"*Your purpose in life is to find your purpose and give your whole heart and soul to it*"

-Gautama Buddha

Dedicated to my family

MOLECULAR GENETIC ANALYSIS OF THE AXIN HOMOLOG PRY-1 IN REGULATING DEVELOPMENTAL AND POST-DEVELOPMENTAL PROCESSES IN *CAENORHABDITIS ELEGANS*

By **Avijit Mallick,**

A Thesis Submitted to the School of Graduate Studies in the Partial Fulfillment of the Requirements for the Degree Doctor of Philosophy

McMaster University

Doctor of Philosophy (2022)

Hamilton, Ontario (Department of Biology)

TITLE: MOLECULAR GENETIC ANALYSIS OF THE AXIN HOMOLOGY PRY-1 IN REGULATING DEVELOPMENTAL AND POST-DEVELOPMENTAL PROCESSES IN *CAENORHABDITIS ELEGANS*

AUTHOR: **Avijit MALLICK** (McMaster University)

SUPERVISOR: Dr. Bhagwati GUPTA

NUMBER OF PAGES: vii, 284

Abstract

My Ph.D. research project in the Bhagwati Gupta lab focuses on understanding the mechanism by which the Axin family of scaffolding proteins functions to regulate biological processes in multicellular eukaryotes. Towards this, I am using the nematode (worm) *Caenorhabditis elegans* as an animal model to investigate the role of one of the Axin homologs, PRY-1. Studies in various model systems and humans have shown that the Axin family of proteins plays crucial roles during cell proliferation, cell differentiation, and organ formation. Such a role of Axin depends on the negative regulation of the WNT signaling cascade. Consistent with these, alterations in Axin function are associated with developmental abnormalities and age-associated diseases such as axis duplication, neuroectodermal defect, and muscle degeneration.

As a scaffolding protein, Axin family members bind to and recruit multiple protein partners that are both WNT dependent and independent. However, how Axin interacts with these factors to regulate molecular events is not well understood. While some Axin-interacting factors have been identified, many more remain to be discovered. My project deals with the identification and functional characterization of *pry-1/Axin* interactors in *C. elegans*.

The key findings of my Ph.D. research are published in five peer-reviewed papers. Collectively, the results demonstrate that PRY-1 is necessary to regulate lipid metabolism, stress response, muscle health, and aging. I have shown that PRY-1 utilizes multiple pathways to control these diverse processes. Specifically, PRY-1 functions via the SREBP transcription factor homolog SBP-1 to regulate yolk lipoprotein expression to promote lipid synthesis. The analysis of *pry-1's* role in aging and muscle health has revealed its interactions with the energy sensor AMPK homolog AAK-2, thereby affecting the function of the Insulin/IGF1 signaling (IIS) transcriptional regulator DAF-16/FOXO. Moreover, I have identified several mRNA genes and microRNAs that function downstream of PRY-1/Axin signaling to either suppress or enhance *pry-1* mutant defects. All these novel interactors have mammalian homologs. Altogether, these findings form the basis to pursue future work to investigate the conserved mechanism of Axin signaling and hold the potential for effective intervention to delay aging and age-associated muscle deterioration.

Acknowledgments

Several people have guided and helped my progress as a student over the years. First, I would like to thank my advisor, Prof. Bhagwati Gupta, for his immense guidance and support. He has always supported me and pushed me to become a better researcher and learn to challenge the odds. He taught me how to stay focused while doing multiple unrelated experiments simultaneously. He was always there during my tough times. Thanks a lot for being so flexible and allowing me to pursue my hypothesis and unrelated project works in the lab.

My committee members, Prof. Andre Bedard and Prof. Brad Doble have been critical, supportive, encouraging, and provided constructive advice and suggestions on critical thinking about research as a whole rather than from worms (model system) perspective. Their advice and knowledge have been extremely important in guiding me and making me a better mature researcher.

I would want to extend my gratitude to Prof. Andrew Dillin from the University of California Berkeley for allowing me to do experiments and sharing resources in his lab as a visiting scholar. His inputs and suggestions have been really helpful for me and our lab. Also, I would thank Wouter van den Berg, Shane Taylor, and Nikita Jhaveri for their encouragement and help during those days when lab work was not going right. I am grateful to my colleagues in the Gupta lab, both past, and present, for their encouragement and help over the years.

Finally, I would like to express my ever gratefulness to my family for their love and support throughout my life. They have encouraged me to dream big and pursue my goals in life. Thanks to my mother (Dr. Shilpi Chowdhury) and father (Dr. Mridul Mallick) for constantly reminding me to stay focused on my studies and the value of biological science. You both have been my true inspiration since childhood. Thanks to my beloved wife (Mrs. Shatabdi Mitra) for her constant support and motivation throughout my time at McMaster. Your deliciously cooked meals always made me happy in difficult times. Thanks to my brother (Dr. Samarjit Mallick), for believing in me. I will be forever grateful to you all. Finally, I would like to thank my friends throughout the globe for reminding me to enjoy small things in life when I got too wrapped up in my work.

Contents

Acronyms

C. br *Caenorhabditis briggsae*

DE Differentially Expressed

Egl Egg-Laying Defect

GO Gene Ontology

HSR Heat Shock Response

IGF Insulin-like Growth Factor-1

IIS Insulin/insulin-like Growth Factor-1

ISR Integrated Stress Response

miRNA microRNA

Muv Multi Vulva

PQ Paraquat

Pvl Protruding Vulva

ROS Reactive Oxygen Species

TEA Tissue Enrichment Analysis

UPR^{ER} Endoplasmic reticulum unfolded protein response

UPR^{mt} Mitochondrial unfolded protein response

VIT Vitellogenins

VPC Vulva Precursor Cell

Declaration of Authorship

I, Avijit Mallick, declare that this thesis titled, “MOLECULAR GENETIC ANALYSIS OF THE AXIN HOMOLOGY PRY-1 IN REGULATING DEVELOPMENTAL AND POST-DEVELOPMENTAL PROCESSES IN *CAENORHABDITIS ELEGANS*” and the work presented in it are my own. Author contributions are listed at the beginning of each chapter.

Chapter 1

Introduction

Signaling pathways control a vast array of biological processes during embryogenesis and in adult life. The development of the complex multicellular organism, ranging from a series of cell fate decisions and morphogenetic movements leads to the generation of different tissues and organs in the body. The network of pathways not only helps in generating tissues and organs (development) but also maintains them during aging (post-development). Consistent with such integral roles, any perturbations of these core pathways lead to various diseases. One such important pathway is the well-studied WNT (*wingless* and *int-1*) signaling pathway that is conserved from the sponges to the vertebrates. WNT signaling activates or regulates several cellular processes, including mitogenic stimulation, cell fate specification, and differentiation. Axin is the central component of the WNT signaling pathway, with its ability to function as a scaffolding protein. With their crucial roles, the Axin family members are evolutionarily conserved

among the eukaryotes. My research utilizes the Axin homolog, PRY-1 (poly ray 1), in the nematode *Caenorhabditis elegans* (*C. elegans*) that negatively regulates WNT signaling, to study the regulation of several different biological events such as reproductive organ development, seam cell development, lipid metabolism, stress response, and aging. In the next few sections, I describe in detail the structure and function of the Axin family of scaffolding proteins, their involvement in WNT and non-WNT signaling pathways followed by how they regulate development, aging, and stress response in the eukaryotes.

1.1 An overview of Axin in WNT signaling

The development of complex multicellular organisms, ranging from a series of cell fate decisions and morphogenetic movements, leads to the generation of different tissues and organs in the body. And one of the central cell-signaling cascades playing a pivotal role in regulating these developments is the evolutionarily conserved WNT-β-catenin pathway. WNT proteins are secreted, lipid-modified glycoproteins present in organisms that range from the sponges to the vertebrates and govern a wide variety of functions, including body axis patterning, cell fate specification, cell proliferation, and cell migration. Upon the completion of developmental stages, this pathway then maintains the stem cells and tissue regeneration in the vertebrates, and mutation of the components involved in this pathway has been shown to cause a wide variety of diseases such as breast and prostate cancer, glioblastoma, type II diabetes and others (Logan and Nusse 2004; Komiya and Habas 2008).

Previous research in Drosophila has shown that WNT can activate several different signaling pathways-canonical and non-canonical WNT signaling pathways. Among these, the most extensively studied pathway is the WNT-β-catenin canonical pathway, which controls the expression of the target genes through the protein β-catenin. This protein is targeted for degradation by a destruction complex, in the absence of WNT signaling, that consists of the scaffold protein Axin, the tumor suppressor gene product APC (adenomatous polyposis coli), and the kinases CKI (casein kinase I), and GSK3 (glycogen synthase kinase-3). Notably, β-catenin has a conserved phosphorylation site at the N-terminus, which upon phosphorylation leads to β-Trcp (F-box protein β-transducin repeats-containing protein**)**-dependent ubiquitination and proteasomal degradation. When FRIZZLED and LRP6 (low-density lipoprotein-related protein 6) receptors are activated upon WNT ligand binding, β-catenin degradation is inhibited through a mechanism involving the cytoplasmic protein DVL (dishevelled) and the recruitment of Axin to the LRP6 in the plasma membrane (Mallick *et al.* 2019b). Then the stabilized β-catenin translocates to the nucleus where it activates the transcription of the target genes by interacting with the members of TCF/LEF1 (T-cell factor/lymphoid enhancer-binding factor 1) family of proteins, HMG-box containing transcription factors.

Axin was first identified as a negative regulator of the WNT-signaling pathway, where it functions as the scaffold of the destruction complex and inhibits axis formation (axis inhibition) in the mouse. Then, its role in other processes, including developmental events like embryogenesis, neuronal differentiation, and tissue homeostasis, has been

shown (Logan and Nusse 2004). Once bound to the destruction complex, β-catenin is phosphorylated and undergoes β-TrCP mediated ubiquitination followed by proteolytic degradation (Clevers 2006; Clevers and Nusse 2012; Nusse and Clevers 2017). When the WNT signaling is ON, destruction complex activity is inhibited by the recruitment of the complex to the cell membrane, thus increasing the cytoplasmic β-catenin content, which translocates to the nucleus and promotes transcription of target genes (Hart *et al.* 1998; Clevers and Nusse 2012). Research has shown previously that the constitutively active β-catenin, due to loss of destruction complex (by loss of Axin function), is involved in various disorders of lungs, heart, muscles, bones and is also associated with different types of cancers (Clevers and Nusse 2012). All these shreds of evidence show that precise regulation of Axin is crucial for WNT-mediated signaling (Also see **Section 1.6).**

The Axin family of scaffolding proteins is conserved in eukaryotes with its ability to recruit and interact with multiple pathway components that are both WNT dependent and independent. In the nematode *C. elegans*, there are two Axin homologs namely, PRY-1 and AXL-1 (Axin like 1), with three characteristic Axin-like domains (RGS, DIX, and GSK3-β-catenin). However, PRY-1 appears to be the major Axin homolog with severe mutant phenotypes and broader expression pattern as described in the subsequent thesis chapters (**Chapters 3, 4, 5,** and **6**). A comprehensive review of this master scaffolding protein Axin and its function in various model systems can be found in the published review article at the end of this chapter (**Section 1.6**).

1.2 Role of Axin in non-WNT pathways

The works described in this thesis and other emerging studies have shown that Axin interacts with many other factors that are WNT independent to carry out its functions. Apart from being the negative regulator of WNT signaling, Axin is involved in several other signal transduction pathways through its scaffolding property. Axin family members cooperate with an increasing number of proteins (MEKK1, MEKK4, Smad3, Smad7, p53 and LKB1-AMPK) in other, non-WNT processes. These interactions involve pathways such as JNK (c-Jun N-terminal kinase), TGF-β (transforming growth factor-beta), p53, and AMPK (AMP-activated protein kinase) (reviewed in Mallick et al. 2019, **Section 1.6**). Moreover, Axin1 facilitates the formation of a destruction complex for c-Myc transcription factor (Arnold *et al.* 2009). Such a property of this scaffolding protein makes it an attractive target to understand the processes regulated by different pathways in an overlapping manner.

1.3 Overview of thesis organization

My research questions described below (**Section 1.5**) focus on uncovering the tissue-specific interacting partners of Axin in *C. elegans* and their role in Axin-mediated regulation of cellular processes such as aging (**Section 1.3**), lipid metabolism (**Section 1.3**) and stress response (**Section 1.4**). In the following sections, I have briefly described the regulation of these major biological processes by Axin that have been discovered as part of my Ph.D. thesis and other published studies. Moreover, key findings are summarized in the following four chapters (**3-6**). In **Chapter 3**, I report the first miRNA

transcriptomic of *pry-1* mutants which revealed six differentially expressed miRNAs (*lin-4, miR-237, miR-48, miR-84, miR-241,* and *miR-246*) involved in seam cell development, stress response, aging, and immunity. Here, we emphasize the role of *pry-1* in regulating seam cell division and miRNA expression via the WNT-asymmetric pathway. In **Chapter 4**, I describe the first mRNA transcriptomic of *pry-1* mutants that laid out the groundwork for the rest of my thesis work. Differentially expressed genes in the *pry-1* mutants were associated with processes such as aging, lipid metabolism, and stress response. Further genetic and molecular analyses demonstrated the important role of PRY-1 in regulating lipid synthesis which may involve the SBP-1/SREBP (Sterol regulatory-element binding proteins) transcription factor. **Chapter 5** reports the role of PRY-1 in the aging process where the protein presumably interacts with the energy sensor AAK-2/AMPK to cell non-autonomously activate DAF-16/FOXO (Forkhead Box subfamily O) in the intestine. Interestingly, I show that PRY-1 acts downstream of the WNT ligand MOM-2 but does not require the β-catenin homolog BAR-1 in this process. Such a mechanism is necessary for maintaining muscle mitochondrial health and the normal lifespan of animals. Finally, in **Chapter 6**, I describe the identification of the genetic network of PRY-1 comprising of the transcription factor CRTC-1/CRTC1 (CREB-regulated transcription coactivator 1), the tyrosine kinase receptor KIN-9/FGFR (Fibroblast growth factor receptor), and eight genes involved in DNA replication, DNA repair, gene expression, oxidation-reduction reaction, and proteostasis. In **chapter 6**, I have demonstrated how PRY-1 may regulate calcineurin signaling, FGF signaling, and control protein homeostasis. Altogether, these findings provide shreds of evidence for the major role of this master scaffolding protein

PRY-1 in regulating processes such as lifespan, lipid metabolism, and stress response by utilizing multiple downstream effectors.

Our finding that PRY-1 is necessary for the regulation of lipid levels, lifespan and muscle health provides a unique opportunity to investigate the conserved role of Axin signaling in age-related diseases. Thus**,** understanding the regulation of Axin and its signaling pathway in different tissues promises to accelerate the development of new tools and methods to effectively modulate Axin function during diseases.

1.4 Aging and lipid metabolism

Aging is an increased rate of fragility that leads to an accelerated mortality rate as a function of time. It is often thought of as a non-specific degeneration outcome of accumulated damage from environmental exposure or metabolic processes. However, genetic components to aging have been extensively studied in the last two decades or so with each species having a characteristic lifespan and rate of aging. Intense research contributions using the nematode *C. elegans* have been made to uncover the genetic components and how they interact with environmental forces to cause changes associated with aging. Some of the well-studied longevity pathways include Insulin/Insulin-like growth factor-1 (IIS) signaling, germline-less signaling, dietary restriction mediated (SKN-1, PHA-4, AMPK-TOR) signaling, and perturbed mitochondrial signaling (Kenyon 2010; Lapierre and Hansen 2012; Uno and Nishida 2016).

Similarly, lipid metabolism plays a vital role in many physiological and pathological processes. All the major aging pathways mentioned above, at least in worms, affect lipid homeostasis (synthesis, transportation, and breakdown) (Hansen *et al.* 2013; Watts and Ristow 2017; Papsdorf and Brunet 2019). Among other processes, it also affects energy storage, intracellular and intercellular signaling, and membrane homeostasis. It has been shown that excessive fat storage in the form of triglycerides (TAGs) is involved with diseases like atherosclerosis and type 2 diabetes in humans (Miller and Bose 2011). Moreover, specific alterations in lipid profiles and even increased lipid storage have been linked to longevity in both invertebrates and mammals (Hansen *et al.* 2013;

Papsdorf and Brunet 2019). Overall, these data suggest that perturbed lipid metabolism may in part contribute to the aging process in animals.

1.4.1 Role of Axin in aging and metabolism

In mammalian systems Axin is necessary to activate the master energy sensor AMPK in glucose deficient cells (Zhang *et al.* 2013, 2014a, 2016) The AMPK/Axin1 signaling pathway mediates contraction-stimulated skeletal muscle glucose uptake (Yue *et al.* 2020). In the first case, Axin docks onto the lysosomal v-ATPase-Ragulator complex to activate AMPK upon glucose deprivation. The Axin-based lysosomal pathway is also required for AMPK activation following metformin treatment, as liver-specific Axin knockout failed to activate this energy sensor (Zhang *et al.* 2016). In the second case, exercise stimulated both AMPK and Rac1 activation while increasing the cellular levels of Axin1. Accordantly reducing Axin1 function blocked GTP loading of Rac1 (Ras-related C3 botulinum toxin substrate 1), AMPK activation, and glucose uptake in the exercising muscles. Both these examples demonstrate the crucial role of Axin tethering in activating AMPK which is responsible for promoting muscle metabolism and benefits linked to exercise (Yue *et al.* 2020). Support for Axin's role in metabolism also comes from a fly study (*Drosophila melanogaster*) where the partial loss of *D-axin* altered the expression of metabolic genes and made the animals hypersensitive to fasting (Zhang *et al.* 2014b). This phenotype was dependent on mTORC1 (mechanistic target of rapamycin complex 1) activity.

Interestingly, the interaction between Axin and AMPK is not a unique phenomenon as other Axin family members have also been found to interact with AMPK in different biological contexts. For example, the *C. elegans* Axin homolog AXL-1 forms a complex with AAK-2 following metformin treatment (Chen *et al.* 2017). Here, AXL-1 is necessary for metformin-mediated lysosomal localization and activation of AAK-2 in a VHA-3-LMTR-3-PAR-4 (v-ATPase-Ragulator-LKB1) complex dependent manner. Metformin-induced lifespan extension of animals is completely abolished in the absence of AXL-1 function (Chen *et al.* 2017). However, the role of the major *C. elegans* Axin homolog PRY-1 in these processes remains to be investigated. Thus, to explore the role of Axin-mediated signaling in aging and lipid metabolism, I investigated whether the Axin homolog PRY-1 in *C. elegans* contributes to these processes in worms which is described in **Chapters 4, and 5**. Published papers in these chapters demonstrate that PRY-1 is crucial for fatty acid synthesis (**Chapter 4**) and for maintaining muscle and mitochondrial health during aging (**Chapter 5**). Altogether, these findings demonstrate the important role of Axin family members in regulating age-related processes in higher eukaryotes.

1.4.2 Axin in WNT-mediated aging

The role of WNT-β-catenin signaling has largely been investigated in development and disease, although the pathway is also involved in other processes, such as aging and cellular senescence (DeCarolis *et al.* 2008). Over the last decade, several lines of evidence have emerged linking WNT pathway components to the aging of cells and

tissues. Studies in both vertebrates and invertebrates have reported age-related expression changes in WNT pathway components. For example, GSK-3β and β-catenin are altered in aged muscle satellite cells (Brack *et al.* 2007). Likewise, mice deficient in Klotho (a WNT antagonist), having reduced lifespan and increased cell senescence, show an increased transcription of WNT ligands, Frizzled (Fz) receptor, as well as WNT downstream targets (Liu *et al.* 2007). In humans, similar changes in the expression of frizzled 4 receptors and several WNT target genes were observed in the mammary artery tissue, a part of the vascular system (Marchand *et al.* 2011).

Studies in *C. elegans* have shown that several WNT ligands (*cwn-1*, *cwn-2, mom-2, egl-20*) are expressed in older adults, consistent with their involvement in post-developmental processes such as aging (Lezzerini and Budovskaya 2014). Loss of *cwn-1, cwn-2,* and *mom-2* function extends lifespan (Lezzerini and Budovskaya 2014), whereas *egl-20* mutants are short-lived (Zhang *et al.* 2018). Moreover, *bar-1/β-catenin* the effector protein of the canonical WNT signaling, has been shown to play a role in aging (Zhang *et al.* 2018; Xu *et al.* 2019). More specifically, in one case *bar-1* was found to be needed for neuronal *egl-20* mediated lifespan extension and mitochondrial unfolded protein response activation, whereas in another case, *bar-1* is required for *miR-235-cwn-1* mediated longer lifespan of dietary restricted *eat-2* mutants (Xu *et al.* 2019).

Although these studies involving nematodes did not report the direct involvement of Axin homologs, research using a mouse model reported elevated *Axin2* transcript levels in aged muscles suggesting that elevated WNT signaling promotes age-associated

deterioration (Brack *et al.* 2007). Specifically, the authors have shown that aged mice muscle satellite cells show conversion from myogenic to a fibrogenic lineage which is mediated by elevated WNT signaling. Exposing aged muscle cells to serum from young mice was able to reduce fibrotic response leading to lower collagen deposition (Brack *et al.* 2007). In addition, mutations in Axin that lead to overactivation of the WNT pathway are known to contribute to the development of many age-related diseases, such as cancer, osteoporosis, and metabolic dysfunction (Clevers 2006).

1.5 Stress response pathways

Eukaryotic cells must accurately monitor proteostasis to adapt to environmental perturbations and respond to physiological cues. Proteostasis is a combination of multiple processes that control the production of proteins which include highly complex pathways mediating protein-translation, folding, maturation, trafficking, degradation, and targeting to the final destination. Each of these processes is regulated at different levels and can be compartmentalized to specific organelles. Protein quality control mechanisms ensure the proper folding of proteins or their degradation that are either organelle-specific or generic. These conserved quality control mechanisms include integrated stress response (ISR), endoplasmic reticulum (ER) induced unfolded protein response (UPR^{ER}), mitochondrial unfolded protein response (UPR^{mt}), and cytosolic heat shock response (HSR) (Pakos-Zebrucka *et al.* 2016; Higuchi-Sanabria *et al.* 2018; Anderson and Haynes 2020; Taylor and Hetz 2020). Interestingly, all these pathways are associated with age-associated physiological deteriorations and affect the lifespan

of animals (Pakos-Zebrucka *et al.* 2016; Higuchi-Sanabria *et al.* 2018; Anderson and Haynes 2020; Taylor and Hetz 2020).

1.5.1 Axin in stress response

There is not much literature on the role of Axin family members in regulating stress response in eukaryotes. The only evidence showing direct involvement of PRY-1/Axin in activating UPR^{mt} comes from *C. elegans* where the authors have shown that loss of PRY-1 activates UPR^{mt} responsive transcription (Zhang *et al.* 2018). My research work in this area not only demonstrated the role of PRY-1 in stress response maintenance but also identified downstream effector genes that contribute to this process (**Chapter 6**). More specifically, I have shown that complete or partial loss of *pry-1* increases the sensitivity of animals to chemical and heat-induced stress. Additionally, mutant RNA transcriptomics revealed differentially expressed genes involved in both UPR^{ER} and UPR^{mt} pathways. Interestingly, *pry-1* also regulates genes that are involved in mitochondrial matrix and membrane formation. Overall, my findings described in **Chapter 6** demonstrate the role of PRY-1 in maintaining protein control machinery. However, it remains to be seen whether PRY-1 also affects global protein synthesis and ER function as proposed in **Chapter 7**.

While there is not much research done on the role of Axin, a significant amount of work has been published that reported the roles of WNT signaling in maintaining stress response. Here I discuss the current developments on the role of WNT signaling in

affecting this protein control machinery that affects both developmental and post-developmental events and regulates cellular health and viability during elevated stress and aging. Research using colon cancer cell lines and zebrafish has shown that while a reduction in mitochondrial ATP downregulates WNT signaling, restoring ATP levels or blocking ER stress activates the WNT pathway (Costa *et al.* 2019). Moreover, heat exposure induces ER stress and downregulates the WNT signaling pathway to disrupt epithelial integrity (Zhou *et al.* 2020). Interestingly, UPR^{ER} activation has been reported to increase the activity of GSK-3 by selectively removing GSK-3 with phosphorylated $Ser^{21/9}$ via autophagy/lysosomal pathway (Nijholt *et al.* 2013).

On a different note, the role of WNT signaling in synaptic plasticity and maintenance is well established (Marzo *et al.* 2016; McLeod *et al.* 2018). Moreover, consistent with its role in aging, WNT signaling is downregulated in the aging brain which increases the susceptibility of synapses to toxic protein aggregation (Folke *et al.* 2019; Palomer *et al.* 2019). Multiple groups have reported that increased deposition of Amyloid-beta (Aβ), a toxic molecule (peptides of 36-43 amino acids) seen in large quantity in the brain of Alzheimer's disease (AD) patients, induces an elevation in DKK1 that antagonizes WNT signaling (Palomer *et al.* 2019). Consistently, blocking DKK1 protects synapses from Aβ (Purro *et al.* 2012). Together with the finding that deletion of LRP6 in the postnatal forebrain leads to synaptic loss and exacerbates AD pathology (Liu *et al.* 2014), suggest that Aβ mediated AD pathology depends on downregulating the WNT pathway.

In the *C. elegans* model, WNT signaling has been implicated in UPR^{mt} and oxidative stress. Specifically, Essers et al have shown that BAR-1/β-catenin function is required for DAF-16/FOXO dependent resistance against oxidative stress (Essers *et al.* 2005). A different study has shown that animals use retromer-dependent EGL-20/WNT signaling to propagate mitochondrial stress signals from the nervous system to peripheral tissues. In this process, loss of PRY-1/Axin and BAR-1/β-catenin activates and suppresses UPR^{mt} respectively in a canonical (opposing) manner (Zhang *et al.* 2018). Subsequently, a follow-up investigation from the same group revealed that WNT signaling is required for transgenerational activation of UPR^{mt} via elevated mitochondrial DNA (mtDNA). This is necessary for the offspring to have an extended lifespan and confer stress resistance (Zhang *et al.* 2021).

1.6 Goals and major findings

Axin negatively regulates WNT signaling and interacts with multiple different signaling pathways. My thesis has focused on non-WNT signaling roles of Axin and characterization of its cellular and molecular mechanisms in regulating diverse processes. To this end, I have investigated the function of *C. elegans* Axin family member *pry-1*.

My project utilized the powerful genetic model system *C. elegans*. However, I also used the closely related species *C. briggsae* in some of my studies. Since the inception of *C. elegans* as a genetic model organism (Brenner 1974), it has led to several scientific

breakthroughs including cell motility, neurobiology, microRNAs, and aging (WormBook 2017). Among the many benefits that these model system offers are their small body size (~1mm), transparent body, definitive cell count of 959 cells from known lineages, large brood size (~300 eggs), relatively short life cycle (~3 days) and lifespan (~3 weeks). Moreover, these animals allow efficient RNAi mediated gene knockdown via feeding, allow efficient gene editing, have 83% of the proteome with human homologs (Lai *et al.* 2000), and conserved pathways and processes of higher eukaryotes. Such a high level of conservation makes research in this model system very valuable to understand the complex regulation of pathways during diseases in the mammalian system.

This project began by carrying out RNA-Seq analysis to identify genes and miRNAs whose expression is changed in the *pry-1(mu38)* mutants at the early larval stage. These analyses revealed differentially expressed genes and miRNAs associated with various biological processes that include seam cell development, reproductive structure development, aging, stress response, and lipid metabolism. To understand the role of PRY-1 in these processes, I started to analyze these genes in a process-specific manner. Detailed genetic, molecular, and biochemical analyses using PRY-1 and other relevant pathway components, uncovered the mechanism of PRY-1 signaling in seam cell development (**Chapter 3**), lipid metabolism (**Chapter 4**), aging and muscle health (**Chapter 5**), reproductive structure development (**Chapter 6**) and stress response maintenance (**Chapter 6**). Over the years, I have generated a lot of resources that included transgenic strains, plasmids, and RNAi clones (**Chapter 2 and Appendix A-**

D) that will help uncover the gaps in our current knowledge described in **Chapter 7**. Moreover, I learned CRISPR-mediated gene editing and high-end confocal microscopy followed by some cutting-edge techniques during my research internship in the Dillin lab at the University of California Berkeley.

As mentioned above, I have uncovered the role of PRY-1 in multiple biological processes such as seam cell development, lipid metabolism, lifespan regulation, and stress response maintenance, which is described in four different chapters (**Chapters 3-6**). Firstly, during seam cell division *pry-1* regulates six miRNAs (*lin-4, miR-237, miR-48, miR-84,* and *miR-241*) involved in heterochronic development. In this, *pry-1* is part of the WNT asymmetric pathway where it inhibits WRM-1/β-catenin-LIT-1/NLK mediated POP-1/TCF nuclear exclusion to determine seam cell fate specification (**Chapter 3**). Secondly, *pry-1* is necessary to maintain normal lipid levels in animals. I have found that loss of *pry-1* leads to a reduction in fatty acid synthesis and overall TAG levels. The findings reveal that PRY-1 utilizes the yolk lipoproteins (vitellogenins) and SBP-1/SREBP transcription factor in this process. While it is known that SBP-1 promotes the expression of fatty acid desaturases, it is unclear how vits are involved in PRY-1 mediated lipid synthesis (**Chapter 4**). Next, I have shown that PRY-1 functions cell non-autonomously in the muscle, where it presumably interacts with AAK-2, to activate DAF-16 in the intestine. This interaction is necessary to promote muscle health and the lifespan of animals (**Chapter 5**). Finally, in **Chapter 6**, I report three different studies where downstream effectors of PRY-1 signaling during stress response and lifespan have been identified. Briefly, PRY-1 negatively regulates

calcineurin signaling and CRTC-1/CRTC transcription factor, PRY-1 inhibits FGF signaling by promoting the *miR-246* expression and acts upstream of genes involved in DNA repair (HIS-7/H2AX), DNA replication (RNR-1/RRM1), DNA damage checkpoint (CLSP-1/CLSPN), proteostasis (CLSP-1/CLSPN, RPN-7/PSMD6, CPZ-1/CTSZ), and oxidation-reduction reaction (ARD-1/ HSD17B10).

1.7 Mallick et al. (2019)- Journal of Developmental Biology

1.7.1 Preface

This section of Chapter 1 includes the following comprehensive review article in its originally published format: "Axin family of scaffolding protein in development: Lesson from *C. elegans*", by Avijit Mallick, Shane Taylor, Ayush Ranawade, and Bhagwati P. Gupta. (Journal of Developmental Biology. 2019 Oct 15; 7(4), 20. DOI: 10.3390/jdb7040020). This is an open-access article distributed under the terms of the Creative Commons Attribution Unported License, which permits unrestricted use, distribution, and reproduction in any medium provided the original work is properly cited.

Contributions: I and Bhagwati Gupta contributed to gathering information from various articles and wrote the initial draft. Shane Taylor performed experiments to analyze *manf-1* expression and neurodegeneration using a *dat-1::GFP* marker in the *pry-1* mutants (Figure 5C-D). I and Bhagwati Gupta made Figures and adopted

copyright permissions from previously published Figures. I, Ayush Ranawade and Bhagwati Gupta edited and finalised the manuscript.

Journal of *Developmental Biology*

MDPI

Review

Axin Family of Scaffolding Proteins in Development: Lessons from *C. elegans*

Avijit Mallick [1], Shane K. B. Taylor [1], Ayush Ranawade [2] and Bhagwati P. Gupta [1,*]

[1] Department of Biology, McMaster University, Hamilton, ON L8S-4K1, Canada; mallia1@mcmaster.ca (A.M.); taylos49@mcmaster.ca (S.K.B.T.)

[2] Department of Bioengineering, Northeastern University, Boston, MA 02115, USA; ayushranawade@gmail.com

* Correspondence: guptab@mcmaster.ca; Tel.: +1-905-525-9140 (ext. 26451); Fax: +1-905-522-6066

Received: 12 August 2019; Accepted: 11 October 2019; Published: 15 October 2019

check for updates

Abstract: Scaffold proteins serve important roles in cellular signaling by integrating inputs from multiple signaling molecules to regulate downstream effectors that, in turn, carry out specific biological functions. One such protein, Axin, represents a major evolutionarily conserved scaffold protein in metazoans that participates in the WNT pathway and other pathways to regulate diverse cellular processes. This review summarizes the vast amount of literature on the regulation and functions of the Axin family of genes in eukaryotes, with a specific focus on *Caenorhabditis elegans* development. By combining early studies with recent findings, the review is aimed to serve as an updated reference for the roles of Axin in *C. elegans* and other model systems.

Keywords: Axin; *C. elegans*; *pry-1*; *axl-1*; WNT signaling; scaffolding protein; signal transduction; development

---

Axin was first discovered as a negative regulator of WNT (*wingless* and *int-1*) signaling in mice while deciphering its role in embryonic axis formation [1]. This protein is the product of the mouse Fu (Fused) gene [2–4] and was named Axin for its initial discovered role in inhibiting axis formation (Axis inhibition). Soon after, Axin and its homolog Axil (for Axin-like, also known as Axin2 or conductin) were discovered in a yeast two-hybrid screen for GSK-3β (glycogen synthase kinase-3 beta)-interacting proteins [5,6]. Since then, involvement of Axin family proteins in WNT signaling has been extensively characterized, revealing that they can bind to and facilitate interactions between several WNT pathway components such as the WNT co-receptor LRP (low-density lipoprotein-related protein), Dvl (Dishevelled), APC (tumor suppressor Adenomatous Polyposis Coli), GSK-3β, β-catenin, CKs (casein kinases), and many others [7–18].

Over the years, Axin homologs have been identified in several organisms. Many of these discoveries were facilitated by the availability of whole-genome sequences. While functional studies are currently limited to a few animal models, the findings and sequence data show that Axin is conserved in metazoans, with invertebrates carrying an ancestral gene and higher eukaryotes possessing two distinct *Axin1* and *Axin2* genes [1,5,19,20]. The nematode lineage contains an additional, divergent, Axin homolog [21] (see Figure 1 and further discussion below). Experiments performed in mice have revealed that while both Axin proteins regulate WNT signaling, they have different functions [22–24]. Whereas Axin1 is ubiquitously expressed in embryos and is essential for viability, Axin2 is restricted to a few tissues and serves as a transcriptional target of WNT signaling [25,26]. Similar to the published literature, the 'Axin1' and 'Axin' names have been used interchangeably in this article, whereas the term 'Axin family' refers to both Axin1 and Axin2 homologs that share conserved protein-interaction domains.

J. Dev. Biol. **2019**, *7*, 20

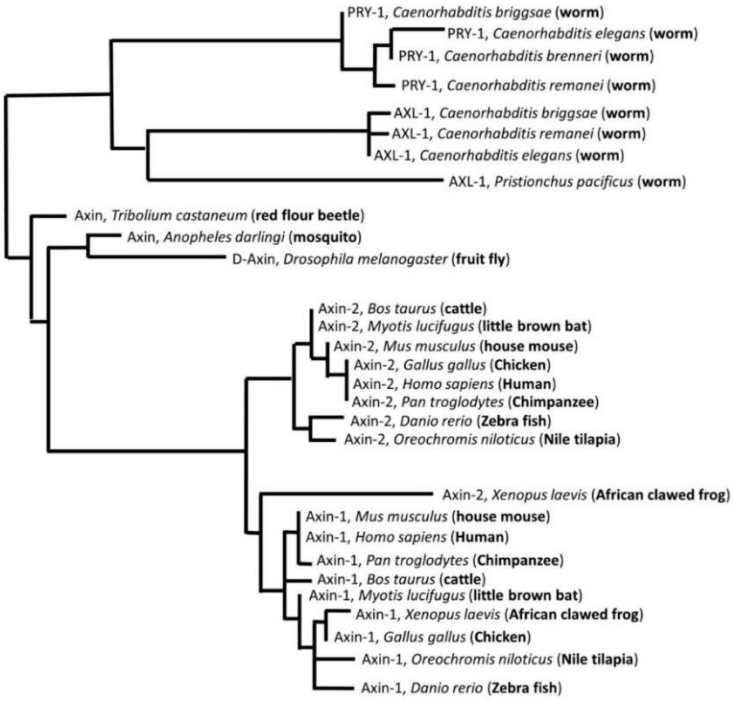

Figure 1. Axin family is conserved in multicellular eukaryotes. Multiple sequence alignment dendrogram was generated by LIRMM (http://www.phylogeny.fr/simple_phylogeny.cgi) using default program parameters.

1. Axin Domains

Axin possesses multiple regions that facilitate its interactions with various proteins (Figure 2). One of these regions is involved in regulating G protein signaling (the RGS domain) near the N-terminus that can bind the APC protein [11] (Figure 2). In the context of the WNT pathway, APC requires Axin to form a destruction complex with GSK-3β and other proteins [27]. The C-terminus of Axin possess a DIX (Dishevelled/Axin homologous) domain that facilitates WNT pathway-specific interactions by forming homodimers and heterodimers with the Axin and Dvl proteins [14,28] (Figure 2). In addition to these well-defined domains, Axin also contains regions between the RGS and DIX domains that bind β-catenin (in Armadillo repeats 2–7) [5] and two serine/threonine kinases GSK-3β [29] and CKIα (casein kinase I) [30] (Figure 2). Through these regions, Axin recruits APC, GSK-3β, CKIα, and β-catenin to form a multimeric complex in the absence of WNT signaling. The complex causes enhanced phosphorylation of β-catenin by GSK-3β and CKIα [31,32] and targets it for ubiquitination and proteasomal degradation. Activation of WNT signaling inhibits the destruction of β-catenin and promotes nuclear translocation of the non-phosphorylated form and activation of WNT-responsive genes [32]. Axin also possesses additional sequences that can facilitate protein–protein interactions, thereby promoting activation of other, non-WNT pathway, factors ([33], also see below).

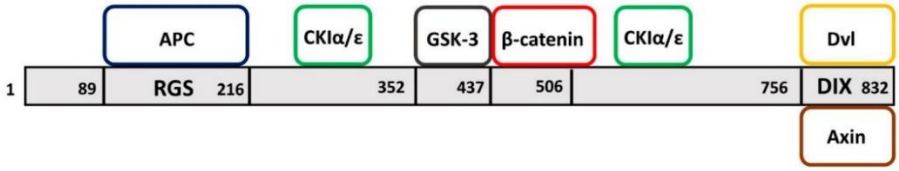

Figure 2. Axin binds to a wide array of proteins. Shown here are the WNT signaling components—APC, CKI, GSK-3, β-catenin and Dvl, with known relative binding positions in Mouse Axin1 (NP_001153070.1). The C-terminus domain (DIX) facilitates formation of homo and hetero dimers.

2. Overview of the Developmental Roles of the Axin Family

2.1. Vertebrate Models

The Axin family of genes are involved in diverse developmental processes. Analyses of mutant and gene knock-down experiments in different animal models have shown defects in anterior–posterior-axis formation and organogenesis. In some cases, these abnormalities may also contribute to early stage lethality. As mentioned above, Axin was initially identified for its role in embryonic axis formation, as mutant mice exhibited axial defects [1]. Subsequently, the gene was also shown to be essential for viability and the formation of many other organs, including the heart, tail, primitive streak, brain, and muscles [24,34–36]. In zebrafish, mutations in Axin cause abnormal fate determination of the eyes and telencephalon, with defective establishment of asymmetries of the nervous system [37,38]. Experiments in *Xenopus laevis* revealed that a failure to regulate Axin activity results in duplication of the dorsal axis due to the constitutive activation of WNT signaling as determined by the expression analysis of target genes [39].

In addition to their requirements for the formation of axis and organs, Axin family members also play crucial roles in neuronal development. Alterations in Axin expression, caused by mutations, knock-down, or dysregulation, show defects in various processes including neurogenesis, neuronal differentiation, axon outgrowth, and synapse formation. As a scaffolding protein, Axin facilitates the recruitment of various proteins to regulate gene expression and cytoskeletal dynamics. Through these actions, Axin affects signaling pathway activities, e.g., WNT-β-catenin, JNK (c-Jun N-terminal kinase) and TGF-β (transforming growth factor-beta) (see below for more details), and organization of proteins such as microtubules (reviewed in [40,41]). Previously, it was shown that ectopic Axin expression in cultured cells blocked neuronal differentiation, a process that involved WNT-3a-β-catenin signaling [42]. In a separate study, it was demonstrated that Axin inhibition in a neuroblastoma cell line, through the application of Li (lithium) and a GSK-3β inhibitor, promoted neurite outgrowth, whereas ectopic Axin expression caused an opposite phenotype [43]. Subsequently, several reports have shown Axin's role in neuronal proliferation and differentiation, axon formation, dendritic spine morphology, and synapse formation [44–48].

Cell proliferation is another process where Axin's involvement has been investigated in considerable detail. The findings have shown that, as a negative regulator of the WNT-β-catenin signaling, Axin functions to inhibit cancerous growth and appears to act as a tumor suppressor [49]. Altered Axin regulation and activity are associated with various types of cancers such as lung cancer, colorectal cancer, and HCC (hepatocellular carcinoma) [50–52]. Characterizations of human HCC cultures identified *Axin1* mutations in many of the cell lines and a corresponding increase in the DNA-binding activities of TCF/LEF (T-cell factor/Lymphoid enhancer-binding factor 1) and β-catenin [53]. Interestingly, when human and mouse HCCs lacking Axin were examined, it was found that in most cases, human HCCs were not associated with increased β-catenin activation [54]. Moreover, HCC induction in mice due to *Axin1* mutation was independent of WNT-β-catenin signaling [54,55]. Further investigations on gene signatures of human and mouse HCCs revealed a significant overlap

between genes affected by Axin1, Notch and YAP (Yes-associated protein), which may provide new avenues for treatments of Axin1-linked tumors [54].

Among its other roles, Axin appears to be necessary for maintaining cell survival, metabolic homeostasis, and thymic adipogenesis. Overexpression studies in transgenic mice and certain cultured cells demonstrated increased apoptosis, possibly due to activation of the cell-death pathway [56,57]. Axin can also regulate the activation of AMPK (AMP (adenosine monophosphate)-activated protein kinase), a sensor of the cellular-energy status [58]. Axin forms a complex with AMPK and a serine-threonine kinase LKB1 (Liver kinase B1), which then leads to AMPK activation to protect cells against increased stress, such as under a condition of low nutrient levels (see below for more discussion on this topic). Finally, in the case of thymus function, Axin promoted age-related adipogenic programming of thymic stromal cells [59]. This process is linked to reduced T-cell production and thymic involution, suggesting that any potential therapeutic intervention to prolong aging may involve lowering Axin activity.

2.2. *Invertebrate Models*

Studies in invertebrates have been instrumental in uncovering the developmental roles of Axin homologs in tissues and organs, in the context of intact animals. The *Drosophila melanogaster* Axin (D-Axin) homolog is necessary for the development of embryos and organs, such as the wings, eyes, heart, gut, and circulatory system [20,60–62]. Analysis of the *Tribolium castaneum* Axin homolog (Tc-Axin) revealed its dynamic expression during embryogenesis. Tc-Axin was initially localized at the anterior pole, extending posteriorly during subsequent development and eventually becoming somewhat ubiquitous [63]. This expression pattern was essential for the formation of head structures, considering that Tc-Axin knockdown led to an absence of the head and thoracic parts. In the case of the nematode *C. elegans*, two divergent Axin-like proteins, specifically PRY-1 (poly ray 1) and AXL-1 (Axin-like 1) have been identified. The roles of both these family members are discussed in a separate section.

In summary, the roles of Axin family of proteins described above rely on its scaffolding properties that are mediated by conserved domains facilitating interactions with WNT-β-catenin pathway components (Figure 2). Additionally, Axins utilize other unique regions (not shown in Figure 2) to recruit non-WNT pathway components involved in other developmental processes that are summarized in the next section (also see Figure 3).

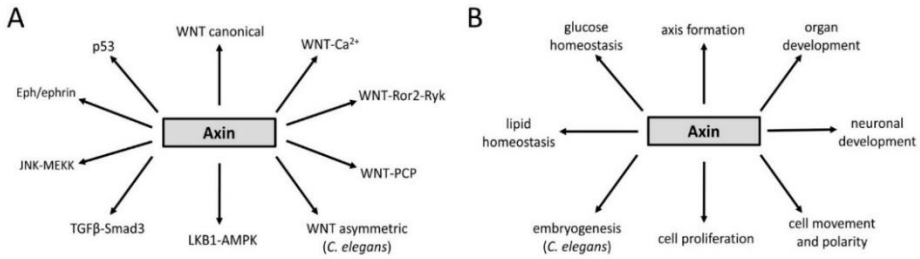

Figure 3. An overview of Axin's involvement in multiple pathways (**A**) and processes (**B**), as described in this review.

3. Axin Proteins Interact with Many Factors Including Signaling Pathway Components

Given that Axins play essential roles in metazoan development, it is not surprising that Axin family members form complexes with various cellular factors and components of signal transduction pathways (Figures 2 and 3A). While much research has focused on their involvement in the canonical WNT-β-catenin signaling pathway, which was summarized in the previous section, additional studies have demonstrated Axin's participation in non-canonical WNT signaling (Figure 3A). These include

the PCP (planar cell polarity) pathway that provides directional information during organ formation, the WNT/calcium pathway that regulates muscle contraction and PKC (protein kinase C) enzyme activation, and the Ror2 (receptor tyrosine kinase-like orphan receptor)- and Ryk (related to tyrosine kinase)-dependent WNT pathway in coordinating cell movement and polarity (Figure 3A) (reviewed in [64]). These WNT pathways are unique in that they do not utilize the canonical effector, β-catenin.

In addition to the above conserved WNT-mediated signaling events, studies in *C. elegans* have shown the presence of a divergent asymmetry pathway that regulates nuclear factor POP-1 in a WRM-1 (worm armadillo 1)/β-catenin-LIT-1 (loss of intestine 1)/NLK (Nemo-like kinase)-dependent manner (see [65] and references therein, [66]). In these cases, PRY-1 affects asymmetric POP-1 localization to control EMS (endomesodermal) precursor division in the embryo and seam cell divisions in larvae (discussed below).

Axin family members also cooperate with an increasing number of proteins in other, non-WNT, processes. These interactions involve pathways such as JNK, TGF-β, p53, and AMPK. Tissue culture experiments involving kidney 293T cells and embryonic fibroblast cells showed that Axin binds to MEKK1 and MEKK4, two members of the MEKK (MAPK (Mitogen-activated protein kinase)/ERK (Extracellular signal-regulated kinase) kinase kinase) family, through domains distinct from those involved in WNT signaling and activates the MKK4- and MKK7- (also belonging to MEKK family) mediated JNK cascade [67,68]. This Axin-dependent JNK activation is inhibited by the WNT pathway components Dvl, GSK-3β, CKIα, and CKIε. Furthermore, during dorsalization of zebrafish embryos, an Axin-interacting protein, Aida, inhibits Axin-mediated JNK activation by disrupting Axin homodimerization [69]. JNK signaling is a key regulator of various cellular processes occurring in response to external signals. Upon activation, JNK translocates to the nucleus and activates gene-expression changes.

Axin's function in TGF-β pathway involves regulation of transcription factor Smad3 activity to affect gene transcription. In human MSCs (mesenchymal stem cells), Axin and GSK-3β physically interact to facilitate Smad3 phosphorylation by the active TβRI (TGF-β type-I receptor) kinase (reviewed in [70]). This interaction is needed to promote MSC proliferation. Axin and GSK-3β also act to regulate ubiquitin-dependent proteasomal degradation of Smad3 in human keratinocytes and hepatocellular carcinoma cells in a manner analogous to the β-catenin degradation process [71]. In yet another study, Axin acted as a scaffold to form a ternary complex with Smad7 and the ubiquitin E3 ligase Arkadia in cultured cells to enhance Sma7 ubiquitination, leading to the activation of TGF-β signaling [72].

While the tumor-suppressor role of Axin has been traditionally investigated in the context of WNT-β-catenin signaling, some studies have demonstrated its interactions with p53, a DNA-binding protein that responds to genotoxic stress and controls cell proliferation and cancerous growth. During p53 signaling, Axin interacts with HIPK2 (homeodomain-interacting protein kinase-2) to facilitate p53 phosphorylation, which stimulates p53-dependent transcription of target genes [73]. Subsequent work showed that this regulatory mechanism involves the formation of distinct complexes consisting of additional proteins such as Pirh2 (p53-induced RING-H2) and the histone acetyl transferase, Tip60 [74,75]. Axin can also associate with a death domain-associated protein, Daxx, to regulate p53 function to induce cell death following exposure to ultraviolet light [76].

Research on Axin has also uncovered its role in controlling cellular energy, nutrient sensing, and metabolic processes. One of these processes involves glucose homeostasis. In *Drosophila*, D-Axin was reported to physically interact with a component of the glucose-transport regulatory complex, DCAP (*Drosophila* catabolite activator protein), to increase glycogen utilization through insulin signaling and glucose transport [77,78]. Additionally, Axin formed a ternary complex with the TNKS2 (ADP (adenosine diphosphate)-ribosylase tankyrase 2) enzyme and the kinesin motor protein KIF3A in cultured cells to facilitate translocation of the insulin-stimulated glucose transporter, GLUT4, and glucose uptake [79]. In an unrelated study, mouse Axin2 was reported to participate in signaling through a *Drosophila* Pygo2 (Pygopus) homolog to affect glucose metabolism [80]. Another energy-homeostasis system involving Axin function is the AMPK signaling network. AMPK is a central player involved

in sensing AMP and ADP levels in response to ATP (Adenosine triphosphate) consumption. During AMPK signaling, accumulation of AMP and glucose-starvation initiates Axin binding to LKB1 to enable AMPK phosphorylation [58]. Because Axin depletion inhibits AMPK stimulation, which results in the loss of lipid homeostasis, Axin acts as a metabolic rheostat and energy sensor [58].

Beyond their other functions, Axins also form complex with Dvl to facilitate cytoskeletal rearrangement during gastrulation (Reviewed in [34]) and orientation of the mitotic spindle during asymmetric cell division [81]. Both these proteins possess a common DIX domain that is responsible for this binding [82]. In addition, Axin interacts with other cellular components to regulate cytoskeletal arrangement. Cowan and Henkemeyer [83] showed that one of the ways that Axin participates in the process is by modulating Eph/ephrin-bidirectional signaling. Specifically, interactions of Axin with Grb4, a SH2/3 domain adaptor protein of the Eph/ephrin pathway, facilitates the recruitment of other proteins leading to cytoskeletal rearrangement during cell and axon growth–cone movement.

In summary, Axin participates in both WNT-dependent and -independent signaling events (Figure 3A). By acting as a scaffold protein, it helps recruit other factors to execute a wide variety of cellular and molecular processes in eukaryotes (Figure 3B). While Axin's role in WNT-β-catenin signaling appears to be conserved in metazoans, several studies have also reported its involvement in other, WNT-independent, pathways. To what extent the later functions of Axin are conserved remains to be established, though it is worth pointing out that Axin-AMPK interaction has been shown in both mice and *C. elegans* systems (see the section 'Regulation of Developmental Processes in *C. elegans*').

4. Regulation of Axin Functions

The crucial roles of Axin family members in metazoans depend on multiple mechanisms that operate at spatiotemporal and subcellular levels. Several reports have shown that Axin is regulated both at transcriptional and post-translational levels. Using an auto-feedback loop, Axin controls its own expression [26,84–86], although the relevance of such a mechanism at the organismal and cellular levels remains to be understood. Modulation of protein functions can also occur via changes in their oligomeric state or through interactions with binding partners. As described above, Axin possesses a DIX domain at the C-terminus, which mediates both homo- and hetero-interactions, thus contributing to its essential activities [87–90]. The same domain is also found in other proteins, such as Dvl. It has been proposed that Dvl might recruit Axin from the destruction complex to the LRP receptor via DIX-domain interactions [91,92].

The post-translational modifications of Axin include phosphorylation, ubiquitination, and SUMOylation. These alterations affect the subcellular localization, stability, or potential interactions of the protein with other factors (reviewed in [93,94]). Similar to β-catenin, under basal conditions, Axin is phosphorylated by both GSK-3β and CKI [10,95,96] to function in the destruction complex and is subsequently dephosphorylated upon WNT pathway activation [10,97,98]. In updated regulation models, Axin phosphorylation occurs during both the 'off' and 'on' states of WNT signaling, and is dependent on another key destruction complex member, APC [99,100]. Another kinase that is reported to phosphorylate Axin is Cdk5 (Cyclin-dependent Kinase 5). During mouse cortex development, Cdk5-mediated phosphorylation was found to be necessary for the interaction of Axin with GSK-3β, leading to microtubules stabilization during axon formation [45].

Axin is subjected to ubiquitin-mediated proteolysis through poly ADP-ribose modification. Experiments in cell culture systems showed that poly ADP-ribosylation of Axin by ADP-ribose polymerase enzymes, tankyrase 1 and tankyrase 2, targeted Axin for proteasomal degradation when the pathway was in the 'off' state [101–103]. The role of tankyrase in Axin regulation has also been demonstrated in the *Drosophila* system [104,105]. Feng et al. [105] reported that Axin levels were moderately higher in Tnks (Tankyrase)-mutant flies. Since a further increase in Axin expression in animals lacking Tnks function disrupted expression of Wingless/WNT reporter gene, it was concluded that Tnks-dependent regulation normally acts to buffer Axin activity. The ubiquitination of Axin is facilitated by several ubiquitin E3 ligases. Ji et al. [106] used human cell lines to investigate the roles of

two RING (really interesting new gene) family ligases, SIAH1 and SIAH2 (seven in absentia homologs 1 and 2), and found that Axin was ubiquitinated and degraded as a feed-forward mechanism to achieve sustained activity of WNT-β-catenin signaling. The *Drosophila* homolog, Iduna (also a RING family member), acts as a key factor in the breakdown of ADP-ribosylated Axin [62,107]. Other ligases (e.g., Smurf2 of HECT (homologous to the E6-AP carboxy terminus) family) also appear to modify Axin's stability [108,109].

Axin is also known to be SUMOylated. The earliest role of SUMOylation in Axin regulation was revealed by the discovery of Axam (Axin associated molecule), an enzyme that possesses deSUMOylation activity [110,111]. Axam formed a complex with Axin and prevented its interactions with Dvl [110]. Later on, studies reported that Axin is SUMOylated and that this modification affects its role in the JNK pathway [112] and may protect Axin from ubiquitination [113].

Adding to its complex mode of regulation, Axin is proposed to utilize an autoinhibitory mechanism. The N-terminus region of the protein was earlier suggested to play an inhibitory role in binding to its partner proteins [7,114] and later shown to associate with the C-terminus, thus forming a closed conformation during the WNT signaling-off state [115]. Thus, Axin can adopt different conformational states depending on its assembly with the destruction complex or the "WNT-LRP5/6 signalosome" (Reviewed in [93]).

Yet another mechanism by which Axin function is modulated involves miRNA (microRNA)-mediated gene silencing. Experiments in the *Drosophila* system showed that *Axin* was negatively regulated by *miR-315* via conserved 3′- UTR (untranslated region) miRNA consensus sequences [116]. Likewise, studies using different human cell types demonstrated that the *Axin2* transcript was targeted by *let-7f* at the 3′ UTR, by *hsa-miR-34a* at both the 5′ UTR and 3′ UTR, and by *miR-205* at the 3′ UTR, which regulated expression of a WNT/β-catenin target gene and a β-catenin-activated reporter [117–119].

The findings summarized above show that Axin is subjected to multiple modes of regulation. Although the full picture of its regulatory mechanism is far from complete, it is evident that alterations help modulate Axin's function and its interactions with other cellular factors and signaling pathway components.

5. Regulation of Developmental Processes in *C. elegans*

As mentioned above, the *C. elegans* genome encodes two Axin family members, PRY-1 and AXL-1. Although both proteins act as scaffolds to recruit other factors, major domains (RGS and DIX) are not well conserved (Figure 4). Of the two, PRY-1 has been investigated in some detail. The protein shows an overall 18–21% amino acid similarity with vertebrate and D-Axin. This level of conservation is primarily restricted to the RGS and DIX domain, with 27% identity (48% similarity) and 31% identity (49% similarity) with the respective domains of D-Axin [120]. Apart from the RGS and DIX domains, PRY-1 has no obvious GSK-3β- and β-catenin binding region(s). Despite this sequence discrepancy, genetic and biochemical experiments showed that PRY-1 acts as a scaffold for components of the destruction complex and negatively regulates canonical WNT signaling [120].

The genetic epistasis experiments confirmed that, similar to mammalian Axin, *pry-1* functions upstream of bar-1 (beta-catenin/armadillo related)/β-catenin and pop-1 (posterior pharynx defect 1)/TCF/LEF and downstream of egl-20 (egg laying defective 20)/WNT and mig-5 (abnormal cell migration 5)/Dvl, thus establishing it as a core component of the canonical WNT signaling pathway in *C. elegans* (reviewed in [121]). Additionally, when introduced in vertebrates, PRY-1 behaves as a functional Axin homolog, as its overexpression in zebrafish rescued the phenotype of Axin-mutation, masterblind, and inhibited WNT signaling in mammalian cells based on a TCF reporter analysis [120]. Consistent with its involvement in many processes, *pry-1* is broadly expressed during development, starting from embryogenesis [120]. At the early L1 stage, *pry-1* is mainly localized to the Q neuroblast cells (QL and QR), seam cells (V5 and V6), ventral hypodermal (P) cells (P7/8 to P11/12), body-wall muscle cells, and neurons in the head, tail, and ventral nerve cord. In addition, *pry-1* continues to be

expressed in all seam cells and QL/R cells through the late-L1 stage. At later stages, *pry-1* expression persists in hypodermal cells and several neurons in the ventral cord, head, and tail ganglia [120]. Furthermore, *pry-1* expression is also observed in reproductive tissues, including vulval precursors and their progeny, as well as the male tail. A similar expression pattern of *pry-1* ortholog, *Cbr-pry-1*, was also seen in Caenorhabditis briggsae, a sister species of *C. elegans* [122]. In agreement with these expression data, constitutive activation of WNT signaling (due to the loss of PRY-1 function) causes a wide range of defects in *C. elegans* that are discussed below.

The other *C. elegans* Axin-like protein, AXL-1, also acts as a functional ortholog of Axin to regulate the canonical WNT signaling [21]. The protein shows an overall 14–16% identity to members of the D-Axin and vertebrate Axin1 and Axin2, and 20% identity to PRY-1. Similar to PRY-1, sequence conservation is restricted to the RGS and DIX domains (24% and 35%, respectively), with no obvious domains for GSK-3β and β-catenin binding [21] (Figure 4). Functional studies revealed that AXL-1 physically interacts with GSK-3/GSK-3β, MIG-5, and DSH-2 (dishevelled related 2)/Dvl, but not APR-1 (APC related 1)/APC to form a destruction complex with BAR-1 [21]. This partial destruction complex is predicted to enable BAR-1 phosphorylation by GSK-3 to inhibit WNT signaling. Furthermore, similar to PRY-1, AXL-1 overexpression inhibited WNT-induced TCF reporter in mammalian cells, suggesting its functional interaction with mammalian GSK-3β and β-catenin.

Although both AXL-1 and PRY-1 are components of the WNT signaling pathway, they are not functionally interchangeable and perform partially overlapping roles in downregulating BAR-1 signaling in developmental processes (see below) [21]. In addition, AXL-1 functions independently of PRY-1 in axonal migration and excretory cell development. Recently, Chen et al. [123] reported a novel role for AXL-1 in aging. The authors showed that following metformin treatment, AXL-1 localizes to lysosomes and regulates the PAR-4 (abnormal embryonic partitioning of cytoplasm 4)/LKB1-dependent lysosome pathway and subsequently activates AAK-2 (AMP activated kinase 2)/AMPK to extend the lifespan of *C. elegans* [123].

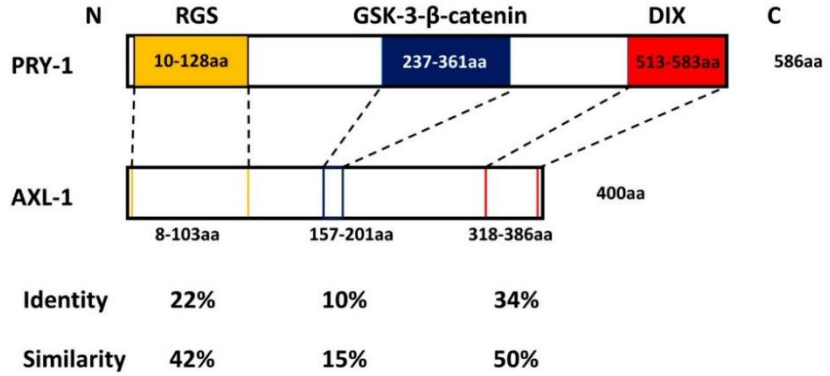

Figure 4. Protein sequence alignment of PRY-1 and AXL-1 in *C. elegans*. The three major domains (RGS, GSK-3-β-catenin, and DIX) in PRY-1 are indicated by colored boxes. The corresponding regions in AXL-1 and their amino acid sequence identity and similarity are also shown. Sequence alignment was done using CLUSTAL W and T-COFFEE (http://www.clustal.org/clustal2/, http://tcoffee.crg.cat) [124,125].

Below, we describe the major developmental events and tissues that depend on PRY-1 and AXL-1 function and their interactions with other cellular factors.

5.1. Neuronal Development

As mentioned earlier, Axin's role in mice was initially discovered based on characterization of fused locus [1]. In the absence of Axin function, mice exhibited neurological defects. Additionally,

the animals showed a neuroectodermal phenotype, which included either incomplete closure or malformation of the head. Since then, Axin family members in other organisms have been found to be essential for neuronal development. In *C. elegans*, *pry-1* mutants exhibit defects in some of their neurons (reviewed in [121]). These include the Q neuroblast system, which consists of a pair of cells, i.e., the QL cell (left lateral side) and QR cell (right lateral side), in the animal (Figure 5A). Interestingly, while the lineages of QL and QR cells are identical, both cells and their descendants migrate in opposite directions, i.e., anterior in the case of QR and posterior in the case of QL (Figure 5A). The progeny of these two neuroblasts give rise to different types of neurons during larval development.

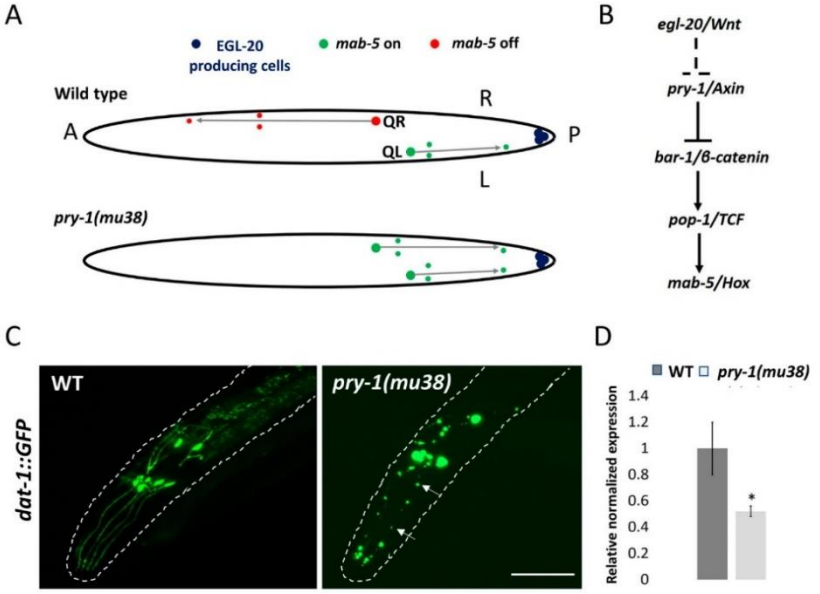

Figure 5. PRY-1 regulates neuronal development in *C. elegans*. (**A**) EGL-20/WNT signaling activates the Hox gene *mab-5* in QL to induce posterior migration of QL descendants. *mab-5* is not activated in QR, and as a consequence, the QR descendants migrate in the default anterior direction. In *pry-1(mu38)* mutant animals, *mab-5* is ectopically expressed in QR leading to the migration of QR descendants towards posterior region. (**B**) PRY-1 acts in the canonical WNT signaling to regulate the expression of *mab-5/ Hox* target gene. The dotted line indicates indirect interaction. (**C**) *pry-1* mutants exhibit defects in dopaminergic neurons (marked with *dat-1p::GFP*). The cell bodies are frequently missing or appear abnormal and dendrites show punctate-like patterns (arrows) (scale bar represents 0.05 μm). (**D**) qPCR experiment shows that *manf-1* is significantly downregulated in *pry-1* mutant adults (* $p < 0.05$, two batches).

Molecular genetic studies have shown that *pry-1*-mediated WNT signaling is essential for the migration of Q-lineage cells and guiding them along specific trajectories [126]. PRY-1 activity is specifically needed in the QR cell to restrict *mab-5 (male abnormal 5)/Hox (homeobox)* expression and to enable anterior migration of their descendants. Loss of PRY-1 function mimics constitutively active WNT pathways with high MAB-5 expression in the QR cell and their progeny, resulting in their migration in an opposite (posterior) direction [120] (Figure 5A,B). Genetic studies have identified other components of the WNT pathway including the ligand, EGL-20, as well as BAR-1 [126] (Figure 5B).

Other neuronal processes in which roles for *pry-1* have been demonstrated include axon guidance and synapse formation. Axonal function was uncovered in a genetic screen using an RNAi (RNA interference)-hypersensitive strain [127]. It was found that *pry-1* RNAi caused defects in ventral

cord neurons, such as branched commissures and abnormal midline crossing. In a separate study, Schneider et al. [128] reported that *pry-1* acts in a canonical WNT-β-catenin pathway to promote synapse formation of a specific motor neuron, based on results showing that *pry-1* mutants enhanced movement defects in animals lacking *unc-4 (uncoordinated 4)/Hox* function.

In addition to its essential function in the development of neurons, *pry-1* may also participate in neuroprotection in adults. This possibility is supported by our findings that *pry-1* mutants show accelerated degeneration of dopaminergic neurons (S. Taylor, unpublished) (Figure 5C). Whether such a role of *pry-1* involves other components of the WNT signaling pathway remains to be investigated. In this regard, it is worth mentioning that WNT signaling has been linked to neurodegenerative diseases, such as Alzheimer's and Parkinson's (reviewed in [129,130]). One of the ways whereby *pry-1*-mediated WNT signaling may protect neurons in *C. elegans* is by regulating the expression of genes that confer neuroprotection. This hypothesis is based on our preliminary observation that the transcription of *manf-1*, a homolog of mammalian MANF (Mesencephalic astrocyte-derived neurotrophic factor) [131], was significantly downregulated in *pry-1* mutant worms (S. Taylor, unpublished) (Figure 5D). In the future, it will be interesting to investigate *pry-1*'s role in *manf-1* regulation and its link to neuroprotection.

5.2. Embryogenesis

Embryogenesis in *C. elegans* is another process that depends on the *pry-1*-mediated, non-canonical WNT signaling pathway. This divergent pathway, known as the WNT-β-catenin-asymmetry pathway, has been shown to control the division of several different types of somatic cell, such as EMS blastomeres in the embryo and larval seam cells (reviewed in [121]). During early embryonic development, the zygote divides into a large anterior blastomere (AB) and a small posterior blastomere (P1) (Figure 6A). P1 then divides to give rise to EMS and P2 blastomeres. The division of EMS has been studied in some detail, which is regulated by the WNT-asymmetry pathway. Upon receiving the WNT ligand, MOM-2, from the adjacent P2 blastomere, the EMS divides to give rise to MS (producing mesoderm) and E (producing endoderm) blastomeres with different cell fates [132,133] (Figure 6A). While cells of the MS lineage contribute to mesodermal tissues (i.e., pharynx and muscles), cells of the E lineage generate endodermal tissues (i.e., intestine).

In the event of asymmetric division, WNT pathway components are asymmetrically localized with MOM-5 (more of MS 5)/Frizzled (Fz), DSH-2, and MIG-5 in the posterior cortex [134,135], and with WRM-1, APR-1, PRY-1, and LIT-1 in the anterior cortex [136,137]. Subsequently, during telophase, WRM-1, SYS-1 (symmetrical sister cell hermaphrodite gonad defect 1)/β-catenin, and LIT-1 preferentially localize to the posterior nucleus [136–140], whereas POP-1 is found mostly in the anterior nucleus (POP-1 asymmetry) [141,142] (Figure 6A). Consistent with its localization in the anterior cortex, PRY-1 antagonizes WRM-1 function, leading to low WRM-1 activity in anterior nucleus that helps establish POP-1 asymmetry [136].

5.3. Seam Cell Development

Similar to the EMS, the PRY-1-mediated WNT-asymmetry pathway is also essential for seam cell development (reviewed in [121]) (Figure 6B). Seam cells are lateral hypodermal cells that give rise to specialized adult cuticular structures, namely the alae (Reviewed in [143]). During early development, a newly hatched L1 stage worm possesses 10 seam cells on either side of the body along the anterior posterior axis [144]. These cells undergo stage-specific divisions (mostly asymmetric) to produce anterior daughters with hypodermal fates and posterior daughters with seam cell fates, and ultimately differentiate to form alae by the end of the L4 stage. The components of WNT-asymmetry pathway in this developmental system are the same as those involved in EMS divisions (Figure 6A, B). Thus, prior to their division, APR-1 and PRY-1 localize to the anterior cortex of a seam cell, whereas MOM-5, DSH-2, and MIG-5 are found in the posterior cortex [134,145–147]. The fates of daughter cells depend on the nuclear levels of SYS-1 and POP-1, such that the anterior nucleus possesses high POP-1 and low SYS-1, and the posterior nucleus possesses low POP-1 and high SYS-1 (Figure 6B).

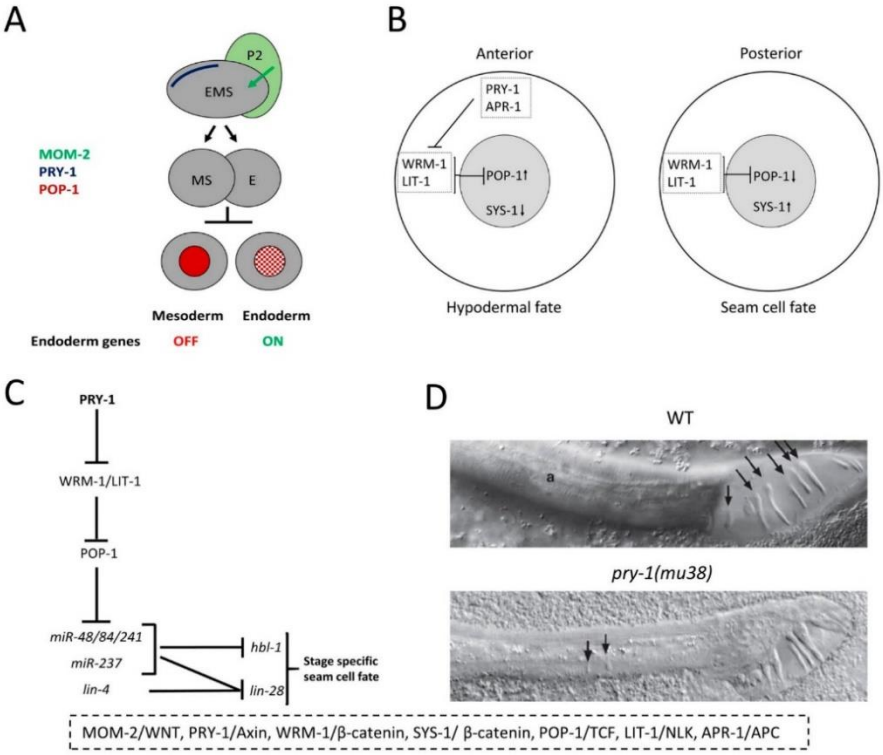

Figure 6. PRY-1 negatively regulates asymmetric cell division during *C. elegans* development. (**A**) Model for EMS division. PRY-1, located in the anterior cortex of EMS during asymmetric division, is involved in conferring endodermal and mesodermal fates of daughter cells. (**B**) Similar to EMS division, a model for seam cell division. PRY-1 negatively regulates WNT signaling in the anterior cell, which ultimately adopts a hypodermal fate. (**C**) A genetic pathway consisting of PRY-1-mediated regulation of heterochronic miRNAs and their targets during seam cell development. (**D**) *pry-1(mu38)* males show defective tail morphology. In wild-type (WT) animals, rays are located in the fan-like region (marked by arrows in the upper panel). In *pry-1* mutants, alae have been replaced with ectopic rays (arrows in the lower panel). The vertebrate homologs of *C. elegans* genes are listed on the bottom. Panels B and C adopted with permission from [66] and panel D from [148].

In support of its role in the asymmetric division of seam cells, *pry-1* mutation disrupts the nuclear localization of WRM-1, SYS-1, and POP-1 [66,134,149], thereby leading to increased seam cell proliferation [65,66]. Work from our lab has shown that in the absence of PRY-1 function, POP-1 localization is disrupted in seam cell daughters [66]. As expected, RNAi knockdown of *wrm-1* and *lit-1* suppressed the seam cell phenotype in *pry-1* mutants whereas *pop-1* RNAi exacerbated the defect.

The temporal division pattern of seam cells relies on several heterochronic miRNAs and their target genes (reviewed in [150,151]. We analyzed the miRNA transcriptome in *pry-1* mutants, which revealed five DE (differentially expressed) miRNAs of *lin-4 (lineage defective 4)* and *let-7 (lethal 7)* families. Further experiments revealed that all DE miRNAs were repressed by PRY-1 in a POP-1-dependent manner [66] (Figure 6C).

In addition, *pry-1* plays a role in V-lineage development in males, where it restricts expression of the Hox gene *mab-5* to posterior V-cell descendants, which ensures correct specification of cell fates and leads to the formation of sensory rays, alae, and the postdeirid [148]. Thus, in males, only the

V5 and V6 cell lineages (expressing *mab-5*) generate rays whereas the V1–V4 lineages (with no *mab-5* expression) give rise to alae [152,153]. Males with no *pry-1* function show defective alae and ectopic rays as the V cells can now differentiate to make more rays due to the inappropriate expression of *mab-5* [148] (Figure 6D). Moreover, altered *mab-5* expression in *pry-1* mutants inhibits the formation of the postdeirid, a sensory structure resulting from the differentiation of V5.pa descendants [148].

5.4. Vulva Development

Although *pry-1* was identified initially based on its role in the Q neuroblast-cell lineage, *pry-1*-mutant animals were subsequently reported to exhibit defects in vulva formation (Figure 7A). *C. elegans* vulva has been studied extensively to understand how signal transduction pathways control cell fates and organogenesis (reviewed in [154]). As a reproductive organ, the vulva serves as a system for mating with males and egg laying. The organ develops from three of the six equipotential groups of P-lineage cells (Pn.p, n = 3–6), termed vulval precursor cells (VPCs), which are induced to adopt primary (1^0 - P6.p) and secondary (2^0 - P5.p and P7.p) cell fates. Mutations in *pry-1* cause more than three VPCs to get induced and lead to the formation of ectopic pseudo-vulvae-like structures in adults, which is referred to as the multivulva (Muv) phenotype [155] (Figure 7A,B). Genetic experiments revealed that the gene acts in the canonical WNT-β-catenin pathway to repress inappropriate induction of vulval precursors. Because of its role as a negative regulator, reduction or elimination of *pry-1* function leads to the constitutive activation of WNT signaling and the dysregulation of downstream targets. One such target is the homeobox family member, *lin-39 (lineage defective 39)*, which is necessary for *pry-1*-mediated vulval development [155].

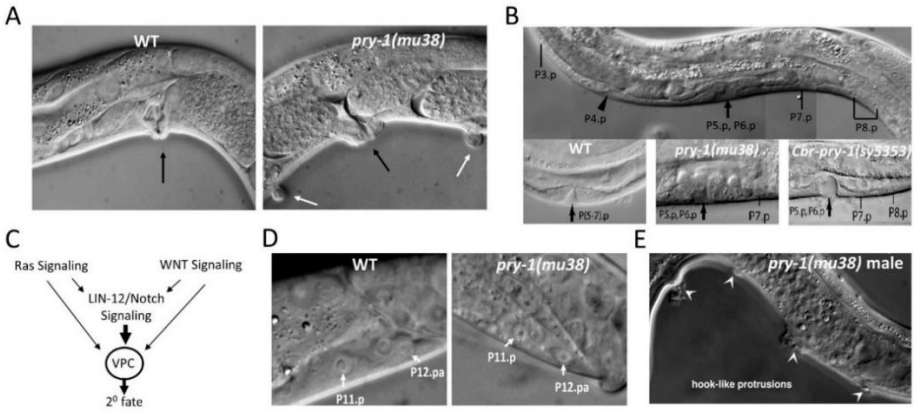

Figure 7. *pry-1* is necessary for the development of P lineage cells. (**A**) Multiple vulva-like protrusions seen in a *pry-1(mu38)* animal (white arrows). Black arrows mark the main vulva. WT, wild-type (**B**) VPC fates are defective in *pry-1(mu38)* animals. Unlike the wild-type, where the progeny of P(5-7).p give rise to the vulva, P7.p in *pry-1(mu38)* and P7.p and P8.p in *Cbr-pry-1(sy5353)* animals remain unfused (panel adapted with permission from [122]). (**C**) A proposed model of interactions between WNT, Ras, and Notch pathways to specify the 2^0 fate of induced VPCs. (**D**) *pry-1(mu38)* mutants show an extra P12.pa-like cell in the place of P11.p. The wild-type P11.p has a large nucleus and a nucleolus compared to P12.pa, which is noticeably smaller. In the case of *bar-1(ga80)* mutants, an opposite phenotype is seen, i.e., two P11.p-like cells [156]. (**E**) Ectopic hook-like structures in *pry-1* mutant males are marked by arrowheads (panel adapted with permission from [157]).

Axin family members have also been genetically characterized in other nematodes. Our laboratory identified mutations in the *C. briggsae pry-1* ortholog (*Cbr-pry-1*) and showed that *Cbr-pry-1* functions in vulva development in a *Cbr-bar-1/β-catenin-*, *Cbr-pop-1/tcf/lef-*, and *Cbr-lin-39/hox*-dependent manner [122]

(Figure 7B). Research in a more distant nematode, *Pristionchus pacificus* (Diplogastridae family), uncovered an Axin family member that is most closely related to *C. elegans axl-1* [158]. Mutations in *Ppa-axl-1* caused a Muv phenotype suggesting that the gene plays an important role in vulva development. Further experiments revealed that *Ppa-axl-1* genetically interacts with WNT-β–catenin pathway components.

Experiments aimed at understanding the mechanism of *pry-1* function have discovered crosstalk between different signaling pathways. Gleason et al. [155] found that *pry-1* mutants bypass the requirements of EGFR–Ras signaling components, which led them to propose that the WNT-β-catenin and EGFR–Ras pathways can act in parallel to promote vulva formation (Figure 7C). Subsequently, our group showed that PRY-1-mediated WNT signaling interacts with the LIN-12/Notch cascade to confer a 2^0 fate on induced VPCs, since the loss of *pry-1* leads to inappropriate activation of the *lin-12* target gene *lip-1 (lateral-signal-induced phosphatase 1)/MAPK phosphatase* [122]. How the three pathways interact to regulate downstream targets (see a model in Figure 7C), leading to correct specification of VPC fates, is currently not understood.

5.5. P11/12 Development

P11 and P12 cells also depend on *pry-1*-mediated signaling for proper differentiation of their progeny. These two cell lineages contribute to the formation of the ventral nervous system [144]. Whereas their anterior daughters, i.e., P11.a and P12.a, are neuroblasts that divide to form several neurons, the posterior daughters, i.e., P11.p and P12.p, take on different fates. The P11.p fuses with the hyp7 syncytium. The P12.p divides to generate two daughters, one of which, P12.pp (posterior daughter), undergoes programmed cell death and the other, P12.pa (anterior daughter), acquires a unique hypodermal cell fate, hyp12. In *pry-1*-mutant animals, P11.p appears to adopt a P12.pa-like fate, based on the presence of two cells having the characteristics of P12.pa [157] (Figure 7D). Mutations in *bar-1* exhibit an opposite phenotype, i.e., two P11.p-like cells [156]. Since these phenotypes may arise due to cell-fate changes at the level of P11 and P12, it is likely that PRY-1–BAR-1-mediated WNT signaling plays a role in conferring the correct fates of these two P cells.

5.6. Male Hook Development

The role of *pry-1* in the development of the male hook has also been investigated. The hook sensillum is a copulatory structure that helps in locating the hermaphrodite vulva during mating [157]. Cell-morphology and -lineage studies have shown that the hook is formed by the progeny of P10.p and P11.p precursors [157]. These two cells are induced to adopt 1^0 (P11.p) and 2^0 (P10.p) fates through the actions of the WNT, EGFR-Ras, and LIN-12 pathways. The P10.p and P11.p progeny differentiate to form a functional hook that includes sensory neurons, structural cell, and support cells. It was found that *pry-1* mutants have ectopic hook-like structures due to inappropriate induction of some of the anterior Pn.p (n = 3–8) cells that normally fuse with the surrounding hypodermal syncytium [157] (Figure 7E). This phenotype was suppressed by mutations in *bar-1* and a downstream target (*mab-5*). Additional genetic experiments led the authors [157] to propose a model in which a graded WNT signal from the tail region causes maximal activation of the pathway in P11.p, leading to inhibition of PRY-1 function and specification of the 1^0 fate. The neighboring P10.p cell receives a comparatively lower signal and thereby adopts a 2^0 fate.

5.7. Lipid Metabolism

The processes described above were related to the development of cells and tissues. Recently, our group uncovered a novel role of PRY-1 that involves the regulation of lipid metabolism [86]. In *C. elegans* and other eukaryotes, fatty acids (such as triacylglycerols, phospholipids, and sphingolipids) serve as building blocks for lipids. Fatty acids are synthesized from thioesters or isoprene units via condensation reactions (Reviewed in [159]). We analyzed the mRNA transcriptome in *pry-1* mutant animals and determined that DE genes are highly linked to biological processes such as lipid

metabolism, cellular responses to lipids, and aging [86]. Functional studies involving a subset of DE genes revealed that *vits* (*vitellogenins*, yolk lipoproteins) and *fats (fatty acid desaturases)* participate in *pry-1*-mediated lipid metabolism. Consistent with these findings, *pry-1* mutants exhibited defects in lipid content (Figure 8A), egg laying, and survival following starvation [86]. Genetic experiments showed that *vits* act downstream of *pry-1*, and RNAi knockdowns of *vit* genes rescued lipid defects in *pry-1* mutants.

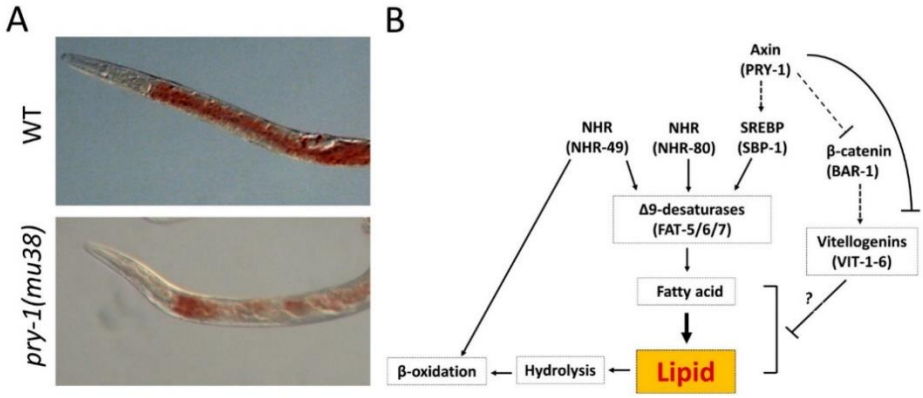

Figure 8. *pry-1* is necessary to regulate lipid metabolism. (**A**) *pry-1* mutant animals show reduced lipid content compared to wild-type (WT) animals as revealed by Oil Red O staining. (**B**) A model for *pry-1* genetic network in regulating lipid synthesis based on findings presented in [86]. *pry-1* acts upstream of *sbp-1* and in parallel to *nhr-49* and *nhr-80*. *pry-1* also regulates the expression of *vit* genes. Whether *bar-1* participates in this process (dotted connecting lines) and how *vits* affect lipid synthesis (question mark) are currently not understood.

In *C. elegans*, MUFAs and PUFAs (monounsaturated and polyunsaturated fatty acids, respectively) can be derived from saturated fatty acid precursors by the actions of fat desaturases (FAT-5, FAT-6, and FAT-7) [159,160]. The expression of desaturases is regulated by transcription factors SBP-1 (sterol regulatory element-binding protein 1, SREBP-1 family) and two HNF4 (hepatocyte nuclear factor 4) families of nuclear receptors NHR-49 (nuclear hormone receptor 49) and NHR-80 (nuclear hormone receptor 80) (Reviewed in [159]). More recently, SBP-1-mediated regulation of MUFA synthesis was shown to extend lifespan when exposed to anti-aging drug combinations [161]. We found that *pry-1* mutants had reduced transcription of fat desaturases and *sbp-1*. However, transcription of the *nhr-49* and *nhr-80* genes was unaltered. Thus, a working model is that *pry-1* acts via *sbp-1* to regulate the expression of *fat* genes that, in turn, regulate lipid synthesis [86]. This model (Figure 8B) is supported by the findings that fatty acid levels were reduced in *pry-1* mutants and supplementing the diet with oleic acid, a MUFA, rescued lipid defects in mutant animals [86].

The requirements of lipids in many biological processes and across multicellular eukaryotes is well documented. These macronutrients are vital for proper growth and reproduction; however, their excessive intake contributes to a variety of diseases in humans. Changes in lipid metabolism could affect a host of processes including signaling, cell structure, and aging [162]. Outside of the *C. elegans* system, Axin family members are reported to function in lipid biology. Axin expression in mice contributes to an age-related increase in adiposity in thymic stromal cells [59]. A recent study showed that Axin knockdown in mouse liver impaired AMPK activation and abrogated AMPK-LKB1 colocalization upon starvation [58]. Therefore, understanding the role of PRY-1 and its homologs in maintaining energy homeostasis is of considerable interest in biomedical research.

6. Major Findings from *C. elegans* Studies

As described in the previous section, PRY-1 and AXL-1 show significant sequence divergence in GSK-3β and β-catenin binding domains. In spite of this, both of these proteins physically interact with BAR-1 and regulate WNT-β-catenin signaling. The functional conservation may be brought about by conserved structures of RGS and DIX domains, thereby making them bona fide Axin family members.

Similar to other eukaryotes, *C. elegans* Axins participate in developmental processes such as cell proliferation, cell differentiation and cell migration. The examples include the formation of the vulva and male hook, P11/12 fate specification, and neuronal development. All of these involve interactions with WNT-β-catenin pathway components, suggesting that this might be the most ancestral mechanism of Axin function. Among other roles of PRY-1, its involvement in lipid metabolism is a recent discovery that may potentially fit into a broader role of Axin as an energy sensor and regulator in eukaryotes.

In addition to their conserved roles, studies in *C. elegans* have also uncovered a unique Axin-mediated WNT signaling during embryogenesis and seam cell development. Typically, interactions between β-catenin and TCF lead to transcriptional regulation of the target genes. However, this divergent WNT signaling has evolved to utilize WRM-1/β-catenin to regulate nuclear localization of POP-1/TCF, leading to the specification of asymmetric cell fates. Thus, research in the *C. elegans* model has shed a new light on the novel mechanism of Axin function in eukaryotes.

7. Concluding Remarks

Axin is a well-characterized scaffold protein that is conserved in eukaryotes. While vertebrate genomes carry two Axin genes, a single ancestral family member is found in invertebrates. Axin's function has been studied mainly in the context of WNT-β-catenin signaling; however, the protein also interacts with multiple factors belonging to WNT-independent signal transduction pathways. Over the years, studies have shown that Axin homologs are necessary for the development of various tissues and cell types. In *C. elegans*, Axin's role has been investigated during embryogenesis and larval development. Given the extensive conservation of genes and signaling mechanisms in *C. elegans*, future studies on PRY-1 and AXL-1 hold the potential to further advance our understanding of shared mechanisms of Axin function in animal development. By harnessing the power of *C. elegans* genetics, new and novel interacting partners of Axin could be identified. Additionally, the discovery of Axin-target genes could help unravel pathways and process-specific functions associated with this family of proteins.

Author Contributions: Contributions of authors is as follows: conceptualization, B.P.G.; experiments on Axin's role in dopaminergic neurons, S.K.B.T., figures, A.M. and S.K.B.T., data curation, B.P.G., A.M.; writing—original draft preparation, A.M., A.R., S.K.B.T.; writing—review and editing, A.M. and B.P.G.; funding acquisition, B.P.G.

Funding: This work was funded by a Discovery grant from the Natural Sciences and Engineering Research Council (http://www.nserc-crsng.gc.ca) to Bhagwati P Gupta.

Conflicts of Interest: The authors declare no conflict of interest.

References

1. Zeng, L.; Fagotto, F.; Zhang, T.; Hsu, W.; Vasicek, T.J.; Perry, W.L., 3rd; Lee, J.J.; Tilghman, S.M.; Gumbiner, B.M.; Costantini, F. The mouse Fused locus encodes Axin, an inhibitor of the Wnt signaling pathway that regulates embryonic axis formation. *Cell* **1997**, *90*, 181–192. [CrossRef]
2. Gluecksohn-Schoenheimer, S. The effects of a lethal mutation responsible for duplications and twinning in mouse embryos. *J. Exp. Zool.* **1949**, *110*, 47–76. [CrossRef]
3. Jacobs-Cohen, R.J.; Spiegelman, M.; Cookingham, J.C.; Bennett, D. Knobbly, a new dominant mutation in the mouse that affects embryonic ectoderm organization. *Genet. Res.* **1984**, *43*, 43–50. [CrossRef]
4. Perry, W.L., 3rd; Vasicek, T.J.; Lee, J.J.; Rossi, J.M.; Zeng, L.; Zhang, T.; Tilghman, S.M.; Costantini, F. Phenotypic and molecular analysis of a transgenic insertional allele of the mouse Fused locus. *Genetics* **1995**, *141*, 321–332.

5. Ikeda, S.; Kishida, S.; Yamamoto, H.; Murai, H.; Koyama, S.; Kikuchi, A. Axin, a negative regulator of the Wnt signaling pathway, forms a complex with GSK-3beta and beta-catenin and promotes GSK-3beta-dependent phosphorylation of beta-catenin. *EMBO J.* **1998**, *17*, 1371–1384. [CrossRef]
6. Yamamoto, H.; Kishida, S.; Uochi, T.; Ikeda, S.; Koyama, S.; Asashima, M.; Kikuchi, A. Axil, a member of the Axin family, interacts with both glycogen synthase kinase 3beta and beta-catenin and inhibits axis formation of Xenopus embryos. *Mol. Cell. Biol.* **1998**, *18*, 2867–2875. [CrossRef]
7. Mao, J.; Wang, J.; Liu, B.; Pan, W.; Farr, G.H., 3rd; Flynn, C.; Yuan, H.; Takada, S.; Kimelman, D.; Li, L.; et al. Low-density lipoprotein receptor-related protein-5 binds to Axin and regulates the canonical Wnt signaling pathway. *Mol. Cell* **2001**, *7*, 801–809. [CrossRef]
8. Wehrli, M.; Dougan, S.T.; Caldwell, K.; O'Keefe, L.; Schwartz, S.; Vaizel-Ohayon, D.; Schejter, E.; Tomlinson, A.; Dinardo, S. *arrow* encodes an LDL-receptor-related protein essential for Wingless signalling. *Nature* **2000**, *407*, 527–530. [CrossRef]
9. Tolwinski, N.S.; Wehrli, M.; Rives, A.; Erdeniz, N.; Dinardo, S.; Wieschaus, E. Wg/Wnt signal can be transmitted through arrow/LRP5,6 and Axin independently of Zw3/Gsk3beta activity. *Dev. Cell* **2003**, *4*, 407–418. [CrossRef]
10. Yamamoto, H.; Kishida, S.; Kishida, M.; Ikeda, S.; Takada, S.; Kikuchi, A. Phosphorylation of Axin, a Wnt Signal Negative Regulator, by Glycogen Synthase Kinase-3β Regulates Its Stability. *J. Boil. Chem.* **1999**, *274*, 10681–10684. [CrossRef]
11. Kishida, S.; Yamamoto, H.; Ikeda, S.; Kishida, M.; Sakamoto, I.; Koyama, S.; Kikuchi, A. Axin, a negative regulator of the wnt signaling pathway, directly interacts with adenomatous polyposis coli and regulates the stabilization of beta-catenin. *J. Boil. Chem.* **1998**, *273*, 10823–10826. [CrossRef]
12. Hart, M.J.; Santos, R.D.L.; Albert, I.N.; Rubinfeld, B.; Polakis, P. Downregulation of beta-catenin by human Axin and its association with the APC tumor suppressor, beta-catenin and GSK3 beta. *Curr. Boil.* **1998**, *8*, 573–581. [CrossRef]
13. Nakamura, T.; Hamada, F.; Ishidate, T.; Anai, K.-I.; Kawahara, K.; Toyoshima, K.; Akiyama, T. Axin, an inhibitor of the Wnt signalling pathway, interacts with beta-catenin, GSK-3beta and APC and reduces the beta-catenin level. *Genes Cells* **1998**, *3*, 395–403. [CrossRef]
14. Hsu, W.; Zeng, L.; Costantini, F. Identification of a Domain of Axin That Binds to the Serine/Threonine Protein Phosphatase 2A and a Self-binding Domain. *J. Boil. Chem.* **1999**, *274*, 3439–3445. [CrossRef]
15. Schwarz-Romond, T.; Asbrand, C.; Bakkers, J.; Kuhl, M.; Schaeffer, H.-J.; Huelsken, J.; Behrens, J.; Hammerschmidt, M.; Birchmeier, W. The ankyrin repeat protein Diversin recruits Casein kinase Iε to the β-catenin degradation complex and acts in both canonical Wnt and Wnt/JNK signaling. *Genome Res.* **2002**, *16*, 2073–2084.
16. Shiomi, K.; Uchida, H.; Keino-Masu, K.; Masu, M. Ccd1, a novel protein with a DIX domain, is a positive regulator in the Wnt signaling during zebrafish neural patterning. *Curr. Boil.* **2003**, *13*, 73–77. [CrossRef]
17. Li, L.; Yuan, H.; Weaver, C.D.; Mao, J.; Farr, G.H., 3rd; Sussman, D.J.; Jonkers, J.; Kimelman, D.; Wu, D. Axin and Frat1 interact with dvl and GSK, bridging Dvl to GSK in Wnt-mediated regulation of LEF-1. *EMBO J.* **1999**, *18*, 4233–4240. [CrossRef]
18. Rubinfeld, B.; Tice, D.A.; Polakis, P. Axin-dependent Phosphorylation of the Adenomatous Polyposis Coli Protein Mediated by Casein Kinase 1epsilon. *J. Boil. Chem.* **2001**, *276*, 39037–39045. [CrossRef]
19. Hedgepeth, C.M.; Deardorff, M.A.; Rankin, K.; Klein, P.S. Regulation of Glycogen Synthase Kinase 3β and Downstream Wnt Signaling by Axin. *Mol. Cell. Boil.* **1999**, *19*, 7147–7157. [CrossRef]
20. Hamada, F.; Tomoyasu, Y.; Takatsu, Y.; Nakamura, M.; Nagai, S.-I.; Suzuki, A.; Fujita, F.; Shibuya, H.; Toyoshima, K.; Ueno, N.; et al. Negative Regulation of Wingless Signaling by D-Axin, a Drosophila Homolog of Axin. *Science* **1999**, *283*, 1739–1742. [CrossRef]
21. Oosterveen, T.; Coudreuse, D.Y.; Yang, P.-T.; Fraser, E.; Bergsma, J.; Dale, T.C.; Korswagen, H.C. Two functionally distinct Axin-like proteins regulate canonical Wnt signaling in *C. elegans*. *Dev. Boil.* **2007**, *308*, 438–448. [CrossRef]
22. Behrens, J.; Jerchow, B.A.; Würtele, M.; Grimm, J.; Asbrand, C.; Wirtz, R.; Kühl, M.; Wedlich, D.; Birchmeier, W. Functional interaction of an axin homolog, conductin, with beta-catenin, APC, and GSK3beta. *Science* **1998**, *280*, 596–599. [CrossRef] [PubMed]

23. Yu, H.-M.I.; Jerchow, B.; Sheu, T.-J.; Liu, B.; Costantini, F.; Puzas, J.E.; Birchmeier, W.; Hsu, W. The role of Axin2 in calvarial morphogenesis and craniosynostosis. *Development* **2005**, *132*, 1995–2005. [CrossRef] [PubMed]
24. Qian, L.; Mahaffey, J.P.; Alcorn, H.L.; Anderson, K.V. Tissue-specific roles of Axin2 in the inhibition and activation of Wnt signaling in the mouse embryo. *Proc. Natl. Acad. Sci. USA* **2011**, *108*, 8692–8697. [CrossRef]
25. Jho, E.-H.; Zhang, T.; Domon, C.; Joo, C.-K.; Freund, J.-N.; Costantini, F. Wnt/β-Catenin/Tcf Signaling Induces the Transcription of Axin2, a Negative Regulator of the Signaling Pathway. *Mol. Cell. Boil.* **2002**, *22*, 1172–1183. [CrossRef]
26. Lustig, B.; Jerchow, B.; Sachs, M.; Weiler, S.; Pietsch, T.; Karsten, U.; Van De Wetering, M.; Clevers, H.; Schlag, P.M.; Birchmeier, W.; et al. Negative Feedback Loop of Wnt Signaling through Upregulation of Conductin/Axin2 in Colorectal and Liver Tumors. *Mol. Cell. Boil.* **2002**, *22*, 1184–1193. [CrossRef]
27. Hinoi, T.; Yamamoto, H.; Kishida, M.; Takada, S.; Kishida, S.; Kikuchi, A. Complex Formation of Adenomatous Polyposis Coli Gene Product and Axin Facilitates Glycogen Synthase Kinase-3β-dependent Phosphorylation of β-Catenin and Down-regulates β-Catenin. *J. Boil. Chem.* **2000**, *275*, 34399–34406. [CrossRef]
28. Kishida, M.; Koyama, S.; Kishida, S.; Matsubara, K.; Nakashima, S.; Higano, K.; Takada, R.; Takada, S.; Kikuchi, A. Axin prevents Wnt-3a-induced accumulation of β-catenin. *Oncogene* **1999**, *18*, 979–985. [CrossRef]
29. Dajani, R.; Fraser, E.; Roe, S.; Yeo, M.; Good, V.M.; Thompson, V.; Dale, T.C.; Pearl, L.H. Structural basis for recruitment of glycogen synthase kinase 3β to the axin–APC scaffold complex. *EMBO J.* **2003**, *22*, 494–501. [CrossRef]
30. Zhang, Y.; Qiu, W.-J.; Chan, S.C.; Han, J.; He, X.; Lin, S.-C. Casein Kinase I and Casein Kinase II Differentially Regulate Axin Function in Wnt and JNK Pathways. *J. Boil. Chem.* **2002**, *277*, 17706–17712. [CrossRef]
31. Liu, C.; Li, Y.; Semënov, M.; Han, C.; Baeg, G.-H.; Tan, Y.; Zhang, Z.; Lin, X.; He, X. Control of β-Catenin Phosphorylation/Degradation by a Dual-Kinase Mechanism. *Cell* **2002**, *108*, 837–847. [CrossRef]
32. Li, V.S.; Ng, S.S.; Boersema, P.J.; Low, T.Y.; Karthaus, W.R.; Gerlach, J.P.; Mohammed, S.; Heck, A.J.; Maurice, M.M.; Mahmoudi, T.; et al. Wnt Signaling through Inhibition of β-Catenin Degradation in an Intact Axin1 Complex. *Cell* **2012**, *149*, 1245–1256. [CrossRef] [PubMed]
33. Luo, W.; Zou, H.; Jin, L.; Lin, S.; Li, Q.; Ye, Z.; Rui, H.; Lin, S.C. Axin contains three separable domains that confer intramolecular, homodimeric, and heterodimeric interactions involved in distinct functions. *J. Biol. Chem.* **2005**, *280*, 5054–5060. [CrossRef] [PubMed]
34. Luo, W.; Lin, S.-C. Axin: A Master Scaffold for Multiple Signaling Pathways. *Neurosignals* **2004**, *13*, 99–113. [CrossRef] [PubMed]
35. Figeac, N.; Zammit, P.S. Coordinated action of Axin1 and Axin2 suppresses β-catenin to regulate muscle stem cell function. *Cell Signal.* **2015**, *27*, 1652–1665. [CrossRef] [PubMed]
36. Huraskin, D.; Eiber, N.; Reichel, M.; Zidek, L.M.; Kravic, B.; Bernkopf, D.; Von Maltzahn, J.; Behrens, J.; Hashemolhosseini, S. Wnt/β-catenin signaling via Axin2 is required for myogenesis and, together with YAP/Taz and Tead1, active in IIa/IIx muscle fibers. *Development* **2016**, *143*, 3128–3142. [CrossRef]
37. Carl, M.; Bianco, I.H.; Bajoghli, B.; Aghaallaei, N.; Czerny, T.; Wilson, S.W. Wnt/Axin1/beta-catenin signaling regulates asymmetric nodal activation, elaboration, and concordance of CNS asymmetries. *Neuron* **2007**, *55*, 393–405. [CrossRef]
38. Heisenberg, C.-P.; Houart, C.; Take-Uchi, M.; Rauch, G.-J.; Young, N.; Coutinho, P.; Masai, I.; Caneparo, L.; Concha, M.L.; Geisler, R.; et al. A mutation in the Gsk3–binding domain of zebrafish Masterblind/Axin1 leads to a fate transformation of telencephalon and eyes to diencephalon. *Genome Res.* **2001**, *15*, 1427–1434. [CrossRef]
39. Kofron, M.; Klein, P.; Zhang, F.; Houston, D.W.; Schaible, K.; Wylie, C.; Heasman, J. The Role of Maternal Axin in Patterning the Xenopus Embryo. *Dev. Boil.* **2001**, *237*, 183–201. [CrossRef]
40. Ye, T.; Fu, A.K.Y.; Ip, N.Y. Emerging roles of Axin in cerebral cortical development. *Front. Cell. Neurosci.* **2015**, *9*, 217. [CrossRef]
41. He, C.-W.; Liao, C.-P.; Pan, C.-L. Wnt signalling in the development of axon, dendrites and synapses. *Open Boil.* **2018**, *8*, 180116. [CrossRef] [PubMed]
42. Lyu, J.; Costantini, F.; Jho, E.-H.; Joo, C.-K. Ectopic Expression of Axin Blocks Neuronal Differentiation of Embryonic Carcinoma P19 Cells. *J. Boil. Chem.* **2003**, *278*, 13487–13495. [CrossRef] [PubMed]

43. Orme, M.H.; Giannini, A.L.; Vivanco, M.D.; Kypta, R.M. Glycogen synthase kinase-3 and Axin function in a beta-catenin-independent pathway that regulates neurite outgrowth in neuroblastoma cells. *Mol. Cell. Neurosci.* **2003**, *24*, 673–686. [CrossRef]
44. Endo, Y.; Beauchamp, E.; Woods, D.; Taylor, W.G.; Toretsky, J.A.; Üren, A.; Rubin, J.S. Wnt-3a and Dickkopf-1 Stimulate Neurite Outgrowth in Ewing Tumor Cells via a Frizzled3- and c-Jun N-Terminal Kinase-Dependent Mechanism. *Mol. Cell. Boil.* **2008**, *28*, 2368–2379. [CrossRef] [PubMed]
45. Fang, W.-Q.; Ip, J.P.K.; Li, R.; Ng, Y.P.; Lin, S.-C.; Chen, Y.; Fu, A.K.Y.; Ip, N.Y. Cdk5-Mediated Phosphorylation of Axin Directs Axon Formation during Cerebral Cortex Development. *J. Neurosci.* **2011**, *31*, 13613–13624. [CrossRef] [PubMed]
46. Fang, W.-Q.; Chen, W.-W.; Fu, A.K.; Ip, N.Y. Axin Directs the Amplification and Differentiation of Intermediate Progenitors in the Developing Cerebral Cortex. *Neuron* **2013**, *79*, 665–679. [CrossRef] [PubMed]
47. Chen, Y.; Fu, A.K.; Ip, N.Y. Axin: An emerging key scaffold at the synapse. *IUBMB Life* **2013**, *65*, 685–691. [CrossRef]
48. Chen, Y.; Liang, Z.; Fei, E.; Chen, Y.; Zhou, X.; Fang, W.; Fu, W.-Y.; Fu, A.K.Y.; Ip, N.Y. Axin Regulates Dendritic Spine Morphogenesis through Cdc42-Dependent Signaling. *PLoS ONE* **2015**, *10*, e0133115. [CrossRef]
49. Peifer, M. Wnt Signaling in Oncogenesis and Embryogenesis—A Look Outside the Nucleus. *Science* **2000**, *287*, 1606–1609. [CrossRef]
50. Jin, L.-H.; Shao, Q.-J.; Luo, W.; Ye, Z.-Y.; Li, Q.; Lin, S.-C. Detection of point mutations of the Axin1 gene in colorectal cancers. *Int. J. Cancer* **2003**, *107*, 696–699. [CrossRef]
51. Yang, L.H.; Xu, H.T.; Li, Q.C.; Jiang, G.Y.; Zhang, X.P.; Zhao, H.Y.; Xu, K.; Wang, E.H. Abnormal hypermethylation and clinicopathological significance of Axin gene in lung cancer. *Tumour Biol.* **2013**, *34*, 749–757. [CrossRef] [PubMed]
52. Clevers, H. Axin and hepatocellular carcinomas. *Nat. Genet.* **2000**, *24*, 206–208. [CrossRef] [PubMed]
53. Satoh, S.; Daigo, Y.; Furukawa, Y.; Kato, T.; Miwa, N.; Nishiwaki, T.; Kawasoe, T.; Ishiguro, H.; Fujita, M.; Tokino, T.; et al. AXIN1 mutations in hepatocellular carcinomas, and growth suppression in cancer cells by virus-mediated transfer of AXIN1. *Nat. Genet.* **2000**, *24*, 245–250. [CrossRef] [PubMed]
54. Abitbol, S.; Dahmani, R.; Coulouarn, C.; Ragazzon, B.; Mlecnik, B.; Senni, N.; Savall, M.; Bossard, P.; Sohier, P.; Drouet, V.; et al. AXIN deficiency in human and mouse hepatocytes induces hepatocellular carcinoma in the absence of β-catenin activation. *J. Hepatol.* **2018**, *68*, 1203–1213. [CrossRef] [PubMed]
55. Feng, G.J.; Cotta, W.; Wei, X.Q.; Poetz, O.; Evans, R.; Jardé, T.; Reed, K.; Méniel, V.; Williams, G.T.; Clarke, A.R.; et al. Conditional Disruption of Axin1 Leads to Development of Liver Tumors in Mice. *Gastroenterology* **2012**, *143*, 1650–1659. [CrossRef] [PubMed]
56. Neo, S.Y.; Zhang, Y.; Yaw, L.P.; Li, P.; Lin, S.-C. Axin-Induced Apoptosis Depends on the Extent of Its JNK Activation and Its Ability to Down-Regulate β-Catenin Levels. *Biochem. Biophys. Res. Commun.* **2000**, *272*, 144–150. [CrossRef] [PubMed]
57. Hsu, W.; Shakya, R.; Costantini, F. Impaired mammary gland and lymphoid development caused by inducible expression of Axin in transgenic mice. *J. Cell Boil.* **2001**, *155*, 1055–1064. [CrossRef]
58. Zhang, Y.-L.; Guo, H.; Zhang, C.-S.; Lin, S.-Y.; Yin, Z.; Peng, Y.; Luo, H.; Shi, Y.; Lian, G.; Zhang, C.; et al. AMP as a Low-Energy Charge Signal Autonomously Initiates Assembly of AXIN-AMPK-LKB1 Complex for AMPK Activation. *Cell Metab.* **2013**, *18*, 546–555. [CrossRef]
59. Yang, H.; Youm, Y.-H.; Sun, Y.; Rim, J.-S.; Galbán, C.J.; Vandanmagsar, B.; Dixit, V.D. Axin expression in thymic stromal cells contributes to an age-related increase in thymic adiposity and is associated with reduced thymopoiesis independently of ghrelin signaling. *J. Leukoc. Boil.* **2009**, *85*, 928–938. [CrossRef]
60. Willert, K.; Logan, C.Y.; Arora, A.; Fish, M.; Nusse, R. A Drosophila Axin homolog, Daxin, inhibits Wnt signaling. *Development* **1999**, *126*, 4165–4173.
61. Song, Y.; Chung, S.; Kunes, S. Combgap Relays Wingless Signal Reception to the Determination of Cortical Cell Fate in the Drosophila Visual System. *Mol. Cell* **2000**, *6*, 1143–1154. [CrossRef]
62. Gultekin, Y.; Steller, H. Axin proteolysis by Iduna is required for the regulation of stem cell proliferation and intestinal homeostasis in Drosophila. *Development* **2019**, *146*. [CrossRef] [PubMed]
63. Fu, J.; Posnien, N.; Bolognesi, R.; Fischer, T.D.; Rayl, P.; Oberhofer, G.; Kitzmann, P.; Brown, S.J.; Bucher, G. Asymmetrically expressed axin required for anterior development in Tribolium. *Proc. Natl. Acad. Sci. USA* **2012**, *109*, 7782–7786. [CrossRef] [PubMed]

64. Foulquier, S.; Daskalopoulos, E.P.; Lluri, G.; Hermans, K.C.M.; Deb, A.; Blankesteijn, W.M. WNT Signaling in Cardiac and Vascular Disease. *Pharmacol. Rev.* **2018**, *70*, 68–141. [CrossRef] [PubMed]
65. Gleason, J.E.; Eisenmann, D.M. Wnt signaling controls the stem cell-like asymmetric division of the epithelial seam cells during *C. elegans* larval development. *Dev. Boil.* **2010**, *348*, 58–66. [CrossRef]
66. Mallick, A.; Ranawade, A.; Gupta, B.P. Role of PRY-1/Axin in heterochronic miRNA-mediated seam cell development. *BMC Dev. Boil.* **2019**, *19*, 17. [CrossRef]
67. Zhang, Y.; Neo, S.Y.; Wang, X.; Han, J.; Lin, S.-C. Axin Forms a Complex with MEKK1 and Activates c-Jun NH2-terminal Kinase/Stress-activated Protein Kinase through Domains Distinct from Wnt Signaling. *J. Boil. Chem.* **1999**, *274*, 35247–35254. [CrossRef]
68. Luo, W.; Ng, W.W.; Jin, L.-H.; Ye, Z.; Han, J.; Lin, S.-C. Axin Utilizes Distinct Regions for Competitive MEKK1 and MEKK4 Binding and JNK Activation. *J. Boil. Chem.* **2003**, *278*, 37451–37458. [CrossRef]
69. Rui, Y.; Xu, Z.; Xiong, B.; Cao, Y.; Lin, S.; Zhang, M.; Chan, S.-C.; Luo, W.; Han, Y.; Lu, Z.; et al. A β-Catenin-Independent Dorsalization Pathway Activated by Axin/JNK Signaling and Antagonized by Aida. *Dev. Cell* **2007**, *13*, 268–282. [CrossRef]
70. Luo, K. Signaling Cross Talk between TGF-β/Smad and Other Signaling Pathways. *Cold Spring Harb. Perspect. Boil.* **2017**, *9*, a022137. [CrossRef]
71. Guo, X.; Ramirez, A.; Waddell, D.S.; Li, Z.; Liu, X.; Wang, X.-F. Axin and GSK3-β control Smad3 protein stability and modulate TGF-β signaling. *Genome Res.* **2008**, *22*, 106–120. [CrossRef] [PubMed]
72. Liu, W.; Rui, H.; Wang, J.; Lin, S.; He, Y.; Chen, M.; Li, Q.; Ye, Z.; Zhang, S.; Chan, S.C.; et al. Axin is a scaffold protein in TGF-β signaling that promotes degradation of Smad7 by Arkadia. *EMBO J.* **2006**, *25*, 1646–1658. [CrossRef] [PubMed]
73. Rui, Y.; Xu, Z.; Lin, S.; Li, Q.; Rui, H.; Luo, W.; Zhou, H.-M.; Cheung, P.-Y.; Wu, Z.; Ye, Z.; et al. Axin stimulates p53 functions by activation of HIPK2 kinase through multimeric complex formation. *EMBO J.* **2004**, *23*, 4583–4594. [CrossRef] [PubMed]
74. Li, Q.; Lin, S.; Wang, X.; Lian, G.; Lu, Z.; Guo, H.; Ruan, K.; Wang, Y.; Ye, Z.; Han, J.; et al. Axin determines cell fate by controlling the p53 activation threshold after DNA damage. *Nature* **2009**, *11*, 1128–1134.
75. Jung, Y.-S.; Qian, Y.; Chen, X. Pirh2 RING-finger E3 ubiquitin ligase: Its role in tumorigenesis and cancer therapy. *FEBS Lett.* **2012**, *586*, 1397–1402. [CrossRef]
76. Li, Q.; Wang, X.; Wu, X.; Rui, Y.; Liu, W.; Wang, J.; Wang, X.; Liou, Y.-C.; Ye, Z.; Lin, S.-C. Daxx Cooperates with the Axin/HIPK2/p53 Complex to Induce Cell Death. *Cancer Res.* **2007**, *67*, 66–74. [CrossRef]
77. Yamazaki, H.; Nusse, R. Identification of DCAP, a drosophila homolog of a glucose transport regulatory complex. *Mech. Dev.* **2002**, *119*, 115–119. [CrossRef]
78. Yamazaki, H.; Yanagawa, S.-I. Axin and the Axin/Arrow-binding protein DCAP mediate glucose–glycogen metabolism. *Biochem. Biophys. Res. Commun.* **2003**, *304*, 229–235. [CrossRef]
79. Guo, H.-L.; Zhang, C.; Liu, Q.; Li, Q.; Lian, G.; Wu, D.; Li, X.; Zhang, W.; Shen, Y.; Ye, Z.; et al. The Axin/TNKS complex interacts with KIF3A and is required for insulin-stimulated GLUT4 translocation. *Cell Res.* **2012**, *22*, 1246–1257. [CrossRef]
80. Xie, Y.Y.; Mo, C.L.; Cai, Y.H.; Wang, W.J.; Hong, X.X.; Zhang, K.K.; Liu, Q.F.; Liu, Y.J.; Hong, J.J.; He, T.; et al. Pygo2 Regulates Adiposity and Glucose Homeostasis via beta-Catenin-Axin2-GSK3beta Signaling Pathway. *Diabetes* **2018**, *67*, 2569–2584. [CrossRef]
81. Gho, M.; Schweisguth, F. Frizzled signalling controls orientation of asymmetric sense organ precursor cell divisions in Drosophila. *Nature* **1998**, *393*, 178–181. [CrossRef] [PubMed]
82. Cadigan, K.M.; Nusse, R. Wnt signaling: A common theme in animal development. *Genes Dev.* **1997**, *11*, 3286–3305. [CrossRef] [PubMed]
83. Cowan, C.A.; Henkemeyer, M. The SH2/SH3 adaptor Grb4 transduces B-ephrin reverse signals. *Nature* **2001**, *413*, 174–179. [CrossRef] [PubMed]
84. Clevers, H. Wnt/β-Catenin Signaling in Development and Disease. *Cell* **2006**, *127*, 469–480. [CrossRef]
85. Gorrepati, L.; Krause, M.W.; Chen, W.; Brodigan, T.M.; Correa-Mendez, M.; Eisenmann, D.M. Identification of Wnt Pathway Target Genes Regulating the Division and Differentiation of Larval Seam Cells and Vulval Precursor Cells in *Caenorhabditis elegans*. *G3 Genes Genomes Genet.* **2015**, *5*, 1551–1566. [CrossRef]
86. Ranawade, A.; Mallick, A.; Gupta, B.P. PRY-1/Axin signaling regulates lipid metabolism in *Caenorhabditis elegans*. *PLoS ONE* **2018**, *13*, e0206540. [CrossRef]

87. Choi, S.-H.; Choi, K.-M.; Ahn, H.-J. Coexpression and protein-protein complexing of DIX domains of human Dvl1 and Axin1 protein. *BMB Rep.* **2010**, *43*, 609–613. [CrossRef]
88. Fiedler, M.; Mendoza-Topaz, C.; Rutherford, T.J.; Mieszczanek, J.; Bienz, M. Dishevelled interacts with the DIX domain polymerization interface of Axin to interfere with its function in down-regulating β-catenin. *Proc. Natl. Acad. Sci. USA* **2011**, *108*, 1937–1942. [CrossRef]
89. Sakanaka, C.; Williams, L.T. Functional domains of axin. Importance of the C terminus as an oligomerization domain. *J. Boil. Chem.* **1999**, *274*, 14090–14093. [CrossRef]
90. Yokoyama, N.; Markova, N.G.; Wang, H.-Y.; Malbon, C.C. Assembly of Dishevelled 3-based supermolecular complexes via phosphorylation and Axin. *J. Mol. Signal.* **2012**, *7*, 8. [CrossRef]
91. Schwarz-Romond, T.; Fiedler, M.; Shibata, N.; Butler, P.J.G.; Kikuchi, A.; Higuchi, Y.; Bienz, M. The DIX domain of Dishevelled confers Wnt signaling by dynamic polymerization. *Nat. Struct. Mol. Boil.* **2007**, *14*, 484–492. [CrossRef] [PubMed]
92. Schwarz-Romond, T.; Metcalfe, C.; Bienz, M. Dynamic recruitment of axin by Dishevelled protein assemblies. *J. Cell Sci.* **2007**, *120*, 2402–2412. [CrossRef] [PubMed]
93. Song, X.; Wang, S.; Li, L. New insights into the regulation of Axin function in canonical Wnt signaling pathway. *Protein Cell* **2014**, *5*, 186–193. [CrossRef] [PubMed]
94. Gao, C.; Xiao, G.; Hu, J. Regulation of Wnt/β-catenin signaling by posttranslational modifications. *Cell Biosci.* **2014**, *4*, 13. [CrossRef]
95. Jho, E.-H.; Lomvardas, S.; Costantini, F. A GSK3β Phosphorylation Site in Axin Modulates Interaction with β-Catenin and Tcf-Mediated Gene Expression. *Biochem. Biophys. Res. Commun.* **1999**, *266*, 28–35. [CrossRef]
96. Gao, Z.-H.; Seeling, J.M.; Hill, V.; Yochum, A.; Virshup, D.M. Casein kinase I phosphorylates and destabilizes the β-catenin degradation complex. *Proc. Natl. Acad. Sci. USA* **2002**, *99*, 1182–1187. [CrossRef]
97. Willert, K.; Shibamoto, S.; Nusse, R. Wnt-induced dephosphorylation of Axin releases beta -catenin from the Axin complex. *Genes Dev.* **1999**, *13*, 1768–1773. [CrossRef]
98. Strovel, E.T.; Wu, D.; Sussman, D.J. Protein Phosphatase 2C Dephosphorylates Axin and Activates LEF-1-dependent Transcription. *J. Boil. Chem.* **2000**, *275*, 2399–2403. [CrossRef]
99. Tacchelly-Benites, O.; Wang, Z.; Yang, E.; Benchabane, H.; Tian, A.; Randall, M.P.; Ahmed, Y. Axin phosphorylation in both Wnt-off and Wnt-on states requires the tumor suppressor APC. *PLoS Genet.* **2018**, *14*, e1007178. [CrossRef]
100. Kim, S.-E.; Huang, H.; Zhao, M.; Zhang, X.; Zhang, A.; Semonov, M.V.; Macdonald, B.T.; Zhang, X.; Abreu, J.G.; Peng, L.; et al. Wnt stabilization of β-catenin reveals principles for morphogen receptor-scaffold assemblies. *Science* **2013**, *340*, 867–870. [CrossRef]
101. Huang, S.-M.A.; Mishina, Y.M.; Liu, S.; Cheung, A.; Stegmeier, F.; Michaud, G.A.; Charlat, O.; Wiellette, E.; Zhang, Y.; Wiessner, S.; et al. Tankyrase inhibition stabilizes axin and antagonizes Wnt signalling. *Nature* **2009**, *461*, 614–620. [CrossRef] [PubMed]
102. Zhang, Y.; Liu, S.; Mickanin, C.; Feng, Y.; Charlat, O.; Michaud, G.A.; Schirle, M.; Shi, X.; Hild, M.; Bauer, A.; et al. RNF146 is a poly(ADP-ribose)-directed E3 ligase that regulates axin degradation and Wnt signalling. *Nature* **2011**, *13*, 623–629. [CrossRef] [PubMed]
103. Callow, M.G.; Tran, H.; Phu, L.; Lau, T.; Lee, J.; Sandoval, W.N.; Liu, P.S.; Bheddah, S.; Tao, J.; Lill, J.R.; et al. Ubiquitin Ligase RNF146 Regulates Tankyrase and Axin to Promote Wnt Signaling. *PLoS ONE* **2011**, *6*, e22595. [CrossRef] [PubMed]
104. Wang, Z.; Tacchelly-Benites, O.; Yang, E.; Ahmed, Y. Dual Roles for Membrane Association of Drosophila Axin in Wnt Signaling. *PLoS Genet.* **2016**, *12*, e1006494. [CrossRef] [PubMed]
105. Feng, Y.; Li, X.; Ray, L.; Song, H.; Qu, J.; Lin, S.; Lin, X. The Drosophila tankyrase regulates Wg signaling depending on the concentration of Daxin. *Cell Signal.* **2014**, *26*, 1717–1724. [CrossRef] [PubMed]
106. Ji, L.; Jiang, B.; Jiang, X.; Charlat, O.; Chen, A.; Mickanin, C.; Bauer, A.; Xu, W.; Yan, X.; Cong, F. The SIAH E3 ubiquitin ligases promote Wnt/β-catenin signaling through mediating Wnt-induced Axin degradation. *Genes Dev.* **2017**, *31*, 904–915. [CrossRef]
107. Wang, Z.; Tacchelly-Benites, O.; Noble, G.P.; Johnson, M.K.; Gagne, J.P.; Poirier, G.G.; Ahmed, Y. A Context-Dependent Role for the RNF146 Ubiquitin Ligase in Wingless/Wnt Signaling in Drosophila. *Genetics* **2019**, *211*, 913–923. [CrossRef]

108. Fei, C.; Li, Z.; Li, C.; Chen, Y.; Chen, Z.; He, X.; Mao, L.; Wang, X.; Zeng, R.; Li, L. Smurf1-Mediated Lys29-Linked Nonproteolytic Polyubiquitination of Axin Negatively Regulates Wnt/β-Catenin Signaling. *Mol. Cell. Boil.* **2013**, *33*, 4095–4105. [CrossRef]
109. Kim, S.; Jho, E.-H. The Protein Stability of Axin, a Negative Regulator of Wnt Signaling, Is Regulated by Smad Ubiquitination Regulatory Factor 2 (Smurf2). *J. Boil. Chem.* **2010**, *285*, 36420–36426. [CrossRef]
110. Kadoya, T.; Kishida, S.; Fukui, A.; Hinoi, T.; Michiue, T.; Asashima, M.; Kikuchi, A. Inhibition of Wnt Signaling Pathway by a Novel Axin-binding Protein. *J. Boil. Chem.* **2000**, *275*, 37030–37037. [CrossRef]
111. Kadoya, T.; Yamamoto, H.; Suzuki, T.; Yukita, A.; Fukui, A.; Michiue, T.; Asahara, T.; Tanaka, K.; Asashima, M.; Kikuchi, A. Desumoylation Activity of Axam, a Novel Axin-Binding Protein, Is Involved in Downregulation of β-Catenin. *Mol. Cell. Boil.* **2002**, *22*, 3803–3819. [CrossRef]
112. Rui, H.-L.; Fan, E.; Zhou, H.-M.; Xu, Z.; Zhang, Y.; Lin, S.-C. SUMO-1 Modification of the C-terminal KVEKVD of Axin Is Required for JNK Activation but Has No Effect on Wnt Signaling. *J. Boil. Chem.* **2002**, *277*, 42981–42986. [CrossRef]
113. Kim, M.J.; Chia, I.V.; Costantini, F. SUMOylation target sites at the C terminus protect Axin from ubiquitination and confer protein stability. *FASEB J.* **2008**, *22*, 3785–3794. [CrossRef]
114. Chen, T.; Li, M.; Ding, Y.; Zhang, L.-S.; Xi, Y.; Pan, W.-J.; Tao, D.-L.; Wang, J.-Y.; Li, L. Identification of Zinc-finger BED Domain-containing 3 (Zbed3) as a Novel Axin-interacting Protein That Activates Wnt/β-Catenin Signaling. *J. Boil. Chem.* **2009**, *284*, 6683–6689. [CrossRef]
115. Wang, S.; Yin, J.; Chen, D.; Nie, F.; Song, X.; Fei, C.; Miao, H.; Jing, C.; Ma, W.; Wang, L.; et al. Small-molecule modulation of Wnt signaling via modulating the Axin-LRP5/6 interaction. *Nat. Methods* **2013**, *9*, 579–585. [CrossRef]
116. Silver, S.J.; Hagen, J.W.; Okamura, K.; Perrimon, N.; Lai, E.C. Functional screening identifies miR-315 as a potent activator of Wingless signaling. *Proc. Natl. Acad. Sci. USA* **2007**, *104*, 18151–18156. [CrossRef]
117. Egea, V.; Zahler, S.; Rieth, N.; Neth, P.; Popp, T.; Kehe, K.; Jochum, M.; Ries, C. Tissue inhibitor of metalloproteinase-1 (TIMP-1) regulates mesenchymal stem cells through let-7f microRNA and Wnt/β-catenin signaling. *Proc. Natl. Acad. Sci. USA* **2012**, *109*, E309–E316. [CrossRef]
118. Lee, I.; Ajay, S.S.; Yook, J.I.; Kim, H.S.; Hong, S.H.; Kim, N.H.; Dhanasekaran, S.M.; Chinnaiyan, A.M.; Athey, B.D. New class of microRNA targets containing simultaneous 5′-UTR and 3′-UTR interaction sites. *Genome Res.* **2009**, *19*, 1175–1183. [CrossRef]
119. Kim, J.S.; Park, S.Y.; Lee, S.A.; Park, M.G.; Yu, S.K.; Lee, M.H.; Park, M.R.; Kim, S.G.; Oh, J.S.; Lee, S.Y.; et al. MicroRNA-205 suppresses the oral carcinoma oncogenic activity via down-regulation of Axin-2 in KB human oral cancer cell. *Mol. Cell. Biochem.* **2014**, *387*, 71–79. [CrossRef]
120. Korswagen, H.C.; Coudreuse, D.Y.; Betist, M.C.; Van De Water, S.; Zivkovic, D.; Clevers, H.C. The Axin-like protein PRY-1 is a negative regulator of a canonical Wnt pathway in C. elegans. *Genome Res.* **2002**, *16*, 1291–1302. [CrossRef]
121. Sawa, H.; Korswagen, H.C. Wnt signaling in C. elegans. *WormBook* **2013**. [CrossRef]
122. Seetharaman, A.; Cumbo, P.; Bojanala, N.; Gupta, B.P. Conserved mechanism of Wnt signaling function in the specification of vulval precursor fates in C. elegans and C. briggsae. *Dev. Biol.* **2010**, *346*, 128–139. [CrossRef]
123. Chen, J.; Ou, Y.; Li, Y.; Hu, S.; Shao, L.-W.; Liu, Y. Metformin extends C. elegans lifespan through lysosomal pathway. *eLife* **2017**, *6*. [CrossRef]
124. Larkin, M.; Blackshields, G.; Brown, N.; Chenna, R.; Mcgettigan, P.; Mc William, H.; Valentin, F.; Wallace, I.; Wilm, A.; López, R.; et al. Clustal W and Clustal X version 2.0. *Bioinformatics* **2007**, *23*, 2947–2948. [CrossRef]
125. Stothard, P. The Sequence Manipulation Suite: JavaScript Programs for Analyzing and Formatting Protein and DNA Sequences. *Biotechniques* **2000**, *28*, 1102–1104. [CrossRef]
126. Rella, L.; Póvoa, E.E.F.; Korswagen, H.C. The *Caenorhabditis elegans* Q neuroblasts: A powerful system to study cell migration at single-cell resolutionin vivo. *Genesis* **2016**, *54*, 198–211. [CrossRef]
127. Schmitz, C.; Kinge, P.; Hutter, H. Axon guidance genes identified in a large-scale RNAi screen using the RNAi-hypersensitive *Caenorhabditis elegans* strain nre-1(hd20) lin-15b(hd126). *Proc. Natl. Acad. Sci. USA* **2007**, *104*, 834–839. [CrossRef]
128. Schneider, J.; Skelton, R.L.; Von Stetina, S.E.; Middelkoop, T.C.; van Oudenaarden, A.; Korswagen, H.C.; Miller, D.M., 3rd. UNC-4 antagonizes Wnt signaling to regulate synaptic choice in the C. elegans motor circuit. *Development* **2012**, *139*, 2234–2245. [CrossRef]

129. Inestrosa, N.C.; Toledo, E.M. The role of Wnt signaling in neuronal dysfunction in Alzheimer's Disease. *Mol. Neurodegener.* **2008**, *3*, 9. [CrossRef]
130. Berwick, D.C.; Harvey, K. The importance of Wnt signalling for neurodegeneration in Parkinson's disease. *Biochem. Soc. Trans.* **2012**, *40*, 1123–1128. [CrossRef]
131. Richman, C.; Rashid, S.; Prashar, S.; Mishra, R.; Selvaganapathy, P.R.; Gupta, B.P. C. elegans MANF Homolog Is Necessary for the Protection of Dopaminergic Neurons and ER Unfolded Protein Response. *Front. Mol. Neurosci.* **2018**, *12*, 544. [CrossRef]
132. Rocheleau, C.E.; Downs, W.D.; Lin, R.; Wittmann, C.; Bei, Y.; Cha, Y.-H.; Ali, M.; Priess, J.R.; Mello, C.C. Wnt Signaling and an APC-Related Gene Specify Endoderm in Early C. elegans Embryos. *Cell* **1997**, *90*, 707–716. [CrossRef]
133. Thorpe, C.J.; Schlesinger, A.; Carter, J.; Bowerman, B. Wnt Signaling Polarizes an Early C. elegans Blastomere to Distinguish Endoderm from Mesoderm. *Cell* **1997**, *90*, 695–705. [CrossRef]
134. Mizumoto, K.; Sawa, H. Cortical β-Catenin and APC Regulate Asymmetric Nuclear β-Catenin Localization during Asymmetric Cell Division in C. elegans. *Dev. Cell* **2007**, *12*, 287–299. [CrossRef]
135. Walston, T.; Tuskey, C.; Edgar, L.; Hawkins, N.; Ellis, G.; Bowerman, B.; Wood, W.; Hardin, J. Multiple Wnt Signaling Pathways Converge to Orient the Mitotic Spindle in Early C. elegans Embryos. *Dev. Cell* **2004**, *7*, 831–841. [CrossRef]
136. Nakamura, K.; Kim, S.; Ishidate, T.; Bei, Y.; Pang, K.; Shirayama, M.; Trzepacz, C.; Brownell, D.R.; Mello, C.C. Wnt signaling drives WRM-1/beta-catenin asymmetries in early C. elegans embryos. *Genes Dev.* **2005**, *19*, 1749–1754. [CrossRef]
137. Takeshita, H.; Sawa, H. Asymmetric cortical and nuclear localizations of WRM-1/beta-catenin during asymmetric cell division in C. elegans. *Genes Dev.* **2005**, *19*, 1743–1748. [CrossRef]
138. Huang, S.; Shetty, P.; Robertson, S.M.; Lin, R. Binary cell fate specification during C. elegans embryogenesis driven by reiterated reciprocal asymmetry of TCF POP-1 and its coactivator {beta}-catenin SYS-1. *Development* **2007**, *134*, 2685–2695. [CrossRef]
139. Lo, M.-C.; Gay, F.; Odom, R.; Shi, Y.; Lin, R. Phosphorylation by the beta-catenin/MAPK complex promotes 14-3-3-mediated nuclear export of TCF/POP-1 in signal-responsive cells in C. elegans. *Cell* **2004**, *117*, 95–106. [CrossRef]
140. Phillips, B.T.; Kidd, A.R., 3rd; King, R.; Hardin, J.; Kimble, J. Reciprocal asymmetry of SYS-1/beta-catenin and POP-1/TCF controls asymmetric divisions in *Caenorhabditis elegans*. *Proc. Natl. Acad. Sci. USA* **2007**, *104*, 3231–3236. [CrossRef]
141. Lin, R.; Hill, R.J.; Priess, J.R. POP-1 and Anterior–Posterior Fate Decisions in C. elegans Embryos. *Cell* **1998**, *92*, 229–239. [CrossRef]
142. Lin, R.; Thompson, S.; Priess, J.R. pop-1 Encodes an HMG box protein required for the specification of a mesoderm precursor in Early C. elegans embryos. *Cell* **1995**, *83*, 599–609. [CrossRef]
143. Page, A.P.; Johnstone, I.L. The cuticle. *WormBook* **2007**, 1–15. [CrossRef] [PubMed]
144. Sulston, J.; Horvitz, H. Post-embryonic cell lineages of the nematode, *Caenorhabditis elegans*. *Dev. Boil.* **1977**, *56*, 110–156. [CrossRef]
145. Park, F.D.; Tenlen, J.R.; Priess, J.R. C. elegans MOM-5/Frizzled Functions in MOM-2/Wnt-Independent Cell Polarity and Is Localized Asymmetrically prior to Cell Division. *Curr. Boil.* **2004**, *14*, 2252–2258. [CrossRef]
146. Baldwin, A.T.; Clemons, A.M.; Phillips, B.T. Unique and redundant β-catenin regulatory roles of two Dishevelled paralogs during C. elegans asymmetric cell division. *J. Cell Sci.* **2016**, *129*, 983–993. [CrossRef]
147. Park, F.D.; Ma, L.; Lei, L.; Eng, S.R.; Turner, E.; Parada, L.F. Establishment of POP-1 asymmetry in early C. elegans embryos. *Development* **2003**, *130*, 3547–3556. [CrossRef]
148. Maloof, J.N.; Whangbo, J.; Harris, J.M.; Jongeward, G.D.; Kenyon, C. A Wnt signaling pathway controls hox gene expression and neuroblast migration in *C. elegans*. *Development* **1999**, *126*, 37–49.
149. Baldwin, A.T.; Phillips, B.T. The tumor suppressor APC differentially regulates multiple β-catenins through the function of axin and CKIα during *C. elegans* asymmetric stem cell divisions. *J. Cell Sci.* **2014**, *127*, 2771–2781. [CrossRef]
150. Moss, E.G. Heterochronic Genes and the Nature of Developmental Time. *Curr. Boil.* **2007**, *17*, R425–R434. [CrossRef]
151. Ambros, V. MicroRNAs and developmental timing. *Curr. Opin. Genet. Dev.* **2011**, *21*, 511–517. [CrossRef] [PubMed]

152. Salser, S.J.; Kenyon, C. A *C. elegans* Hox gene switches on, off, on and off again to regulate proliferation, differentiation and morphogenesis. *Development* **1996**, *122*, 1651–1661. [PubMed]
153. Emmons, S.W. Male development. *WormBook* **2005**, 1–22. [CrossRef] [PubMed]
154. Sternberg, P.W. Vulval development. *WormBook* **2005**. [CrossRef] [PubMed]
155. Gleason, J.E.; Korswagen, H.C.; Eisenmann, D.M. Activation of Wnt signaling bypasses the requirement for RTK/Ras signaling during *C. elegans* vulval induction. *Genome Res.* **2002**, *16*, 1281–1290. [CrossRef] [PubMed]
156. Eisenmann, D.M.; Kim, S.K. Protruding vulva mutants identify novel loci and Wnt signaling factors that function during *Caenorhabditis elegans* vulva development. *Genetics* **2000**, *156*, 1097–1116. [PubMed]
157. Yu, H.; Seah, A.; Sternberg, P.W. Re-programming of *C. elegans* male epidermal precursor fates by Wnt, Hox, and LIN-12/Notch activities. *Dev. Boil.* **2010**, *345*, 1–11. [CrossRef]
158. Wang, X.; Sommer, R.J. Antagonism of LIN-17/Frizzled and LIN-18/Ryk in nematode vulva induction reveals evolutionary alterations in core developmental pathways. *PLoS Boil.* **2011**, *9*, e1001110. [CrossRef]
159. Watts, J.L.; Ristow, M. Lipid and Carbohydrate Metabolism in Caenorhabditis elegans. *Genetics* **2017**, *207*, 413–446.
160. Watts, J.L.; Browse, J. A palmitoyl-CoA-specific delta9 fatty acid desaturase from *Caenorhabditis elegans*. *Biochem. Biophys. Res. Commun.* **2000**, *272*, 263–269. [CrossRef]
161. Admasu, T.D.; Batchu, K.C.; Barardo, D.; Ng, L.F.; Lam, V.Y.M.; Xiao, L.; Cazenave-Gassiot, A.; Wenk, M.R.; Tolwinski, N.S.; Gruber, J. Drug Synergy Slows Aging and Improves Healthspan through IGF and SREBP Lipid Signaling. *Dev. Cell* **2018**, *47*, 67–79. [CrossRef] [PubMed]
162. Hou, N.S.; Taubert, S. Function and Regulation of Lipid Biology in *Caenorhabditis elegans* Aging. *Front. Physiol.* **2012**, *3*, 143. [CrossRef] [PubMed]

Chapter 2

Materials and Methods

2.1 Worm strains and culture conditions

Nematodes were grown under standard conditions at 20°C unless otherwise noted. The following strains were used in this study. All wild type, mutant and transgenic strains used in the later chapters are listed here.

AF16 *(C. briggsae wild type),*
AGD1664 *uthSi17[myo-3p::MLS::GFP::unc-54 3' UTR:: cb-unc-119(+)]*
AGD2192 *uthSi60[vha-6p::ERss::mRuby::HDEL::unc-54 3' UTR]*
AGD3311 *uthIs526(unc-54p::pry-1-cDNA + myo-3::YFP)*
AGD3312 *uthIs527(unc-54p::pry-1-cDNA + myo-3::YFP)*
AGD3313 *uthIs528(pry-1p::PRY-1-GFP + glr-1p::RFP)*
AGD3314 *uthIs529(pry-1p::PRY-1-GFP + glr-1p::RFP)*
AGD418 *uthIs205 [crtc-1p::crtc-1::RFP::unc-54 3'UTR + rol-6(su1006)]*
AGD927 *uthIs270[rab-3p::xbp-1s + myo-2p::tdTomato]*
AU78 *agIs219[T24B8.5p::GFP + ttx-3p::GFP]*
CB1370 *daf-2(e1370) III*

CB4037 *glp-1(e2141) III*
CF1038 *daf-16(mu86) I*
CF1553 *muIs84 [(pAD76) sod-3p::gfp + rol-6(su1006)]*
DA1116 *eat-2(ad1116) II*
DA2123 *adIs2122 [lgg-1p::GFP::lgg-1 + rol-6(su1006)]*
DR1572 *daf-2(e1368) III*
DY220 *pry-1(mu38) I*
DY230 *pry-1(mu38) I; bhEx80[myo-2::gfp+unc-119(+)+ pGLC37(hs::cel-pry-1)]*
DY250 *Cbr-pry-1(sy5353) I*
DY252 *Cbr-pry-1(sy5353); bhEx93[unc-119(+)+myo-2::gfp+pGLC37(hs::cel-pry-1)]*
DY319 *Cbr-pry-1(sy5353) I; mfEx[myo-2::RFP + Cel-dlg-1::GFP]*
DY596 *pry-1(mu38) I; bhEx246[pDC10(pry-1p::PRY-1-GFP) + glr-1::RFP]*
DY612 *bhEx259[pGLC135(Cel-manf-1p::GFP) + pRF4(rol-6(su1006))]*
DY629 *pry-1(mu38) I; wIs78*
DY630 *pry-1(mu38) I; maIs150*
DY631 *pry-1(mu38) I; maIs140*
DY636 *pry-1(mu38); maIs138*
DY637 *pry-1(mu38); maIs236*
DY638 *pry-1(gk3682) I; wIs78*
DY641 *miR-246(n4636) IV; zcIs13[hsp-6::gfp]*
DY642 *miR-246(n4636) IV; zcIs4[hsp-4::gfp]*
DY643 *miR-246(n4636) IV; muIs84 [(pAD76) sod-3p::GFP + rol-6(su1006)]*
DY646 *miR-246(n4636) IV; stIs11597*
DY647 *bhEx273[pGLC144(kin-9p::gfp) + myo-2p::gfp]*
DY648 *bhEx274[pGLC144(kin-9p::gfp) + myo-2p::gfp]*
DY649 *miR-246(n4636) IV; wIs51 [scm::gfp] V*
DY654 *pry-1(mu38) I; muIs84 [(pAD76) sod-3p::gfp + rol-6(su1006)]*
DY656 *pry-1(mu38) I; ldrIs2 [mdt-28p::mdt-28::mCherry + unc-76(+)]*
DY657 *miR-246(n4636) IV; bcIs39 [lim-7p::ced-1::gfp]*
DY658 *pry-1(mu38); zcIs4[hsp-4::GFP]*

DY659 *pry-1(mu38); adIs2122[lgg-1p::gfp::lgg-1 + rol-6(su1006)]*
DY661 *pry-1(mu38) I; zIs356 [daf-16p::daf-16a/b::GFP + rol-6(su1006)]*
DY662 *kin-9(tm3973) X*
DY663 *kin-9(tm3973) X*
DY664 *bhEx277[pGLC153(unc-54p::pry-1-cDNA) + myo-3::YFP + unc-119(+)]*
DY665 *bhEx278[pGLC153(unc-54p::pry-1-cDNA) + myo-3::YFP + unc-119(+)]*
DY666 *pry-1(mu38) I; (bh39)*
DY667 *bhEx279[pGLC154(lin-26p::pry-1-cDNA) + myo-3::YFP + unc-119(+)]*
DY668 *bhEx280[pGLC154(lin-26p::pry-1-cDNA) + myo-3::YFP + unc-119(+)]*
DY669 *unc-119(tm4063) III; bhEx281[pGLC155(elt-2p::pry-1-cDNA) + myo-2::gfp + unc-119(+)]*
DY670 *unc-119(tm4063) III; bhEx282[pGLC155(elt-2p::pry-1-cDNA) + myo-2::gfp + unc-119(+)]*
DY671 *pry-1(mu38) I; bhEx279[pGLC154(lin-26p::pry-1-cDNA)+myo-3::gfp+unc-119(+)]*
DY672 *bhEx283[pGLC157(unc-119p::pry-1-cDNA) + myo-3::gfp]*
DY673 *bhEx284[pGLC157(unc-119p::pry-1-cDNA) + myo-3::gfp]*
DY674 *pry-1(mu38)I;bhEx277[pGLC153(unc-54p::pry-1-cDNA)+myo-3::YFP+ unc-119(+)]*
DY675 *pry-1(mu38)I;bhEx281[pGLC155(elt-2p::pry-1-cDNA) + myo-2::gfp + unc-119(+)]*
DY676 *bhEx285[pGLC146(hsp-16::kin-9) + myo-3::wCherry]*
DY677 *bhEx286[pGLC146(hsp-16::kin-9) + myo-3::wCherry]*
DY678 *bhEx287[pGLC150(F56E10.1p::gfp) + myo-3::wCherry]*
DY679 *bhEx246[pDC10(pry-1p::PRY-1-GFP) + glr-1::RFP]*
DY680 *pry-1(mu38)I;bhEx283[pGLC157(unc-119p::pry-1-cDNA)+myo-3::YFP+unc119(+)]*
DY681 *pry-1(mu38); zcIs9 [hsp-60::GFP + lin-15(+)]*
DY682 *rde-1(ne219) V; kzIs20; bhEx288[pGLC153(unc-54p::pry-1-cDNA)+myo-3::YFP]*
DY683 *pry-1(mu38); zcIs14 [myo-3::GFP(mit)]*

DY685 *zIs356 [daf-16p::daf-16a/b::gfp + rol-6(su1006)]; bhEx277[pGLC153(unc-54p::pry-1-cDNA)+myo-3::YFP+ unc-119(+)]*
DY686 *pry-1(mu38); bhEx120[pGLC72(Cel-dat-1::yfp)+unc-119(+)]*
DY688 *kagIs1[Pdyc-1S::GFP::lgg-1]+Pmyo-2::mCherry;bhEx277[pGLC153(unc-54p::pry-1-cDNA)+myo-3::YFP+ unc-119(+)]*
DY689 *pry-1(mu38); kagIs1[Pdyc-1S::GFP::lgg-1]+Pmyo-2::mCherry*
DY690 *rde-1(ne219) V; kbIs7 [nhx-2p::rde-1 + rol-6(su1006)];bhEx277[pGLC153(unc-54p::pry-1-cDNA)+myo-3::gfp+ unc-119(+)]*
DY691 *unc-119(tm4063) III; bhEx289[pGLC158(Pkin-9abc::GFP)+unc-119(+)]*
DY692 *unc-119(tm4063) III; bhEx290[pGLC144(Pkin-9bc::GFP)+unc-119(+)]*
DY694 *F56E10.1(gk3701) V*
DY697 *pry-1(mu38) I; uthIs248*
DY698 *F56E10.1(bh40) V*
DY700 *bhEx293[pGLC160(kin-9p::GFP::3'UTR)]*
DY701 *bhEx294[pGLC162(miR-246oe) + pJH1774(myo-3p::wCherry)](use this),*
DY702 *bhEx295[pGLC162(miR-246oe) + pJH1774(myo-3p::wCherry)],*
DY703 *pry-1(mu38) I; bhEx293[pGLC160(kin-9p::GFP::3'UTR)],*
DY704 *bhEx294[pGLC162(miR-246oe)+pJH1774(myo-3p::wCherry)]; bhEx293[pGLC160(kin-9p::GFP::3'UTR)]*
DY705 *miR-246(n4636); bhEx293[pGLC160(kin-9p::GFP::kin-9 3'UTR)],*
DY706 *bhEx296[pGLC161(myo-3p::mAxin1::YFP) + pJH1774(myo-3p::wCherry)]*
DY707 *F56E10.1(bh40); wIs78[(scm::GFP) + (ajm-1p::GFP)]*
DY708 *bhEx297[pGLC162(miR-26(oe) + pPD136.64(myo-3p::YFP)]*
DY709 *bhEx298[pGLC165(F09A5.2p::GFP)]*
DY710 *bhEx299[pGLC165(F09A5.2p::GFP)]*
DY713 *zcIs14 [myo-3::GFP(mit)]; bhEx285[pGLC146(hsp-16::kin-9) + myo-3::wCherry]*
DY716 *pry-1(gk3682); kin-9(tm3973)*
DY717 *miR-246(tm4831)*
DY718 *F09A5.2(tm7493)*

DY719 *miR-246(tm4679)*
DY720 *bhEx294[pGLC162(miR-246oe) + pJH1774(myo-3p::wCherry)]; bhEx259[pGLC135(Cel-manf-1p::GFP) + pRF4(rol-6(su1006)]*
DY721 *bhEx300[pGLC153(unc-54p::pry-1-cDNA)+pGLC160(kin-9::GFP)]; zcIs14 [myo-3::GFP(mit)]*
DY722 *rde-1(ne219) V; kzIs20; zcIs14(myo-3p::GFP(mito))*
DY723 *bhEx301[pDYH5(Cel-daf-16p::DAF-16-GFP)+ myo-2p::mCherry]*
DY725 *pry-1(mu38); F56E10.1(bh40)*
DY726 *Cbr-daf-16(syb3672) (2X)*
DY727 *Cbr-daf-2(sy5445); mfIs42[Cel-sid-2::gfp + Cel-myo-2::Ds-red]*
DY728 *Cbr-daf-2(sy5445); mfIs42[Cel-sid-2::gfp + Cel-myo-2::Ds-red]*
DY730 *pry-1(mu38) I; pkIs2386 [unc-54p::alpha synuclein::YFP]*
DY731 *pry-1(gk3682) I; hjIs14 [vha-6p::GFP::C34B2.10(SP12) + unc-119(+)]*
DY732 *pry-1(gk3682); uthSi17[myo-3p::MLS::GFP::unc-54 3' UTR:: cb-unc-119(+)]*
DY733 *pry-1(gk3682); ldrIs[dhs-3p::dhs-3::GFP + unc-76(+)]*
DY734 *pry-1(gk3682); uthIs270 [rab-3p::xbp-1s + myo-2p::tdTomato]*
DY735 *bhEx277[pGLC153(unc-54p::pry-1-cDNA) + myo-3::YFP]; uthIs205[crtc-1p::crtc-1::RFP + rol-6(su1006)]*
DY736 *pry-1(mu38); agIs219[T24B8.5p::GFP + ttx-3p::GFP]*
DY737 *pry-1(gk3682); uthSi60[vha-6p::ERss::mRuby::HDEL::unc-54 3' UTR]*
DY740 *pry-1(gk3682); uthIs205[crtc-1p::crtc-1::RFP + rol-6(su1006)]*
EU384 *dpy-11(e1180) mom-2(or42) V/nT1 [let-?(m435)] (IV;V)*
EW15 *bar-1(ga80) X*
GR2245 *skn-1(mg570) IV*
HT1189 *daf-16(mgDf50) I; unc-119(ed3) III; lpIs14*
JK3437 *him-5(e1490) V, qIs74 [sys-1p::GFP::pop-1 + unc-119(+)]*
JR667 *unc-119(e2498::Tc1) III; wIs51[scmp::gfp + unc-119(+)] V*
JU1018 *mfIs42[Cel-sid-2::gfp + Cel-myo-2::Ds-red]*
JU1078 *mfEx33[myo-2::RFP + Cel-dlg-1::GFP]*
KAG238 *kagIs1[Pdyc-1S::GFP::lgg-1]+ Pmyo-2::mCherry*

KK300 *par-4(it57) V*
KN562 *pop-1(hu9) I*
KN611 *axl-1(tm1095) I*
LIU1 *ldrIs[dhs-3p::dhs-3::GFP + unc-76(+)]*
LIU2 *ldrIs2[mdt-28p::mdt-28::mcherry]*
MD701 *bcIs39 [lim-7p::ced-1::GFP]*
MGH171 *sid-1(qt9) V; alxIs9 [vha-6p::sid-1::SL2::gfp]*
MQ887 *isp-1(qm150) IV*
MT10430 *lin-35(n745)*
MT15020 *miR-246(n4636) IV*
N2 *(C. elegans wild type)*
NL2098 *rrf-1(pk1417)*
NL5901 *pkIs2386 [unc-54p::alphasynuclein::YFP + unc-119(+)]*
NR222 *rde-1(ne219) V; kzIs9 [(pKK1260) lin-26p::NLS::gfp + (pKK1253) lin-26p::rde-1 + rol-6(su1006)]*
NR350 *rde-1(ne219) V; kzIs20 [hlh-1p::rde-1 + sur-5p::NLS::GFP]*
PHX3672 *Cbr-daf-16(syb3672)*
PS4943 *huIs[dpy-20(+); hsp-16-2delta NTbar-1]; syIs148*
PS5531 *Cbr-daf-2(sy5445)*
RB1566 *F09A5.2(ok1900)*
RB754 *aak-2(ok524) X*
RG733 *wIs78*
RW11597 *stIs11597*
SJ4005 *zcIs4[hsp-4::gfp]*
SJ4058 *zcIs9 [hsp-60::GFP + lin-15(+)]*
SJ4100 *zcIs13[hsp-6::gfp]*
SJ4103 *zcIs14 [myo-3::GFP(mit)]*
TJ356 *zIs356 [daf-16p::daf-16a/b::gfp + rol-6(su1006)]*
TTV310 *unc-119(ed3) III; eluIs300[Pdaf-16d/f::gfp+unc-119(+)]*
TTV421 *unc-119(ed3) III; eluEx370[Pdaf-16a::gfp+unc-119(+)]*
TU3311 *uIs60 (unc-119p::yfp + unc-119p::sid-1)*

VC3709 *pry-1(gk3681) I; F56E10.1(gk3701) V*
VC3710 *pry-1(gk3682) I*
VC636 *cwn-2(ok895) IV*
VP303 *rde-1(ne219) V; kbIs7 [nhx-2p::rde-1 + rol-6(su1006)]*
VS25 *hjIs14 [vha-6p::GFP::C34B2.10(SP12) + unc-119(+)]*
VT1160 *maIs138*
VT1189 *maIs140*
VT1259 *maIs150*
VT1607 *maIs236*
WBM60 *uthIs248[aak-2p::aak-2(genomicaa1-321)::GFP::unc-54-3'UTR+myo-2p::tdTOMATO]*
WM27 *rde-1(ne219)*

2.2 Molecular biology and transgenic

2.2.1 List of Plasmids

Plasmid #	Construct	Purpose
pGLC142	*C. elegans pry-1* RNAi plasmid	To knockdown *pry-1*
pGLC144	*kin-9bc::GFP::unc-54 UTR*	Transcriptional reporter of *kin-9 b* and *c* isoforms.
pGLC145	*C. elegans lin-28* RNAi plasmid	To knockdown *lin-28*
pGLC146	*hsp-16.2::kin-9*	Overexpression of full-length *kin-9* transcript.
pGLC150	*F56E10.1p::GFP::unc-54 3' UTR*	Transcriptional reporter of *F56E10.1*
pGLC151	*pry-1 cDNA entry clone vector*	Used to create tissue-specific overexpression plasmids

pGLC152	*unc-54 3' UTR entry clone vector*	Used to create tissue-specific overexpression plasmids
pGLC153	*unc-54p::pry-1-cDNA::unc-54 UTR*	Overexpression of *pry-1* in the muscle
pGLC157	*unc-119p::pry-1-cDNA::unc-54 UTR*	Overexpression of *pry-1* in the pan neurons
pGLC154	*lin-26p::pry-1-cDNA::unc-54 UTR*	Overexpression of *pry-1* in the hypodermis
pGLC155	*elt-2p::pry-1-cDNA::unc-54 UTR*	Overexpression of *pry-1* in the intestine
pGLC156	*pie-1p::pry-1-cDNA::unc-54 UTR*	Overexpression of *pry-1* in the germline
pGLC163	*C. elegans par-4* RNAi plasmid	To knockdown *par-4*
pGLC158	*kin-9abc::GFP::unc-54 UTR*	Transcriptional reporter of *kin-9 a, b* and *c* isoforms
pGLC160	*kin-9bc::GFP::kin-9 UTR*	Transcriptional reporter of *kin-9 b* and *c* isoforms with *kin-9* 3' UTR.
pGLC165	*F09A5.2p::GFP::unc-54 UTR*	Transcriptional reporter of *F09A5.2*
pGLC170	*manf-1p::GFP::kin-9 UTR*	Transcriptional reporter of *manf-1* with *kin-9* 3' UTR.
pGLC164	*kin-9p::kin-9::UTR (genomic fragment)*	*kin-9* overexpression
pGLC162	*miR-246 full length transcript (genomic fragment)*	*miR-246* overexpression

pGLC175	*C. briggsae daf-16* RNAi plasmid	To knockdown *Cbr-daf-16*
pGLC172	*C. briggsae aak-2* RNAi plasmid	To knockdown *Cbr-aak-2*
pGLC173	*C. briggsae hsf-1* RNAi plasmid	To knockdown *Cbr-hsf-1*

2.2.2 Transgenic animals

All the transgenic animals carrying extrachromosomal arrays were generated by standard microinjection technique (Mello *et al.* 1991). The concentration for plasmids containing the gene of interest ranged from 10 ng/µL to 50 ng/µL whereas plasmid concentration for microinjection markers (*myo-3p::GFP, myo-3p::wCherry, myo-2p::GFP* and *unc-119* rescue) ranged from 20ng/µL to 40 ng/µL. More details regarding transgenics can be found in the respective chapters.

2.2.3 Genetic Crosses

Genetic crosses to obtain *miR::GFP* reporter expressing lines in a mutant background were performed in *C. elegans* by crossing 8-10 wildtype (either N2) males and 2-4 GFP reporter-expressing hermaphrodites on agar plates. Animals were allowed to mate and produce Fl progeny for 3-4 days at which point the Fl heterozygous males were isolated. F1 heterozygous males were then crossed to the mutant of interest. Fl progeny that was heterozygous for the mutation and the reporter were obtained and cloned. Cloned Fl progenies were allowed to self-fertilize and reporters expressing F2 progeny, which was homozygous for the phenotype caused by the mutation of interest, were cloned onto separate plates. These F2 progenies were allowed to self-fertilize and clones that produced only reporter expressing progeny were selected. One homozygous population, for both the reporter and mutation, was used as the reference strain and frozen.

2.2.4 RNA extraction and expression analysis

See **Chapter 4** – Methods section.

2.2.5 List of primers used.

Gene	**GL #**	**Orientation**	**Purpose**	**Sequence (5'-3')**
miR-2-5p	1247	Forward	cDNA synthesis	CTCAACTGGTGTCGTGGAGTCGGCAATTCAGTTGAGGCACATCA
lin-4-5p	1331	Forward	cDNA synthesis	CTCAACTGGTGTCGTGGAGTCGGCAATTCAGTTGAGTCACACTT
miR-48-5p	1245	Forward	cDNA synthesis	CTCAACTGGTGTCGTGGAGTCGGCAATTCAGTTGAGTCGCATCT
miR-84-5p	1246	Forward	cDNA synthesis	CTCAACTGGTGTCGTGGAGTCGGCAATTCAGTTGAGTCTACAAT
miR-237-5p	1355	Forward	cDNA synthesis	CTCAACTGGTGTCGTGGAGTCGGCAATTCAGTTGAGAGCTGTTC
miR-241-5p	1332	Forward	cDNA synthesis	CTCAACTGGTGTCGTGGAGTCGGCAATTCAGTTGAGTCATTTCT
miR-246-3p	1244	Forward	cDNA synthesis	CTCAACTGGTGTCGTGGAGTCGGCAATTCAGTTGAGGCTCCTAC
Cbr-miR-84-5p	1255	Forward	cDNA synthesis	CTCAACTGGTGTCGTGGAGTCGGCAATTCAGTTGAGGACAGCAT
Cbr-miR-237-5p	1357	Forward	cDNA synthesis	CTCAACTGGTGTCGTGGAGTCGGCAATTCAGTTGAGAGATGTCG

miR-2-5p	1252	Forward	qPCR	ACACTCCAGCTGGGTATCACAGCCAG CTTT
lin-4-5p	1333	Forward	qPCR	ACACTCCAGCTGGGTCCCTGAGACCT CAAG
miR-48-5p	1250	Forward	qPCR	ACACTCCAGCTGGGTGAGGTAGGCTC AGTA
miR-84-5p	1251	Forward	qPCR	ACACTCCAGCTGGGTGAGGTAGTATG TAAT
miR-237-5p	1356	Forward	qPCR	ACACTCCAGCTGGGTCCCTGAGAATT CTCG
miR-241-5p	1334	Forward	qPCR	ACACTCCAGCTGGGTGAGGTAGGTGC GAGA
miR-246-3p	1249	Forward	qPCR	ACACTCCAGCTGGGTTACATGTTTCG GGTA
Cbr-miR-84-5p	1256	Forward	qPCR	ACACTCCAGCTGGGTGAGGTAGTTTG CAAT
Cbr-miR-237-5p	1358	Forward	qPCR	ACACTCCAGCTGGGTCCCTGAGAATG CTCC
Cbr-miR-246-3p	1257	Forward	qPCR	ACACTCCAGCTGGGTTACATGTATTG GGTA
All miRNA gene	1254	Reverse	qPCR	CTCAACTGGTGTCGTGGAGTCGGCAA
pmp-3	747	Forward	qPCR	CTTAGAGTCAAGGGTCGCAGTGGAG
pmp-3	748	Reverse	qPCR	ACTGTATCGGCACCAAGGAAACTGG

pry-1	741	Forward	qPCR	CGCCAACACGAGGAGTTTGTGG
	742	Reverse	qPCR	TGTGATGAATGGTGGGCGGAGC
hbl-1	1258	Forward	qPCR	TTGGCACAAAGAGCAAAGCC
hbl-1	1259	Reverse	qPCR	GGCCATTCTGATCCTATTAAAGGTG
lin-14	1262	Forward	qPCR	TGCGAGGAATGGGGAAATGG
lin-14	1263	Reverse	qPCR	GTCGAAGATCGGTTACTTCTTTCC
lin-28	1264	Forward	qPCR	AAGTTGAAGATAGGCTGCCAGA
	1265	Reverse	qPCR	GTGTTGGTGACGGGAGCC
lin-29	1266	Forward	qPCR	TTTGGTGTTGGAACAAACTTGAGA
	1267	Reverse	qPCR	GCTGGTGTGGATCCAGTTGA
let-60	1260	Forward	qPCR	TCAGCACTCACCATTCAACTCA
	1261	Reverse	qPCR	CACCGTCTATCACAACCTGCT
miR-246	1325	Forward	PCR	CGTCGGAAGATTCACTCCTG
miR-246	1326	Reverse	PCR	CCTCACTGGTCATACTTCCC
pry-1(gk3682)	1307	Forward	PCR	CATCGCCTTCTATCGCCTTCTTGA
	1308	Reverse	PCR	GCGAAGAACAAGTCGAGGTACTG
cah-4	1337	Forward	qPCR	GGTGACTGTTGCGATGTCCT
	1338	Reverse	qPCR	GTTGGCGGTAAGGAATGTGC

pbs-5	1339	Forward	qPCR	GGAGGCGTCTGCAATTTGTG
	1340	Reverse	qPCR	CAGCTTGCTCACGTCCATTG
kin-9	1341	Forward	qPCR	CCACGTCATTTGCCAACAACA
	1342	Reverse	qPCR	GCAACTGCATTTACGCCTCC
sbp-1	1398	Forward	qPCR	GGACCATCACAACAACCGGA
	1399	Reverse	qPCR	GCAGGGAGTGTAAGGTGCTT
F56E10.1	1329	Forward	qPCR	CCCAGGCCGCTTCTACTATG
	1330	Reverse	qPCR	GGATGGAGAATTCTGGAACGAAGT
pry-1 RNAi (pGLC142)	1343	Forward	PCR	ATTACCCGGGCTCCGCCCACCATTCATCAC
	1344	Reverse	PCR	TGCTGAGCTCGAGCCTTTCTGTGCTGCCT
kin-9bcp::GFP (pGLC144)	1350	Forward	PCR	TAAGGCATGCTCAAGCTGTTCAAACACGAC
	1352	Reverse	PCR	TAAGGTCGACCTTCGTGAGAGTCGTCAACG
hsp-16::kin-9abc (pGLC146)	1353	Forward	PCR	TAAGGGTACCAGCCAATGCTCATCCAGTACC
	1354	Reverse	PCR	TAAGGAGCTCCATGTTGTGCGGACCCGTT
lin-28 RNAi	1359	Forward	PCR	TAAGGGTACCGTAGTATCGGAGGGAAGGAATG

(pGLC145)	1360	Reverse	PCR	TAAGGCTAGCGGTGGTAGTATGGTTTAGAGGG
F56E10.1p::gfp (pGLC150)	1372	Forward	PCR	AGGTCGACGTGGTGTCAAGCTGTCTCATTGC
	1373	Reverse	PCR	AGGGTACCCAAACCTCTCCGTCGGAAGACTC
kin-9(tm3973)	1417	Forward	PCR	CTAGTACAATTCCTGGGGTC
	1418	Reverse	PCR	CCAATCCATTGCTAATCTGC
kin-9 all isoforms	1419	Forward	qPCR	GCTGCCCGTAACGTCTTAGT
	1420	Reverse	qPCR	CTCCTCGGGCAGTGTACAAA
pry-1-cDNA (pGLC151)	1384	Forward	PCR	GGGGACAACTTTCTATACAAAGTTGTAATGGAGACCCATCTCGGTTGG
	1385	Reverse	PCR	GGGGACAACTTTATTATACAAAGTTGTCTATCGGAGCTCGGCGGCAATT
unc-54 3'UTR (pGLC152)	1396	Forward	PCR	GGGGACAACTTTGTATAATAAAGTTGTAACTTCTAAGTCCAATTACTC
	1397	Reverse	PCR	GGGGACCACTTTGTACAAGAAAGCTGGGTTCACTACTCCACTTTCAAATT
unc-54p::pry-1-cDNA (pGLC153)	1394	Forward	PCR	GGGGACAAGTTTGTACAAAAAAGCAGGCTTAATGAATCCGAGAAATATGAG
	1395	Reverse	PCR	GGGGACAACTTTGTATAGAAAAGTTGGGTGGATTTCTCGCTTCTTTCAAAT
	1412	Forward	PCR	GGGGACAAGTTTGTACAAAAAAGCA

lin-26p::pry-1-cDNA (pGLC154)				GGCTTATCTGAAATATACGGCGGTAGATC
	1413	Reverse	PCR	GGGGACAACTTTGTATAGAAAAGTTGGGTGGTAAGCGAGGGATGAAGGTATTC
elt-2p::pry-1-cDNA (pGLC155)	1388	Forward	PCR	GGGGACAAGTTTGTACAAAAAAGCAGGCTTAATCTTCAGATTCTTCTACTC
	1389	Reverse	PCR	GGGGACAACTTTGTATAGAAAAGTTGGGTGTCTATAATCTATTTTCTAGTTTCTATTTTATT
pie-1p::pry-1-cDNA (pGLC156)	1390	Forward	PCR	GGGGACAAGTTTGTACAAAAAAGCAGGCTTATTGAAAGTTTTGTGGGGAAA
	1391	Reverse	PCR	GGGGACAACTTTGTATAGAAAAGTTGGGTGTGGGAAACGAAATACTGCAA
unc-119p::pry-1-cDNA (pGLC157)	1392	Forward	PCR	GGGGACAAGTTTGTACAAAAAAGCAGGCTTAATGTCGATTTACGGGCTCAG
	1393	Reverse	PCR	GGGGACAACTTTGTATAGAAAAGTTGGGTGATATGCTGTTGTAGCTGAAAATTTTG
Pkin-9abc::gfp (pGLC158)	1431	Forward	PCR	AGGTCGACTCAAGCTGTTCAAACACGAC
	1432	Reverse	PCR	AGGGTACCTCTGCATTTACGCCTCCTTCAC
daf-16 all isoforms	1364	Forward	qPCR	TACCGGGTGCCTATGGAAAC
	1365	Reverse	qPCR	GAATATGCTGCCCTCCAGCT

daf-16a	1366	Forward	qPCR	TCAGGAATCGTCAGCAACC
	1367	Reverse	qPCR	CACGGAACTGCCAGAAGAT
daf-16b/c	1368	Forward	qPCR	CTCCACGTCCACCTCATCTG
	1369	Reverse	qPCR	GTTGAGTGGTGGTTCGAGTT
daf-16d/f/h/i/k	1370	Forward	qPCR	CGACCTCCATCAACAAGAGC
	1371	Reverse	qPCR	CTTCCGCTGTCAACAGTCTC
rde-1(ne219)	1454	Internal Forward	PCR sequencing	CTTTCCTGGACATTCGATCATCTG
	1455	Internal Reverse	PCR sequencing	GGTAAATCGGACAGAGGAAGAA
rde-1(ne219)	1468	External Forward	PCR sequencing	AGGAAACAGCGCAAATGACGAC
	1469	External Reverse	PCR sequencing	GATTTCCCGCTGTTTCGTTGACT
tnt-4	1456	Forward	qPCR	CGGAGGAAGACATCCACCAA
	1457	Reverse	qPCR	TCATAAACCTGACGGCGCTC
mlc-1	1458	Forward	qPCR	TGCGGAAAGATCAAGGAGGAC
	1459	Reverse	qPCR	CGATTGGTGGCTTTCCCTTG
unc-96	1460	Forward	qPCR	GGCACTCCGTACTCCGAAAT
	1461	Reverse	qPCR	TGGACGATTTCTGTTGATGCTC

lgg-1	1462	Forward	qPCR	AAACGCATCCAACTTCGTCC
	1463	Reverse	qPCR	CCTCGTGATGGTCCTGGTAG
F56E10.1 (gk3701)	1482	Forward	PCR	AGAGGATGAGGACAATGGTGA
	1483	Reverse	PCR	GATTCTCCTGGTTGTATGTGGC
	1484	Forward	PCR	CGCGCTGTGTTTATCGTAAATC
F56E10.1(bh40)	1486		ssODN	AATTTTTTTATTAAACTAAAATTTAGA AATGGAAGATTAGTAGGTAGTAGCTA GTAGTAACAGGAAACAGCTATGACCG TATGAAGACGACGAGTCTTCCGACGG ATAGGTTTGTAGCAAAGCTTAAAATT CACGGAAACCAGCATTTTAATTC
	1480		crRNA1	TTGCTTGCGCCCAATTCTGA
	1487		crRNA2	TCTTCCGACGGAGAGGTTTG
	1488	M13 Forward (internal)	PCR	CAGGAAACAGCTATGACCGT
	1489	Forward	PCR	CATCAGAATTGGGCGCAAGC
	1483	Reverse	PCR	GATTCTCCTGGTTGTATGTGGC
Pkin-9bc::GFP::kin-9 3'UTR (pGLC160)	1497	Forward	PCR	AAGGAATTCCAATGCGATAATGTGTA ACACTATG
	1498	Reverse	PCR	AAGACTAGTCGACCGTCAATATATGA AACTAATT
kin-9p::kin-9	1561	Forward	PCR	CATTCAAGCTGTTCAAACACGACAC

overexpression	1562	Reverse	PCR	TTCCACATCGTCATCTGTTCTCATC
par-4 RNAi plasmid (pGLC163)	1559	Forward	PCR	AAGGGTACCCGTCCAACGTGTCTCGAAAC
	1560	Reverse	PCR	AAGACTAGTGGTACGAGAACGAAAGATACACG
myo-3p::mAxin1::YFP	1499	Forward (mAxin1 insert)	PCR	CCACTTTTACCGTCTAATTTTCAGATGCAGAGTCCCAAAATGAATGTC
	1500	Reverse (mAxin1 insert)	PCR	AGTTCTTCTCCTTTACTCATGTCCACCTTTTCCACCTTGC
	1501	Forward (pPD136_64 vector)	PCR	ATGAGTAAAGGAGAAGAACTTTTCAC
	1502	Reverse (pPD136_64)	PCR	CTGCATCTGAAAATTAGACGGTAAAAGTGG
miR-246p::miR-246 (pGLC162)	1509	Forward	PCR	CTTACACCAAATGGGTTTACATGTG
	1510	Reverse	PCR	ATTTCCTCACTGGTCATACTTCC
F09A5.2p::GFP (pGLC165)	1599	Forward	PCR	AAGAAGCTTTATGCGTCAATGCTTGCACC
	1600	Reverse	PCR	AAGGGTACCAGGTGGGAGTAAGAAGGATTAGA
	1621	Forward	qPCR	AAACAGCTCCATGCTCCACTC

F09A5.2	1622	Reverse	qPCR	CGTTTGCCTCGCATTGATTTCG
F09A5.2 (ok1900)	1623	Forward	PCR	CAGCAAGACCTTAATCTCCACG
	1624	Reverse	PCR	GTCACTCACCATCAGCACATAATC
F09A5.2 (tm7493)	1625	Forward	PCR	CAGCAAGACCTTAATCTCCACG
	1626	Reverse	PCR	GTCTTCTTTCTTCCCACTGGG
xbp-1	1446	Forward	qPCR	CGCAGCCCAAAATGCTAGAG
	1447	Reverse	qPCR	AGATCGCGCATCACATCCTC
atf-6	1452	Forward	qPCR	TTGTTCAGCCCTTGATGCCA
	1453	Reverse	qPCR	AGCGGACCACTTTTTGGTTG
ire-1	1448	Forward	qPCR	TGGCTTCCGGAATGATCACG
	1449	Reverse	qPCR	TCCAAAGCTCTCAAACGTCCA
pek-1	1450	Forward	qPCR	AACGCATTGCCAGAGCTTTC
	1451	Reverse	qPCR	TGAAGCACCAATCGCAAGGT
hsf-1	1631	Forward	qPCR	ATGCAGCCAGGATTGTCGAA
	1632	Reverse	qPCR	GCACGTTTTGAGTTGGGTCC
atfs-1	1633	Forward	qPCR	CGAGCCGAGAAGAAGGGAAG
	1634	Reverse	qPCR	GCGCCCATTTTACGAAGCTC

pop-1	1335	Forward	qPCR	GAACGGTATCCGGAGTGGTC
	1336	Reverse	qPCR	TGATCGTTGTTCTCCGATGGAAT
mig-5	1629	Forward	qPCR	TCCTCCAAAAGGCAGAACACT
	1630	Reverse	qPCR	TAGTTGCCGTTTGCTCCTGT
kin-19	1627	Forward	qPCR	ACGTCACTGCAACAAGCTCT
	1628	Reverse	qPCR	ATTCCCAAGTGGGCGTTGAT
cdk-1	1421	Forward	qPCR	GGCGAAGGAACATACGGAGT
	1422	Reverse	qPCR	CCGTTGATGGAACACCCTCAT
rnr-1	1423	Forward	qPCR	ATTTTGTCGATCCGGTCGCT
	1424	Reverse	qPCR	GGTCATGGAAGCAGCAGTCT
his-7	1425	Forward	qPCR	CAGTTGGTCGTCTTCACCGT
	1426	Reverse	qPCR	CTCAAGAACAGCAGCCAGGT
cpz-1	1427	Forward	qPCR	GGTGCATGGATGGGGTGTAG
	1428	Reverse	qPCR	TTGAACCATCCGTGCTCTCC
clsp-1	1635	Forward	qPCR	TCGTCAGCATCTGCAAAACG
	1636	Reverse	qPCR	TGTCAGAGGTTTTGAGGGGTA
ard-1	1637	Forward	qPCR	AATGTCGGCACTCAGAAGCA
	1638	Reverse	qPCR	CTTTCCCAGTCCAGACGCTC

spp-1	1639	Forward	qPCR	AGCCAATCCAGCTAACCCAC
	1640	Reverse	qPCR	GACGAGAGCCTTGCAGACAT
rpn-7	1641	Forward	qPCR	AGGATGACAGAGGCTGCCAA
	1642	Reverse	qPCR	GCTGCTGTCTACTTCGGGAT
hsp-4	1643	Forward	qPCR	AAGCTTCTGAGGAGCCATCG
	1644	Reverse	qPCR	GGGGTTGGGTTGGGAAAGAA
hsp-6	1645	Forward	qPCR	AACCATTGAGCCATGCCGTA
	1646	Reverse	qPCR	CTTGAACAGTGGCTTGCACC
sod-3	956	Forward	qPCR	TATTAAGCGCGACTTCGGTTCC
	957	Reverse	qPCR	CTTGCAATATCCCAACCATCCC
hsp-16.2	1647	Forward	qPCR	GTCCAGCTCAACGTTCCGT
	1648	Reverse	qPCR	TCTCAGAAGACTCAGATGGAGAGAT
SL1	539	Forward	PCR	GGTTTAATTACCCAAGTTTGAG
Cbr-iscu-1	1406	Forward	qPCR	GCTTCAAATCAGTCTCGCTGC
	1407	Reverse	qPCR	GTGCCGACGTTCTTGTCGTTT
Cbr-daf-2(sy5445)	1667	Forward	PCR	GGTATTCGACGAGAACAACTGC
	1668	Reverse	PCR	CCAATTCTAGCTGAATCCTACTGC
	1711	Forward	PCR	AAACTGTATGATTGATAAAACGGAAT

				TGA
Cbr-daf-2	1669	Forward	qPCR	TATAATCCGCCTGAGGAGCTGG
	1670	Reverse	qPCR	GGAACCCATCGAGATCGTCGAA
Cbr-sod-2	1673	Forward	qPCR	TTGGAGCCAGTTATCAGCCATG
	1674	Reverse	qPCR	GCTTCCTTGACGTTTCCCTTTGAA
Cbr-lipl-4	1671	Forward	qPCR	ACTTTGCACTTGCTCCAGTTG
	1672	Reverse	qPCR	CCAGTTCTCACTAGACGTTCCAA
Cbr-fat-6	1677	Forward	qPCR	GCTCACATGGGATGGCTTCT
	1678	Reverse	qPCR	GGCAAGGACTGGATCGTTCT
Cbr-vit-2	1679	Forward	qPCR	TGCCACTGAGTGTGCTAAGG
	1680	Reverse	qPCR	TATGCGGAGGCGATCATCTG
Cbr-daf-16(syb3672)	1687	Forward	PCR	GATTCAGAAGAGCGATTCCAGTG
	1688	Reverse	PCR	CGTGGTATGATGGTGGAGCAAT
Cbr-daf-16e::DAF-16	1689	Forward	nested PCR	GTAGAAGTGCCTATTAAGCTCCTC
	1690	Reverse	nested PCR	TACCGGTACCCTCCAAGGGTCCTCCAAATCGAAATGAATACTTTGCCCT
GFP + unc-54 UTR from pPD95.81	1691	Forward	nested PCR	GAGGACCCTTGGAGGGTACCGGTA
	1692	Reverse	nested PCR	AAGGGCCCGTACGGCCGACTAG

Cbr-daf-16e::DAF-16::GFP	1693	Forward	nested PCR	GATCTTTAGAATTAGGGCTGAAATTCCTTCAGG
	1694	Reverse	nested PCR	GGAAACAGTTATGTTTGGTATATTGGGAATGT
Cbr-hsp-4	1695	Forward	qPCR	CCACTTACTCGTGCGTTGGA
	1696	Reverse	qPCR	ATGAGCCGTTCTCCTTGCTC
Cbr-hsp-6	1697	Forward	qPCR	CGAAGGAGTCAGAACCACCC
	1698	Reverse	qPCR	GGCGTCTCCATTACTGGCTT
Cbr-hsp-70	1699	Forward	qPCR	ACAAGGGTGCCAAAGGTTCA
	1700	Reverse	qPCR	TGTCATCTTTGACGCCGGAA
Cbr-hsp-16.2	1701	Forward	qPCR	CCGTCCAAGACCATTCTCTGT
	1702	Reverse	qPCR	ACTGGGAGACGTTGAGGTTG
Cbr-hsp-12.3	1703	Forward	qPCR	AGGAACCAAGTGGGATTGGC
	1704	Reverse	qPCR	TCCGAACTTGTCGTCCTTGG
Cbr-aak-2 RNAi plasmid	1705	Forward	PCR	TAAGGTCGACTTGTCATCGTCACATGGTTGTTC
	1706	Reverse	PCR	TAAGGGTACCCAATACTCGCCTCCATGCTCAT
Cbr-daf-16 RNAi plasmid	1707	Forward	PCR	TAAGGTCGACTCTCTACTTTCGGGAACGATC

	1708	Reverse	PCR	TAAGGGTACCCAACGCATCCACATCC ATATCC
Cbr-hsf-1 RNAi plasmid	1709	Forward	PCR	TAAGGTCGACTGAAATAGTTACAGCG GTGTGC
	1710	Reverse	PCR	TAAGGGTACCCTCTCCATCAGCGTCG TAATAC
Cbr-daf-16 all isoforms	1712	Forward	qPCR	AGGAGCATTCGGAGGTTATCAG
	1713	Reverse	qPCR	CAACGCATCCACATCCATATCCA
Cbr-daf-16a/c	1714	Forward	PCR of cDNA	GACAGTGGAACAAACAGCCTGTT
	1717	Reverse	qPCR	CACCAAACAGGGCATCTCCATTC
Cbr-daf-16b/d	1715	Forward	PCR of cDNA	GAAGATCCGGACCTGTTTGGAAG
	1717	Reverse	qPCR	CACCAAACAGGGCATCTCCATTC
Cbr-daf-16e	1716	Forward	PCR of cDNA	CCGGATGGAAGAACTCGATCCG
	1718	Reverse	qPCR	GATTGATGACCCACCACGAACTC
Cbr-daf-16 all isoforms	1713	Common Reverse Primer for PCR	PCR of cDNA	CAACGCATCCACATCCATATCCA
dod-24	1727	Forward	qPCR	GTGTCCAACACAACCTGCAT
	1728	Reverse	qPCR	TCCTCCGGCTCTTAACTCGT

asp-12	1729	Forward	qPCR	GTCCCATCTACCACTTTCGGT
	1730	Reverse	qPCR	CCGTCGACTGCAAGAGATGT

Underlined sequences correspond to restriction enzyme sites, recombination sites or CRISPR site.

2.3 Lifespan assay

See **Chapter 5** – Methods section.

2.4 Stress sensitivity assay

See **Chapter 6** – Methods section.

2.5 Microscopy

See **Chapter 3** – Methods section.

2.6 RNA-interference (RNAi) mediated knock down

See **Chapter 6** – Methods section.

2.7 Statistical analysis

See Methods section of **Chapters 4, 5 and 6** for relevant statistical analysis.

Chapter 3

Role of PRY-1/Axin in heterochronic miRNA mediated seam cell development

3.1 Preface

This chapter includes the following article in its originally published format: "Role of PRY-1/Axin in heterochronic miRNA mediated seam cell development", by Avijit Mallick, Ayush Ranawade and Bhagwati P. Gupta. BMC Developmental Biology. 19(17): 1-8 (DOI: 10.1186/s12861-019-0197-5). This is an open-access article distributed under the terms of the Creative Commons Attribution Unported License, which permits unrestricted use, distribution, and reproduction in any medium, provided the original work is properly cited.

3.2 Mallick, Ranawade and Gupta (2019)- BMC Developmental Biology

In this study, we characterised the role of the Axin homolog PRY-1 in regulating heterochronic microRNAs (miRNAs) that regulate seam cell development. We found that *pry-1* mutants in *C. elegans* exhibit seam cell, cuticle, and alae defects. To understand the regulation better, we carried out a miRNA transcriptome analysis, which showed that *let-7 (miR-48, miR-84, miR-241)* and *lin-4 (lin-4, miR-237)* family members were upregulated in the absence of *pry-1* function. Similar phenotypes and patterns of miRNA overexpression were also observed in *C. briggsae pry-1(sy5353)* mutants, a species that is closely related to *C. elegans*. RNA interference-mediated silencing of *wrm-1/β-catenin* and *lit-1/NLK* in the *C. elegans pry-1* mutants rescued the seam cell defect, whereas *pop-1/TCF* silencing enhanced the phenotype, suggesting that all three proteins are likely important for PRY-1 function in seam cell development. We also found that these miRNAs were overexpressed in *pop-1(hu9)* hypomorphic mutants, suggesting that PRY-1 is required for POP-1-mediated miRNA suppression. Analysis of the *let-7* and *lin-4*-family heterochronic targets, *lin-28* and *hbl-1*, showed that both genes were significantly downregulated in *pry-1* mutants, and furthermore, *lin-28* silencing reduced the number of seam cells in mutant animals. Altogether our results show that PRY-1 plays a conserved role to maintain normal expression of heterochronic miRNAs in nematodes and functions upstream of the WNT asymmetry pathway components WRM-1, LIT-1, and POP-1, and miRNA target genes in seam cell development.

Contributions: I performed experiments and provided data for Figures 1, 2, 3, 4, 5, 6 and 7. Ayush Ranawade performed the RNA-seq analysis in the *pry-1(mu38)* animals at the L1 stage and the I carried out the analysis for target prediction coupled with GO enrichment analysis. Data for Figure 3C, Figures 5B-C and 6A-B were also replicated by Ayush Ranawade. I and Bhagwati Gupta created all the Figures and illustrations. Bhagwati Gupta conceived and supervised the project. I and Bhagwati Gupta wrote the manuscript. It was finally revised with addressed reviewers concerns by me and Bhagwati Gupta.

Mallick *et al. BMC Developmental Biology* (2019) 19:17
https://doi.org/10.1186/s12861-019-0197-5

BMC Developmental Biology

RESEARCH ARTICLE Open Access

Role of PRY-1/Axin in heterochronic miRNA-mediated seam cell development

Avijit Mallick[1], Ayush Ranawade[1,2] and Bhagwati P. Gupta[1*]

Abstract

Background: *Caenorhabditis elegans* seam cells serve as a good model to understand how genes and signaling pathways interact to control asymmetric cell fates. The stage-specific pattern of seam cell division is coordinated by a genetic network that includes WNT asymmetry pathway components WRM-1, LIT-1, and POP-1, as well as heterochronic microRNAs (miRNAs) and their downstream targets. Mutations in *pry-1*, a negative regulator of WNT signaling that belongs to the Axin family, were shown to cause seam cell defects; however, the mechanism of PRY-1 action and its interactions with miRNAs remain unclear.

Results: We found that *pry-1* mutants in *C. elegans* exhibit seam cell, cuticle, and alae defects. To examine this further, a miRNA transcriptome analysis was carried out, which showed that *let-7* (*miR-48, miR-84, miR-241*) and *lin-4* (*lin-4, miR-237*) family members were upregulated in the absence of *pry-1* function. Similar phenotypes and patterns of miRNA overexpression were also observed in *C. briggsae pry-1* mutants, a species that is closely related to *C. elegans*. RNA interference-mediated silencing of *wrm-1* and *lit-1* in the *C. elegans pry-1* mutants rescued the seam cell defect, whereas *pop-1* silencing enhanced the phenotype, suggesting that all three proteins are likely important for PRY-1 function in seam cells. We also found that these miRNAs were overexpressed in *pop-1* hypomorphic animals, suggesting that PRY-1 may be required for POP-1-mediated miRNA suppression. Analysis of the *let-7* and *lin-4*-family heterochronic targets, *lin-28* and *hbl-1*, showed that both genes were significantly downregulated in *pry-1* mutants, and furthermore, *lin-28* silencing reduced the number of seam cells in mutant animals.

Conclusions: Our results show that PRY-1 plays a conserved role to maintain normal expression of heterochronic miRNAs in nematodes. Furthermore, we demonstrated that PRY-1 acts upstream of the WNT asymmetry pathway components WRM-1, LIT-1, and POP-1, and miRNA target genes in seam cell development.

Keywords: *C. elegans*, *C. briggsae*, *Pry-1*, Axin, WNT asymmetry pathway, Seam cell, miRNA, Heterochronic development

Background

Caenorhabditis elegans hypodermal seam cells serve as a good model to elucidate spatiotemporal patterns of division and differentiation that enable cells to adopt sex-specific fates. They comprise two lateral rows of multipotent somatic cells which extend from the anterior to the posterior of the nematode (Fig. 1), and that divide in a stem cell-like manner to both self-renew, and generate daughter hypodermal, neuronal, and neuronal-support cells [1]. At the early L2 stage of development, the six seam cells (V1–6) undergo symmetric division to give rise to a total of 16 seam cells. By the end of the L4 stage, the cells terminally differentiate and fuse with their neighbors to give rise to adult cuticular structures called alae [2].

Multiple genes and pathways have been shown to regulate seam cell division and differentiation. These include the *lin-4* (*lin-4* and *miR-237*) and *let-7* (*let-7, miR-48, miR-84,* and *miR-241*) families of heterochronic microRNAs (miRNAs) that regulate the relative timing of developmental events [3–7]. Specifically, *lin-4* is required for the L1–L2 transition [2, 8], while the *let-7* family members act at later stages of development [9]. Mutations in *lin-4, miR-48, miR-84,* and *miR-241* cause cells to reiterate stages, which ultimately affects both the number of differentiated seam cells, and cuticle development [9].

Previous studies have shown that heterochronic miRNAs regulate a number of targets, including *hbl-1*, *lin-*

* Correspondence: guptab@mcmaster.ca
[1]Department of Biology, McMaster University, ON L8S-4K1, Hamilton, Canada
Full list of author information is available at the end of the article

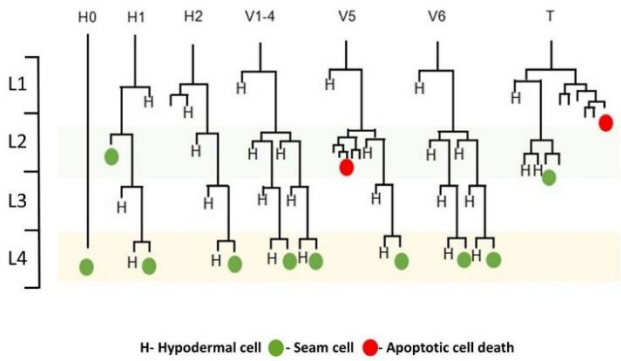

Fig. 1 Seam cell asymmetric divisions during postembryonic development in *C. elegans*. During postembryonic development, *C. elegans* larvae undergo a series of molts, each of which is associated with carefully timed seam cell divisions. In the V1–4, and V6, cells undergo stem cell-like division where the anterior daughter fuses with the hyp7 syncytium. The posterior daughter then self-renews as another 'stem cell-like' seam cell. The exception to the asymmetric divisions is in early L2 stage where they undergo one symmetrical division prior to dividing again in an asymmetric manner

14, and *lin-28* [10]. HBL-1 is a zinc-finger transcription factor that critically mediates embryogenesis [11], and that controls developmental timing during post-embryonic development [9]. LIN-14 is a novel class of transcription factor [12] that is initially expressed at high levels in hypodermal blast cells in newly hatched L1 animals but at lower levels by the L2 stage [13]. LIN-28 is a conserved RNA-binding protein that controls the maturation of *let-7* miRNA [5, 14–16]. Hypomorphic and null alleles of *lin-14* and *hbl-1* cause an increase whereas *lin-28* mutants cause a decrease in the overall number of seam cells [9, 17, 18].

In addition to heterochronic miRNAs and their targets, seam cell division is also regulated by the divergent WNT asymmetry pathway, whose components include the β-catenins WRM-1 and SYS-1, the NEMO-like kinase (NLK) LIT-1, and the T-cell factor/lymphoid enhancer factor (TCF/LEF) POP-1 [18, 19]. Removal of POP-1 activity causes seam cells to divide symmetrically, and thereby leads to an increase in their number. Conversely, since LIT-1 normally forms a complex with WRM-1 to phosphorylate and thus stimulate POP-1 export from the nucleus, disrupting WRM-1 and/or LIT-1 activity reduces the number of seam cells [19]. Similarly, the ratio of nuclear POP-1/SYS-1 activity affects the fate of daughter cells, such that those with lower POP-1 (and hence comparatively higher SYS-1) levels retain their seam cell fate, whereas those with higher POP-1 (and hence comparatively lower SYS-1) levels differentiate [20–23]. Genetic studies have also shown that WNT asymmetry pathway components interact with heterochronic genes to control seam cell development [17, 18].

While investigating the role of *pry-1* in developmental and post-developmental processes, we observed that *pry-1(mu38)* animals exhibit weaker cuticle and abnormal alae. Further analysis revealed that they also display a higher number of seam cells, a phenotype that was previously reported [19]. Similar defects were also seen in a *C. briggsae pry-1* mutant *Cbr-pry-1(sy5353)* [24], suggesting a conserved role for *pry-1* in seam cell development and cuticular alae formation. These observations are in line with our recent *pry-1(mu38)* mRNA transcriptome profiling (RNA-Seq), which identified differentially expressed (DE) genes associated with 'cuticle development' [25]. Given that the heterochronic pathway involves both protein-coding and miRNA genes, in the present study we conducted an miRNA-specific whole genome RNA-Seq experiment, which uncovered six DE miRNAs that include members of *lin-4* and *let-7* families. To understand the interaction of *pry-1* with miRNAs during seam cell development, we knocked-down WNT asymmetry pathway components. Reducing *wrm-1* and *lit-1* expression suppressed, while silencing *pop-1* exacerbated the *pry-1* phenotype. Furthermore, an miRNA expression analysis conducted in a *pop-1* hypomorph revealed a similar upregulation of miRNAs to that observed in *pry-1(mu38)* worms, suggesting both that POP-1 is critical for asymmetric seam cell division, and that its nuclear levels are likely reduced in *pry-1* mutants. Overall, our data demonstrates the importance of PRY-1 and its interactions with the WNT asymmetry pathway components for the regulation of miRNAs (and their targets) during asymmetric cell division. Since the WNT pathway and miRNAs are conserved in eukaryotes, similar interactions with Axin family members may control stem cell division in other systems.

Results

We observed that *pry-1* mutant worms have a weaker cuticle (Fig. 2a) and abnormal alae that frequently includes

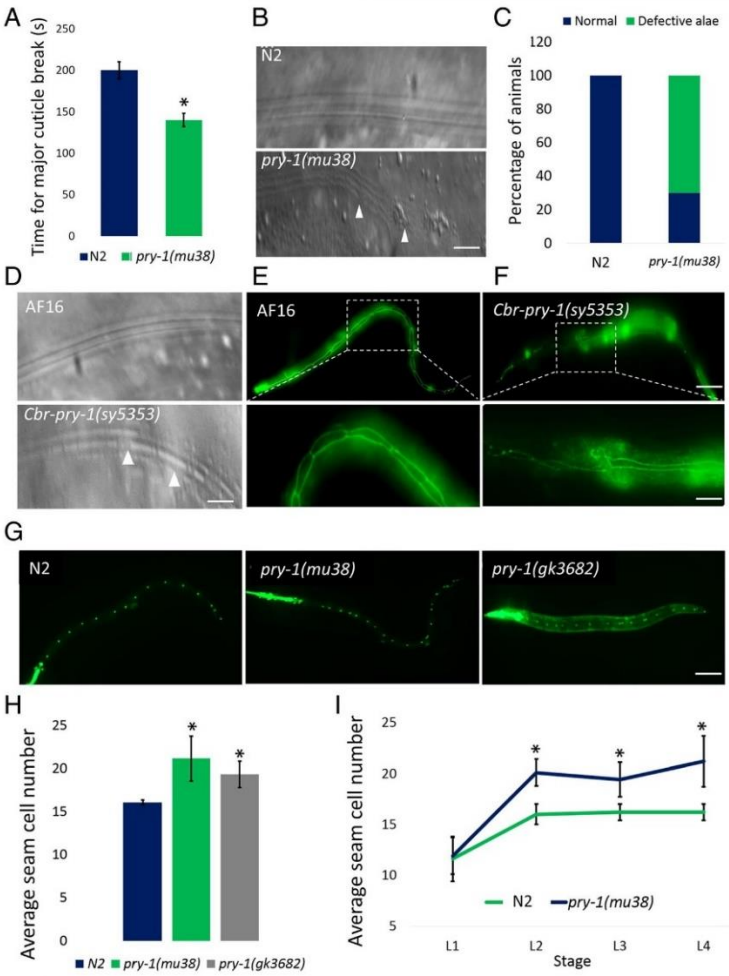

Fig. 2 *pry-1* mutants display seam cell defects in *C. elegans* and *C. briggsae*. Mutations in *pry-1* lead to somatic defects. (**a**) Cuticle is weaker as demonstrated by the cuticle break assay. (**b, c**) *pry-1* mutants having defective alae formation. (**b**) Control N2 animals have distinct rows of alae. *pry-1(mu38)* mutants have defect with frequent breaks (see arrow). (**c**) Quantification of alae defect in control N2 and *pry-1(mu38)* animals. (**d**-**f**) Heterochronic phenotypes in *C. briggsae* AF16 and *Cbr-pry-1* mutants. (**d**) Alae defects are visible in *Cbr-pry-1(sy5353)*. (**e**, **f**) Seam cells in control AF16 (**e**) and *Cbr-pry-1(sy5353)* (**f**) are visualized by adherens-junction-associated marker *Cel-dlg-1p::GFP*. *Cbr-pry-1(sy5353)* animals show defects in cell fusion (scale bar 0.1 mm). Boxed areas, marked by dotted lines, have been enlarged in the second row. Scale bars in **b**, **d**-**f** are 0.01 mm. (**g**) Both the *pry-1(mu38)* and *pry-1(gk3682)* animals show increased seam cell numbers compared to control N2 (scale bar 0.1 mm). (**h**) Each control animal has exactly 16 seam cells, whereas an average of 21 and 19 cells are found in *pry-1(mu38)* and *pry-1(gk3682)* mutants, respectively. (**i**) *pry-1(mu38)* animals show increased seam cell number by the end of the L2 stage. In panels **a**, **h**, and **i**, each data point represents the mean of at least two replicates (each batch with 30 or more worms) and error bar represents the STD. Student's *t*-test was used to determine the statistical significance: $*p < 0.05$

gaps (Fig. 2b, c). The phenotypic analysis of *C. briggsae pry-1* mutants, *Cbr-pry-1(sy5353)* [24], revealed similar gaps in alae as well as defective seam cell morphologies (Fig. 2d-f). Given these hypodermis-associated phenotypes, we investigated the role of *pry-1* in seam cell development.

pry-1 mutants exhibit an increased number of seam cells

In *C. elegans*, seam cells divide asymmetrically at each larval stage to produce two daughter cells, one of which fuses with the hypodermal syncytium, while the other retains the seam cell fate (Fig. 1). The L2 stage is unique

because it also includes a symmetric division that causes an increase in the number of seam cells (Fig. 1). We found that the *pry-1(mu38)* mutants have an average of approximately five extra seam cells (Fig. 2g, h), consistent with a previously report [19]. A similar phenotype was also observed in *pry-1(gk3682)*, a new CRISPR/Cas9-induced mutant strain (provided by Don Moerman's lab) (Fig. 2g, h; Additional file 1: Figure S1). A stage-specific analysis conducted using *scm::GFP* and *ajm-1::GFP* markers [26] revealed a higher number of seam cells in *pry-1* mutants by the end of the L2 stage, likely due to an increase in symmetric cell divisions (Fig. 2h, i). Together, these findings suggest that *pry-1* appears to play a role in L2-specific seam cell division.

Heterochronic miRNA expression is altered in *pry-1* mutants

As described above, seam cell asymmetry is mediated by two interacting pathways. While heterochronic genes, such as members of the *lin-4* and *let-7* miRNA families, control cell division, the WNT asymmetry pathway plays a role in the specification of anterior/posterior daughter cell fates. To evaluate the involvement of miRNAs in *pry-1*-mediated seam cell development, we performed RNA-Seq experiment in L1-stage animals. The results revealed six DE miRNAs in the *pry-1(mu38)* mutants. Additionally, 61 novel miRNAs were recovered in the *C. elegans* reference sample (N2) (see Methods and Additional files 2-4: Table S1, S2, S3) that serve as a resource to further investigate the miRNA biology in worms.

Of the six DE miRNAs, five (*lin-4*, *miR-48*, *miR-84*, *miR-237*, and *miR-241*) were upregulated and one (*miR-246*) was downregulated (Fig. 3a, b). Notably, all of these except *miR-246* are known to be involved in both heterochronic development and a range of other processes [8, 9, 27, 28], a fact that was further supported by our tissue-enrichment analysis (Additional file 5: Figure S2). We next performed quantitative real-time PCR (qRT-PCR) validations which revealed similar, if comparatively lower (3–22-fold versus 2–12-fold in RNA-Seq and qRT-PCR, respectively), DE trends (Fig. 3B, C). Moreover, the *C. briggsae* orthologs of DE miRNAs were found to be likewise altered in *Cbr-pry-1(sy5353)* animals (Fig. 3d).

To elucidate whether *pry-1*-mediated miRNA regulation is stage-specific, we examined miRNA transcript levels by qRT-PCR in adult nematodes. While the expression of miRNAs was either unchanged or downregulated in *pry-1(mu38)* (Additional file 6: Figure S3A), the pattern was different in *Cbr-pry-1(sy5353)* animals, i.e., three miRNA orthologs were up, two were down, and one was unchanged (Additional file 6: Figure S3B). We also used the existing *C. elegans miRNA::GFP* transgenic strains [29] to determine changes in miRNA expression in *pry-1(mu38)* animals and confirmed the qRT-PCR results (Additional file 7: Figure S4). Overall, the dissimilar expression trends of the analyzed miRNAs in adults from L1-stage nematodes suggests that the *pry-1*-miRNA network is likely temporally regulated.

miR-246, which a previous study showed to be involved in aging, oxidative stress, and thermo-sensation [30, 31], was the only miRNA to be downregulated in the *pry-1(mu38)* nematodes. Although no role in heterochronic development has yet been reported for *miR-246*, we herein demonstrate that *miR-246(n4636)* adults exhibit alae defects (Fig. 3e). Conversely, *scm::GFP* and *ajm-1::GFP* reporter-based expression analyses of the *miR-246(n4636)* adults did not reveal any significant change to the seam cells (Fig. 3f). This finding was supported by the results of the tissue-enrichment analysis (Additional file 5: Fig. S2). Interestingly, a hypodermal cell marker, *dpy-7::H1-wcherry*, revealed that the number of hypodermal cells was reduced in the mutant compared to control worms (45.1 ± 1.7, $n = 20$ and 51.9 ± 1.6, $n = 20$, respectively; also see Additional file 8: Figure S5). Further study is needed to determine the exact fate of these hypodermal cells in *miR-246* mutants.

Many predicted gene targets of the mis-regulated heterochronic miRNAs are differentially expressed in the *pry-1(mu38)* mRNA transcriptome

miRNAs mediate the degradation or translational inhibition of their target mRNAs via binding between their seed sequence and an miRNA response element (MRE) in the 3′ untranslated region of their target. Therefore, we searched for miRNA targets using TargetScan online program (http://www.targetscan.org/vert_72/), and resultantly identified 453 unique targets. The gene ontology (GO) analysis revealed that these predicted miRNA targets were predominantly associated with processes such as the regulation of heterochrony (29-fold enrichment), the positive regulation of nematode larval development (8-fold enrichment), the molting cycle (5-fold enrichment), and collagen and cuticulin-based cuticle development (7-fold enrichment) (Fig. 4a).

A comparison of the predicted miRNA target genes with our recently published *pry-1(mu38)* mRNA transcriptome [25] revealed a significant overlap (111 genes, Representation factor: 1.6, hyp.geo $p < 7.862$ e-08) (Fig. 4b). Furthermore, a tissue-enrichment analysis showed that this subset of overlapping genes is frequently associated with the hypodermal syncytium (i.e. the third-most enriched subset) (Fig. 4c). Together, these findings suggest that PRY-1 is likely necessary for normal miRNA expression during seam cell development.

Knockdowns of WNT asymmetric pathway components affect both the *pry-1(mu38)* phenotype and miRNA expression

We induced RNAi-mediated silencing to examine interactions between *pry-1* and WNT asymmetry pathway components

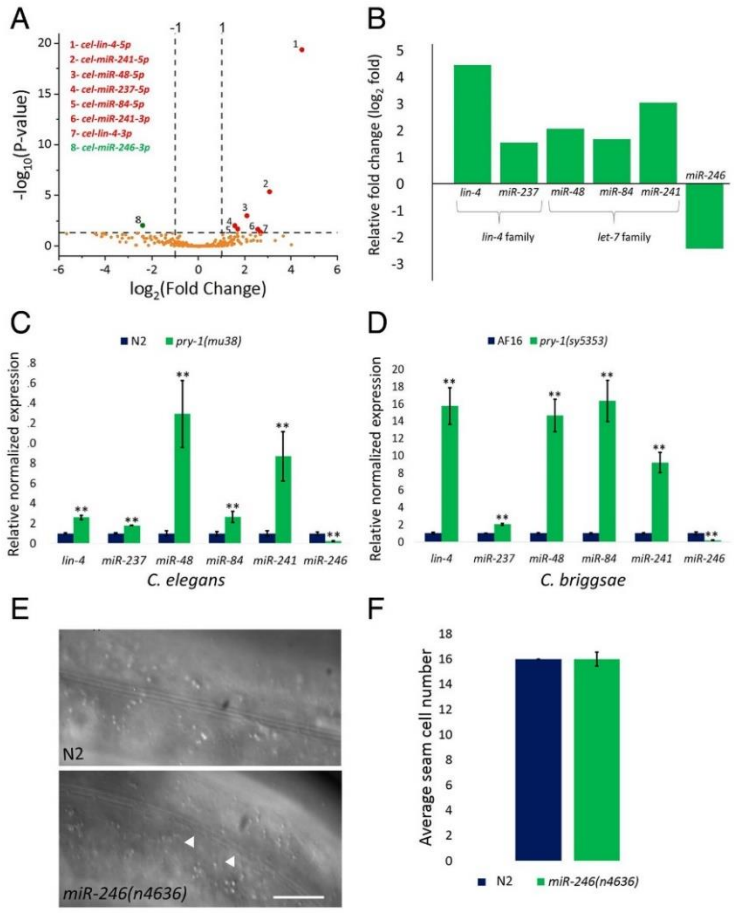

Fig. 3 *pry-1* is necessary for normal miRNA expression in both *C. elegans* and *C. briggsae*. (**a**) Volcano plot of differentially expressed miRNA genes in *pry-1(mu38)*. Red and green dots mark significantly altered upregulated and downregulated transcripts, respectively, with a *p*-adj value of < 0.05. Orange dots mark transcripts that are not significantly altered (*p*-adj > 0.05). (**b**) Data showing $\log_2$ fold expression of miRNAs from RNA-Seq analysis. (**c**, **d**) qRT-PCR analysis of miRNAs in *Cel-pry-1(mu38) and Cbr-pry-1(sy5353)* animals at the L1 stage showed upregulation of all but *miR-246*. Each data point represents the mean of two replicates and error bar represents the SEM, $^{**}p < 0.01$. (**e**, **f**) *miR-246(n4636)* mutants exhibit alae defect in the form of gaps (scale bar 0.01 mm) (**e**) but show no change in the number of seam cells (**f**). Each data point represents the mean of at least two replicates (each batch with at least 20 worms) and error bar represents the STD

during seam cell development. The fates of seam cell daughters are specified by the nuclear levels of POP-1 that are high in the anterior cell (hypodermal fate) and low in the posterior cell (seam cell fate) [19, 32] (Fig. 5a). The results of our experiments revealed that knockdowns of *wrm-1* or *lit-1* suppresses the *pry-1(mu38)* seam cell phenotype (Fig. 5b), likely because PRY-1 promotes asymmetric division by negatively regulating both of these factors in anterior daughter cells (Fig. 5a). This is consistent with PRY-1 being localized to the anterior cortex of dividing seam cells [23]. A similar genetic interaction between *pry-1*, *wrm-1*, and *lit-1* was previously reported to occur during the asymmetric division of embryonic EMS cells [33].

In contrast to *wrm-1* and *lit-1*, *pop-1* RNAi exacerbated the *pry-1(mu38)* phenotype, resulting in a significant increase in the number of seam cells (35.9 ± 10.8 in *pry-1(mu38); pop-1(RNAi)*, compared to 20.8 ± 2.1 in *pry-1(mu38)*, and 23.5 ± 5.7 in *pop-1(RNAi)*) (Fig. 5b, c). We also examined nuclear POP-1 asymmetry following

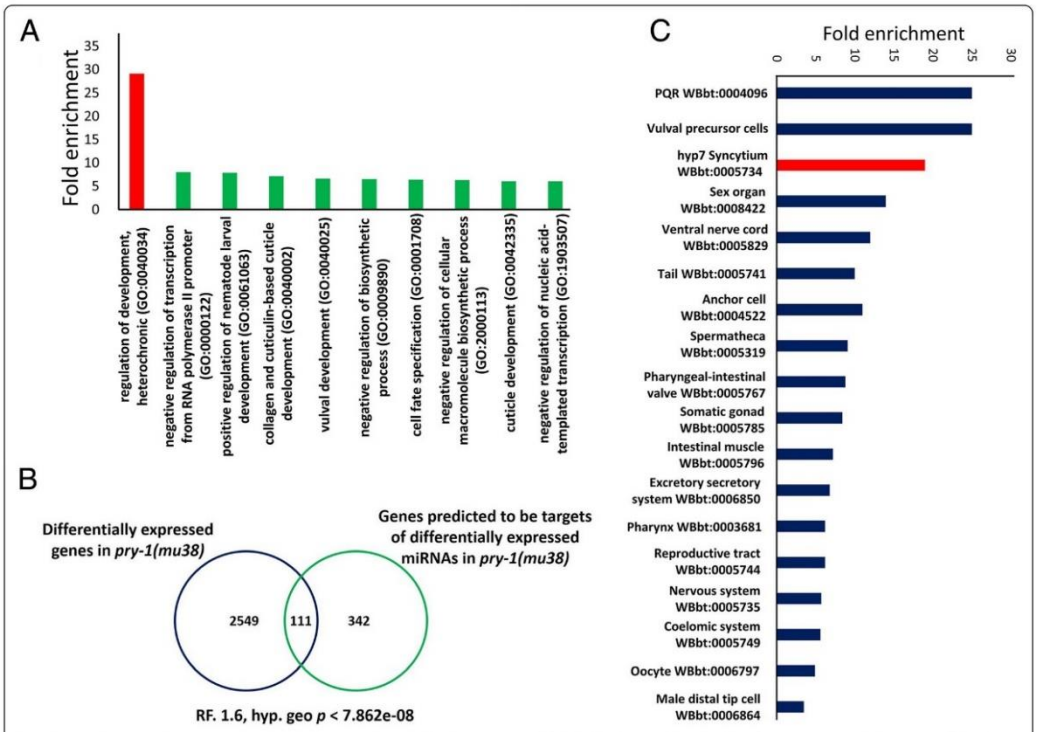

Fig. 4 DE miRNAs and their predicted target genes in *pry-1(mu38)* are mostly linked to heterochronic development. (**a**) Enrichment analysis of potential targets of DE miRNAs using GO-terms associated with biological processes. A significant number of genes (29-fold enrichment) are linked to heterochronic development (colour coded in orange). (**b**) Venn diagram showing the overlap between previously reported protein-coding DE genes (2,660 genes, [25]) and predicted targets of DE miRNAs identified by Targetscan (435 genes, this study) in *pry-1(mu38)* animals. Further analysis revealed that 435 potential targets are shared between DE miRNAs (36 by *lin-4*, 115 by *miR-48*, 115 by *miR-84*, 36 by *miR-237*, 115 by *miR-241*, and 102 by *miR-246*). A total 111 genes are common between the two data sets, a number that is statistically significant based on the hypergeometric test. (**c**) Tissue-enrichment analysis of the common set of genes (111) revealed third highest fold enrichment in hypodermal syncytium cells (colour coded in orange)

RNAi knockdown of *pry-1* and found that it was disrupted (Fig. 5d). These results agree with nuclear POP-1 levels being differentially regulated by WRM-1 and LIT-1 to be higher in the anterior, and lower in the posterior daughter cell [19, 32] (Fig. 5a) Together, our findings support that *pop-1* likely limits the number of seam cells that are produced by promoting the asymmetric division of their precursors. Since the asymmetric localization of WRM-1, LIT-1, and POP-1 are known to mediate fate specification in presumptive seam cells, our results suggest that PRY-1 likely facilitates the maintenance of these asymmetric expression patterns.

Given that the nuclear POP-1 and SYS-1 ratio determines the fate of daughter cells and SYS-1 localization is disrupted in animals lacking PRY-1 function [34], we also examined the effect of *sys-1* knockdown. The results of this analysis showed no effect on seam cell division in *pry-1(mu38)* animals (Fig. 5b). We likewise knocked down another β-Catenin family member, *bar-1*, in the mutant strain and found that doing so did not alter the number of seam cells (Fig. 5b). Overall, the data support the possibility that β-Catenin family members are functionally redundant during seam cell division, consistent with previous studies [19], although do not exclude the possibility that PRY-1 role in seam cells is independent of BAR-1 and SYS-1.

To examine whether WRM-1, LIT-1, and POP-1 asymmetries affect miRNA expression during seam cell division, we next quantified miRNA levels in animals in which POP-1 function was compromised. As in *pry-1(mu38)* mutants, the expression levels of *lin-4*, *miR-48*, *miR-84*, *miR-237*, and *miR-241*, were found to be significantly upregulated in both *pop-1(hu9)* and *pop-1(RNAi)* worms; however, no change to *miR-246* expression was

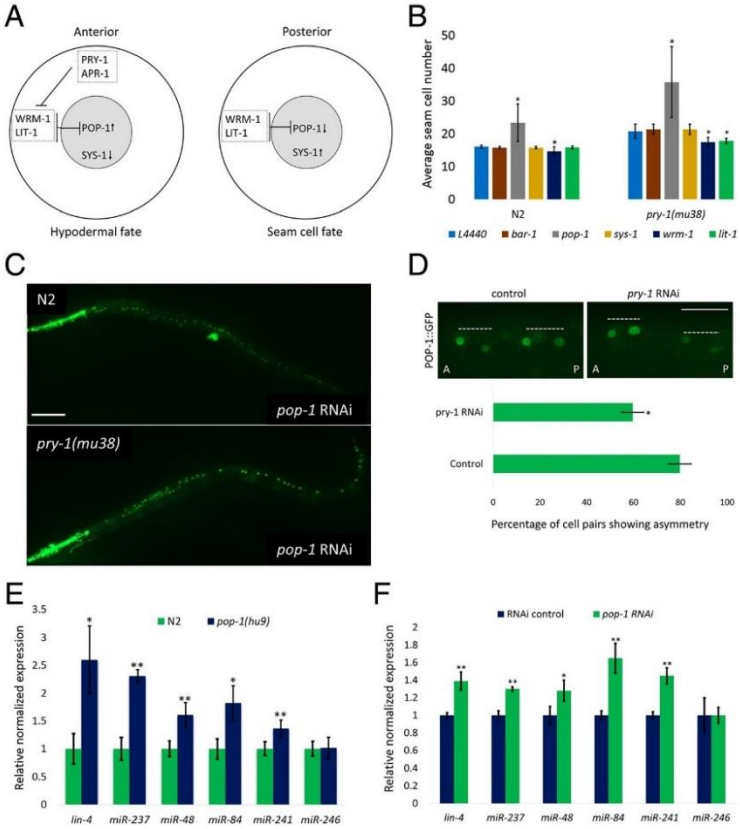

Fig. 5 WNT asymmetry pathway components WRM-1, LIT-1, and POP-1 are important for PRY-1-mediated expression of miRNAs and seam cell development. (**a**) Schematic diagram showing the involvement of PRY-1 and other WNT asymmetry pathway components in the specification of seam cell fates. The levels of nuclear POP-1 are high in the anterior cell but low in the posterior cell. (**b**) RNAi knockdowns of *bar-1*, *pop-1*, *wrm-1*, *sys-1* and *lit-1* in control N2 and *pry-1(mu38)* animals. Each data point represents the mean of at least two batches (each batch with at least 30 worms) and error bar represents the STD. Student's *t*-test was used to determine the statistical significance: $*p < 0.05$ (compared to L4440 control). (**c**) Representative images of control N2 and *pry-1(mu38)* animals following *pop-1* RNAi. The numbers of seam cells are increased in both cases. The phenotype is particularly enhanced in *pry-1* mutants (scale bar 0.1 mm). (**d**) Representative images of two adjacent POP-1::GFP fluorescing cell pairs from V1-V5 seam cell lineages following control and *pry-1* RNAi treatments (A-anterior, P- posterior, each dotted line marks a cell pair, scale bar 20 μm). POP-1 asymmetry is disrupted after *pry-1* RNAi, resulting in fewer cell pairs having asymmetric localisation of POP-1::GFP in their nuclei. (**e, f**) qRT-PCR analysis of miRNAs in *pop-1(hu9)* and *pop-1(RNAi)* worms at the L1 stage. Similar to *pry-1(mu38)*, all miRNAs, except *miR-246*, are overexpressed in both *pop-1(hu9)* (**e**) and *pop-1(RNAi)* (**f**) animals. Each data point represents the mean of two replicates and error bar represents the SEM, $*p < 0.05$, $**p < 0.01$

observed (Fig. 5e, f). Furthermore, the bioinformatic analysis revealed multiple TCF/LEF consensus binding sites (SCTTTGATS; S = G/C) [35, 36] in the 5′ regulatory region of each of these miRNAs, except for *miR-246* where a single site is found near the transcriptional start site (See Methods, Additional file 9: Figure S6), suggesting that their transcription may be inhibited by POP-1. Together, these data allow us to conclude that miRNAs act downstream of POP-1, which agrees with a previous model [18], and also suggest that PRY-1 may interact with WRM-1, LIT-1, and POP-1 to negatively regulate the expression of heterochronic miRNAs during seam cell development.

HBL-1 and LIN-28 act genetically downstream of PRY-1 and POP-1 signaling during asymmetric seam cell division

To further examine the role of *pry-1* in miRNA-mediated heterochronic development, we focused on three known miRNA targets, *hbl-1*, *lin-14*, and *lin-28*. Previous studies have shown that *lin-14* and *lin-28* are

targeted by *lin-4* [3, 5, 37, 38], whereas *hbl-1* and *lin-28* are targeted by another *lin-4* family member *miR-237* [8, 39, 40] as well as *let-7* family members *miR-48*, *miR-84*, and *miR-241* [9, 17].

The qRT-PCR analysis showed that while *lin-14* expression levels were unchanged, *hbl-1* and *lin-28* were significantly downregulated in L1-stage *pry-1(mu38)* animals (Fig. 6a). Together with results described in previous sections, this observation allows us to propose that *pry-1* may function upstream of miRNAs to promote expression of *hbl-1* and *lin-28*. To further examine the regulatory network of *pry-1*, RNAi was carried out. The results revealed that while *lin-14* and *hbl-1* RNAi had no marked impact on seam cells, *lin-28* RNAi caused a significant reduction in the seam cell number in both *pry-1(mu38)* and control animals (Fig. 6b).

Discussion

In this paper we describe a genetic pathway of PRY-1/Axin signaling in seam cell development. Using a combination of mutant analysis and reporter gene expression we show that PRY-1 is involved in L2-specific seam cell division. To identify the genes regulated by *pry-1*, we performed whole genome miRNA profiling at the late-L1 stage. The results revealed six DE miRNAs in *pry-1* mutants. Five of these, belonging to *lin-4* and *let-7* families (*lin-4*, *miR-48*, *miR-84*, *miR-237*, and *miR-241*), were upregulated whereas *miR-246* was the only miRNA that was downregulated. A similar trend was also observed in *C. briggsae pry-1* mutants suggesting that *pry-1* plays a conserved role in miRNA regulation in *Caenorhabditis* nematodes.

Three of the overexpressed miRNAs in *pry-1* mutants, namely *miR-48*, *miR-84*, and *miR-241* (*let-7* family members), are known to redundantly control the L2-L3 larval-stage transition [9]. While *C. elegans* nematodes carrying a mutation in any one of these three miRNAs have been shown to exhibit a normal phenotype, *miR-48/miR-84* double mutants display retarded molting and a higher number of seam cells as a result of reiterated symmetric divisions during the L2 stage [9]. This seam cell phenotype is further exacerbated in *miR-48/miR-84/miR-241* triple mutants [9], while conversely, *miR-48*-overexpression mutants were shown to exhibit a reduced number of seam cells due to 'skipping' of L2-specific symmetric divisions [41]. The other two miRNAs upregulated in the *pry-1(mu38)* mutants are *lin-4* and *miR-237* (*lin-4* family members [42]). A previous study showed that, although a *miR-237*-knock-out mutant does not directly incur a heterochronic defect, it enhances the seam cell phenotype exhibited by *lin-4(e912)*; *lin-14(n179ts)* double mutant animals [8].

Unlike *lin-4* and *let-7* family of DE miRNAs, *miR-246* is not known to play a role in heterochronic development although it is involved in other processes [30, 31]. Consistent with previous studies, our analysis of *miR-246* mutants did not reveal any changes in the number of seam cells. Thus, *pry-1*-mediated *miR-246* regulation may participate in other biological events.

The fact that all but one DE miRNAs in *pry-1* mutants are involved in heterochronic pathway suggests an important role of *pry-1* in this developmental process. This was further strengthened by our data showing a high enrichment for miRNA predicted target genes associated with GO-term processes such as regulation of heterochrony. Moreover, we observed a significant overlap between DE miRNA predicted targets and *pry-1(mu38)* mRNA transcriptome [25] that included many genes expressed in hypodermal syncytium.

To understand the regulation of miRNAs by *pry-1* we studied the involvement of WNT asymmetry pathway components using an RNAi approach. It was shown

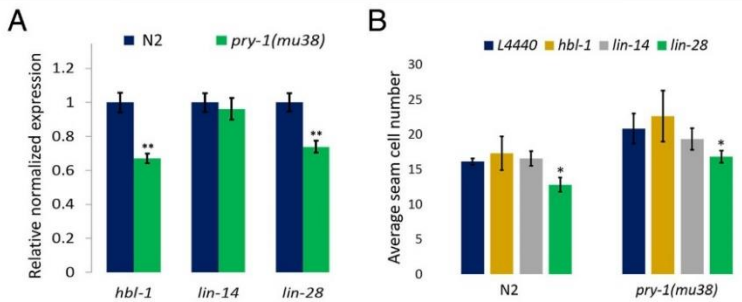

Fig. 6 Analysis of heterochronic genes in *pry-1*-mediated seam cell development. (**a**) qRT-PCR experiments at the L1 stage showed that *hbl-1* and *lin-28* are significantly downregulated in *pry-1(mu38)* animals. Each data point represents the mean of two replicates and error bar represents the SEM, $^{**}p < 0.01$. (**b**) RNAi KD of *lin-28* in *pry-1(mu38)* mutants rescued the seam cell defect. Each data point represents the mean of three batches (each batch with at least 30 worms) and error bar represents the STD. Student's *t*-test was used to determine the statistical significance: $^{*}p < 0.05$ (compared to L4440 control)

earlier that in the absence of PRY-1, localizations of WRM-1, LIT-1, and SYS-1 are disrupted [23, 34]. As expected, the examination of seam cell phenotypes in *pry-1(mu38)* animals following RNAi knockdowns of these genes revealed that *wrm-1* and *lit-1* are necessary for *pry-1* function. Thus, PRY-1 may affect seam cell number by localizing in the anterior cortex of dividing seam cells [23] and thereby lowering WRM-1 and LIT-1-mediated nuclear POP-1 levels in anterior daughters. This plausible explanation is supported by our finding that POP-1 asymmetry is affected in animals with reduced PRY-1 function. To test this further, we examined miRNA expression in *pop-1(hu9)* and *pop-1(RNAi)* worms. As expected, all five (*lin-4, miR-48, miR-84, miR-237,* and *miR-241*) were found to be overexpressed. Moreover, multiple TCF/LEF binding sites were detected in the 5′ regulatory regions of miRNAs. Together, these findings raise the possibility of POP-1 acting as a transcriptional regulator of miRNAs.

We thus propose a model summarizing our findings (Fig. 7), in which PRY-1 acts upstream of WRM-1, LIT-1, POP-1, and DE miRNAs (except *miR-246*). Since the miRNAs regulate the expression of protein-coding genes during heterochronic development, we tested three of their known targets *hbl-1, lin-14,* and *lin-28*. The results of our experiments suggested that *hbl-1* and *lin-28* act downstream of *pry-1*; however, only *lin-28* appears to function in *pry-1*-mediated asymmetric cell division. The above genetic interactions are consistent with earlier findings where *lin-28* was shown to act downstream of the WNT asymmetry pathway components and included in a network consisting of *lin-4* and *let-7*-family of miRNAs and their targets during seam cell development [17, 18]. Our model is unique in that it places PRY-1 upstream of WRM-1, LIT-1, and POP-1-mediated miRNA transcriptional network.

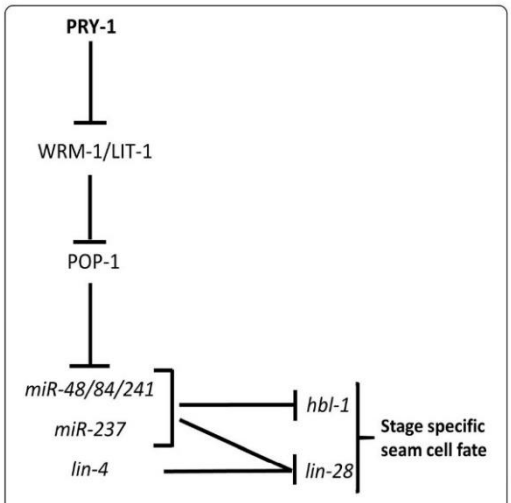

Fig. 7 A model summarizing genetic interactions between PRY-1, WNT asymmetric pathway components (WRM-1, LIT-1, and POP-1), heterochronic miRNAs, and the targets of heterochronic miRNAs during L2 stage seam cell development. Our data supports the Ren and Zhang model [18] and places the WNT asymmetric pathway upstream of miRNAs

Conclusions

Overall, the data presented in this paper demonstrate the important role of PRY-1/Axin in the regulation of miRNAs and their heterochronic gene targets in a pathway that involves WNT asymmetry pathway components WRM-1, LIT-1, and POP-1 during seam cell development. Furthermore, since seam cell defects are also exhibited by *C. briggsae pry-1* mutants, and that *Cbr-pry-1* is necessary for the normal expression of these miRNA orthologs, our work has revealed that the role of *pry-1* in seam cell development is conserved amongst nematodes.

Methods

Strains, culture condition, and RNAi

Nematodes were grown on standard NG-agar culture plates seeded with *E. coli* bacteria (OP50) [43]. Cultures were maintained at 20 °C. Strains used in the study are listed in a supplementary table (Additional file 10: Table S4). RNAi-mediated gene silencing was performed using a protocol previously published by our laboratory [24].

Microscopy

Nematodes were mounted on a glass slide containing 2% agarose and 0.02 M NaN_3 and observed using an Axiovision Zeiss microscope. Seam cell nuclei were counted, and adult lateral alae were scored using Nomarski differential interference contrast and epifluorescence optics. Images were acquired using NIS Element software (Nikon, USA) with a Hamamastu Camera that was mounted on a Nikon 80i upright microscope.

Analysis of seam cell division

The fates of daughter seam cells were determined in *C. elegans* using *scm::GFP* and *ajm-1::GFP* markers, and in *C. briggsae* using the seam cell adherens-junction marker, *Cel-dlg-1::GFP*. After 8 h of feeding, nematodes expressing GFP that had completed the first larval seam cell division, and that had 10 seam cells per side, were chosen for analysis. Seam cell divisions were monitored at approximately 6 h intervals until the late L4 stage, when divisions ceased.

Cuticle integrity assay

A solution containing 1% hypochlorite and 0.25 M NaOH was prepared as previously reported [44], and aliquoted (500 μl) into a 48-well plate. Individual gravid

adult worms were transferred to each well, and the plate was agitated at 30 s intervals. The time to the first major cuticle break was recorded by direct observation using a dissecting stereoscope (SMZ 645; Nikon Corporation, Japan).

Molecular biology and bioinformatics

For qRT-PCR experiments, synchronous cultures were prepared by bleaching gravid hermaphrodites as described previously [45] except that eggs were allowed to hatch on the NG-agar plates. The bleaching process was repeated. The eggs were finally transferred onto plates and grown till the desired stage. Because *pry-1* mutants grow slower than controls, RNA was extracted from age-matched animals. The L1 larvae were grown till 16 h (N2/AF16) and 18 h (*pry-1* mutants) whereas adults were incubated for 52 h (N2/AF16) and 58 h (*pry-1* mutant). Total RNA was extracted from animals using the trizol reagent (Catalog Number T9424, Sigma-Aldrich, Canada), according to the manufacturer's instructions. cDNAs for protein-encoding genes and miRNAs were synthesized using oligo-dT and specific stem-loop primers, respectively (Additional file 11: Table S5), and by using the qScript cDNA synthesis kit (Catalog Number 95047–025, Quantabio, Canada) according to manufacturer's instructions.

qRT-PCR was performed (in triplicate) in the Bio-Rad cycler CFX 96 using appropriate primers (Additional file 11: Table S5), and SensiFAST SYBR Green Kit (Catalog Number BIO-98005, BIOLINE, USA), according to the manufacturer's instructions. The expression levels of miRNAs and protein-coding genes were normalized to those of *miR-2* and *pmp-3,* respectively. Ct and *p* values were calculated using CFX manager software (Bio-Rad, Canada).

A *lin-28* RNAi plasmid was constructed by inserting 2949 bp of the *lin-28* coding sequence into the L4440 vector. A DNA fragment was obtained via PCR using the listed primers (Additional file 11: Table S5), under the specified PCR conditions.

To identify TCF/LEF family binding sites in the 5′ upstream genomic region of the miRNAs, MatInspector software (https://www.genomatix.de/) was used with default settings.

RNA-Seq experiment

The steps for miRNA RNA-Seq in *pry-1(mu38)* mutants were similar to mRNA RNA-Seq that we reported earlier [25]. The *pry-1* miRNA transcriptome profile can be found in the GEO archive with accession number GSE130039. Synchronized L1 worms were harvested by two successive bleaching to obtain a homogenous population and total RNA was isolated. Small RNA sequencing libraries were prepared, and samples were analysed using the Genome Analyzer IIx platform (Illumina Inc., USA) at the McGill University Genome Quebec sequencing facility.

A total of 36,656,022 reads of small RNAs (15–25 nt) were generated from the four samples of *C. elegans* examined, of which 10,453,527 sequences aligned perfectly to the *C. elegans* genome. Overall, we detected perfect matches to the precursor forms of 161 out of the 250 miRNAs annotated in miRBase (http://www.mirbase.org) WBcel235 for *C. elegans*. DE analysis of the known miRNAs led to identification of eight miRNAs that were altered in *pry-1* mutants, of which two (*miR-353* and *miR-2208a*) were excluded due to false predictions (Additional file 2: Table S1).

Although previous studies have reported miRNAs in the *C. elegans* genome (e.g., see [42, 46], due to increased depth of our sequencing data we expected to uncover additional new candidates. After eliminating rRNA, tRNA, and ncRNA reads, the remaining unannotated reads were processed for novel miRNA discovery, as discussed below. We focused on the 30,300 non-redundant un-annotated reads that aligned to the *C. elegans* genome in control N2 and *pry-1(mu38)* animals. To discover novel miRNAs, the miRNA discovery package miRDeep2 (https://www.mdc-berlin.de/n-rajewsky#t-data,software&resources) was used. The analysis predicted a total of 243 miRNAs using read count cut-off of 5-fold (or 187 with cut-off of 10-fold) (Additional file 3: Table S2). We then used an additional criterion to further examine these candidates, i.e., a higher miRDeep Score (> 10). This led to the identification of 64 novel miRNAs at the 5-fold read count cut-off (or 61 when the read count was set at 10-fold) (Additional file 3-4: Table S2, S3). The authenticity of these novel miRNAs was tested by RNAfold, which confirmed that these produce miRNA stem loop structure [47].

Statistical analyses

Statistics were performed by two-tailed student's *t* test after testing for equal distribution of the data and equal variances within the data set. The *p* values of 0.05 and less were considered statistically significant. The data are presented as either mean ± standard deviation of the mean (STD) or mean ± standard error of mean (SEM). Graphs were prepared using Microsoft Excel. Hypergeometric probability related tests were done using an online program (http://nemates.org/MA/progs/overlap_stats.html).

Additional files

Additional file 1: Figure S1. *C. elegans pry-1* open reading frame showing the region affected by *gk3682* mutation. The exons and introns are indicated by boxes and lines, respectively. The translational start and stop sites are marked. The sequence deleted in *gk3682* allele (738 bp) is shown by a rectangle. As part of the CRISPR editing process, the excised

portion is replaced by a 5419 bp *myo-2::GFP* containing cassette. The allele and sequencing data were kindly provided by Dr. Moerman's lab. (TIF 157 kb)

Additional file 2: Table S1. A list of miRNAs in *pry-1(mu38)* animals. The file contains two spreadsheets that list all miRNAs identified by RNA-Seq experiment (used for volcano plot, see Fig. 3a) and DE miRNAs. (DOCX 33 kb)

Additional file 3: Table S2. Total number of novel miRNAs in *C. elegans*. The table shows the number of predicated miRNAs based on different miRDeep scores and read count cut-offs. (DOCX 16 kb)

Additional file 4: Table S3. A list of novel miRNAs in *C. elegans*. The IDs of miRNAs are based on the sequential numbering of unique reads in our analysis. For each novel miRNA, the table lists the miRDeep score, read count, chromosomal location, and the sequence. (XLSX 25 kb)

Additional file 5: Figure S2. Tissue-enrichment analysis of DE miRNAs. The analysis was done using the miRNA discovery tool miRDeep2 (see the RNA-Seq section in Methods). For each miRNA, colored areas represent tissue-specific expression. (DOCX 13 kb)

Additional file 6: Figure S3. Adult stage qRT-PCR analysis of heterochronic miRNAs in *C. elegans* and *C. briggsae pry-1* mutants. (A) *pry-1(mu38)* adults show differences in the pattern of miRNA expression compared to the L1 stage. All miRNAs, except *lin-4* and *miR-48*, are downregulated. (B) *Cbr-pry-1(sy5353)* adults show altered expression of *miR-246*, *miR-48* and *miR-84*. Each data point represents the mean of two replicates and error bar represents the SEM, $*p < 0.05$, $**p < 0.01$ (XLSX 380 kb)

Additional file 7: Figure S4. miRNA expression analysis in *pry-1(mu38)* adults using a *GFP* reporter. (A) Representative images of *PmiR-48::GFP*, *PmiR-84::GFP*, *PmiR-241::GFP*, and *PmiR-246::GFP* reporters in control N2 and *pry-1(mu38)* animals. The scale bar is 0.1 mm. (B) Quantification of fluorescence intensity using an arbitrary unit (a.u.) scale. Each data point represents the mean of two replicates (at least 20 animals each) and error bar represents the STD. Student's *t*-test was used to determine the statistical significance: $*p < 0.05$. (TIF 9966 kb)

Additional file 8: Figure S5. Representative images of control N2 and *miR-246(n4636)* mutants showing hypodermal cells (based on *dpy-7::H1-wcherry* reporter). The mutant animal shows fewer hypodermal cells. *(TIF 4047 kb)*

Additional file 9: Figure S6. Line drawings of TCF/LEF putative binding sites in the 5′ upstream regions of miRNA genes (within 1500 bp of transcriptional start site). Each putative binding site is shown by a coloured square box. The numbers in brackets next to boxes show matrix similarity scores. (TIF 8102 kb)

Additional file 10: Table S4. A list of strains used in this study. (TIF 10153 kb)

Additional file 11: Table S5. A list of primers used in this study. (TIF 7309 kb)

Abbreviations

DE: Differentially expressed; GO: Gene ontology; miRNAs: microRNAs; MRE: miRNA response element; NLK: NEMO-like kinase; qRT-PCR: quantitative real-time PCR; SEM: Standard error of the mean; STD: Standard deviation; TCF/LEF: T-cell factor/lymphoid enhancer factor

Acknowledgements

We are grateful to Brian Golding (McMaster University) for providing access to his lab computer server and Don Moerman's lab (University of British Columbia) for generating the *pry-1(gk3682)* CRISPR/Cas9 allele. Lesley MacNeil and Ian Chin-Sang kindly provided comments on a previous draft of the manuscript. Some of the strains were obtained from Caenorhabditis Genetic Center (CGC), which is funded by the NIH Office of Research Infrastructure Programs (P40OD010440).

Authors' contributions

AM, AR, and BG designed the study. AM and AR performed experiments. AM and BG wrote the manuscript. BG supervised the project. All authors have read and approved the manuscript.

Funding

This work was supported by a Discovery grant from the Natural Sciences and Engineering Research Council of Canada (http://www.nserc-crsng.gc.ca) to Bhagwati Gupta. The funder had no role in study design, data collection and analysis, decision to publish, or preparation of the manuscript.

Availability of data and materials

The datasets supporting the conclusions of this article are provided in figures, tables, and additional files. miRNA transcriptome data of *pry-1* mutants can be found in the NCBI GEO archive database with accession number GSE130039.

Ethics approval and consent to participate

Not Applicable.

Consent for publication

Not Applicable.

Competing interests

The authors declare that they have no competing interests.

Author details

[1]Department of Biology, McMaster University, ON L8S-4K1, Hamilton, Canada. [2]Department of Physics, Harvard University, NW256, 52 Oxford St, Cambridge, MA 02138, USA.

Received: 28 May 2019 Accepted: 4 July 2019
Published online: 15 July 2019

References

1. Hall DH, Altun ZF. *C. elegans* Atlas. New York: Cold Spring Harbor Laboratory Press; 2008.
2. Ambros V, Horvitz HR. Heterochronic mutants of the nematode Caenorhabditis elegans. Science. 1984;226(4673):409–16.
3. Lee RC, Feinbaum RL, Ambros V. The C. elegans heterochronic gene lin-4 encodes small RNAs with antisense complementarity to lin-14. Cell. 1993; 75(5):843–54.
4. Wightman B, Ha I, Ruvkun G. Posttranscriptional regulation of the heterochronic gene lin-14 by lin-4 mediates temporal pattern formation in C. elegans. Cell. 1993;75(5):855–62.
5. Moss EG, Lee RC, Ambros V. The cold shock domain protein LIN-28 controls developmental timing in C. elegans and is regulated by the lin-4 RNA. Cell. 1997;88(5):637–46.
6. Slack FJ, Basson M, Liu Z, Ambros V, Horvitz HR, Ruvkun G. The lin-41 RBCC gene acts in the C. elegans heterochronic pathway between the let-7 regulatory RNA and the LIN-29 transcription factor. Mol Cell. 2000;5(4):659–69.
7. Reinhart BJ, Slack FJ, Basson M, Pasquinelli AE, Bettinger JC, Rougvie AE, Horvitz HR, Ruvkun G. The 21-nucleotide let-7 RNA regulates developmental timing in Caenorhabditis elegans. Nature. 2000;403(6772):901–6.
8. Tsialikas J, Romens MA, Abbott A, Moss EG. Stage-specific timing of the microRNA regulation of lin-28 by the Heterochronic gene lin-14 in Caenorhabditis elegans. Genetics. 2017;205(1):251–62.
9. Abbott AL, Alvarez-Saavedra E, Miska EA, Lau NC, Bartel DP, Horvitz HR, Ambros V. The let-7 MicroRNA family members mir-48, mir-84, and mir-241 function together to regulate developmental timing in Caenorhabditis elegans. Dev Cell. 2005;9(3):403–14.
10. Banerjee D, Slack F. Control of developmental timing by small temporal RNAs: a paradigm for RNA-mediated regulation of gene expression. Bioessays. 2002;24(2):119–29.
11. Fay DS, Stanley HM, Han M, Wood WB. A Caenorhabditis elegans homologue of hunchback is required for late stages of development but not early embryonic patterning. Dev Biol. 1999;205(2):240–53.
12. Hong Y, Lee RC, Ambros V. Structure and function analysis of LIN-14, a temporal regulator of postembryonic developmental events in Caenorhabditis elegans. Mol Cell Biol. 2000;20(6):2285–95.
13. Ruvkun G, Giusto J. The Caenorhabditis elegans heterochronic gene lin-14 encodes a nuclear protein that forms a temporal developmental switch. Nature. 1989;338(6213):313–9.
14. Viswanathan SR, Daley GQ, Gregory RI. Selective blockade of microRNA processing by Lin28. Science. 2008;320(5872):97–100.

15. Lehrbach NJ, Armisen J, Lightfoot HL, Murfitt KJ, Bugaut A, Balasubramanian S, Miska EA. LIN-28 and the poly(U) polymerase PUP-2 regulate let-7 microRNA processing in Caenorhabditis elegans. Nat Struct Mol Biol. 2009; 16(10):1016–20.
16. Tsialikas J, Romer-Seibert J. LIN28: roles and regulation in development and beyond. Development. 2015;142(14):2397–404.
17. Harandi OF, Ambros VR. Control of stem cell self-renewal and differentiation by the heterochronic genes and the cellular asymmetry machinery in Caenorhabditis elegans. Proc Natl Acad Sci U S A. 2015;112(3):E287–96.
18. Ren H, Zhang H. Wnt signaling controls temporal identities of seam cells in Caenorhabditis elegans. Dev Biol. 2010;345(2):144–55.
19. Gleason JE, Eisenmann DM. Wnt signaling controls the stem cell-like asymmetric division of the epithelial seam cells during C. elegans larval development. Dev Biol. 2010;348(1):58–66.
20. Maduro MF, Lin R, Rothman JH. Dynamics of a developmental switch: recursive intracellular and intranuclear redistribution of Caenorhabditis elegans POP-1 parallels Wnt-inhibited transcriptional repression. Dev Biol. 2002;248(1):128–42.
21. Phillips BT, Kidd AR 3rd, King R, Hardin J, Kimble J. Reciprocal asymmetry of SYS-1/beta-catenin and POP-1/TCF controls asymmetric divisions in Caenorhabditis elegans. Proc Natl Acad Sci U S A. 2007;104(9):3231–6.
22. Shetty P, Lo MC, Robertson SM, Lin R. C. elegans TCF protein, POP-1, converts from repressor to activator as a result of Wnt-induced lowering of nuclear levels. Dev Biol. 2005;285(2):584–92.
23. Mizumoto K, Sawa H. Cortical beta-catenin and APC regulate asymmetric nuclear beta-catenin localization during asymmetric cell division in C. elegans. Dev Cell. 2007;12(2):287–99.
24. Seetharaman A, Cumbo P, Bojanala N, Gupta BP. Conserved mechanism of Wnt signaling function in the specification of vulval precursor fates in C. elegans and C. briggsae. Dev Biol. 2010;346(1):128–39.
25. Ranawade A, Mallick A, Gupta BP. PRY-1/Axin signaling regulates lipid metabolism in Caenorhabditis elegans. PLoS One. 2018;13(11):e0206540.
26. Koh K, Rothman JH. ELT-5 and ELT-6 are required continuously to regulate epidermal seam cell differentiation and cell fusion in C. elegans. Development. 2001;128(15):2867–80.
27. Ren Z, Ambros VR. Caenorhabditis elegans microRNAs of the let-7 family act in innate immune response circuits and confer robust developmental timing against pathogen stress. Proc Natl Acad Sci U S A. 2015;112(18):E2366–75.
28. Lee H, Han S, Kwon CS, Lee D. Biogenesis and regulation of the let-7 miRNAs and their functional implications. Protein Cell. 2016;7(2):100–13.
29. Martinez NJ, Ow MC, Reece-Hoyes JS, Barrasa MI, Ambros VR, Walhout AJ. Genome-scale spatiotemporal analysis of Caenorhabditis elegans microRNA promoter activity. Genome Res. 2008;18(12):2005–15.
30. de Lencastre A, Pincus Z, Zhou K, Kato M, Lee SS, Slack FJ. MicroRNAs both promote and antagonize longevity in C. elegans. Curr Biol. 2010;20(24): 2159–68.
31. Pincus Z, Smith-Vikos T, Slack FJ. MicroRNA predictors of longevity in Caenorhabditis elegans. PLoS Genet. 2011;7(9):e1002306.
32. Banerjee D, Chen X, Lin SY, Slack FJ. Kin-19/casein kinase Ialpha has dual functions in regulating asymmetric division and terminal differentiation in C. elegans epidermal stem cells. Cell Cycle. 2010;9(23):4748–65.
33. Nakamura K, Kim S, Ishidate T, Bei Y, Pang K, Shirayama M, Trzepacz C, Brownell DR, Mello CC. Wnt signaling drives WRM-1/beta-catenin asymmetries in early C. elegans embryos. Genes Dev. 2005;19(15):1749–54.
34. Baldwin AT, Phillips BT. The tumor suppressor APC differentially regulates multiple beta-catenins through the function of axin and CKIalpha during C. elegans asymmetric stem cell divisions. J Cell Sci. 2014;127(Pt 12):2771–81.
35. Cadigan KM, Waterman ML: TCF/LEFs and Wnt signaling in the nucleus. Cold Spring Harb Perspect Biol 2012, 4(11).
36. Bhambhani C, Ravindranath AJ, Mentink RA, Chang MV, Betist MC, Yang YX, Koushika SP, Korswagen HC, Cadigan KM. Distinct DNA binding sites contribute to the TCF transcriptional switch in *C. elegans* and Drosophila. *PLoS Genet*. 2014;10(2):e1004133.
37. Arasu P, Wightman B, Ruvkun G. Temporal regulation of lin-14 by the antagonistic action of two other heterochronic genes, lin-4 and lin-28. Genes Dev. 1991;5(10):1825–33.
38. Feinbaum R, Ambros V. The timing of lin-4 RNA accumulation controls the timing of postembryonic developmental events in Caenorhabditis elegans. Dev Biol. 1999;210(1):87–95.
39. Abrahante JE, Daul AL, Li M, Volk ML, Tennessen JM, Miller EA, Rougvie AE. The Caenorhabditis elegans hunchback-like gene lin-57/hbl-1 controls developmental time and is regulated by microRNAs. Dev Cell. 2003;4(5): 625–37.
40. Lin SY, Johnson SM, Abraham M, Vella MC, Pasquinelli A, Gamberi C, Gottlieb E, Slack FJ. The C elegans hunchback homolog, hbl-1, controls temporal patterning and is a probable microRNA target. Dev Cell. 2003;4(5):639–50.
41. Li M, Jones-Rhoades MW, Lau NC, Bartel DP, Rougvie AE. Regulatory mutations of mir-48, a C. elegans let-7 family MicroRNA, cause developmental timing defects. Dev Cell. 2005;9(3):415–22.
42. Lim LP, Lau NC, Weinstein EG, Abdelhakim A, Yekta S, Rhoades MW, Burge CB, Bartel DP. The microRNAs of Caenorhabditis elegans. Genes Dev. 2003; 17(8):991–1008.
43. Brenner S. The genetics of *Caenorhabditis elegans*. Genetics. 1974;77:71–94.
44. Watts JL, Phillips E, Griffing KR, Browse J. Deficiencies in C20 polyunsaturated fatty acids cause behavioral and developmental defects in Caenorhabditis elegans fat-3 mutants. Genetics. 2003;163(2):581–9.
45. Sharanya D, Thillainathan B, Marri S, Bojanala N, Taylor J, Flibotte S, Moerman DG, Waterston RH, Gupta BP: Genetic control of vulval development in *Caenorhabditis briggsae. G3 (Bethesda)* 2012, 2(12):1625–1641.
46. Grad Y, Aach J, Hayes GD, Reinhart BJ, Church GM, Ruvkun G, Kim J. Computational and experimental identification of C. elegans microRNAs. Mol Cell. 2003;11(5):1253–63.
47. Hofacker IL. Vienna RNA secondary structure server. Nucleic Acids Res. 2003; 31(13):3429–31.

Publisher's Note

Springer Nature remains neutral with regard to jurisdictional claims in published maps and institutional affiliations.

Chapter 4

PRY-1/Axin signaling regulates lipid metabolism in *Caenorhabditis elegans*

4.1 Preface

This chapter includes the following two articles in its originally published format: "PRY-1/Axin signaling regulates lipid metabolism in *Caenorhabditis elegans*", by Ayush Ranawade, Avijit Mallick and Bhagwati P. Gupta. PLoS One. 13(11): e0206540 (DOI: 10.1371/journal.pone.0206540) and "Vitellogenin-2 acts downstream of PRY-1/Axin to regulate lipids and lifespan in *C. elegans*", by Avijit Mallick and Bhagwati P. Gupta. micropublication Biology (DOI: 10.17912/micropub.biology.000281). These are open-access articles distributed under the terms of the Creative Commons

4.2 Ranawade, Mallick and Gupta (2018)- PLoS One

In this study, we report the mRNA transcriptomic of *pry-1(mu38)* mutants at the L1 stage. Our analysis of the RNAseq data revealed differentially expressed genes associated with various biological processes. Among those, one of the most enriched GO term biological processes was lipid metabolism. These set of genes were linked to lipid synthesis (fatty acid desaturases), lipid transportation (vitellogenin), lipid oxidation (*acdh-1*, -6, *-11*, *-23*, *acs-2*, *-11*, and *-17*, *cpt-1*, *-4*, and *ech-9)*, and lipid breakdown (lipases). Consistent with this analysis, *pry-1* mutants exhibited depleted lipid storage coupled with poor brood size and poor survivability of L1 starved animals. Such a reduced lipid storage seen in these animals is mostly due to compromised fatty acid synthesis as revealed by our GC-MS analysis. Supporting this finding, Oleic acid supplementation rescued the lipid levels in the *pry-1* mutants. Furthermore, we focused on the vitellogenin species (*vit-1 to vit-6*) known for their role in lipid uptake from the intestine to the gonad during the reproductive period. Knocking down *vits* by RNAi rescued the lipid defect in the *pry-1(mu38)* animals suggesting that vitellogenin act downstream of PRY-1 to regulate lipid level. Overall, our data demonstrated that PRY-1 plays an important role in regulating lipid synthesis and utilises SBP-1/SREBP transcription factor to modulate fatty acid synthesis.

Contributions: I performed experiments and provided data for Figures 4, 5C-F, S3, S4, S6, S7, S8 and S9. Ayush Ranawade performed the RNA-seq analysis in the *pry-*

1(mu38) animals at the L1 stage and carried out the analysis for target prediction coupled with GO enrichment analysis. Rest of the data were provided by Ayush Ranawade. I and Bhagwati Gupta created all the Figures and illustrations. Bhagwati Gupta conceived and supervised the project. Ayush Ranawade, I and Bhagwati Gupta wrote the manuscript. It was finally revised with addressed reviewers concerns by me and Bhagwati Gupta.

PLOS ONE

RESEARCH ARTICLE

PRY-1/Axin signaling regulates lipid metabolism in *Caenorhabditis elegans*

Ayush Ranawade[☯¤], **Avijit Mallick**[☯], **Bhagwati P. Gupta***

Department of Biology, McMaster University, Hamilton, Ontario, Canada

☯ These authors contributed equally to this work.
¤ Current address: Department of Physics, Harvard University, Cambridge, Massachusetts, United States of America
* guptab@mcmaster.ca

Check for updates

OPEN ACCESS

Citation: Ranawade A, Mallick A, Gupta BP (2018) PRY-1/Axin signaling regulates lipid metabolism in *Caenorhabditis elegans*. PLoS ONE 13(11): e0206540. https://doi.org/10.1371/journal.pone.0206540

Editor: Juan J Loor, University of Illinois, UNITED STATES

Received: June 27, 2018

Accepted: October 15, 2018

Published: November 7, 2018

Data Availability Statement: The pry-1 transcriptome profile can be found in the GEO archive with accession number GSE94412 (https://www.ncbi.nlm.nih.gov/geo/query/acc.cgi?acc=GSE94412).

Funding: This work was supported by a Discovery grant from the Natural Sciences and Engineering Research Council of Canada to Bhagwati Gupta (http://www.nserc-crsng.gc.ca). The funder had no role in study design, data collection and analysis, decision to publish, or preparation of the manuscript.

Abstract

The nematode *Caenorhabditis elegans* constitutes a leading animal model to study how signaling pathway components function in conserved biological processes. Here, we describe the role of an Axin family member, PRY-1, in lipid metabolism. Axins are scaffolding proteins that play crucial roles in signal transduction pathways by physically interacting with multiple factors and coordinating the assembly of protein complexes. Genome-wide transcriptome profiling of a *pry-1* mutant revealed differentially regulated genes that are associated with lipid metabolism such as vitellogenins (yolk lipoproteins), fatty acid desaturases, lipases, and fatty acid transporters. Consistent with these categorizations, we found that *pry-1* is crucial for the maintenance of lipid levels. Knockdowns of *vit* genes in a *pry-1* mutant background restored lipid levels, suggesting that vitellogenins contribute to PRY-1 function in lipid metabolic processes. Additionally, lowered expression of desaturases and lipidomic analysis provided evidence that fatty acid synthesis is reduced in *pry-1* mutants. Accordingly, an exogenous supply of oleic acid restored depleted lipids in somatic tissues of worms. Overall, our findings demonstrate that PRY-1/Axin signaling is essential for lipid metabolism and involves the regulation of yolk proteins.

Introduction

Axin was identified initially as a negative regulator of the WNT-signaling pathway [1]. Subsequently, Axin family members were shown to also be essential in numerous developmental events including embryogenesis, axis formation, cell differentiation, and tissue homeostasis [2–5]. As a scaffolding protein Axin plays a key role in the regulation of canonical WNT pathway function. It contains multiple domains that facilitate homodimerization and interactions with the destruction-complex proteins Dishevelled, APC, and GSK-3β [4, 6]. In turn, the destruction complex initiates the phosphorylation and consequent proteolysis of the transcriptional regulator β-Catenin, which promotes expression of WNT target genes [4, 6]. Constitutive activation of β-Catenin, consequent to the loss of destruction-complex function, is often associated with cancers and various other disorders affecting the lungs, heart, muscles, and

Competing interests: The authors have declared that no competing interests exist.

bones [4]. Thus, Axin function is crucial toward ensuring precise regulation of β-Catenin-mediated WNT signaling. In addition to WNT pathway components, Axin homologs also interact with various other factors such as Smad3, MEKK4, and LKB1 to affect diverse processes, for example cell proliferation, metabolic homeostasis, and tissue aging [7–10]. However, the mechanism of Axin function in these processes is not fully understood.

In *Caenorhabditis elegans*, PRY-1 is a member of the Axin family that is involved in multiple events such as cell fate specification, neuronal differentiation, and tissue formation [11–13]. Molecular genetic experiments have shown that PRY-1 interacts with APR-1/APC and GSK-3/GSK-3β to regulate BAR-1/β-Catenin-mediated gene transcription [14]. The phenotypes of *pry-1* mutants are consistent with overactivation of WNT signaling, such as Q cell migration and vulval induction [13, 14]. Our group has been investigating *pry-1* role in developmental as well as post-developmental processes. To identify genes that interact with *pry-1*, we performed a genome-wide transcriptome profiling experiment. Among the genes that were differentially expressed many were found to be associated with lipid metabolism. Consistent with this, *pry-1* mutant animals showed reduced lipid level. We examined a subset of differentially regulated genes, specifically yolk lipoproteins vitellogenins (VITs), which are important for lipid distribution [15], in mediating *pry-1* function. Knockdowns of *vit* genes by RNA interference (RNAi) rescued lipid defects in *pry-1* mutants. We also found that the expression of three conserved stearoyl-CoA-desaturases, *fat-5*, *fat-6*, and *fat-7*, which are involved in the synthesis of monounsaturated fatty acids such as oleic acid (OA) [16–18], was reduced in *pry-1* mutants. In support of this, supplementing the bacterial diet of mutant animals with OA partially rescued the lipid phenotype. These results provide evidence for the important role of PRY-1 in lipid metabolism through the regulation of vitellogenesis.

Materials and methods

Strains

Worms were grown on standard Nematode Growth Medium (NGM) agar plates using procedure described previously [19]. Cultures were maintained at 20 ˚C unless mentioned otherwise. The *mu38* allele of *pry-1* was obtained from CGC. All strains were outcrossed at least three times before doing the experiments.

The genotypes of the strains used in this study are: N2 (wild-type), DY220 *pry-1(mu38) I*, DY656 *pry-1(mu38) I; ldrIs2[mdt-28p::mdt-28::mCherry]*, EW15 *bar-1(ga80) X*, LIU2 *ldrIs2 [mdt-28p::mdt-28::mCherry]*, PS4943 *huIs[dpy-20;hsp16-2::dNT-bar-1]; syIs148[pT00.49 + unc-119(+)]*, RB1982 *vit-1(ok2616) X*, RB2365 *vit-2(ok3211) X*, RB2202 *vit-4(ok2982) X*, RB2382 *vit-5(ok3239) X*, STE68 *nhr-49(nr2041) I*, STE70 *nhr-80(tm1011) III*.

Heat shock treatments

For lipid quantification, *hsp-16-2::dNT-bar-1* (termed as *hs::dNT-bar-1*) animals were age synchronized and grown at 20 ˚C till young adult after which they were heat treated at 38 ˚C for 30 min or 30 ˚C for 12 hours. Subsequently, the animals were incubated at 20 ˚C for one hour before carrying out lipid staining. For qPCR analysis, *hs::dNT-bar-1* eggs were incubated for 16 hours. The hatched L1 animals were heat treated at 38 ˚C for 30 min. They were then allowed to recover for 90 min at 20 ˚C prior to extraction of RNA.

Molecular Biology

For qRT-PCR experiments mRNA was extracted from bleach synchronized worms by Tri-reagent (Catalog Number T9424, Sigma-Aldrich Canada) according to the manufacturer's

instructions. cDNA was synthesized from total RNA using oligo (dT) primers and other reagents in the ProtoScript First Strand cDNA Synthesis Kit (Catalog Number E6300S, NEB, Canada). Quantitative real-time PCR (qRT-PCR) analysis was performed on a CFX 96 BioRad cycler in triplicate with SensiFAST SYBR Green Kit (Catalog Number BIO-98005, USA), according to manufacturer's instructions. *pmp-3* was used as a reference gene in all assays. CFX manager was used for the Ct and *p*-value calculations. The primers used in this study are listed in S1 Table.

RNAi

For RNAi experiments, *Escherichia coli* HT115 expressing target specific dsRNA were grown on plates containing β-lactose [20]. Worms were age synchronized by bleach treatment and seeded onto plates. After becoming young adults, worms were transferred to fresh plates every other day and the numbers of dead worms were recorded. For adult specific RNAi, synchronized worms were cultivated on NGM/OP50 plates until the young adult stage and then transferred to the RNAi plates.

Lipid analysis by Oil Red O staining and fluorescence measurements

Oil Red O (Sigma-Aldrich, Canada, Catalog number O0625-25G) staining was performed as previously reported [21]. Briefly, worms were collected from NGM plates, washed with 1x phosphate-buffered saline (PBS) buffer (pH 7.4), and re-suspended in 60 μl of 1x PBS, 120 μl of 2x MRWB buffer (160 mM KCl, 40 mM NaCl, 14 mM Na_2-EGTA, 1 mM spermidine-HCl, 0.4 mM spermine, 30 mM Na-PIPES [Na-piperazine-*N*, *N*′-bis (2-ethanesulfonic acid); pH 7.4], 0.2% β-mercaptoethanol), and 60 μl of 4% paraformaldehyde. The worms were then freeze-thawed three times and washed twice with 1x PBS. They were then incubated at room temperature in 60% isopropyl alcohol for 10 minutes for dehydration and stained with freshly prepared Oil Red O solution for at least 48 hours on a shaker. For direct and consistent comparison, all Oil Red O images from the same experiment were acquired under identical settings and exposure times. Animals were mounted and imaged using Q-imaging software and a Micropublisher 3.3 RTV color camera outfitted with DIC optics on a Nikon 80i microscope. NIH ImageJ software (https://imagej.nih.gov/ij/) was used to quantify Oil Red O intensities as described previously [21]. A total of 15 to 30 worms were randomly selected from each category in at least two separate batches.

For lipid quantification using fluorescent mCherry marker, animals were paralyzed in 10 mM Sodium Azide and mounted on glass slide carrying 2% agar pads. Images were acquired using NIS Element software (Nikon, USA) and a Hamamatsu Camera attached to a Nikon Eclipse 80i upright Nomarski microscope. At least two batches of animals, each containing 20 or more, were examined. All images were acquired under fixed software settings. Quantification of pixel densities was performed using Image J.

Brood assay

Worms were bleach synchronized and allowed to grow to L4 stage for determining the progression of egg-laying and the brood size. Individual worms were picked onto a separate NGM plate with *E. coli* OP50 bacteria and allowed to grow for several days. Worms were transferred routinely to freshly seeded NGM plates and progeny were counted every 24 hours. Data from escaping or dying mothers were omitted from the analyses [22].

Oleic acid supplementation assay

To make Oleic acid (OA) supplemented NGM agar plates, a 0.1 M water-based stock solution of OA sodium salt (NuCheck Prep, USA, Catalog number U-46-A) was prepared and stored at –20 °C in the dark. The OA solution was added continuously to the NGM and promptly poured into the plates. The plates were covered with aluminum foil and kept at room temperature overnight to dry. The *E. coli* OP50 strain was seeded onto each plate and allowed to further dry for one to two days in the dark. Oil Red O staining was performed as described above [23].

Lipase assay

Lipase activity was estimated using commercially available QuantiChrom Lipase Assay Kit (BioAssay Systems, USA, Catalog number DLPS-100) and processed according to the manufacturer's instructions. 1 unit of Lipase catalyzes the cleavage of 1 μmol substrate per minute. Three independent samples of one-day-adult worms were prepared by homogenizing in a solution (20% glycerol, 0.1 M KCl, 20 mM HEPES pH 7.6). Measurements were done as described earlier [24].

L1 survival assay

Worms were bleach synchronized and kept in a 1.5 ml centrifuge tube. The progeny were seeded onto NGM plates approximately 24 hours later and transferred regularly for 12 days. Worms were grown to young adult stage before counting the survivors. The data was statistically compared using an analysis of covariance (ANCOVA) model.

RNA-Seq and data analysis

pry-1 targets were examined in synchronized L1 stage animals. At this stage WNT ligands, receptors, and targets are highly expressed as revealed by microarray studies from SPELL database [25, 26] (S1A–S1D Fig). Also, our qRT-PCR experiments showed significant upregulation of three of the WNT targets, *lin-39*, *egl-5* and *mab-5*, in *pry-1* mutants at L1 stage (S1D Fig). The *pry-1* transcriptome profile can be found in the GEO archive with accession number GSE94412. For RNA-Seq experiments synchronized L1 stage animals were obtained by two successive bleach treatments and RNA was isolated using Trizol-reagent (Sigma, USA, Catalog Number T9424) [27]. The quality of total purified RNA was confirmed using bioanalyzer (Agilent 2100 and Nanodrop 1000). cDNA libraries were constructed from 100–200ng mRNA using an Illumina-specific commercial kit (TruSeq RNA Sample Preparation Kit v2, Set A, Catalog number RS-122-2001). RNA sequencing was carried out using Illumina Hi-Seq 2000 system at the McGill University Genome Quebec sequencing facility. For each of the N2 and *pry-1(mu38)* strains two biological replicates were used. For each cDNA library, 100 bp paired-end reads were obtained. In total, 30 to 38 million reads were obtained for each sample analyzed for differential gene expression.

The adapters were trimmed using cutadapt/trimgalore, reads with QC values (Phred score) lower than 30 bases were discarded after trimming [28]. Later, processed sequencing reads were mapped to the reference genome (ce6) (UCSC 2013) using the software package Bowtie 1.0.0 [29]. 92–95% of total sequenced fragments could be mapped to the genome (S2 Table). Transcript-level abundance estimation was performed using eXpress 1.5 software package [30]. Among all genes analyzed, we were able to map 18,867 to known transcripts by at least one sequencing fragment in *C. elegans*. To avoid biases between samples, the gene counts were

quantile normalized [28, 31]. Using a negative binomial distribution model of DESeq package in R, differentially-expressed genes were called at a false discovery rate (FDR) of 0.05% [32].

GO analysis was carried out with default setting using GoAmigo (http://amigo.geneontology.org). A GO-term containing at least three genes with a p-value adjusted for multiple comparisons and < 0.05 (Benjamini-Hochberg method) was counted significant [33]. Tissue enrichment analysis was performed using Wormbase online TEA tool that employs a tissue ontology previously developed by WormBase [34].

Gas chromatography mass spectrophotometry (GC-MS)

We modified the fatty Acid analysis protocol from a previously published method [16, 35]. Eppendorf tubes, glass vials or any containers used for the extraction process were sonicated in dichloromethane (Caledon Laboratories Ltd., Canada, Catalog number 3601-2-40) for 30 minutes to eliminate lipid contamination. To determine FA composition, we collected few thousand adult worms from three 6-cm plates and removed residual bacteria by washing the animals with sterile water. Washed worms were placed into a screw-capped centrifuge tube and spun at 2,500 RPM for 45 seconds. The residual water was removed using a Pasteur pipette and worms were transferred to glass vials (Agilent, part number 5182–0714) and accurately weighed to 50–100 mg. Fatty acids were then extracted from tissues and transmethylated by adding 1 ml of 2.5% H_2SO_4 (Caledon Laboratories Ltd., Canada, Catalog number 8825-1-05) diluted in methanol (Caledon Laboratories Ltd., Canada, Catalog number 6701-7-40). We spiked the samples with 10 μl of a recovery standard (stearic acid 120 ng/μl, Sigma-Aldrich Canada, Catalog number S4751-1G) and incubated at 80 ˚C for an hour in a water bath. To this, a mixture of 0.2 ml of hexane (Caledon Laboratories Ltd., Canada, Catalog number 3201-7-40) and 1.5 ml of water was added and slowly spun to extract fatty acid methyl esters into the hexane layer. Agilent 6890 series gas chromatographer equipped with a 30 × 0.25 mm SP-2380 fused silica capillary column (Supelco USA), helium as the carrier gas at 1.4 ml/minute, and a flame ionization detector was used for fatty acid analysis. Automatic injections of 1 μl samples in the organic phase were made, without splitting, into the GC inlet set to 250 ˚C. The thermal program began at 50 ˚C for 2 minutes, then increased linearly to 300 ˚C at a ramping rate of 8 ˚C/minute and held this temperature for 15 minutes. A constant flow rate of 1 ml/minute helium carrier gas under electronic pressure control was maintained for the fatty acid composition determination by TIC method using standard software. For quantitation of fatty acids, the peaks across all GC-MS runs were aligned using both chromatographic information (retention times) and mass-spectral data (m/z components) to establish the chemical identity of peaks being compared. We calculated the relative fatty acid amounts by dividing each peak area by the sum of areas for all fatty acid peaks appearing on the same chromatogram. For each fatty acid, the quantities determined by GC-MS were successively normalized in two ways: 1) to an internal standard naphthalene-d8, 10 ng/μl (1 ng/μl in injection sample) added to each sample prior to sonication and lipid extraction), and 2) to the weight of the samples.

Statistical analysis

The statistics were performed using Microsoft Office Excel 2016. If not specifically mentioned, p values for the fertility, motility, fat content, L1 survival, and enzyme activities were calculated using the Student's t test after testing for equal distribution of the data and equal variances within the data set. Experiments were performed in triplicates except where stated otherwise. Differences were considered statistically significant at $p < 0.05$, thereby indicating a probability of error lower than 5%. Hypergeometric probability tests and statistical significance of the

overlap between two gene sets were done using an online program (http://nemates.org/MA/progs/overlap_stats.html).

Results

Identification of PRY-1 targets

To gain insights into the mechanism of *pry-1*-mediated signaling, a genome-wide transcriptome analysis was carried out to identify the potential downstream targets. The RNA-Seq was performed in *pry-1* mutant animals carrying a nonsense allele, *mu38*, that causes constitutive activation of WNT signaling [14]. We identified a total of 2,665 genes (767 upregulated and 1898 downregulated, False Discovery Rate (FDR) *p*-adj 0.05) that were differentially expressed in *pry-1(mu38)* animals during the L1 larval stage (Fig 1A, S3 Table, also see Methods). Of these, the transcription of 1,331 genes was altered twofold or more (FDR, *p*-adj 0.05) (248 upregulated and 1083 downregulated) (S3 Table). The average and median fold changes in the expression were 2.2 and 2.0, respectively. Fig 1A shows a scatter plot of all expressed genes. A subset of these genes was also tested by quantitative polymerase chain reaction (qPCR), which revealed an 85% validation rate (Fig 1F).

We next carried out gene ontology (GO) analysis (www.geneontology.org) to investigate the processes affected in *pry-1(mu38)* animals. Genes with altered expression were found to be enriched in GO terms associated with "determination of adult lifespan", "aging", "response to unfolded protein", "oxidation-reduction process", "metabolism", "stress response and cell signaling", "steroid hormone mediated signaling", "lipid metabolic processes", and "cellular response to lipids" (Fig 1B; a complete list is provided in S4 Table). This suggests that *pry-1* plays a role in stress response, lipid metabolism, and lifespan regulation. We also observed enrichment in neuron-related GO terms such as "axon", "synapse", "synaptic transmission", and "neuron development", which was expected from the requirements of *pry-1* in neuronal development [14]. Other categories included "molting cycle", "regulation of transcription", "DNA-template", and the "reproductive process". In addition to these known categories, the dataset included numerous non-annotated genes (S3 Table) whose functions remain uncharacterized.

Analysis of genes and gene families revealed that several components of Hedgehog (HH) signaling are downregulated in *pry-1(mu38)* animals including warthog genes *wrt-1* and *wrt-9*; groundhog-like genes *grl-1*, *grl-4*, *grl-5*, *grl-6*, *grl-7*, *grl-13*, *grl-16*, and *grl-21*; hedgehog-like genes *grd-3*, *grd-5*, *grd-12*, *grd-14*, and *grd-15*; and patched-related genes *daf-6*, *ptr-1*, *ptr-13*, *ptr-16*, *ptr-19*, *ptr-2*, *ptr-20*, *ptr-21*, *ptr-22*, *ptr-23*, and *ptr-8*. This suggests that *hh*-signaling is affected by *pry-1*. Some of these genes were also recovered earlier in *bar-1* transcriptome studies [36–38], discussed further below. The *ptc* and *ptr* genes promote molting and the trafficking of proteins, sterols, and lipids [39, 40]. In support of such function, we found molting and other cuticle-related defects in *pry-1* mutants (e.g., rollers, defective alae, and weaker cuticle) (Mallick *et al*., manuscript in preparation). These data are consistent with the role of WNT signaling in cuticle development [36].

Alterations in the expression of some of the WNT pathway components were noted as well. For example, *pry-1* was up 1.3 fold (on log2 scale, S3 Table, Fig 1F). Although such upregulation of *pry-1* was not reported previously in *pry-1* mutants, prior studies have shown that Axin constitutes a target of WNT signaling and its expression is increased in overactivated WNT backgrounds [6, 36, 38, 41]. Thus, positive regulation of Axin by the canonical WNT signaling represents a conserved mechanism in eukaryotes. Other WNT pathway components that were differentially expressed in *pry-1(mu38)* included *mom-2/wnt* (1.5-fold increase), *cfz-2/fz* (1.7-fold decrease), *lin-17/fz* (1.6-fold increase), and *pop-1/tcf* (1.7-fold increase) (S3 Table).

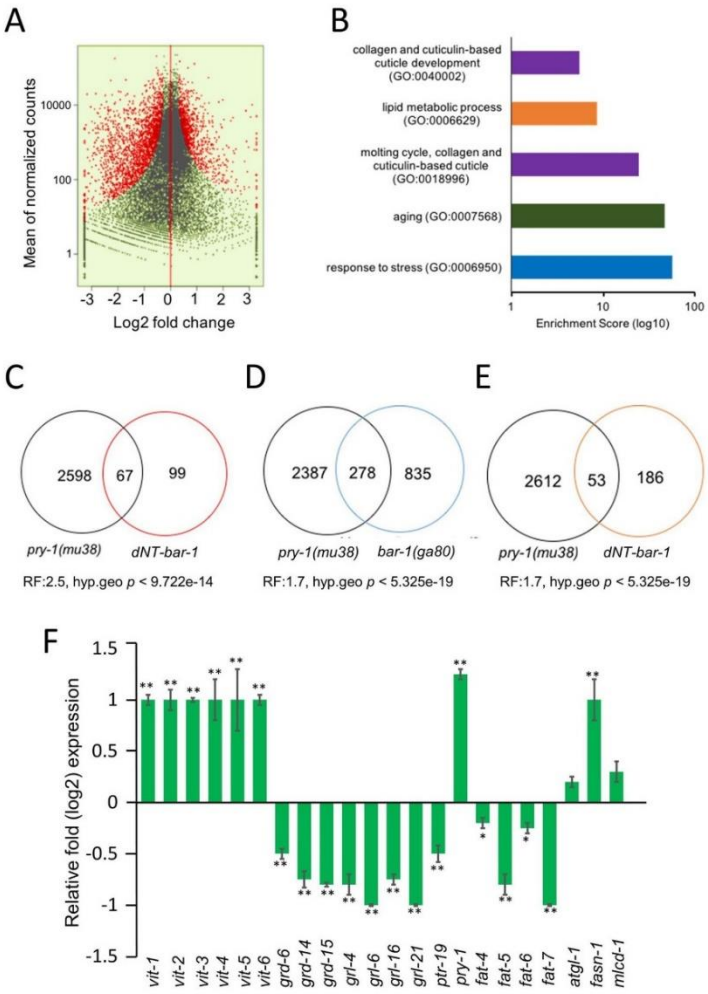

Fig 1. *pry-1(mu38)* transcriptome analysis. (A) Scatter plots of differentially expressed genes in *pry-1(mu38)*. Red dots mark significantly altered transcripts with a FDR *p*-adj of < 0.05, whereas black dots mark transcripts that are not significantly altered (FDR *p*-values of > 0.05). (B) Selected GO categories enriched in *pry-1(mu38)* targets are identified by GO Amigo, (*p*-adj < 0.05). (see S4 Table for a detailed list). (C-E) Venn diagrams showing the overlap between *pry-1(mu38)*, *hs::dNT-bar-1*, and *bar-1(ga80)* transcriptional targets. P values are shown in each case. (C) Overlap between *pry-1(mu38)* and *hs::dNT-bar-1*whole animal transcriptome data [36]. (D) Overlap between *pry-1 (mu38)* and *bar-1(ga80)* whole animal transcriptome data [37]. (E) Overlap between *pry-1(mu38)* and *hs::dNT-bar-1* vulva and seam cell-specific transcriptome data [38]. (F) qPCR analysis of selected genes in the *pry-1(mu38)* mutant. Data represents the mean of at least two replicates and error bar represents the SEM. $^{*}p < 0.05$, $^{**}p < 0.01$.

https://doi.org/10.1371/journal.pone.0206540.g001

A comparison of *pry-1* RNA-Seq dataset with three previously reported WNT transcriptome microarray studies involving *bar-1(ga80)* [37], which is a genetic null, and constitutively active *bar-1* (*hs*::*dNT-bar-1*, heat-shock promoter-driven *bar-1* carrying a small deletion in the *N*-terminus) [13, 36, 38] revealed shared genes and families. Of the two *hs*::*dNT-bar-1* studies, one was specific to the vulva and seam cells [38] and the other involved whole animal analysis [36]. A total of 12% [38], 18% [37], and 30% [36] *bar-1* set of genes overlapped with our *pry-1* set (Fig 1C–1E, S5 Table). These include several *hh* family members. Altogether, from the three *bar-1* studies mentioned above, 10 *hh* genes, namely *grl-5*, *grl-10*, *grl-14*, *grl-15*, *hog-1*, *grd-1*, *grd-2*, *grd-12*, *wrt-4*, and *wrt-6* were reported, of which three (*grl-5*, *grl-14*, and *grd-12*) are present in our *pry-1* list. The other shared genes include those involved in cuticle synthesis (*col* and *cutl* families), defense response, embryo development, oxidation-reduction processes, and proteolysis. We also analyzed shared genes based on their expression trend, i.e., up or down, using GO terms. The analysis revealed over-representation of categories, namely immunity, stress response, and lipid catabolic processes (S6 Table), suggesting that these genes might act downstream of both PRY-1 and BAR-1.

pry-1 mutants exhibit altered lipid metabolism

Throughout the lifespan of an animal, lipids are persistently mobilized to supply energy demands for growth, cellular maintenance, tissue repair, and reproduction [42, 43]. Changes in lipid levels also affect an organism's ability to survive in stressful conditions [44, 45]. Notably, many genes that are involved in the synthesis, breakdown, and transport of lipids are differentially expressed in *pry-1* mutants (S2 Fig). These include vitellogenins (yolk protein/apolipoprotein-like): *vit-1–6*; fatty acid transporters: *lbp-1*, *-2*, *-4*, *-5*, *-7*, and *-8*; lipases: *lips-3*, *-4*, *-7*, *-10*, and *-17*; desaturases: *fat-4-6*; elongases: *elo-3* and *-6*; and fatty acid oxidation: *acdh-1*, *-6*, *-11*, *-23*, *acs-2*, *-11*, and *-17*, *cpt-1*, *-4*, and *ech-9* (S2 Table). The expression of *vit* genes and desaturase was measured by qPCR and all but *fat-4* were successfully validated (Fig 1F) as levels of the latter were decreased by 20%, unlike the 1.5-fold increase observed by RNA-Seq. We also tested another desaturase, *fat-7*, which functions redundantly with *fat-6* [46] but was not present in our dataset. The *fat-7* mRNA level was significantly reduced (Fig 1F); thus, all four *fat* desaturase genes are downregulated in *pry-1(mu38)* animals.

Enrichment of several lipid metabolism genes in the *pry-1* transcriptome led us to examine lipid accumulation in worms. Staining with Oil Red O revealed that the lipid content was less than half in *pry-1(mu38)* one-day-old young adults compared with controls (Fig 2A and 2B). Examination of total fat at each larval stage revealed that *pry-1* mutants had lower somatic lipid stores (25–80%) at all stages except for L2 (Fig 3A). In addition, the lipid distribution was altered such that the staining was mostly restricted to gonadal tissue (Fig 2C). These results suggested that *pry-1* plays a role in lipid metabolism. Consistent with this model, we found that *pry-1(mu38)* animals laid fewer fertilized eggs and had poor survival upon starvation-induced L1 diapause (Fig 2E and 2F).

One explanation for the reduced lipid phenotype may be that lipids are being rapidly utilized. However, this is unlikely because several lipases (*lips* family members) were downregulated. We also measured lipase activity in one-day-old adults from whole worm lysates. As expected, the total activity was 34% lower in the mutant compared with the N2 control (Fig 2D). Next, we examined lipids in *pry-1(mu38)* animals following knockdown of *lipl-4* or *lips-7*, which comprise lipase genes that regulate the gonad-dependent somatic lipid levels [42, 43, 47] but observed no change in the pattern of lipid distribution (Fig 2G and 2H). We concluded that the lower somatic lipids in animals lacking *pry-1* function were not due to increased utilization, raising the possibility of the involvement of other metabolic processes.

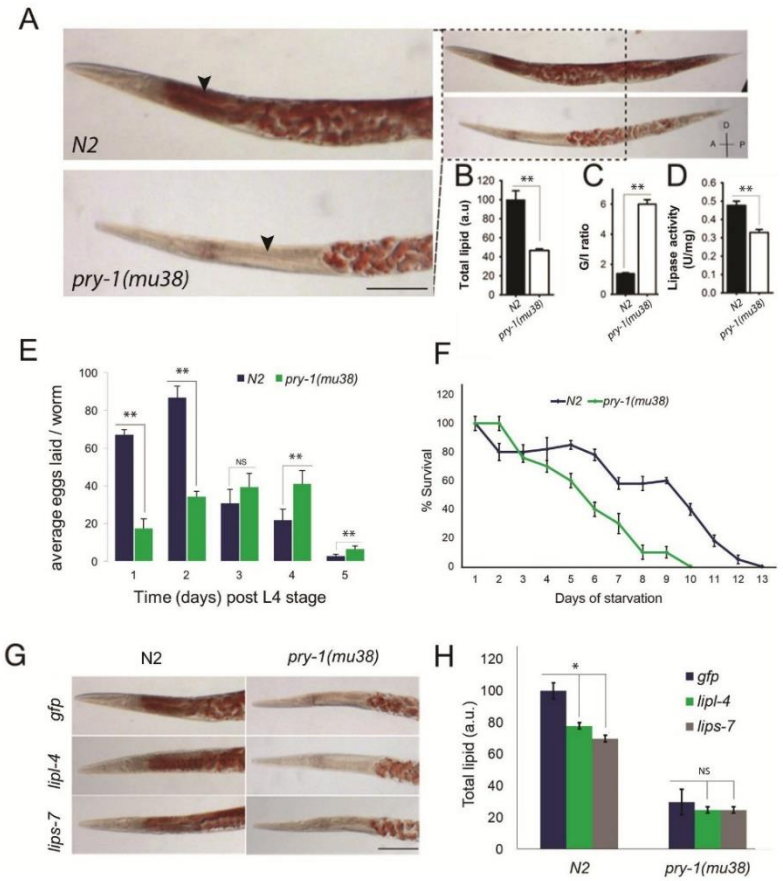

Fig 2. Lipid levels and distribution are altered in *pry-1(mu38)* mutants. Arrowheads indicate intestine and dotted areas gonad. (A) Representative DIC images of N2 and *pry-1(mu38)*, stained with Oil Red O. D: dorsal; V: ventral; A: anterior; and P: posterior. (B, C) Quantification of Oil Red O staining. Data represents the mean of at least two replicates and error bar in this and subsequent graphs represents the SEM. (C) Ratio of gonadal to intestinal (G/I) lipid. (D) The lipase activity is decreased in *pry-1(mu38)*. The activity per mg of protein has been plotted. (E) The average number of eggs laid by wild-type and *pry-1(mu38)* animals on different days over the duration of their reproductive period. (F) *pry-1(mu38)* displayed significant reduction in L1 survival following starvation. Percent survival of L1 larvae in the absence of food has been plotted. Graph represents the average of three independent experiments. (G) Representative images of N2 and *pry-1(mu38)* RNAi-treated animals stained with Oil Red O. (H) Histograms show Oil Red O intensities. Scale bar, 50 μm. $^{*}p < 0.01$, $^{**}p < 0.001$.

https://doi.org/10.1371/journal.pone.0206540.g002

Vitellogenins contribute to lipid metabolism defects in *pry-1* mutants

To understand the molecular basis of low lipid levels in *pry-1(mu38)* worms we focused on the vitellogenin family of genes, whose expression is repressed by *pry-1*. VITs comprise the major yolk proteins in *C. elegans*, which are synthesized in the intestine and mediate lipid transport from the intestine to the gonad during the reproductive period [15]. Examination of *vit* levels

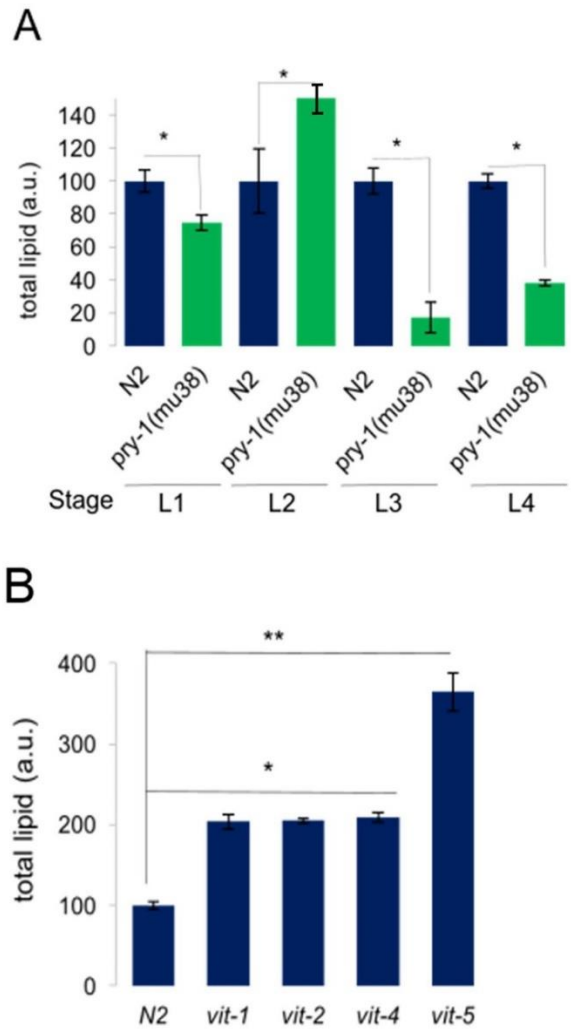

Fig 3. Lipid levels in *pry-1(mu38)* and *vit* mutants. (A) Quantification of Oil Red O staining intensity in *pry-1(mu38)* and wild-type animals at different developmental stages. Lipids are lower in *pry-1* mutants at all stages except L2. (B) Quantification of Oil Red O staining in N2 and *vit* mutants during the young adult stage. Lipid levels are higher in *vit-1(ok2616), vit-2(ok3211), vit-4(ok2982), and vit-5(ok3239)* animals. Data represents the mean of at least two replicates and error bar represents the SEM. $^{*}p < 0.01$, $^{**}p < 0.001$.

https://doi.org/10.1371/journal.pone.0206540.g003

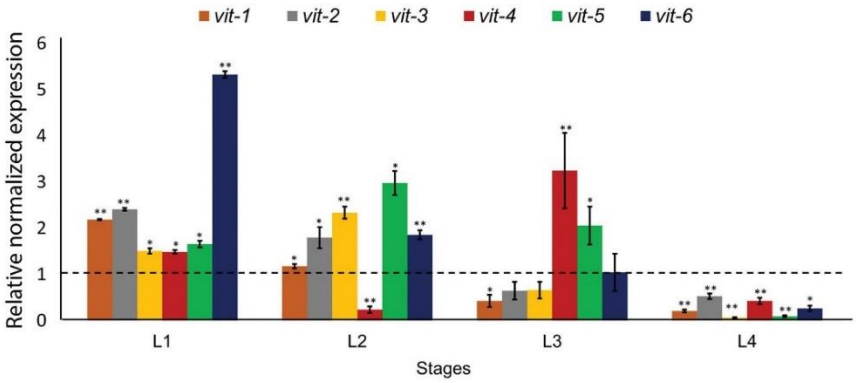

Fig 4. Expression of *vit* genes in *pry-1(mu38)*. (A) qRT-PCR of *vit* genes at larval stages in *pry-1(mu38)* mutants. Relative normalized expression has been plotted. Data represents the mean of at least two replicates and error bar represents the SEM. $^{*}p<0.05$ and $^{**}p<0.01$, compared to wild-type which is normalized to 1.

https://doi.org/10.1371/journal.pone.0206540.g004

in *pry-1(mu38)* animals revealed abnormal expression at all developmental stages. Thus, beginning with the L1 stage where all six *vit* genes were upregulated, the number of overexpressed genes was five in L2, two in L3, and zero in L4 stage (Fig 4).

We next examined lipid contents in worms using mutants and RNAi knockdowns of specific *vit* genes. The results revealed altered lipid distributions in all cases such that lipids accumulated at higher levels in somatic tissues (Figs 3B, 5A and 5B, S3A Fig). A quantification of overall lipids following *vit* knockdowns revealed a significantly higher accumulation in mutants compared to wild-type (2.5–3 fold and 1.3–1.4 fold, respectively, using *gfp* RNAi knockdown as a control in each case) (Fig 5A and 5B). A similar observation was made using the *mdt-28p*::*mCherry* reporter (S3B–S3D Fig) that marks lipid droplets [48]. Lipid accumulation following *vit* knockdown has also been reported in wild-type animals [49]. Sequence comparisons indicated that *vit-1* RNAi may also target *vit-2* owing to significant identity in the genomic region used to perform KDs (S7 Table), which was validated by qPCR (S4 Fig). Similarly, any one of the *vit-3*, *4*, or *5* RNAi could simultaneously effect knockdown of the other two (S7 Table). Thus, multiple VITs appear to play roles in the regulation of both the level as well as the distribution of lipids, and their misregulation contributes to lipid metabolism defects in *pry-1* mutants.

Lipoprotein receptors RME-2 and LRP-2 may not contribute to lipid defects in *pry-1* mutants

To understand how *pry-1* and *vit* genes might function to regulate lipid levels, we examined the involvement of *rme-2* in the *pry-1*-mediated pathway to regulate lipid accumulation as VITs are transported via the RME-2 receptor [15]. The knockdown of *rme-2* by RNAi led to intestinal accumulation and ectopic deposition of lipids (Fig 5C and 5D) consequent to blockage of yolk protein transport to the developing oocytes [15]. Specifically, *rme-2(RNAi)* animals showed an approximately 45% increase in total lipid content such that the gonad-to-somatic ratio was roughly 30% lower compared with that in controls. However, this phenotype was not observed in *pry-1(mu38)* owing to a reduction in lipid levels both in somatic and gonadal tissues (Fig 5C and 5D). These results allow us to suggest that VITs act independently of the

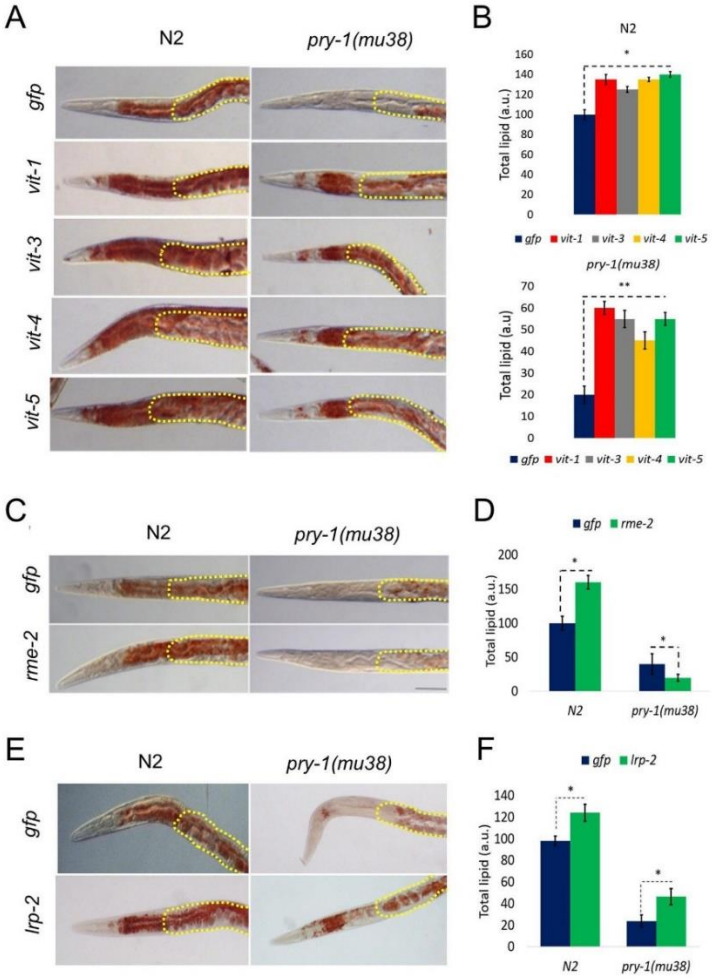

Fig 5. Vitellogenin mediated lipid metabolism in *pry-1* mutants. (A) DIC micrographs of representative N2 and *pry-1(mu38)* adults stained with Oil Red O following *vit* RNAi. Areas marked with dotted lines show germline and eggs. (B) The corresponding Oil Red O quantifications following each treatment. (C) Representative images of N2 and *pry-1(mu38)* following *rme-2* RNAi knockdown. (D) The histogram shows Oil Red O intensity in N2 and *pry-1(mu38)*. (E) Representative images of N2 and *pry-1(mu38)* following *lrp-2* RNAi knockdown. (F) The histogram shows Oil Red O intensity in N2 and *pry-1(mu38)*. Data represents the mean of at least two replicates and error bar represents the SEM. At least 50 animals were quantified in each batch. $^{*}p < 0.01$, $^{**}p < 0.001$.

https://doi.org/10.1371/journal.pone.0206540.g005

RME-2 transport mechanism to regulate lipid metabolism in response to *pry-1* signaling. Moreover, as lipid levels are further reduced in *pry-1(mu38)* animals following *rme-2* knock-down, *rme-2* may have an unknown non-vitellogenin-mediated role in lipid accumulation. Other possibilities also exist for such a phenotype.

We also examined other VIT-interacting factors for their involvement in PRY-1-mediated regulation of lipids. Our transcriptome dataset contained one LDL-like receptor gene, *lrp-2*, which was overexpressed in *pry-1* mutants (S3 Table). It was shown previously that *lrp-2* positively regulates yolk protein synthesis [22]. To test whether lipid levels are affected by *lrp-2*, RNAi knockdown experiments were performed, which showed a small but significant rescue of the lipid phenotype in *pry-1(mu38)* animals (Fig 5E and 5F). However, as *lrp-2* knockdown in wild-type animals also caused an increase in lipids, it is unclear whether PRY-1-mediated signaling utilizes LRP-2 function to affect lipid levels.

pry-1 mutants show reduced fatty acid levels

The *pry-1* transcriptome contains genes predicted to participate in fatty acid desaturation and elongation (5), binding/transport (6), and β-oxidation pathway (16) (S2 Fig). The Δ9-desaturase enzymes are required to produce C16:1 and C18:1 monounsaturated fatty acids (S2 Fig). Whereas *fat-5* converts palmitic acid (C16:0) to palmitoleic acid (C16:1n7), *fat-6* and *fat-7* are involved in stearic acid (C18:0) to OA (C18:1n9) conversion [17]. The downregulation of Δ9-desaturases, observed in *pry-1(mu38)* animals, may lead to reduced fatty acid synthesis. To investigate this, we quantified lipids using a gas chromatography-mass spectrometry (GC-MS) approach. The results showed that whereas the relative ratios of fatty acids in *pry-1* mutants were normal, the absolute level of each species was significantly reduced (Fig 6A, S5 Fig). The

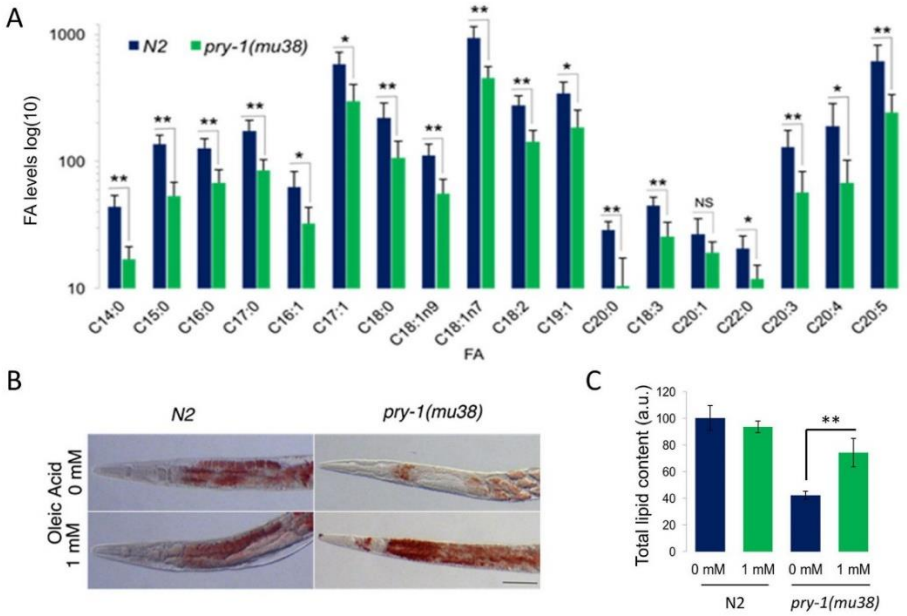

Fig 6. GC-MS analysis of fatty acids in *pry-1* mutants and partial rescue of lipid defects following OA treatments. (A) Total FA levels of selected fatty acid species expressed in $\log_{10}$ value as determined by GC-MS analysis. The *pry-1* mutants have low levels of FA. Error bars represent the standard deviation. Significant differences between wild type and *pry-1* mutant are marked with stars, * $p < 0.03$, ** $p < 0.015$. (B) Lipid staining of N2 and *pry-1(mu38)* adults supplemented with 1 mM OA. **C)** Quantification of total lipid, $p < 0.001$.

https://doi.org/10.1371/journal.pone.0206540.g006

result agrees with the overall low lipid levels in *pry-1(mu38)* animals and together supports the important role of PRY-1 signaling in lipid metabolism in *C. elegans*.

Because the expression of *fat* genes depends on the nuclear hormone receptors *nhr-49* and *nhr-80* [18, 35], we determined levels of these NHR transcripts in *pry-1* mutant animals. Although RNA-Seq transcriptome data showed no change in either gene, qPCR revealed a subtle but significant upregulation of *nhr-80* whereas *nhr-49* was unchanged (S6 Fig). Thus, transcriptional regulation of these two NHRs is unlikely to be a mechanism affecting *pry-1*-mediated expression of Δ9-desaturase genes, although we cannot rule out the possibility that activities of one or both may be regulated post-transcriptionally in response to PRY-1 function. To further examine the involvement of *nhr* genes, two types of RNAi experiments were carried out. In one of these, *pry-1* was knocked down in *nhr-49(nr2041)* and *nhr-80(tm1011)* animals which reduced lipid levels in both mutant backgrounds (S7 Fig). In the other case, *nhr* genes were knocked down in *pry-1(mu38)* animals. While *nhr-49 RNAi* increased the lipid level likely due to *nhr-49* role in β-oxidation [35], no change was observed following *nhr-80* knockdown (S7 Fig). Overall, these results suggest that PRY-1 and the NHRs may act in parallel to regulate lipid levels.

OA (18C:1n9) supplementation partially rescues the somatic depletion of lipids in *pry-1* mutants

OA constitutes one of the fatty acid species that showed 50% reduced levels in our GC-MS analysis (Fig 6A). OA is required for fatty acid metabolism and is synthesized by *C. elegans* as it cannot be obtained through the normal *E. coli* (OP50) diet. OA acts as a precursor for the synthesis of polyunsaturated fatty acids and triacylglycerides, which are used for fat storage [16]. The addition of exogenous OA as a fat source has been shown to rescue several fat-deficient mutants including *fat-6* and *fat-7* by restoring their fat storage, resulting in improved fertility and increased locomotion [46]. Moreover, the addition of OA in *sbp-1*, *fat-6*, and *fat-7* animals fully rescued defects in satiety quiescence [17, 18, 50]. We therefore reasoned that supplementation of OA may improve lipid levels in *pry-1(mu38)* mutants. Treatment with 1 mM OA resulted in the restoration of lipids in animals lacking *pry-1* function (up to 2-fold higher compared with the untreated control, Fig 6B and 6C). No significant changes were seen in the gonadal lipid levels, suggesting that lipid metabolism in the gonad was unaffected.

Discussion

PRY-1 is necessary for normal expression of genes involved in lipid metabolism

To understand the mechanism of PRY-1/Axin function, we performed transcriptome profiling on a *pry-1* mutant. The analysis revealed altered expression of many genes including those that affect hypodermis, stress-response, aging, and lipid metabolism. The hypodermal-related genes included collagens, cuticulins, and hedgehogs. Previously, expression of some of the hedgehog genes was found to be altered in *bar-1* mutants [37, 38]. Considering that cuticular defects are observed in *bar-1* [36, 38] and *pry-1* mutants (Mallick *et al*., manuscript in preparation), and that hedgehog family members play roles in cuticle shedding and the formation of alae [39], these results lead us to suggest that a genetic pathway involving *pry-1* and *bar-1* may interact with hedgehogs for normal cuticle development.

One of the key findings of our *pry-1(mu38)* transcriptome analysis was the enrichment of genes related to lipid metabolism. In particular, we found that multiple lipogenic and lipolytic genes exhibited altered expression. For example, all four fatty acid desaturases (Δ5 and Δ9

desaturases) were downregulated in *pry-1* mutants. Whereas single *fat* gene mutants affect fatty acid composition without altering overall lipid levels, double mutants have low lipid levels [17, 46], suggesting that *pry-1* positively regulates fatty acid synthesis. With regard to lipolytic genes, such as those involved in β-oxidation, changes in gene expression between peroxisomal and mitochondrial β-oxidation genes showed an opposite trend (4 of 5 upregulated and 8 of 11 downregulated, respectively). This may indicate selective utilization of long-chain over short-chain fatty acids by the *pry-1* pathway. We also observed that all four lipases (*lips* family) were downregulated including *lips-7*, which was previously shown to be involved in lifespan extension and the maintenance of lipid levels [47]. Although *lips-7* RNAi did not alter the *pry-1(mu38)* phenotype, it remains to be seen whether *pry-1* affects any of the remaining three *lips* gene(s) to modulate lipids.

In addition to lipogenic and lipolytic genes, several lipid transporters are also present in the *pry-1(mu38)* transcriptome, including two lipid-binding proteins (*lbp-5* and *lbp-8*; both downregulated), six lipoproteins (*vit-1* to *-6*; all upregulated), and a LDL-like receptor protein (*lrp-2*). Knockdown of *lbp-5* and VITs negatively affect lipid storage [51], which further emphasizes the important role of *pry-1* in the maintenance of lipids and suggests that *pry-1*-mediated signaling is involved in the utilization of lipids for energetics as well as signaling mechanisms.

PRY-1-mediated lipid metabolism involves vitellogenins

Reduced lipids may affect tissue function and physiology in different ways; for example, owing to altered membrane structure and compartmentalization, altered signaling, reduced energy demands, and impact on autophagy. The Oil Red O staining of *pry-1(mu38)* showed a severe reduction in lipid content with a marked decline in the somatic lipid storage. It is worth mentioning that a reduced lipid phenotype was also observed in *hs::dNT-bar-1* animals that carry a constitutively active form of BAR-1 (S8 Fig) [13], suggesting that *pry-1* may interact with *bar-1* to maintain lipid levels.

To understand the mechanism of *pry-1* signaling in lipid regulation, we examined the possibility of increased lipid breakdown. The results showed that total lipase activity was not increased in *pry-1* mutants. Additionally, knockdowns of *lipl-4* (lysosomal lipase) and *lips-7* (cytosolic lipase), both of which negatively regulate lipid levels [42, 43], in *pry-1(mu38)* had no observable effect. Thus, selective and rapid lipid catabolism does not appear to be a factor in lipid depletion in the absence of *pry-1* function.

We then investigated the role of VIT proteins, which are the distant homologs of human apolipoprotein B [52], in maintaining lipid levels. As major yolk proteins, VITs are involved in somatic mobilization of lipids to the developing germline. Moreover, previous studies demonstrated that reducing VITs in wild-type animals increases both lifespan and lipid accumulation, with overexpression having an opposite effect in long-lived mutants [49, 53]. Both RNA-Seq and qPCR experiments showed that the expression of all six *vit* genes was upregulated in *pry-1* mutants. We also observed a similar trend in *vit* expression in *hs::dNT-bar-1* animals (S9 Fig), which together with lipid defects (S8 Fig) support the possibility of *bar-1* being involved in *pry-1*-mediated *vit* transcription.

To examine whether PRY-1 signaling utilizes VITs to affect lipid levels, RNAi experiments were performed. The results showed that knocking down *vit* genes (*vit-1/2* and vit-3/4/5) suppressed low lipid phenotype of *pry-1* mutant animals, providing evidence that VITs play an important role in PRY-1-mediated lipid metabolism. We have also shown that such a role of VITs may not utilize lipoprotein receptors RME-2 (VIT transporter) or LRP-2 (VIT synthesis). Overall, these findings along with the role of VITs in regulating lipid levels [49], allow us to

propose that PRY-1-mediated signaling involves VITs to regulate processes that depend on energy metabolism and lipid signaling [42, 43].

Although it remains unclear how VITs participate in *pry-1* signaling, one possibility may involve downregulation of the autophagy pathway. Manipulating VIT levels has been shown to affect the lifespan by altering autophagy [49]. Autophagy is a complex process that involves multiple enzymes to recycle cellular contents by converting them into usable metabolites. Despite the *pry-1* transcriptome not containing known autophagy-related candidates, the pathway may still be involved. This could be tested by examining the roles of specific autophagosome genes in lipoprotein synthesis and autophagy, which in turn should reveal a link with *pry-1*-mediated lipid metabolism.

A potential role of PRY-1 in fatty acid synthesis

While lipid catabolism appears to be unaffected in *pry-1* mutants, the low lipid phenotype may be caused by reduced fatty acid synthesis. In agreement with this, the expression of three conserved stearoyl-CoA desaturases, *fat-5*, *fat-6*, and *fat-7*, which are involved in the synthesis of monounsaturated fatty acids such as OA [16–18] was reduced in *pry-1* mutants. Because these *fat* desaturases are regulated by *nhr-49* and *nhr-80*, we examined genetic interactions between *pry-1* and *nhr* genes. Our qPCR and RNAi experiments (S6 and S7 Figs) did not reveal a clear epistatic relationship, suggesting that *pry-1* is likely to act in parallel to these two transcription factors. Besides NHR-49 and NHR-80, the mammalian homolog of SREBP, SBP-1, is another transcription factor that regulates expression of *fat* genes [50, 54, 55]. Although our RNA-Seq dataset did not include *sbp-1*, we found the *sbp-1* transcript levels to be reduced in *pry-1 (mu38)* animals (S6 Fig), suggesting that *pry-1* may interact with *sbp-1* to affect expression of *fat* genes. However, more experiments are needed to validate this regulatory relationship.

The GC-MS analysis of fatty acid composition revealed that *pry-1* is needed to maintain normal levels of every fatty acid species analyzed. A global reduction in fatty acids may affect processes that require utilization of lipids such as aging. However, the relationship between lipid levels and lifespan is not well understood. It is likely that rather than absolute levels, the quality of lipids may be more important for cellular processes [45]. We investigated this possibility using OA, one of the species involved in fatty acid signaling. Exogenous treatment with OA restored lipid levels in *pry-1* mutants. Thus, *pry-1* may play a role in maintaining the levels of beneficial fatty acids, possibly by affecting their synthesis. However, additional mechanisms are also likely to be involved, such as reduced conversion of acetyl-CoA to saturated fatty acid (palmitate), lower synthesis of diglycerides, and increased peroxisomal β-oxidation (S2 Fig). It would therefore be worthwhile to examine these possibilities in future studies.

It is also unclear whether PRY-1 is required in one or more tissues to maintain lipid levels. In preliminary studies using *pry-1::gfp* transgenic animals, we observed fluorescence in several tissues including seam cells, neuronal cells, muscles, and hypodermis. This suggests a broader requirement of PRY-1 in *C. elegans*, however more experiments are needed to fully understand its tissue-specific role in lipid regulation.

Our study provides the first evidence of PRY-1/Axin function in lipid metabolism. The involvement of lipids in age-related disorders in humans, as well as animal models, is well documented. Genetic and acquired lipid diseases are associated with the loss of subcutaneous fat, accumulation of visceral and ectopic fat, and metabolic syndromes such as insulin resistance, glucose intolerance, dyslipidemia, and hypertension [56]. In addition, Yang et al. showed that Axin expression in mice contributes to an age-related increase in adiposity in thymic stromal cells [10]. Although the role of PRY-1/Axin in fat storage needs to be investigated further, whether Axin family members play roles in any of these lipid-related diseases remains

unknown. Therefore, the findings that PRY-1/Axin is necessary for the regulation of lipid levels provide a unique opportunity to investigate the role of Axin signaling in age-related lipid metabolism.

Supporting information

S1 Fig. Expression profile of WNT ligands, receptors, and target genes. (A-C) Developmental expression patterns of known WNT ligands, receptors and target genes from published microarray sources (see Methods). (D) qPCR validations of selected WNT target genes during the L1 and L4 stages. Each data sample represents the mean of two replicates and error bar represents the SEM. $^{*}p < 0.01$.
(JPG)

S2 Fig. Overview of lipid metabolism and genes with altered expression in *pry-1(mu38)*. The lipid anabolic and catabolic pathway is adapted from a previously published study [57, 58]. Lipid anabolic processes involve initiation, desaturation and elongation of fatty-acid (FA), followed by triglyceride (TAG) formation. Initiation involves conversion of Acetyl CoA to the saturated fatty-acid (SFA) Palmitate (C16:0). Elongase (*elo*) and desaturase (*fat*) enzymes act on Palmitate to modify it to long chain mono- and poly-unsaturated fatty acids (MUFAs and PUFAs, respectively). MUFAs and PUFAs are collectively termed as free fatty acids (FFAs). The FFAs are linked with glycerol 3-phosphate (Glycerol 3P) to produce lysophosphatidic acid (LPA) and phosphatidic acid (PA). PA and monoglycerides (MAG) serve as building blocks of diglycerides (DAG) synthesis. DAGs are converted into neutral lipids (TAGs). Lipid catabolism begins with the breakdown of TAGs into DAGs by ATGL-1, and other lipases and lipase-like enzymes (abbreviated as '*lipl*' and '*lips*') to release FFAs. FFAs are further broken down to Acetyl CoA through peroxisomal- and mitochondrial- β-oxidation and release energy. Putative genes involved in lipid metabolism are shown at the appropriate step. Genes with altered expression in *pry-1(mu38)* are highlighted in blue (DOWN) and red (UP).
(JPG)

S3 Fig. Quantification of lipids in *vit* and *pry-1* mutants. (A) Representative images of wild-type (WT) and *vit* mutant animals stained with Oil Red O. Refer to Fig 3 for lipid quantification in these worms. (B) Representative images of *mdt-28p*::*mCherry* and *pry-1(mu38)*; *mdt-28p*::*mCherry* animals treated with *gfp* (control) and *vit* RNAi. (C,D) Histograms showing quantification of fluorescence intensity. Data represents the mean of two replicates and error bar represents the SEM. $^{*}p < 0.05$, $^{**}p < 0.01$.
(JPG)

S4 Fig. *vit-1* RNAi causes almost complete elimination of *vit-2* transcripts. qPCR analysis of *vit-2* in the *pry-1(mu38)* day 3 mutants after adult specific *vit-1* RNAi knockdown. Data represents the mean of three replicates and error bar represents the SEM. $^{*}p < 0.01$.
(JPG)

S5 Fig. Relative fatty acid abundance in *pry-1(mu38)*. (A) Relative abundance of selected fatty acid species expressed in percentage of total fatty acid as determined by GC-MS analysis. *pry-1* mutants have marginally lower levels of C15:0, C16:0 and higher levels of C20:1, C22:0 than N2 (marked with star, $p < 0.05$). Error bar represents the standard deviation. (B, C) A representative GC-MS Total Ion Chromatogram (TIC) traces of populations of the N2 and *pry-1(mu38)* worms, respectively. The peaks corresponding to fatty acid species are identified.
(JPG)

S6 Fig. *sbp-1* is downregulated in *pry-1(mu38)*. qPCR analysis of *nhr-49*, *nhr-80* and *sbp-1* genes in *pry-1(mu38)* animals at the L1 stage. Data represents the mean of two replicates and error bar represents the SEM. $^{*}p < 0.05$, $^{*}p < 0.01$.
(JPG)

S7 Fig. Genetic interaction analysis of *pry-1* with *nhr-49* and *nhr-80*. (A) Representative images after RNAi knockdown of *nhr-49* and *nhr-80* in wild-type and *pry-1(mu38)* animals. (B) Lipid quantification after *nhr-49* and *nhr-80* RNAi. (C) Representative images of *nhr-49* and *nhr-80* mutant animals fed with *gfp* (control) and *pry-1* RNAi bacteria. (D) Lipid quantification in wild-type, *nhr-49*, and *nhr-80* mutants. Data represents the mean of at least two replicates and error bar represents the SEM. $n > 30$, $^{*}p < 0.05$.
(JPG)

S8 Fig. Lipid staining and quantification in *hs::dNT-bar-1* animals. (A) Representative DIC images of N2 and *hs::dNT-bar-1* at 20 ˚C, after heat shock at 30 ˚C for 12hrs and 38 ˚C for 30 minutes, stained with Oil Red O. (B) Quantification of total lipids in *hs::dNT-bar-1* animals after heat shock treatments. Data represents the mean of at least two replicates and error bar represents the SEM. $n > 50$ for each trial; $p < 0.01$ for all mutants compared to the control (marked with *).
(JPG)

S9 Fig. qPCR analysis of *vit* genes in *hs::dNT-bar-1* animals. (A) qRT-PCR of *vit* genes at L1 stage in *hs::dNT-bar-1* mutants after heat shock at 38 ˚C for 30 min. Data represents the mean of at least two replicates and error bar represents the SEM. The dotted horizontal line marks the control which is normalized to one. $^{*}p < 0.01$.
(JPG)

S1 Table. List of primers used in this study.
(PDF)

S2 Table. mRNA transcripts mapped to the *C. elegans* genome.
(PDF)

S3 Table. An Excel spreadsheet listing differentially regulated genes.
(XLSX)

S4 Table. An Excel spreadsheet showing GO-term enrichment.
(XLSX)

S5 Table. An Excel spreadsheet showing transcriptome comparison.
(XLSX)

S6 Table. An Excel spreadsheet showing analysis of the shared genes based on expression trends.
(XLSX)

S7 Table. Conservation of *vit* gene sequences used in RNAi experiments. RNAi clones are from the Ahringer library. ns: no significant identity observed.
(PDF)

Acknowledgments

We are grateful to Brian Golding for providing server space and Paul Sternberg lab for help with RNA-Seq computational analysis. GC-MS experiments were performed at McMaster Regional

Centre for Mass Spectrometry (MRCMS) facility. Some of the strains were obtained from CGC, which is funded by the NIH Office of Research Infrastructure Programs (P40OD010440). We thank Lesley Macneil and anonymous reviewers for comments on previous versions of the manuscript, Jessica Knox for assistance with initial quantitative real time-PCR experiments, and Gupta lab members for helpful discussions.

Author Contributions

Conceptualization: Ayush Ranawade, Avijit Mallick, Bhagwati P. Gupta.

Data curation: Ayush Ranawade, Avijit Mallick.

Funding acquisition: Bhagwati P. Gupta.

Investigation: Ayush Ranawade, Avijit Mallick, Bhagwati P. Gupta.

Methodology: Ayush Ranawade, Avijit Mallick.

Project administration: Bhagwati P. Gupta.

Resources: Bhagwati P. Gupta.

Supervision: Bhagwati P. Gupta.

Validation: Avijit Mallick, Bhagwati P. Gupta.

Writing – original draft: Ayush Ranawade, Avijit Mallick, Bhagwati P. Gupta.

Writing – review & editing: Ayush Ranawade, Avijit Mallick, Bhagwati P. Gupta.

References

1. Zeng L, Fagotto F, Zhang T, Hsu W, Vasicek TJ, Perry WL 3rd, et al. The mouse Fused locus encodes Axin, an inhibitor of the Wnt signaling pathway that regulates embryonic axis formation. Cell. 1997; 90 (1):181–92. PMID: 9230313.
2. Logan CY, Nusse R. The Wnt signaling pathway in development and disease. Annu Rev Cell Dev Biol. 2004; 20:781–810. https://doi.org/10.1146/annurev.cellbio.20.010403.113126 PMID: 15473860.
3. Luo W, Lin SC. Axin: a master scaffold for multiple signaling pathways. Neurosignals. 2004; 13(3):99–113. Epub 2004/04/07. https://doi.org/10.1159/000076563 PMID: 15067197.
4. Clevers H, Nusse R. Wnt/beta-catenin signaling and disease. Cell. 2012; 149(6):1192–205. Epub 2012/06/12. https://doi.org/10.1016/j.cell.2012.05.012 PMID: 22682243.
5. Chen Y, Fu AK, Ip NY. Axin: an emerging key scaffold at the synapse. IUBMB Life. 2013; 65(8):685–91. Epub 2013/07/13. https://doi.org/10.1002/iub.1184 PMID: 23847014.
6. Clevers H. Wnt/beta-catenin signaling in development and disease. Cell. 2006; 127(3):469–80. https://doi.org/10.1016/j.cell.2006.10.018 PMID: 17081971.
7. Furuhashi M, Yagi K, Yamamoto H, Furukawa Y, Shimada S, Nakamura Y, et al. Axin facilitates Smad3 activation in the transforming growth factor beta signaling pathway. Mol Cell Biol. 2001; 21(15):5132–41. https://doi.org/10.1128/MCB.21.15.5132-5141.2001 PMID: 11438668.
8. Luo W, Ng WW, Jin LH, Ye Z, Han J, Lin SC. Axin utilizes distinct regions for competitive MEKK1 and MEKK4 binding and JNK activation. J Biol Chem. 2003; 278(39):37451–8. Epub 2003/07/25. https://doi.org/10.1074/jbc.M305277200 PMID: 12878610.
9. Zhang YL, Guo H, Zhang CS, Lin SY, Yin Z, Peng Y, et al. AMP as a low-energy charge signal autonomously initiates assembly of AXIN-AMPK-LKB1 complex for AMPK activation. Cell Metab. 2013; 18 (4):546–55. Epub 2013/10/08. https://doi.org/10.1016/j.cmet.2013.09.005 PMID: 24093678.
10. Yang H, Youm YH, Sun Y, Rim JS, Galban CJ, Vandanmagsar B, et al. Axin expression in thymic stromal cells contributes to an age-related increase in thymic adiposity and is associated with reduced thymopoiesis independently of ghrelin signaling. J Leukoc Biol. 2009; 85(6):928–38. https://doi.org/10.1189/jlb.1008621 PMID: 19299626.
11. Sawa H, Korswagen HC. Wnt signaling in C. elegans. WormBook. 2013;ed. The C. elegans Research Community, WormBook, http://www.wormbook.org. PMID: 25263666

12. Maloof JN, Whangbo J, Harris JM, Jongeward GD, Kenyon C. A Wnt signaling pathway controls hox gene expression and neuroblast migration in C. elegans. Development. 1999; 126(1):37–49. PMID: 9834184.
13. Gleason JE, Korswagen HC, Eisenmann DM. Activation of Wnt signaling bypasses the requirement for RTK/Ras signaling during *C. elegans* vulval induction. Genes Dev. 2002; 16(10):1281–90. https://doi.org/10.1101/gad.981602 PMID: 12023306.
14. Korswagen HC, Coudreuse DY, Betist MC, van de Water S, Zivkovic D, Clevers HC. The Axin-like protein PRY-1 is a negative regulator of a canonical Wnt pathway in *C. elegans*. Genes Dev. 2002; 16 (10):1291–302. https://doi.org/10.1101/gad.981802 PMID: 12023307.
15. Grant B, Hirsh D. Receptor-mediated endocytosis in the Caenorhabditis elegans oocyte. Mol Biol Cell. 1999; 10(12):4311–26. https://doi.org/10.1091/mbc.10.12.4311 PMID: 10588660.
16. Watts JL, Browse J. Genetic dissection of polyunsaturated fatty acid synthesis in Caenorhabditis elegans. Proc Natl Acad Sci U S A. 2002; 99(9):5854–9. https://doi.org/10.1073/pnas.092064799 PMID: 11972048.
17. Brock TJ, Browse J, Watts JL. Genetic regulation of unsaturated fatty acid composition in C. elegans. PLoS Genet. 2006; 2(7):e108. https://doi.org/10.1371/journal.pgen.0020108 PMID: 16839188.
18. Goudeau J, Bellemin S, Toselli-Mollereau E, Shamalnasab M, Chen Y, Aguilaniu H. Fatty acid desaturation links germ cell loss to longevity through NHR-80/HNF4 in C. elegans. PLoS Biol. 2011; 9(3): e1000599. https://doi.org/10.1371/journal.pbio.1000599 PMID: 21423649.
19. Brenner S. The genetics of *Caenorhabditis elegans*. Genetics. 1974; 77:71–94. PMID: 4366476
20. Ranawade AV, Cumbo P, Gupta BP. Caenorhabditis elegans histone deacetylase hda-1 is required for morphogenesis of the vulva and LIN-12/Notch-mediated specification of uterine cell fates. G3 (Bethesda). 2013; 3(8):1363–74. https://doi.org/10.1534/g3.113.006999 PMID: 23797102.
21. Soukas AA, Kane EA, Carr CE, Melo JA, Ruvkun G. Rictor/TORC2 regulates fat metabolism, feeding, growth, and life span in Caenorhabditis elegans. Genes Dev. 2009; 23(4):496–511. https://doi.org/10.1101/gad.1775409 PMID: 19240135.
22. Van Rompay L, Borghgraef C, Beets I, Caers J, Temmerman L. New genetic regulators question relevance of abundant yolk protein production in C. elegans. Sci Rep. 2015; 5:16381. https://doi.org/10.1038/srep16381 PMID: 26553710.
23. Watts JL, Phillips E, Griffing KR, Browse J. Deficiencies in C20 polyunsaturated fatty acids cause behavioral and developmental defects in Caenorhabditis elegans fat-3 mutants. Genetics. 2003; 163 (2):581–9. PMID: 12618397.
24. Narbonne P, Roy R. Caenorhabditis elegans dauers need LKB1/AMPK to ration lipid reserves and ensure long-term survival. Nature. 2009; 457(7226):210–4. https://doi.org/10.1038/nature07536 PMID: 19052547.
25. Hillier LW, Reinke V, Green P, Hirst M, Marra MA, Waterston RH. Massively parallel sequencing of the polyadenylated transcriptome of C. elegans. Genome Res. 2009; 19(4):657–66. Epub 2009/02/03. https://doi.org/10.1101/gr.088112.108 PMID: 19181841.
26. Yook K, Harris TW, Bieri T, Cabunoc A, Chan J, Chen WJ, et al. WormBase 2012: more genomes, more data, new website. Nucleic Acids Res. 2012; 40(Database issue):D735–41. https://doi.org/10.1093/nar/gkr954 PMID: 22067452.
27. Chomczynski P, Sacchi N. Single-step method of RNA isolation by acid guanidinium thiocyanate-phenol-chloroform extraction. Anal Biochem. 1987; 162(1):156–9. https://doi.org/10.1006/abio.1987.9999 PMID: 2440339.
28. Martin M. Cutadapt Removes Adapter Sequences From High-Throughput Sequencing Reads. EMBnetjournal. 2011; 17(1). https://doi.org/10.14806/ej.17.1.200
29. Langmead B, Trapnell C, Pop M, Salzberg SL. Ultrafast and memory-efficient alignment of short DNA sequences to the human genome. Genome Biol. 2009; 10(3):R25. https://doi.org/10.1186/gb-2009-10-3-r25 PMID: 19261174.
30. Roberts A, Pachter L. Streaming fragment assignment for real-time analysis of sequencing experiments. Nat Methods. 2013; 10(1):71–3. https://doi.org/10.1038/nmeth.2251 PMID: 23160280.
31. Bullard JH, Purdom E, Hansen KD, Dudoit S. Evaluation of statistical methods for normalization and differential expression in mRNA-Seq experiments. BMC Bioinformatics. 2010; 11:94. https://doi.org/10.1186/1471-2105-11-94 PMID: 20167110.
32. Anders S, Huber W. Differential expression analysis for sequence count data. Genome Biol. 2010; 11 (10):R106. https://doi.org/10.1186/gb-2010-11-10-r106 PMID: 20979621.
33. Carbon S, Ireland A, Mungall CJ, Shu S, Marshall B, Lewis S, et al. AmiGO: online access to ontology and annotation data. Bioinformatics. 2009; 25(2):288–9. https://doi.org/10.1093/bioinformatics/btn615 PMID: 19033274.

34. Angeles-Albores D, RY NL, Chan J, Sternberg PW. Tissue enrichment analysis for C. elegans genomics. BMC Bioinformatics. 2016; 17(1):366. https://doi.org/10.1186/s12859-016-1229-9 PMID: 27618863.

35. Van Gilst MR, Hadjivassiliou H, Jolly A, Yamamoto KR. Nuclear hormone receptor NHR-49 controls fat consumption and fatty acid composition in C. elegans. PLoS Biol. 2005; 3(2):e53. https://doi.org/10.1371/journal.pbio.0030053 PMID: 15719061.

36. Jackson BM, Abete-Luzi P, Krause MW, Eisenmann DM. Use of an activated beta-catenin to identify Wnt pathway target genes in caenorhabditis elegans, including a subset of collagen genes expressed in late larval development. G3 (Bethesda). 2014; 4(4):733–47. https://doi.org/10.1534/g3.113.009522 PMID: 24569038.

37. van der Bent ML, Sterken MG, Volkers RJ, Riksen JA, Schmid T, Hajnal A, et al. Loss-of-function of beta-catenin bar-1 slows development and activates the Wnt pathway in Caenorhabditis elegans. Sci Rep. 2014; 4:4926. https://doi.org/10.1038/srep04926 PMID: 24819947.

38. Gorrepati L, Krause MW, Chen W, Brodigan TM, Correa-Mendez M, Eisenmann DM. Identification of Wnt Pathway Target Genes Regulating the Division and Differentiation of Larval Seam Cells and Vulval Precursor Cells in Caenorhabditis elegans. G3 (Bethesda). 2015; 5(8):1551–66. https://doi.org/10.1534/g3.115.017715 PMID: 26048561.

39. Zugasti O, Rajan J, Kuwabara PE. The function and expansion of the Patched- and Hedgehog-related homologs in C. elegans. Genome Res. 2005; 15(10):1402–10. https://doi.org/10.1101/gr.3935405 PMID: 16204193

40. Ewald CY, Landis JN, Porter Abate J, Murphy CT, Blackwell TK. Dauer-independent insulin/IGF-1-signalling implicates collagen remodelling in longevity. Nature. 2015; 519(7541):97–101. https://doi.org/10.1038/nature14021 PMID: 25517099.

41. Lustig B, Jerchow B, Sachs M, Weiler S, Pietsch T, Karsten U, et al. Negative feedback loop of Wnt signaling through upregulation of conductin/axin2 in colorectal and liver tumors. Mol Cell Biol. 2002; 22(4):1184–93. https://doi.org/10.1128/MCB.22.4.1184-1193.2002 PMID: 11809809.

42. Hou NS, Taubert S. Function and Regulation of Lipid Biology in Caenorhabditis elegans Aging. Front Physiol. 2012; 3:143. https://doi.org/10.3389/fphys.2012.00143 PMID: 22629250.

43. Lemieux GA, Ashrafi K. Investigating Connections between Metabolism, Longevity, and Behavior in Caenorhabditis elegans. Trends Endocrinol Metab. 2016; 27(8):586–96. https://doi.org/10.1016/j.tem.2016.05.004 PMID: 27289335.

44. Lynn DA, Dalton HM, Sowa JN, Wang MC, Soukas AA, Curran SP. Omega-3 and -6 fatty acids allocate somatic and germline lipids to ensure fitness during nutrient and oxidative stress in Caenorhabditis elegans. Proc Natl Acad Sci U S A. 2015; 112(50):15378–83. https://doi.org/10.1073/pnas.1514012112 PMID: 26621724.

45. Steinbaugh MJ, Narasimhan SD, Robida-Stubbs S, Moronetti Mazzeo LE, Dreyfuss JM, Hourihan JM, et al. Lipid-mediated regulation of SKN-1/Nrf in response to germ cell absence. Elife. 2015; 4:e07836. https://doi.org/10.7554/eLife.07836 PMID: 26196144.

46. Brock TJ, Browse J, Watts JL. Fatty acid desaturation and the regulation of adiposity in Caenorhabditis elegans. Genetics. 2007; 176(2):865–75. https://doi.org/10.1534/genetics.107.071860 PMID: 17435249.

47. Chen S, Whetstine JR, Ghosh S, Hanover JA, Gali RR, Grosu P, et al. The conserved NAD(H)-dependent corepressor CTBP-1 regulates Caenorhabditis elegans life span. Proc Natl Acad Sci U S A. 2009; 106(5):1496–501. https://doi.org/10.1073/pnas.0802674106 PMID: 19164523.

48. Na H, Zhang P, Chen Y, Zhu X, Liu Y, Liu Y, et al. Identification of lipid droplet structure-like/resident proteins in Caenorhabditis elegans. Biochim Biophys Acta. 2015; 1853(10 Pt A):2481–91. Epub 2015/05/31. https://doi.org/10.1016/j.bbamcr.2015.05.020 PMID: 26025681.

49. Seah NE, de Magalhaes Filho CD, Petrashen AP, Henderson HR, Laguer J, Gonzalez J, et al. Autophagy-mediated longevity is modulated by lipoprotein biogenesis. Autophagy. 2016; 12(2):261–72. https://doi.org/10.1080/15548627.2015.1127464 PMID: 26671266.

50. Yang F, Vought BW, Satterlee JS, Walker AK, Jim Sun ZY, Watts JL, et al. An ARC/Mediator subunit required for SREBP control of cholesterol and lipid homeostasis. Nature. 2006; 442(7103):700–4. https://doi.org/10.1038/nature04942 PMID: 16799563.

51. Xu M, Joo HJ, Paik YK. Novel functions of lipid-binding protein 5 in Caenorhabditis elegans fat metabolism. J Biol Chem. 2011; 286(32):28111–8. https://doi.org/10.1074/jbc.M111.227165 PMID: 21697096.

52. Smolenaars MM, Madsen O, Rodenburg KW, Van der Horst DJ. Molecular diversity and evolution of the large lipid transfer protein superfamily. J Lipid Res. 2007; 48(3):489–502. Epub 2006/12/07. https://doi.org/10.1194/jlr.R600028-JLR200 PMID: 17148551.

53. Murphy CT, McCarroll SA, Bargmann CI, Fraser A, Kamath RS, Ahringer J, et al. Genes that act downstream of DAF-16 to influence the lifespan of Caenorhabditis elegans. Nature. 2003; 424(6946):277–83. https://doi.org/10.1038/nature01789 PMID: 12845331.

54. Kniazeva M, Crawford QT, Seiber M, Wang CY, Han M. Monomethyl branched-chain fatty acids play an essential role in Caenorhabditis elegans development. PLoS Biol. 2004; 2(9):E257. https://doi.org/10.1371/journal.pbio.0020257 PMID: 15340492.

55. Nomura T, Horikawa M, Shimamura S, Hashimoto T, Sakamoto K. Fat accumulation in Caenorhabditis elegans is mediated by SREBP homolog SBP-1. Genes Nutr. 2010; 5(1):17–27. Epub 2009/11/26. https://doi.org/10.1007/s12263-009-0157-y PMID: 19936816.

56. Garg A, Agarwal AK. Lipodystrophies: disorders of adipose tissue biology. Biochim Biophys Acta. 2009; 1791(6):507–13. https://doi.org/10.1016/j.bbalip.2008.12.014 PMID: 19162222.

57. Amrit FR, Steenkiste EM, Ratnappan R, Chen SW, McClendon TB, Kostka D, et al. Correction: DAF-16 and TCER-1 Facilitate Adaptation to Germline Loss by Restoring Lipid Homeostasis and Repressing Reproductive Physiology in C. elegans. PLoS Genet. 2016; 12(10):e1006381. https://doi.org/10.1371/journal.pgen.1006381 PMID: 27716821.

58. Amrit FR, Steenkiste EM, Ratnappan R, Chen SW, McClendon TB, Kostka D, et al. DAF-16 and TCER-1 Facilitate Adaptation to Germline Loss by Restoring Lipid Homeostasis and Repressing Reproductive Physiology in C. elegans. PLoS Genet. 2016; 12(2):e1005788. https://doi.org/10.1371/journal.pgen.1005788 PMID: 26862916.

4.3 Mallick and Gupta (2020)- micropublication Biology

In this study we show that only *vit-2* is significantly in the *pry-1* mutants during day-2 and day-4 of adulthood. Given that *pry-1* mutants only have a mean lifespan of 3 days, we hypothesized whether knocking down *vit-2* could rescue the lifespan and lipid defects in these animals. Our results revealed that knocking down *vit-2* by using dsRNA specific for *vit-1/2* in adults rescued both the lipid level and short lifespan of *pry-1(mu38)* animals. These findings further supported our model (4.1.1) of vitellogenins acting downstream of PRY-1 signalling to regulate lipid synthesis that in part also affect lifespan of animals.

Contributions: I performed experiments and provided data. I and Bhagwati Gupta created all the Figures and illustrations. Bhagwati Gupta conceived and supervised the project. I and Bhagwati Gupta wrote the manuscript. It was finally revised with addressed reviewers concerns by me and Bhagwati Gupta.

microPublication BIOLOGY

7/21/2020 - *Open Access*

Vitellogenin-2 acts downstream of PRY-1/Axin to regulate lipids and lifespan in *C. elegans*

Avijit Mallick[1§] and Bhagwati P Gupta[1]

[1]Department of Biology, McMaster University

[§]To whom correspondence should be addressed: mallia1@mcmaster.ca

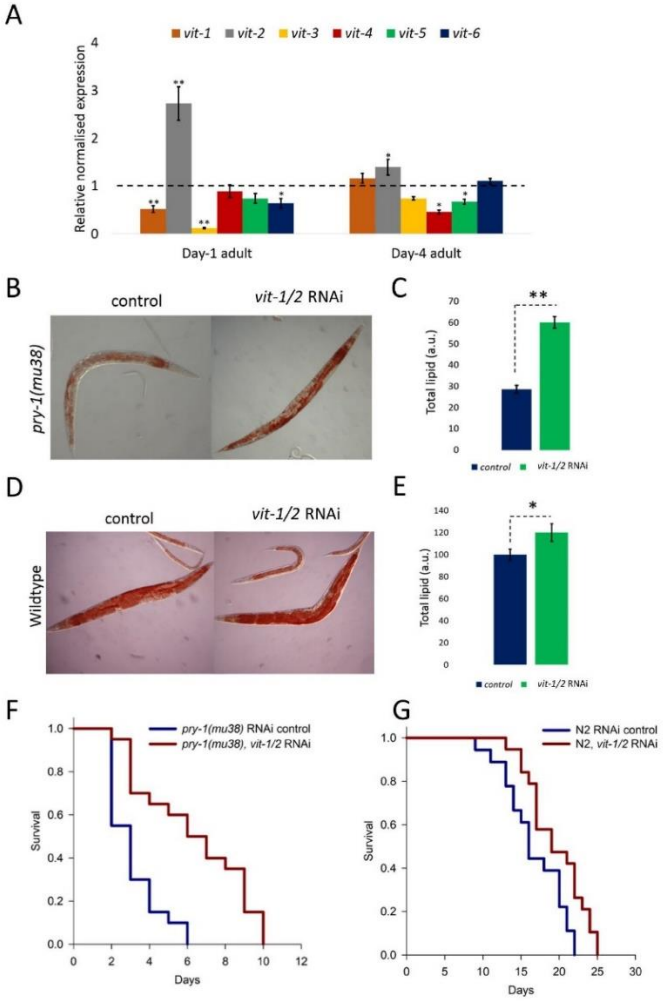

Figure 1: *vit-2* functions downstream of *pry-1* to regulate lipid levels and lifespan. (A) qRT-PCR analysis of *vit* genes in day-1 and day-4 *pry-1(mu38)* adults. The relative normalized expression has been plotted. Each data point represents the mean of at least two replicates and the error bar represents the SEM. *$p<0.05$ and **$p<0.01$, compared to wildtype (N2) which is normalized to one. **(B-E)** Oil Red O analysis of N2 and *pry-1* mutants following control and *vit-1/2* RNAi treatments. B, D) DIC micrographs of representative *pry-1(mu38)* and N2 day-4 adults. **(C, E)** Quantification of Oil Red O signal from two replicates. **(F, G)** Lifespan analysis of *pry-1(mu38)* and N2 animals following adult-specific knockdown of *vit-1/2*. Mean lifespan increased by 102% (6.3 ± 0.6 compared to 3.1 ± 0.3, $p<0.001$) for *pry-1(mu38)* and 16.6% (19.6 ± 0.8 compared to 16.7 ± 0.8, $p<0.01$) for N2.

microPublication BIOLOGY

7/21/2020 - *Open Access*

Description

Lipid metabolism plays an essential role in the survival and adaptation of animals under variable environmental conditions. Lipids are important macromolecules that store energy, serve as structural components, and function as signaling molecules (Watts and Ristow 2017; Papsdorf and Brunet 2019). Defects in lipid metabolism are linked to various diseases and aging in eukaryotes. Therefore, understanding the regulation of this process is critical to modulating disease progression (Wymann and Schneiter 2008).

We have shown earlier that lipid metabolism in *C. elegans* is regulated by an Axin family member, PRY-1 (Ranawade *et al.* 2018). While the signaling network of PRY-1 in this process remains to be investigated, Axin family of proteins are known to function in both WNT dependant and independent pathways to regulate various developmental events (Mallick, *et al.* 2019). Our transcriptomic analysis of both mRNA and miRNA genes revealed that PRY-1 is involved in lipid synthesis by affecting the expression of genes such as fatty acid desaturases (*fat-5, fat-6,* and *fat-7*) and vitellogenins (*vit-1, vit-2, vit-3, vit-4, vit-5* and *vit-6*) (Ranawade *et al.* 2018; Mallick, *et al.* 2019).

Vitellogenins are yolk lipoproteins, similar to mammalian apolipoprotein B, that bind to complex lipids and aid in their transportation from the intestine to the gonad (Kimble and Sharrock 1983; Grant and Hirsh 1999). Moreover, *vit-2* has been shown to negatively regulate longevity and such a role of *vit-2* depends on autophagy, lysosomal lipases, DAF-16/FOXO and HLH-30/TFEB (Seah *et al.* 2016). In this study, we report a new, adult-specific role of *vit-2* in *pry-1*-mediated regulation of lipid levels and lifespan. We analyzed the transcript levels of *vit* genes in day-1 and day-4 adults and found that *vit-2* was the only vitellogenin whose expression was significantly upregulated in *pry-1* mutants (Figure 1A). This suggested to us that *vit-2* is negatively regulated by *pry-1* and may be involved in *pry-1*-mediated adult-specific processes. To investigate this further, we examined whether *vit-2* knockdown during adulthood can rescue the lipid and lifespan defect (Mallick, *et al.* 2020) of *pry-1* mutants. This was done using a *vit-1* dsRNA that also knocks down *vit-2* due to the sequence similarity (Ranawade *et al.* 2018). The results showed that the knockdown of *vit-1/2* during adulthood significantly rescued lipid levels in *pry-1(mu38)* (almost 2-fold) (Figures 1B and 1C). Similar experiments in wildtype animals showed a modest increase (by 1.2-fold). We also examined the lifespan phenotype following *vit-1/2* RNAi and observed a marked rescue of the lifespan defect (Mallick *et al.* 2020) in *pry-1(mu38)* (102% increase in mean lifespan). The wildtype animals showed a comparatively lower increase in the mean lifespan (16.6%) (Figures 1F and 1G). Overall, these findings show that *vit-2* functions downstream of *pry-1* to regulate both lipid levels and lifespan.

Methods

Request a detailed protocol

Strain and growth conditions

Worms were grown at 20°C on standard nematode growth media plates seeded with *E. coli* OP50. The strains are N2 (wildtype *C. elegans*) and DY220 *pry-1(mu38)* I.

Lifespan analysis

Lifespan experiments were performed as described previously (Murphy *et al.* 2003) at 20°C. All experiments were performed on RNAi plates with HT115 cells expressing either empty vector (L4440) or dsRNA of *vit-1/2* gene (The Ahringer *C. elegans* RNAi feeding library, sjj_K09F5.2, location X-4A17, FP: CATGCTTGCTTTGTGGAGAA and RP: TTTGAGAATCCTGGGAAACG). Synchronized animals were transferred onto RNAi plates at L4 stage and observed every day throughout the lifespan.

Oil Red O staining

Oil Red O staining was performed as previously reported (Ranawade *et al.* 2018). Animals at day-1 adulthood were collected after washing with 1X PBS buffer from the plate and treated as described in the protocol. Animals were mounted and imaged with a Q imaging software and Micropublisher 3.3 RTV color camera outfitted with DIC optics on a Nikon 80i microscope. NIH ImageJ software was used to quantify Oil Red O intensities (Soukas *et al.* 2009). 15 to 30 worms were randomly selected from each category in at least two separate batches.

qPCR analysis

Total RNA was extracted from bleach synchronized worms by Tri-reagent (Catalog Number T9424, Sigma-Aldrich Canada) according to the manufacturer's instructions. Using oligo (dT) primers cDNA was made from total RNA with SensiFAST™ cDNA kit (Catalog Number BIO-65054, USA). Quantitative real-time PCR (qRT-PCR) analysis was performed on a CFX 96 BioRad cycler in triplicate with SensiFAST™ SYBR® Green Kit (Catalog Number BIO-98005, USA), according to the manufacturer's instructions. Primers used in the study are listed below: *pmp-3* (FP: CTTAGAGTCAAGGGTCGCAGTGGAG and RP: ACTGTATCGGCACCAAGGAAACTGG), *vit-1* (FP: GGTTCGCTTTGACGGATACAC and RP: AACTCGTTGGTGGACTCATC), *vit-2* (FP: GACACCGAGCTCATCCGCCCA and RP: TTCCTTCTCTCCATTGACCT), *vit-3* (FP: GGCTCGTGAGCAAACTGTTG and RP: TTAATAGGCAACGCAGGCGG), *vit-4* (FP:

microPublication BIOLOGY

7/21/2020 - *Open Access*

TGTCAACGGACAAGAGGTTG and RP: TCCTTTGGTCCAGAGACCTTC), *vit-5* (FP: GGCAATTTGTTAAGCCACAA and RP: CCTCCTTTGGTCCAGAAACCT) and *vit-6* (FP: AGTCGCTATTGTCGAGCGTC and RP: AGACGGAGGTCACCTTTTGC).

Statistical analysis

For lifespan analysis, all statistics were performed using SigmaPlot software 11. Survival curves were estimated using the Kaplan-Meier test, and differences among groups were assessed using the log-rank test. Survival data are expressed relative to the control group. Other statistics were performed using Microsoft Office Excel 365. Bio-Rad CFX manager was used for Ct and *p* values of qPCR analysis.

Acknowledgments: N2 strain was provided by Caenorhabditis Genetics Centre (CGC).

References

Grant B, Hirsh D. 1999. Receptor-mediated endocytosis in the Caenorhabditis elegans oocyte. Mol Biol Cell. 10(12):4311–4326. DOI: 10.1091/mbc.10.12.4311 | PMID: 10588660.

Kimble J, Sharrock WJ. 1983. Tissue-specific synthesis of yolk proteins in Caenorhabditis elegans. Dev Biol. 96(1):189–196. DOI: 10.1016/0012-1606(83)90322-6 | PMID: 6825952.

Mallick A, Ranawade A, Gupta BP. 2020. Axin-mediated regulation of lifespan and muscle health in C . elegans involves AMPK-FOXO signaling. bioRxiv:1–39. DOI: 10.1101/2020.04.22.055962

Mallick A, Ranawade A, Gupta BP. 2019. Role of PRY-1/Axin in heterochronic miRNA-mediated seam cell development. BMC Dev Biol. 19(1):1–12. DOI: 10.1186/s12861-019-0197-5. | PMID: 31307392.

Mallick A, Taylor SKB, Ranawade A, Gupta BP. 2019. Axin Family of Scaffolding Proteins in Development: Lessons from C. elegans. J Dev Biol. 7(4):20. DOI: 10.3390/jdb7040020 | PMID: 31618970.

Murphy CT, McCarroll SA, Lieb JD, Bargmann CI, Kamath RS, Fraser A, Ahringer J, Li H, Kenyon CJ. 2003. Genes that act downstream of DAF-16 to influence C. elegans lifespan. Nature. 424:277–283. DOI: 10.1038/nature01789 | PMID: 12845331.

Papsdorf K, Brunet A. 2019. Linking Lipid Metabolism to Chromatin Regulation in Aging. Trends Cell Biol. 29(2):97–116. DOI: 10.1016/j.tcb.2018.09.004 | PMID: 30316636.

Ranawade A, Mallick A, Gupta BP. 2018. PRY-1/Axin signaling regulates lipid metabolism in Caenorhabditis elegans. PLoS One. 13(11):e0206540. DOI: 10.1371/journal.pone.0206540 | PMID: 30403720.

Seah NE, de Magalhaes Filho CD, Petrashen AP, Henderson HR, Laguer J, Gonzalez J, Dillin A, Hansen M, Lapierre LR. 2016. Autophagy-mediated longevity is modulated by lipoprotein biogenesis. Autophagy. 12(2):261–272. DOI: 10.1080/15548627.2015.1127464 | PMID: 26671266.

Soukas AA, Kane EA, Carr CE, Melo JA, Ruvkun G. 2009. Rictor/TORC2 regulates fat metabolism, feeding, growth, and life span in Caenorhabditis elegans. Genes Dev.:496–511. DOI: 10.1101/gad.1775409.2004. | PMID: 19240135.

Watts JL, Ristow M. 2017. Lipid and carbohydrate metabolism in Caenorhabditis elegans. Genetics. 207(2):413–446. DOI: 10.1534/genetics.117.300106. | PMID: 28978773.

Wymann MP, Schneiter R. 2008. Lipid signalling in disease. Nat Rev Mol Cell Biol. 9(2):162–176. DOI: 10.1038/nrm2335. | PMID: 18216772.

Funding: This work was supported by NSERC Discovery grant to Bhagwati Gupta.

Author Contributions: Avijit Mallick: Investigation, Data curation, Conceptualization, Validation, Writing - original draft. Bhagwati P Gupta: Conceptualization, Supervision, Writing - review and editing, Funding acquisition.

Reviewed By: Anonymous

History: Received July 6, 2020 **Revision received** July 17, 2020 **Accepted** July 17, 2020 **Published** July 21, 2020

Citation: Mallick, A; Gupta, BP (2020). Vitellogenin-2 acts downstream of PRY-1/Axin to regulate lipids and lifespan in *C. elegans*. microPublication Biology. https://doi.org/10.17912/micropub.biology.000281

Chapter 5

Axin-mediated regulation of lifespan and muscle health in *C. elegans* requires AMPK-FOXO signaling

5.1 Preface

This chapter includes the following two articles in its originally published format: "Axin-mediated regulation of lifespan and muscle health in *C. elegans* requires AMPK-FOXO signaling", by Avijit Mallick, Ayush Ranawade, Wouter van den Berg and Bhagwati P. Gupta. iScience. 23, 101843 (DOI: https://doi.org/10.1016/j.isci.2020.101843). This is an open-access article distributed under the terms of the Creative Commons Attribution Unported License, which permits

5.2 Mallick, Ranawade, van den Berg and Gupta (2020)- iScience

In this study, we reported the role of PRY-1/Axin in maintaining lifespan and muscle health of animals. PRY-1 functions in the muscle is crucial to delay fragmentation of muscle mitochondrial morphology and for normal expression of muscle-specific genes involved in muscle development and function (contraction). Such a role of PRY-1 in muscle requires AMPK catalytic subunit homolog AAK-2, where AAK-2 is activated by PRY-1 probably via complex formation, and cell autonomously regulate DAF-16/FOXO localisation in the intestine. This is also supported by the transcriptomic analyses of *pry-1*, *aak-2* and *daf-16* mutants which revealed significant overlap of differentially expressed genes between these three data sets. Moreover, overexpression of *pry-1* in the muscle leads to longer lifespan, better muscle mitochondrial morphology, muscle activity and increased lipid level. Taken together, our data demonstrate that PRY-1 functions in muscles to promote the life span of animals. This study establishes Axin as a major regulator of muscle health and aging.

Contributions: I performed experiments and provided data for Figures 1A-D, 2, 3, 4B-E, 5, 6A-E, 7, S1A, S2C-D, and S3-7. Ayush Ranawade performed experiments and provided data for Figures 1E-F, 4A, SB-C and S2A-B. Wouter van den Berg performed experiments and provided data for Figure 6F. I and Bhagwati Gupta created all the Figures and illustrations. Bhagwati Gupta conceived and supervised the project. I and

Bhagwati Gupta wrote the manuscript. It was finally revised with addressed reviewers concerns by me and Bhagwati Gupta.

iScience

CellPress
OPEN ACCESS

Article

Axin-Mediated Regulation of Lifespan and Muscle Health in *C. elegans* Requires AMPK-FOXO Signaling

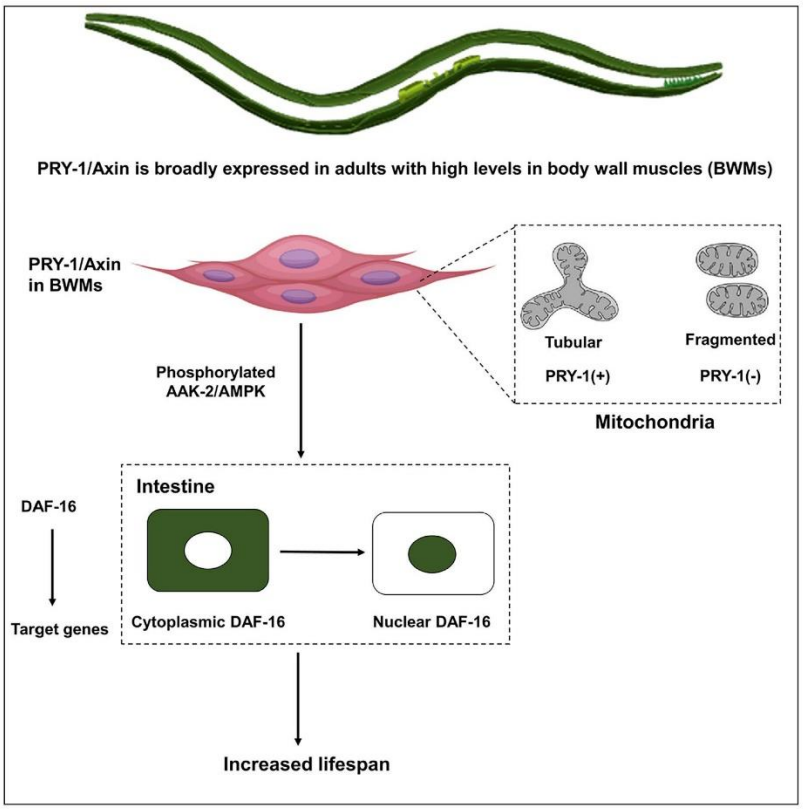

Avijit Mallick, Ayush Ranawade, Wouter van den Berg, Bhagwati P. Gupta

guptab@mcmaster.ca

HIGHLIGHTS

pry-1 transcriptome contains genes linked to aging and muscle function

pry-1 functions in muscles to maintain life span and mitochondrial network

Muscle-specific overexpression of *pry-1* extends life span and promotes muscle health

PRY-1-mediated life span extension depends on AAK-2-DAF-16 signaling

Mallick et al., iScience *23*, 101843
December 18, 2020 © 2020 The Authors.
https://doi.org/10.1016/j.isci.2020.101843

iScience

CellPress
OPEN ACCESS

Article

Axin-Mediated Regulation of Lifespan and Muscle Health in *C. elegans* Requires AMPK-FOXO Signaling

Avijit Mallick,[1] Ayush Ranawade,[1,2] Wouter van den Berg,[1] and Bhagwati P. Gupta[1,3,*]

SUMMARY

Aging is a significant risk factor for several diseases. Studies have uncovered multiple signaling pathways that modulate aging, including insulin/insulin-like growth factor-1 signaling (IIS). In *Caenorhabditis elegans*, the key regulator of IIS is DAF-16/FOXO. One of the kinases that affects DAF-16 function is the AMPK catalytic subunit homolog AAK-2. In this study, we report that PRY-1/Axin plays an essential role in AAK-2 and DAF-16-mediated regulation of life span. The *pry-1* mutant transcriptome contains many genes associated with aging and muscle function. Consistent with this, *pry-1* is strongly expressed in muscles, and muscle-specific overexpression of *pry-1* extends life span, delays muscle aging, and improves mitochondrial morphology in AAK-2-DAF-16-dependent manner. Furthermore, PRY-1 is necessary for AAK-2 phosphorylation. Taken together, our data demonstrate that PRY-1 functions in muscles to promote the life span of animals. This study establishes Axin as a major regulator of muscle health and aging.

INTRODUCTION

Aging is defined as a progressive functional decline in living organisms. It is characterized by hallmarks such as genomic instability, epigenetic alterations, mitochondrial dysfunction, and telomere attrition, and is thought to be regulated in part by genetic pathways (Lopez-Otin et al., 2013). Several genes and pathways have been identified that govern and modulate life span and are conserved in higher eukaryotes (Kenyon, 2010; Lapierre and Hansen, 2012; Uno and Nishida, 2016). Insulin/insulin-like growth factor-1 signaling (IIS) was the first pathway shown to be involved in the regulation of aging in *Caenorhabditis elegans* (Kenyon, 2011; Kenyon et al., 1993). Subsequent studies have demonstrated that the IIS pathway is conserved across eukaryotes (Uno and Nishida, 2016). In *C. elegans*, reduction in the activity of the IIS receptor homolog DAF-2 leads to a prolonged life span, which is dependent on DAF-16, a FOXO transcription factor homolog (Kenyon et al., 1993). This modulation of life span by DAF-16 involves translocation to the nucleus followed by either the activation or repression of genes involved in stress response, metabolism, and autophagy (Lee et al., 2003; Melendez et al., 2003; Murphy et al., 2003).

The activity of DAF-16 is regulated by phosphorylation (Kenyon, 2010). One of the kinases involved in this process is the α2 catalytic subunit homolog of AMPK, AAK-2 (Greer et al., 2007a), a phenomenon that is conserved in the mammalian system (Greer et al., 2007b). AAK-2 also plays a crucial role in aging. It is essential for DAF-2-mediated life span extension, and its overexpression extends the life span of animals (Apfeld et al., 2004; Mair et al., 2011). Interestingly, a truncated version of AAK-2 bearing only the catalytic domain was found to be more effective than the full-length wild-type form, suggesting that AAK-2 activity is regulated during the normal aging process (Mair et al., 2011). As in *C. elegans*, AMPK in *Drosophila* is also involved in life span regulation. Specifically, overexpression of the α2 subunit in muscles and fat bodies extends the life span of transgenic animals (Stenesen et al., 2013).

AMPK is an established energy sensor in eukaryotes that is phosphorylated by several kinases, including LKB1 (Burkewitz et al., 2014; Hardie et al., 2012). Studies in mouse and human cell culture models have shown that, under the condition of glucose starvation, AMPK forms a complex with LKB1 and the scaffolding protein Axin (Zhang et al., 2013b). The multimeric complex regulates AMPK activation, leading to phosphorylation of downstream targets (Hardie and Lin, 2017; Hardie et al., 2012). The involvement of Axin in AMPK complex formation is essential, since Axin knockdown drastically reduces AMPK activity,

[1]Department of Biology, McMaster University, Hamilton, ON L8S-4K1, Canada

[2]Present address: Department of Bioengineering, Northeastern University, 360 Huntington Avenue, Boston, MA 02115

[3]Lead Contact

*Correspondence: guptab@mcmaster.ca

https://doi.org/10.1016/j.isci.2020.101843

CellPress OPEN ACCESS

iScience
Article

leading to fatty liver in starved mice (Zhang et al., 2013b). In addition to their role in AMPK regulation, Axin family members are also involved in multiple biological processes during development and post-development (Mallick et al., 2019b). Since its discovery as a negative regulator of WNT signaling, Axin has been demonstrated to participate in other, non-WNT, pathways as well. In all cases, a common thread is Axin's role as a scaffold protein in recruiting other factors to form complexes (Mallick et al., 2019b). However, whether the scaffolding role of Axin affects FOXO activity remains to be investigated.

In this study, we report that the *C. elegans* Axin homolog PRY-1, which is necessary for embryonic and larval processes, is also essential for normal life span maintenance. Previously, it was found that metformin-mediated life span extension depends on another *C. elegans* Axin-like gene, *axl-1*. However, *axl-1* mutants do not show defects in aging and age-related processes (Chen et al., 2017). Our work has revealed that animals lacking *pry-1* function during adulthood are short-lived and show increased deterioration in aging-associated processes. Consistent with this, *pry-1* mutant transcriptome contains many aging-related protein-coding and miRNA genes. We found that *pry-1* is broadly expressed in adults, with high levels in body wall muscles (BWMs). Moreover, muscle-specific knockdown of *pry-1* caused an increase in the proportion of fragmented mitochondria and led to a reduction in life span. Conversely, overexpression of *pry-1* in muscles improved both phenotypes. Thus, *pry-1* appears to affect life span by regulating muscle mitochondria health. Interestingly, muscle-specific expression of mouse Axin (*mAxin1*) in *C. elegans* also extended life span, suggesting that Axin's role in aging may be conserved. It is worth mentioning that Axin is expressed in mouse and human skeletal muscles (Smith et al., 2019; Uhlen et al., 2015). To investigate PRY-1's mechanism of action, we performed a combination of molecular genetics and biochemical experiments. The results revealed that PRY-1's role in aging depends on AAK-2 and DAF-16. Our data suggest that PRY-1 presumably forms a complex with AAK-2 leading to its phosphorylation, thereby promoting nuclear localization of DAF-16 in the intestine and life span maintenance.

RESULTS

pry-1 Transcriptome Contains Genes Involved in Life Span Regulation

The involvement of PRY-1 in multiple signaling pathways and biological events is well documented (Mallick et al., 2019b). Earlier, we reported both mRNA and microRNA (miRNA) transcriptome profiles of *pry-1* mutant that revealed 2,665 differentially expressed protein-coding genes and six miRNAs (Mallick et al., 2019a; Ranawade et al., 2018). The characterization of differentially expressed genes showed *pry-1*'s crucial role in miRNA-mediated seam cell development (Mallick et al., 2019a) and lipid metabolism (Ranawade et al., 2018). In this study, we have specifically focused on the genes linked to aging. Of the differentially expressed miRNAs, *mir-246* is involved in aging and stress response (de Lencastre et al., 2010). The mRNA transcriptome dataset was analyzed using Gene Ontology (GO) terms, which revealed that aging-related protein-coding genes and gene families are overrepresented (69 in total; relative frequency (RF): 2, $p < 4.91 \times 10^{-9}$; 33% upregulated and 67% downregulated) and that they are linked to biological activities such as cellular processes (26 genes), metabolic processes (24 genes), and biological regulation (13 genes) (Figure 1A; Table S1). Within cellular processes, candidates include genes linked to lipid metabolism (*aap-1, hyl-1, elo-2, ctl-2, cat-1,* and *lipl-4*), which further supports the essential role of lipids in *pry-1*-mediated signaling (Ranawade et al., 2018) and suggests that *pry-1* may affect lipid metabolism to regulate aging.

Further GO term analysis of protein-coding aging-related genes showed that they are linked to 32 distinct signaling pathways and include well-known factors such as AAP-1 (PI3K adapter subunit) and DAF-16, both belonging to the IIS pathway (Lapierre and Hansen, 2012; Uno and Nishida, 2016), and XBP-1, a human XBP1 ortholog that acts downstream of IRE-1 and PEK-1-mediated signaling (Ron and Walter, 2007). Thus, *pry-1* appears to interact with multiple genetic networks. We also compared the *pry-1* transcriptome with differentially expressed genes of the DAF-2-DAF-16 signaling pathway (Lin et al., 2018) and found a significant overlap (415 genes; RF: 1.7, $p < 2.228 \times 10^{-31}$, Table S3). Additionally, 29 of 109 DAF-16 direct targets (Li and Zhang, 2016) are present in the *pry-1* dataset (27% overlap, $p < 0.01$; two-thirds downregulated), including four (*dod-17, prdx-3, nnt-1,* and *daf-16*) that are directly involved in aging (Figure 1B; Table S3). Taken together, these *in silico* analyses suggest that *pry-1* acts in part via DAF-16 to regulate life span in *C. elegans*.

Mutations in *pry-1* Reduce Life Span

In accordance with the above data suggesting *pry-1*'s role in aging, *pry-1* expression was found to be significantly higher in older adults (Figure S1A).We also found that the mean life span of *pry-1(mu38)* animals was 80% ($p < 0.001$) shorter compared with that of wild-type animals (Figure 1C; Table S2). A similar reduction in

iScience
Article

CellPress
OPEN ACCESS

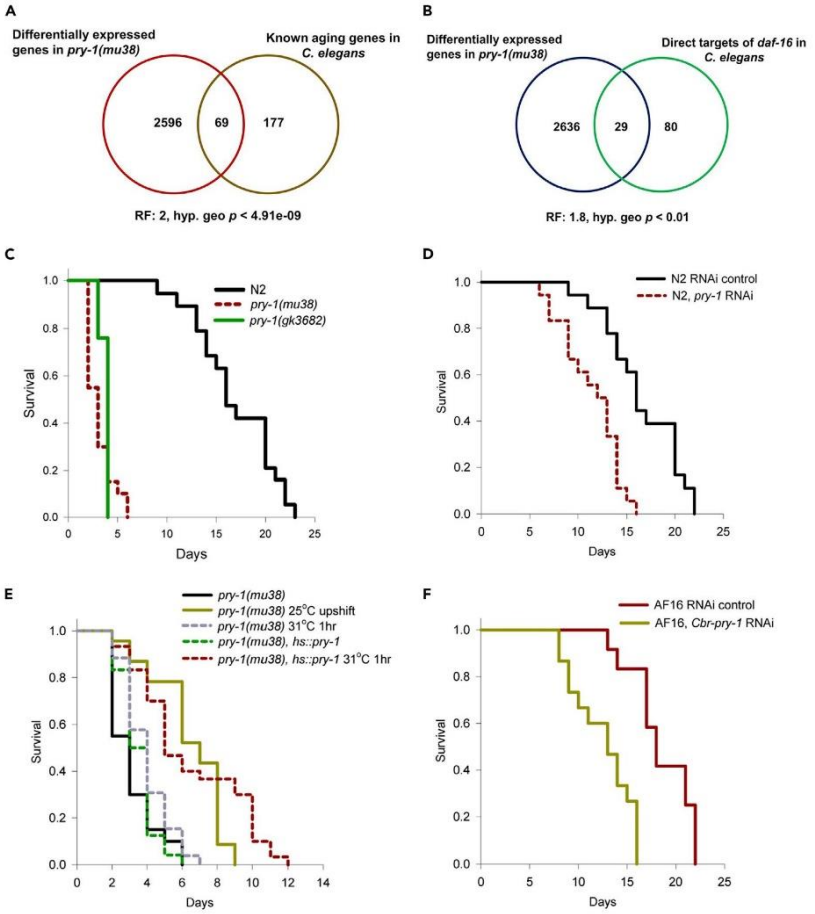

Figure 1. *pry-1* is Required for the Normal Life Span of Animals

(A) Sixty-nine differentially expressed genes in *pry-1* mutant transcriptome are linked to aging.

(B) More than a quarter of DAF-16 direct targets is present in *pry-1* mutant transcriptome.

(C) Life span of *pry-1(mu38)* animals.

(D) Life span of Adult-specific *pry-1(RNAi)* animals.

(E) Life span rescue experiments following two different treatments during adulthood, namely subjecting *pry-1(mu38)* to a 25°C upshift and 31°C 1hr heat-shock to *pry-1(mu38); hs::pry-1* animals. The control worms consist of *pry-1(mu38)* alone, *pry-1(mu38)* subjected to 31°C 1hr heat shock, and *pry-1(mu38); hs::pry-1* without heat shock.

(F) Life span analysis of *Cbr-pry-1(RNAi)* animals.

(E and F) See Transparent Methods and Table S2 for life span data and statistical analyses.

life span was also observed with a CRISPR allele, *gk3682*, that deletes a roughly 750-bp region, including the 5′ UTR and the first exon (Mallick et al., 2019a) (Figure 1C; Table S2). As *pry-1* is also involved in developmental processes (Mallick et al., 2019b), we took an RNAi approach to knock down the gene function specifically during adulthood. As expected, *pry-1(RNAi)* animals were found to be short-lived, with 22–31% ($p < 0.01$) reduced mean life span (Figure 1D; Table S2).

To further investigate whether *pry-1* affects aging, we performed two sets of rescue experiments. One of these involved making use of the cold-sensitive allele *mu38*. While the life span defect of *pry-1(mu38)* was

CellPress OPEN ACCESS

iScience Article

severe at 20°C (mean life span 81% lower than N2, $p < 0.001$, Figure 1E; Table S2), the animals appeared healthier and showed an improved life span at 25°C (50% lower than N2, $p < 0.01$, Figure 1E; Table S2). When day-1 *pry-1(mu38)* adults were upshifted from 20°C to 25°C, life span was extended by 107% (6.4 ± 0.4 days mean life span compared with 3.2 ± 0.1 days for untreated *mu38* control, $p < 0.01$). In the other experiment, transgenic animals were generated carrying a heat-shock promoter-driven *pry-1*. The *hs::pry-1* transgene efficiently rescued the life span defect of *pry-1(mu38)* animals upon heat-shock during adulthood (58% longer mean life span compared to control animals, $p < 0.001$, Figure 1E; Table S2). Interestingly, no such effect was observed when the transgene was expressed in wild-type background (Figure S1B; Table S2).

Since our lab had previously reported a conserved role of *C. briggsae pry-1* during development (Seetharaman et al., 2010), we investigated whether *Cbr-pry-1* is also involved in aging. The results revealed both the *sy5353* mutant allele and adult RNAi caused a shorter life span in animals (Figures 1F and S1C; Table S2). These data show that *pry-1* function in life span maintenance is conserved in nematodes.

pry-1 Knockdown in Adults Causes Accelerated Aging and Increased Expression of Stress Response Markers

Several physiological and molecular changes occur in animals during the aging process. These include a decline in tissue function, oxidative stress, accumulation of mis/unfolded proteins, and altered lipid distributions (Huang et al., 2004; Lopez-Otin et al., 2013). To characterize such changes in *pry-1(RNAi)* animals, we analyzed the age-dependent decline in pharyngeal pumping and body bending. Adult-specific knockdown led to a significant reduction in rates of pharyngeal pumping and body bending starting on days 7 and 2, respectively (Figures 2A and 2B). Similar phenotypes were also observed in *pry-1(mu38)* mutants, although the defects were more severe (Figures S2A and S2B). Consistent with the adult-specific role of *pry-1*, we found that heat-shocked *pry-1(mu38); hs::pry-1* adults showed significant improvements in both these aging-related markers (Figures S2C and S2D). Together, the results demonstrate that *pry-1* is needed to delay aging-associated physical deterioration in animals.

Next, we measured lipofuscin levels in adults. In *C. elegans*, lipofuscin, a product of oxidative damage and autophagy, is visible as auto fluorescent granules in the intestine and serves as a biomarker of aging (Davis et al., 1982). Quantification of the intestinal autofluorescence showed a 30% increase ($p < 0.05$) in *pry-1(RNAi)* adults compared with that in N2 control animals (Figures 2C and 2D). The expression of an oxidative stress marker, manganese superoxide dismutase (*sod-3*), was also investigated (Lopez-Otin et al., 2013). The RNAi-mediated knockdown of *pry-1* caused no significant change in *sod-3:GFP* fluorescence (Figures 2C and 2D), suggesting that *pry-1* function is not essential for the maintenance of oxidative stress.

Other indicators of premature aging include unfolded protein response (UPR) associated with mitochondria and ER (UPR^{MT} and UPR^{ER}, respectively) (Lopez-Otin et al., 2013). Upon activation, these UPR pathways increase the expression of chaperones and heat shock proteins such as *hsp-6* and *hsp-60* (UPR^{MT}) (Tran and Van Aken, 2020) and *hsp-4/Bip* (UPR^{ER}) (Ron and Walter, 2007). We found that GFP fluorescence of all three markers, namely *hsp-6::GFP*, *hsp-60::GFP*, and *hsp-4::GFP*, was significantly increased in *pry-1(RNAi)* day-8 adults compared with that in controls (70%, 40%, and 50% higher, respectively, $p < 0.01$) (Figures 2C and 2D). Moreover, it was observed that *pry-1* transcriptome contains genes involved in IRE-1/IRE1 and PEK-1/PERK-mediated UPR^{ER} signaling (57 genes, 49% overlap, R.F. 3.2, $p < 5.87 \times 10^{-18}$; and 10 genes, 43% overlap, R.F. 2.9, $p < 0.001$, respectively) (Table S4), including the key downstream factor, XBP-1, which activates *hsp-4* expression (Ron and Walter, 2007).

Collectively, the above data provide evidence that *pry-1* plays an essential role in the maintenance of aging-associated processes and stress response in animals. One possibility may be that *pry-1* affects aging by regulating lipid metabolism. This is supported by our previous results demonstrating that lipid synthesis is compromised in *pry-1* mutant animals (Mallick and Gupta, 2020; Ranawade et al., 2018). More importantly, adult-specific knockdown of *pry-1* caused a significant reduction in lipid content in day-8 adults (Figure 2E). Given that *daf-16* is also necessary for lipid synthesis (Murphy et al., 2003; Ogg et al., 1997; Zhang et al., 2013a) and *pry-1* and *daf-16* transcriptomes contain a common set of lipid synthesis and transport genes (such as *fat-5-7* and *vit-1/3/4/5*) (Table S3), it is conceivable that *pry-1* and *daf-16* interact to regulate lipid levels, leading to a normal life span of animals.

iScience
Article

CellPress
OPEN ACCESS

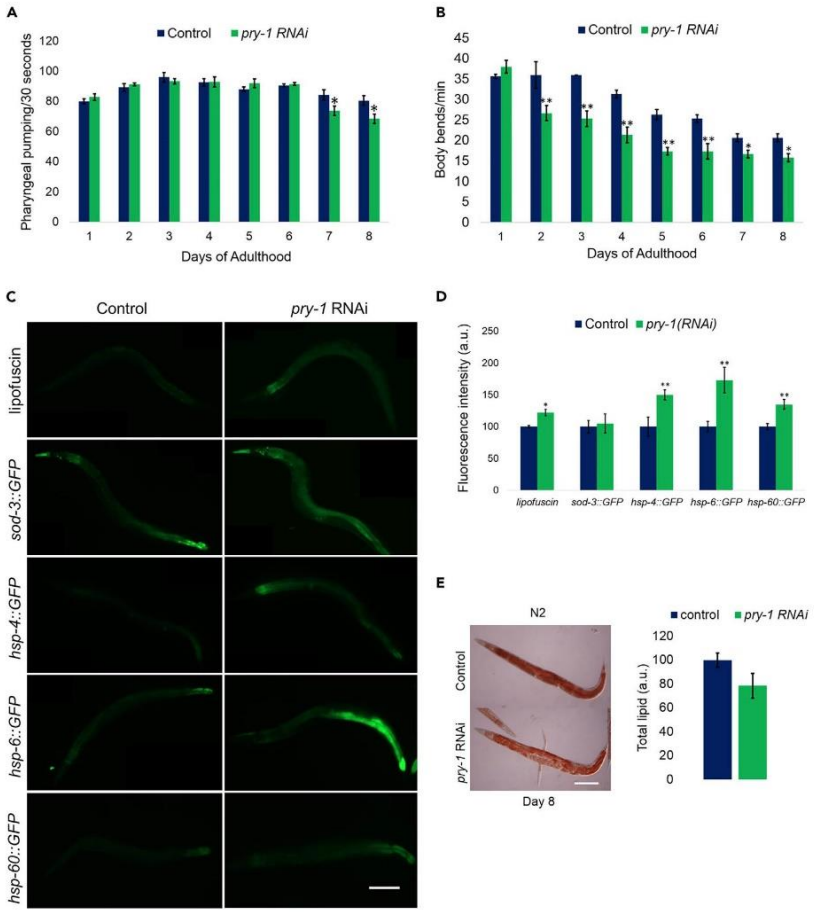

Figure 2. Adult-Specific Lowering of *pry-1* Accelerates Aging-Associated Markers

(A and B) Pharyngeal pumping of RNAi-treated *pry-1* in day-7 and day-8 adults (A) and body bending starting day-2 of adulthood (B). Data represent the mean of at least two replicates ($n \geq 30$ animals) and error bars represent the standard deviation. Significance was calculated using Student's t-test $^{*}p < 0.05$, $^{**}p < 0.01$.

(C) Representative images of animals showing aging pigment (lipofuscin), ROS marker (*sod-3::GFP*), UPR-ER marker (*hsp-4::GFP*), and UPR-MT markers (*hsp-6::GFP* and *hsp-60::GFP*). Scale bar is 0.1mm.

(D) Quantification of fluorescence intensity shown in panel C.

(E) Oil red O staining of total lipid droplets in day-8 control and *pry-1(RNAi)* animals. Scale bar is 0.1mm. (D and E) Data represent the mean of two replicates ($n \geq 15$ animals in each), and error bars represent the standard deviation. Significance was calculated using Student's t-test. $^{**}p < 0.01$.

pry-1 Knockdown Suppresses Life Span Extension of *mom-2/WNT* Mutants

As PRY-1 is an established negative regulator of WNT signaling, we examined its genetic interactions with WNT ligands. Of the five known ligands, loss-of-function mutations in *mom-2* and *cwn-2* cause an extension of life span (Lezzerini and Budovskaya, 2014). When *pry-1* was knocked down in *mom-2(or42)* and *cwn-2(ok895)* backgrounds, life span extension was significantly reduced in *mom-2* mutants (13.6% reduction in mean life span, $p < 0.05$, Figure 3A; Table S2) but remained unchanged in the *cwn-2* animals (Figure 3B; Table S2). We also analyzed the requirements of *bar-1/β-catenin*, a component of the canonical WNT signaling that plays a role in aging (Xu et al., 2019; Zhang et al., 2018), in the *mom-2-pry-1* pathway. Since

CellPress OPEN ACCESS

iScience
Article

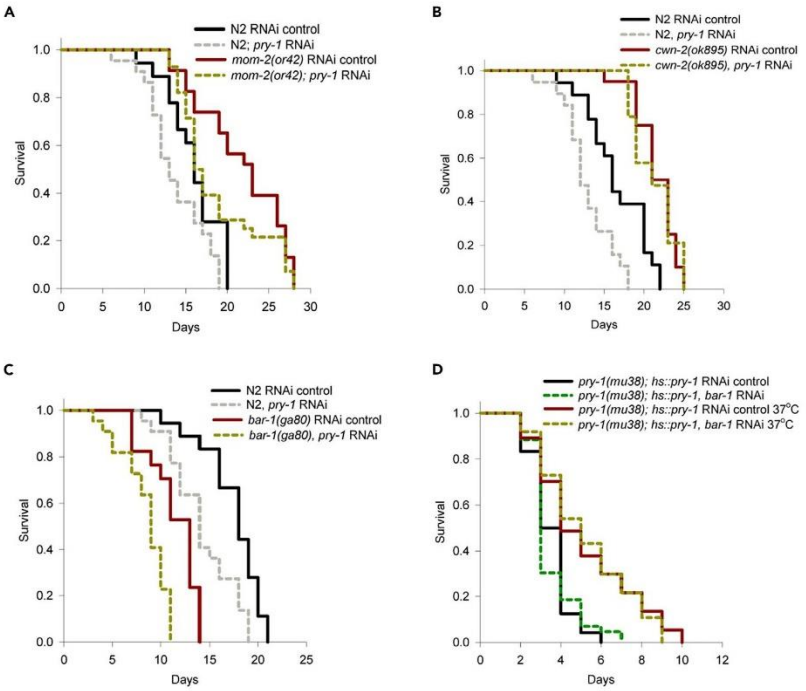

Figure 3. *pry-1* Functions Downstream of WNT Ligand *mom-2* and Independently of β-Catenin *bar-1* to Regulate Life Span

(A–C) Life span analysis following RNAi knockdown of *pry-1* in WNT pathway mutants, *mom-2(or42)* (A), *cwn-2(ok895)* (B), and *bar-1(ga80)* (C).

(D) Effect of *bar-1* RNAi in *pry-1(mu38); hs::pry-1* animals.

(A–D) See Transparent Methods and Table S2 for life span data and statistical analyses.

pry-1-mediated WNT signaling negatively regulates *bar-1*, removing *bar-1* function is expected to suppress the phenotype of *pry-1* mutants. However, we observed that the life span of *bar-1* null mutants was further shortened by *pry-1* RNAi (Figure 3C; Table S2), suggesting that *bar-1* is unlikely to participate in the *pry-1*-mediated aging process. Further support for this model comes from a *bar-1* RNAi experiment that failed to suppress the life span phenotype of *pry-1(mu38); hs::pry-1* animals (Figure 3D; Table S2). These data suggest that PRY-1 may act downstream of MOM-2 in a pathway that is independent of BAR-1 and likely to utilize DAF-16-mediated signaling.

Tissue-Specific Analysis Shows that *pry-1* is Needed in Muscles and Hypodermis

To investigate the requirements of *pry-1* in life span regulation, we examined its *in vivo* expression pattern. Previously, a 3.6-kb *pry-1* proximal promoter was used to drive the coding sequence of *pry-1* fused to a *GFP* reporter, which showed fluorescence throughout development, specifically in the vulval precursor cells, neurons, BWM, and some hypodermal cells (Korswagen et al., 2002). We further characterized *pry-1* expression, which revealed expression in almost all tissues during development. Expression in seam cells, neuronal cells, muscles, hypodermis, and intestine was readily visible (Figure 4A). This pattern of localization matches well with tissue enrichment of differentially expressed genes in the *pry-1* transcriptome using WormBase tissue ontology tool (Table S5, see Transparent Methods). The most enriched tissues include neurons and muscles.

A closer examination of GFP localization in developing animals revealed bright fluorescence in the ventral cord region, which includes neuronal and non-neuronal cells. The expression was largely similar in adults, although

iScience
Article

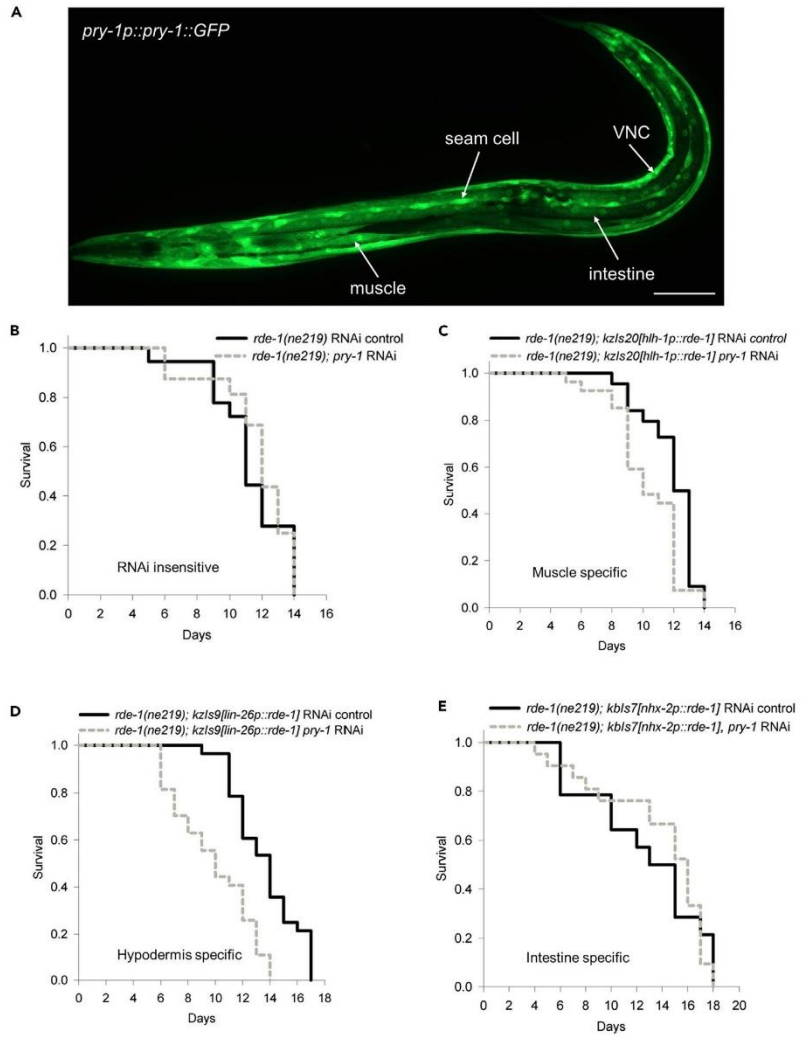

Figure 4. Expression Pattern of *pry-1* in Adults and Its Tissue-Specific Requirements for Life Span Maintenance
(A) Representative image of *pry-1p::pry-1::GFP* animals showing GFP fluorescence in muscles, intestine, seam cells, and neurons. Also see Figure S3. Scale bar is 0.1mm.
(B–E) Life span analysis after tissue-specific RNAi knockdown of *pry-1*. Also see Figures S4B and S4C *pry-1* RNAi knockdown control (B) and *pry-1* RNAi knockdown in muscle (C), hypodermis (D), and intestine (E). (B–E) See Transparent Methods and Table S2 for life span data and statistical analyses.

the fluorescence was much higher in BWMs (Figures 4A, S3A, and S3B). The posterior end of the intestine, near the rectal opening, showed a strong signal in L4 and adult animals; however, the rest of the intestine lacked a detectable expression. In general, GFP was diffused and not localized to any specific subcellular structures except in the case of muscles and posterior intestine, where nuclei are visible (see arrows in Figures S3B and S3C). The fluorescence continued to persist in older adults, consistent with the role of *pry-1* in aging. A similar pattern of expression for *pry-1* was also observed in *C. briggsae* transgenic animals, with a marked increase in

CellPress OPEN ACCESS

iScience
Article

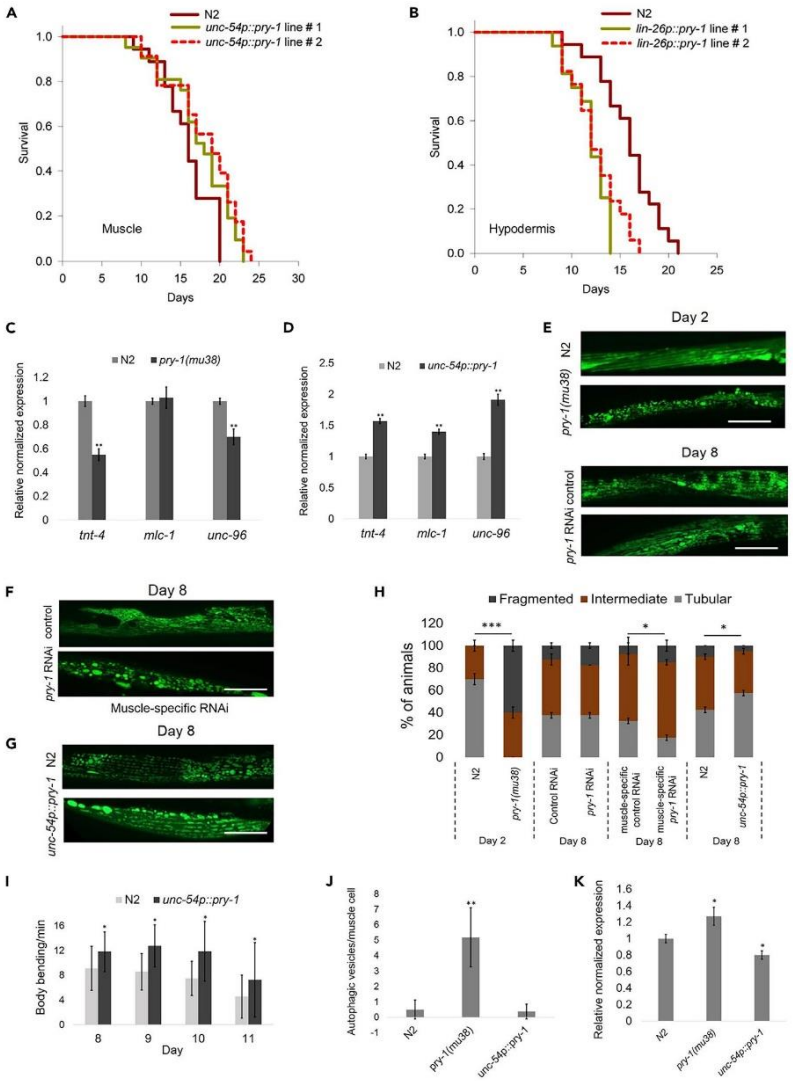

Figure 5. *pry-1* Overexpression in the Muscle Extends Life Span and Improves Muscle Physiology

(A and B) Effects of tissue-specific overexpression of *pry-1*. Overexpression in muscle (A), also see Figure S5B and Table S2, and in hypodermis (B). See Transparent Methods and Table S2 for life span data and statistical analyses.

(C and D) qPCR analysis of muscle genes *tnt-4*, *mlc-1* and *unc-96* in day-1 *pry-1(mu38)* (C) and *unc-54p::pry-1* (D) adults. Data represent the mean of two replicates and error bars represent the SEM. Significance was calculated using Bio-Rad software (t test). $^{**}p < 0.01$.

(E–G) Representative images of muscle mitochondrial morphologies revealed by *myo-3p::GFP(mito)* reporter in the control, *pry-1(mu38)*, *pry-1(RNAi)*, and *unc-54p::pry-1* transgenic animals. The control for whole-animal RNAi experiment was N2 (E) and for muscle-specific RNAi was an RNAi-sensitive strain (F), each fed with bacteria carrying an empty vector (L4440) (see Transparent Methods for genotypes). Day-2 adults were used for *pry-1(mu38)*, whereas day-8 adults for *pry-1(RNAi)* and *unc-54p::pry-1* animals. Scale bar is 25μm.

iScience
Article

CellPress
OPEN ACCESS

Figure 5. *Continued*

(H) Quantification of phenotypes in panels E, F, and G. Data represent the mean of two replicates (n = 20 animals in each) and error bars standard deviations. Statistical analyses were carried out using the two-tailed Fisher's exact test by comparing mitochondrial morphology between normal (tubular) and defective (intermediate and fragmented) categories and indicated by stars (*). *p < 0.05, ***p < 0.0001. See Transparent Methods for details.

(I) Body bending analysis of *unc-54p::pry-1* adults between day-8 and day-11. Also see Figure S5D.

(J) Number of autophagic vesicles per muscle cell at day-2 of adulthood revealed by *dyc-1S::lgg-1::GFP*, a GFP marker of autophagic vesicles in body-wall muscles. (I-J) Data represent the mean of two replicates (n ≥ 15 animals in each) and error bars standard deviations. Significance was calculated using Student's t-test. *p < 0.05, **p < 0.01.

(K) *lgg-1* transcript levels in *pry-1(mu38)* and *unc-54p::pry-1* animals. Data represent the means of two replicates and error bars the SEM. Significance was calculated using Bio-Rad software (t test). *p < 0.05.

fluorescence in muscles throughout adulthood (Figure S4A). This pattern of *pry-1* expression in both nematodes suggests that the gene may play a conserved role in maintaining muscle health during aging.

Given that *pry-1* is expressed in muscles as well as other tissues, we examined its tissue-specific requirements for life span maintenance. To this end, RNAi experiments were performed in adults using strains that allow tissue-specific knockdowns in muscles, hypodermis, intestine, and neurons (see Transparent Methods). The results showed that *pry-1* RNAi caused a significant reduction in mean life span when knocked down in the hypodermis and muscles (26% lower mean life span in hypodermis RNAi and 12% in muscle RNAi, $p < 0.05$) (Figures 4B–4D). No such effect was observed in other tissues (Figures 4E, S4B, and S4C). We conclude that *pry-1* functions in muscles and hypodermis to maintain the life span of animals. Further support for this comes from the analysis of transgenic strains in which *pry-1* expression was driven by hypodermal and muscle-specific promoters (*lin-26p::pry-1* and *unc-54p::pry-1*, respectively). In both cases, the life span defect of *pry-1(mu38)* animals was significantly rescued (41% and 56% increases in mean life span by *lin-26p::pry-1* and *unc-54p::pry-1*, respectively, $p < 0.01$) (Figures S5A and S5B; Table S2).

Having uncovered the role of *pry-1* in hypodermis and muscles, we examined whether overexpression of the gene in these two tissues can extend the life span. Interestingly, while muscle-specific expression (*unc-54p::pry-1*) extended the life span significantly (13% increase in mean life span, $p < 0.05$), no such effect was observed in the case of hypodermis-specific expression (*lin-26p::pry-1*) (Figures 5A and 5B; Table S2). In fact, *lin-26p::pry-1* animals were short-lived, suggesting that a lack of spatiotemporal control is detrimental (Figure 5B; Table S2). These data, together with RNAi and rescue experiments, firmly establish that *pry-1* functions in both muscles and hypodermis for the maintenance of life span, and its hypodermal expression needs to be tightly regulated. Furthermore, the results have revealed a role of *pry-1* in muscles that is beneficial to animals throughout the life span. Interestingly, muscle-specific expression of *mAxin1* also caused animals to live longer (14% increase in mean life span, $p < 0.05$) (Figure S5C; Table S2).

Overexpression of *pry-1* in Muscles Improves Muscle Health and Mitochondrial Morphology

The life span extension observed in *unc-54p::pry-1* animals led us to investigate the cellular and molecular basis of *pry-1*'s role in muscle health. Based on GO analysis, we found that *pry-1* transcriptome contains a significant number of muscle-associated genes (31 of 123, 25.2%, R.F. 1.7, $p < 0.002$) (Table S5). A majority of these genes are downregulated (90.3%, 28 of 31 genes), suggesting that *pry-1* is needed to maintain their expression. Further investigation identified two broad categories, namely muscle structure development (21 genes) and muscle contraction (15 genes) (Table S5), both of which include core components of the sarcomere, such as the subunits of troponin complex (*tnt-3, tnt-4*), twitchin/titin (*unc-22*), myosin complex (*mlc-1, unc-15, unc-54*), and voltage-gated potassium channels (*unc-58, unc-103, slo-1*) (Table S5). We chose three genes at random to validate changes in their expression by quantitative Polymerase Chain Reaction (qPCR): *mlc-1* and *tnt-4* (involved in muscle contraction and structure development), and *unc-96* (involved in muscle structure development). The results confirmed that *tnt-4* and *unc-96* were indeed downregulated in *pry-1(mu38)* mutants, whereas *mlc-1* expression was unchanged (Figure 5C). As expected, all three genes were upregulated in *unc-54p::pry-1* animals (Figure 5D).

Since muscle health is linked to mitochondrial homeostasis (Gouspillou and Hepple, 2016; Hood et al., 2019; Mergoud Dit Lamarche et al., 2018; Regmi et al., 2014), we speculated that *pry-1* is necessary to maintain the expression of mitochondrial genes. Indeed, genes associated with mitochondrial structure and function are overrepresented in the *pry-1* transcriptome (173 genes, 27%, R.F. 1.8, $p < 1.691 \times 10^{-15}$) (Table S6). These include genes that function in the mitochondrial membrane (52 of 220, 24% overlap, R.F. 1.6, p <

CellPress OPEN ACCESS

iScience Article

5.567 × 10^{-4}), mitochondrial outer membrane (10 of 30, 33% overlap, R.F. 2.2, $p < 0.01$), mitochondrial matrix (37 of 137, 27% overlap, R.F. 1.8, $p < 2.298 \times 10^{-4}$), and mitochondrial gene expression (18 of 53, 34% overlap, R.F. 2.2, $p < 5.146 \times 10^{-4}$) (See also Table S6).

Further support of *pry-1*'s role in mitochondrial health comes from examination of BWMs using an organelle-specific GFP reporter, mitoGFP (Benedetti et al., 2006). The mitoGFP was used earlier to demonstrate age-dependent fragmentation of muscle mitochondria and, consequently, the loss of muscle function, since significantly fewer adults exhibited a tubular mitochondrial morphology (Mergoud Dit Lamarche et al., 2018; Regmi et al., 2014). We found that while muscle-specific, but not whole animal, *pry-1* RNAi caused a subtle but statistically significant defect in mitochondria in older adults, *pry-1(mu38)* animals exhibited a drastic increase in fragmented mitochondria (Figures 5E, 5F, and 5H). In contrast, the morphology was better preserved in *unc-54p::pry-1* adults compared with wild-type controls (Figures 5G and 5H), demonstrating that *pry-1* is needed to maintain muscle mitochondrial homeostasis.

The above results led us to investigate whether the mitochondrial network architecture mirrors the functional state of muscles. Studies have shown that the loss of locomotion and pharyngeal pumping are associated with fragmented mitochondrial structure in older worms (Mergoud Dit Lamarche et al., 2018; Regmi et al., 2014). Since a similar correlation is also seen in *pry-1(mu38)* day-1 adults, we wondered whether *unc-54p::pry-1* animals will appear healthier with respect to these aging-related markers. The experiments revealed that, while overexpression of *pry-1* in muscles led to a significantly improved body bending rate in adults, pharyngeal pumping and thrashing were comparable to that of controls (Figures 5I and S5D–S5F). These results are consistent with *pry-1*'s role in maintaining the mitochondrial network, which may contribute to the improvement of muscle health.

Another process that affects muscle aging is autophagy, in which damaged mitochondria are selectively removed (Madeo et al., 2015; Twig and Shirihai, 2011). While autophagy is beneficial for longevity, its effect is detrimental in the presence of increased mitochondrial permeability, which triggers mitochondrial fragmentation (Zhou et al., 2019). Since muscle autophagy increases with age (Mergoud Dit Lamarche et al., 2018), we investigated whether the process is affected in *pry-1* mutants that are short-lived. The analysis of autophagic vesicles, using *dyc-1S::lgg-1::GFP* marker (Mergoud Dit Lamarche et al., 2018), revealed that vesicle number per muscle cell was significantly higher in *pry-1(mu38)* animals compared with that in controls (Figure 5J). Similar results were also obtained by the analysis of *lgg-1* transcripts (Figure 5K). As expected, no such effect was found in the *unc-54p::pry-1* genetic background (Figures 5J and 5K). Overall, our data demonstrate that *pry-1* regulates muscle mitochondrial morphology to maintain muscle structure and function.

daf-16/FOXO Functions Downstream of *pry-1* to Maintain Life Span

As described above, we found that *daf-16* is downregulated in the *pry-1* transcriptome. *daf-16* encodes several isoforms, three of which, R13H8.1b, d, and f (WormBase WS261 release), influence the rate of the aging process (Chen et al., 2015; Kwon et al., 2010). To examine whether *pry-1* affects these isoforms, we performed qPCR analysis. In the case of *pry-1(mu38)*, transcripts for R13H8.1b/c (*daf-16a*) and R13H8.1d/f/h/i/k (*daf-16d/f/h/i/k*) were significantly downregulated (Figure S6A). An opposite trend was observed in *unc-54p::pry-1* animals (Figure S6B). How might *pry-1* regulate transcription of *daf-16*? Previously, two intestinal GATA transcription factors, *elt-2* and *elt-4*, were shown to promote *daf-16* transcription, leading to longevity (Bansal et al., 2014). Using qPCR, we found that the expression of both *elt-2* and *elt-4* was significantly upregulated in the muscle-specific line (*unc-54p::pry-1*) (Figure S6C). Thus, *pry-1* may use these GATA factors directly or indirectly to affect *daf-16* transcription.

To investigate whether the interaction of *pry-1* with *daf-16* is affected by *daf-2* signaling (IIS), we knocked down *pry-1* in both *daf-2* and *daf-16* mutant backgrounds. While the knockdown caused a reduction in *daf-2(e1370ts)* life span (Figure S6D), no change was observed in *daf-16(mu86)* animals (Figure 6A), suggesting that *pry-1* may act genetically downstream of *daf-2* but upstream of *daf-16*. The results of the following two experiments are most consistent with the possibility of *daf-16* acting downstream of *pry-1*: One, *daf-16* RNAi suppressed the life span extension observed in *pry-1(mu38); hsp::pry-1* animals (Figure S6E), and, two, life span defect of *pry-1(mu38)* animals is significantly rescued by *daf-16* overexpression (Figure 6B).

Since DAF-16's function depends on its nuclear localization (Kenyon, 2010), we investigated whether PRY-1 plays a role in this process. The fluorescence of DAF-16:GFP in *unc-54p::pry-1* animals was localized

iScience
Article

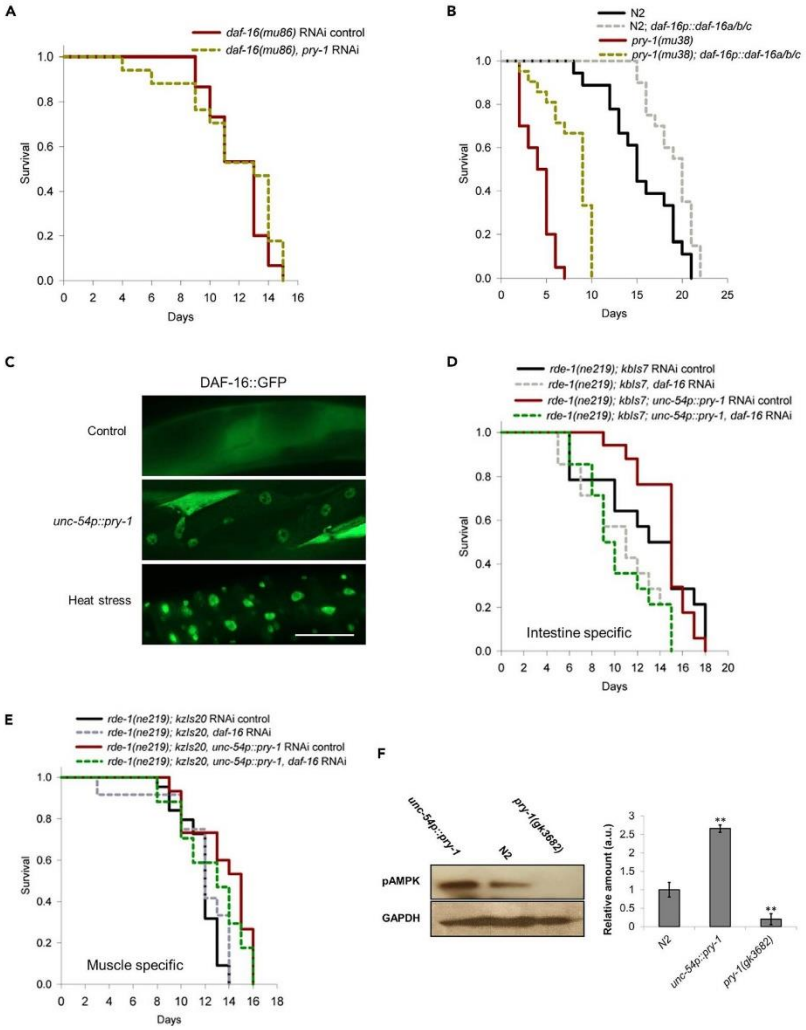

Figure 6. Life Span Regulation by *pry-1* Depends on *daf-16* Function in the Intestine

(A) *pry-1* RNAi knockdown in *daf-16(mu86)* animals.

(B) *daf-16* overexpression in *pry-1(mu38)* animals.

(C) Localization of GFP fluorescence in *unc-54p::pry-1* intestinal nuclei. Scale bar is 50μm. 100% of the *unc-54p::pry-1* animals (n = 30) showed nuclear localization for DAF-16:GFP.

(D and E) Intestine-specific *daf-16* RNAi knockdown (D) and muscle-specific knockdown (E) in *unc-54p::pry-1* animals.

(A, B, D, and E) See Transparent Methods and Table S2 for life span data and statistical analyses.

(F) Western blot analysis of AAK-2 phosphorylation in control, *pry-1* mutant, and *unc-54p::pry-1* animals. Data represent the means of two replicates and error bars the standard deviation. Significance was calculated using Student's t-test. $^{**}p < 0.01$.

CellPress OPEN ACCESS

iScience
Article

frequently to intestinal nuclei (Figure 6C). Consistent with this, *sod-3*, a direct target of *daf-16*, was overexpressed (Figure S6F). The transgenic worms also exhibited a higher level of lipids (Figures S7A and S7B), which supports *pry-1's* role in lipid synthesis (Mallick and Gupta, 2020; Ranawade et al., 2018). Moreover, there was a significant up-regulation of fatty acid desaturases (*fat-5, fat-6,* and *fat-7*) and the SREBP homolog *sbp-1* (Figure S7C). These findings, along with the known role of *daf-16* in promoting lipid synthesis (Papsdorf and Brunet, 2019), lead us to propose that *pry-1* interacts with *daf-16* to regulate lipids.

To examine whether *daf-16* acts locally in the intestine or via a long-range signal by functioning in the muscle, we performed tissue-specific RNAi experiments. Life span extension of *unc-54p::pry-1* was completely abolished by *daf-16* knockdown in the intestine (Figure 6D), the tissue where it acts primarily to regulate life span (Libina et al., 2003). No such effect was observed following muscle-specific knockdown (Figure 6E). Overall, the results show that *daf-16* is involved in *pry-1*-mediated life span regulation and that life span extension observed in muscle-overexpressed *pry-1* animals depends on *daf-16* function in the intestine.

DAF-16-Mediated PRY-1 Signaling Depends on AAK-2 Function

Next, we determined the nature of interaction between *pry-1* and *daf-16*. In the mammalian system, Axin forms a complex with AMPK and LKB1 upon glucose starvation, resulting in phosphorylation of AMPK (Zhang et al., 2013b). The activated AMPK, in turn, phosphorylates a number of targets, including FOXO family members, preferentially FOXO3 (Greer et al., 2007b; Mihaylova and Shaw, 2011). Since the AMPK-FOXO interaction also occurs in *C. elegans* where AAK-2 phosphorylates DAF-16 and plays a role in DAF-16-dependent life span extension (Greer et al., 2007a; Mair et al., 2011), we investigated whether PRY-1 is involved in activating AAK-2. For this, AAK-2 phosphorylation was quantified in worm protein extracts. The results showed that, while the phosphorylated AAK-2 level was drastically reduced in *pry-1* mutants when probed with phospho-AMPK (T172) antibody, it was significantly increased in *unc-54p::pry-1* animals (Figure 6F). To determine whether a reduced AAK-2 signal in *pry-1* mutants is due to a lower abundance of protein, we examined GFP fluorescence in *aak-2p::aak-2::GFP* transgenic animals and found no change in fluorescence intensity in *pry-1(mu38)* mutants compared with that in the control (Figure S7D). Thus, PRY-1 is necessary for AAK-2 phosphorylation.

Three additional experiments support PRY-1 playing a role in AAK-2 activation: First, *pry-1* RNAi did not exacerbate the life span defect of *aak-2(ok524)* animals (Figure 7A; Table S2). Second, a constitutively active form of AMPKα2 (due to increased T172 phosphorylation), which causes a long-lived phenotype in worms (Mair et al., 2011), was unable to rescue the life span defect of *pry-1(mu38)* (Figure 7B; Table S2). And, three, *aak-2* is expressed in BWMs and neurons during adulthood in a pattern that resembles *pry-1* (Lee et al., 2008; Mair et al., 2011) (Figure S7E). Moreover, similar to *aak-2* mutants, *pry-1* mutant animals exhibited significantly reduced life span of dauers (55-70% reduction in mean life span in two different alleles compared to the control, $p < 0.01$) (Figure S7F; Table S2) (Narbonne and Roy, 2009). Taken together, these data support a model of PRY-1 promoting AAK-2 activation, likely through protein-protein interaction. The LKB1 homolog, PAR-4, required for AAK-2 activation (Lee et al., 2008) may also be involved in this process, since the life span defect of *par-4* mutant was not enhanced by *pry-1(RNAi)* (Figure S7G). The activated AAK-2 may, in turn, act in a cell non-autonomous manner to affect DAF-16 function in the intestine.

The model above suggests that PRY-1 and AAK-2 affect the expression of a common set of genes. Indeed, the transcriptome data sets of *pry-1* and *aak-2* mutants (Ranawade et al., 2018; Shin et al., 2011) showed a significant overlap (192 shared genes, 132 upregulated and 60 downregulated; RF: 1.2, hyp.geo $p < 0.006$) (Figure 7F; Table S7). Of these, 60 (45%) are mutually upregulated and 28 (47%) mutually downregulated in both mutants. The overlapping set of differentially expressed genes are linked to GO processes such as muscle structure development (*act-1, mel-26, unc-52, emb-9, unc-15,* and *unc-54*), muscle contraction (*unc-54*), aging (*daf-16, prmt-1, mpk-1, chc-1, cgh-1, dao-5,* and *glp-4*), lipid metabolic processes (*tat-4, ldp-1, sptl-3, pmt-1, lipin-1,* and *cgt-3*), and regulation of lipid localization (*daf-16, prmt-1, sams-1, tat-4, lea-1, vit-1, vit-3, vit-4,* and *vit-6*). Moreover, a significant number of genes are associated with stress response (27) and catabolic process (25) (Table S7).

To further investigate the interaction of *aak-2* with *pry-1*, tissue-specific knockdown experiments were performed. Both muscle and intestine-specific *aak-2* RNAi abolished life span extension in *unc-54p::pry-1* animals (Figures 7C and 7D; Table S2). Additionally, RNAi caused significantly fewer animals to show nuclear-localized DAF-16:GFP (Figures 7E and 7F). As with *aak-2*, RNAi knock-down of *par-4* in the muscle suppressed the life span extension of *unc-54p::pry-1* (Figure S7H), providing further evidence for PAR-4's

iScience
Article

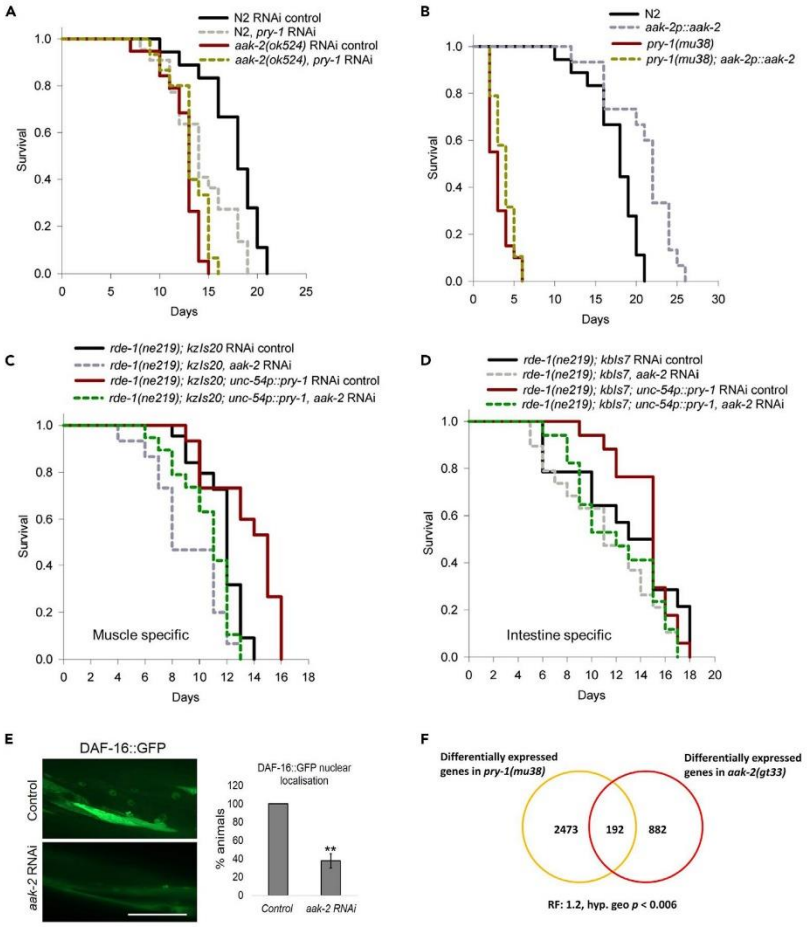

Figure 7. PRY-1 Interacts with AAK-2 to Regulate DAF-16 Localization and Life Span Extension

(A) *pry-1* RNAi knockdown in *aak-2(ok524)* animals.

(B) Constitutive activation of *aak-2* in *pry-1(mu38)* animals.

(C and D) *aak-2* RNAi knockdown in the muscle and intestine in *unc-54p::pry-1* animals.

(A–D) See Transparent Methods and Table S2 for life span data and statistical analyses.

(E) *aak-2* RNAi effect on DAF-16:GFP localization in *unc-54p::pry-1* animals. Scale bar is 50 μm.

Data represent the means of two replicates (15 animals each) and error bars the standard deviation. Significance was calculated using Student's t-test. **p < 0.01.

(F) Venn diagram showing an overlapping set of genes between *pry-1(mu38)* and *aak-2(gt33)* transcriptomes.

involvement in PRY-1 and AAK-2 interaction. Collectively, the results described in this section lead us to conclude that PRY-1 interacts with PAR-4 and AAK-2 in the muscle, thereby affecting DAF-16 localization in the intestine and, ultimately, the life span of animals.

DISCUSSION

Our results demonstrate the role of *C. elegans* Axin family member PRY-1 in life span maintenance, which involves AAK-2/AMPK-mediated DAF-16/FOXO signaling. We found that the *pry-1* mutant transcriptome

CellPress OPEN ACCESS

iScience Article

contains a significant number of aging-associated genes, including IIS and UPR^{ER} pathway components as well as those linked to lipid maintenance. Moreover, a significant number of DAF-16 direct targets are altered in *pry-1* mutants, and a majority of these are downregulated. Consistent with these findings, previous studies have shown that both DAF-16 and XBP-1-mediated UPR^{ER} signaling regulate stress response, lipid metabolism, and longevity (Imanikia et al., 2019; Lee et al., 2003; Lin et al., 2018; Murphy et al., 2003; Taylor and Dillin, 2013). As expected from misregulation of aging-related genes, a partial or complete loss of PRY-1 activity resulted in a shorter life span. The aging phenotype was associated with physiological changes such as slower rates of body bending and pharyngeal pumping, an increase in aging pigment (lipofuscin), and higher expression of UPR^{ER} and UPR^{MT} chaperones. Altogether, these data suggest that *pry-1* affects multiple conserved pathways involved in stress maintenance and aging.

The characterization of *pry-1* expression uncovered muscles as a major tissue for gene action. Other tissues showing a relatively lower abundance of *pry-1* include neurons, hypodermis, and intestine. Since the WNT ligands, *mom-2* and *cwn-2*, are localized in some of these tissues (Song et al., 2010) and both ligands affect life span (Lezzerini and Budovskaya, 2014), we investigated the possibility of *pry-1* acting in a WNT-dependent manner. The results of genetic interaction experiments suggest that *mom-2*-mediated signaling may affect *pry-1* function to maintain life span. However, such a mechanism may not involve the canonical WNT effector protein β-catenin. It is worth noting that WNT signaling has been shown to play roles in cellular senescence, aging, and age-related diseases (Brack et al., 2007; Gruber et al., 2016; Naito et al., 2010; Zhang et al., 2019). However, the regulation and function of Axin in the pathway is poorly understood.

The finding that *pry-1* is expressed in multiple tissues led us to investigate its tissue-specific function. The results of RNAi-mediated knockdowns and rescue experiments revealed that the gene is needed in the muscle and hypodermis to maintain life span. Interestingly, forced expression of *pry-1* in muscles, but not in hypodermis, allowed animals to live longer. Considering that Axin homologs are expressed in muscles (Smith et al., 2019; Uhlen et al., 2015) and mouse Axin (*mAxin1*) extended the life span of *C. elegans* when ectopically expressed in the muscle tissue, we propose that the beneficial role of Axin in the muscle is evolutionarily conserved.

pry-1's involvement in muscle health was further investigated using the transcriptome data, which uncovered a significant number of genes involved in muscle structure development and function. Almost all of these were downregulated. Another group of genes regulated by *pry-1* are associated with mitochondria and include those that function in the mitochondrial membrane, mitochondrial matrix, and mitochondrial ATP synthesis, suggesting that *pry-1* plays a major role in maintaining the health of this vital organelle. As expected, mutant animals showed increased fragmentation of mitochondria, which may contribute to muscle aging and a shorter life span (Gouspillou and Hepple, 2016; Hood et al., 2019; Mergoud Dit Lamarche et al., 2018). In contrast, muscle-specific overexpression of *pry-1* resulted in marked improvements in mitochondrial morphology and locomotion. The relationship between aging and muscle mitochondrial function is well described. For example, *daf-2* mutants that have a longer life span show preservation of mitochondrial morphology and delayed muscle aging (Mergoud Dit Lamarche et al., 2018; Wang et al., 2019). Additionally, *daf-16* is essential for the maintenance of muscle mitochondrial health (Wang et al., 2019). We found that both transcription and subcellular localization of DAF-16 is regulated by PRY-1. Moreover, genetic experiments revealed that the *pry-1*-mediated life span depends on *daf-16*. Interestingly, DAF-16 was nuclear localized in the intestine of *unc-54p::pry-1* worms. This localization appears to be important, since the intestine-specific knockdown of *daf-16* abolished the life span extension of transgenic animals.

We investigated the mechanism of PRY-1-mediated DAF-16 regulation and uncovered the role of AMPK homolog AAK-2 in this process. Specifically, PRY-1 is essential for the activation of AAK-2, which, in turn, promotes DAF-16 nuclear localization and life span extension of *unc-54p::pry-1* animals. Previous work has reported the involvement of AAK-2 in regulating DAF-16 function (Chen et al., 2013; Greer et al., 2007a). Hence, these data, along with genetic interactions, *aak-2::GFP* expression, and *pry-1* and *aak-2* transcriptome analysis, support the following model: PRY-1, PAR-4, and AAK-2 form a complex in the muscle, leading to AAK-2 phosphorylation. Activated AAK-2 initiates cell non-autonomous signaling to regulate DAF-16 activity in the intestine to maintain the life span. This model is consistent with the previously reported role of AAK-2 (Burkewitz et al., 2014).

One of the outcomes of *pry-1* interaction with *daf-16* could be to affect lipid metabolism, since lipids are implicated in aging (Papsdorf and Brunet, 2019) and both genes promote monounsaturated fatty acid

synthesis by transcriptionally regulating fatty acid desaturases such as *fat-7* (Murphy et al., 2003; Ranawade et al., 2018; Zhang et al., 2013a). Other possibilities are also likely because DAF-16 interacts with multiple factors to regulate life span (Lapierre and Hansen, 2012; Uno and Nishida, 2016). We should point out that AXL-1, another Axin homolog in *C. elegans*, was reported previously to be necessary for metformin-induced life span extension, although *axl-1* mutants have no aging-related phenotypes of their own (Chen et al., 2017). Thus, our work on PRY-1 provides the first evidence of an Axin family member regulating muscle health as well as life span.

Interactions between Axin and AMPK have been reported previously in mammalian systems. Specifically, the Axin-AMPK complex formation was enhanced in cultured cells when subjected to glucose deprivation, and Axin knockdown in the mouse liver impaired AMPK activation (Zhang et al., 2013b). AMPK is known to promote mitochondrial biogenesis and mitochondrial function in human umbilical vein cells and mice aorta (Marin et al., 2017). Moreover, AMPK phosphorylates all four human FOXO family members (Greer et al., 2007b). Similar to that with AMPK, AAK-2-mediated life span extension depends on mitochondrial network maintenance and DAF-16 regulation (Greer et al., 2007a; Uno and Nishida, 2016; Weir et al., 2017). Thus, it is plausible that Axin-AMPK-FOXO interact in a conserved manner to regulate disparate biological processes in eukaryotes. Studies in humans and other higher systems have established a connection between aging, muscle health, mitochondrial dysfunction, and diseases (Gouspillou and Hepple, 2016; Hood et al., 2019). Furthermore, Axin is essential for muscle maintenance, since myogenesis is abrogated in mutant animals (Huraskin et al., 2016) and *Axin2* upregulation is associated with increased muscle fibrosis in aging mice (Arthur and Cooley, 2012; Brack et al., 2007). Since muscle mass and function progressively decline with age, understanding the mechanism of Axin's function in this tissue promises to uncover potential interventions for aging-associated muscle deterioration.

Limitations of the Study

We have shown that *pry-1* is necessary to maintain muscle health and life span in *C. elegans*. However, it remains to be determined whether Axin homologs in other systems also regulate similar processes. Our conclusion that muscle-specific expression of *pry-1* extends life span is based on the analysis of transgenic animals that constitutively express the gene throughout developmental and post-developmental periods. In the future, it will be worthwhile to investigate *pry-1*'s role by activating its expression specifically during adulthood. The analysis of the *pry-1* role in muscles led us to investigate its interactions with *aak-2/AMPK* and *daf-16/FOXO*. While our data demonstrates that the muscle-specific expression of *pry-1* causes an increase in AAK-2 phosphorylation, whether PRY-1 physically interacts with AAK-2 is yet to be examined. Finally, we found that PRY-1-AAK-2-mediated signaling acts cell non-autonomously to promote nuclear localization of DAF-16 in the intestine, which is necessary for life span extension. However, the factors that facilitate communication between PRY-1 and DAF-16 remain to be identified.

Resource Availability

Lead Contact

Further information and requests for resources and reagents should be directed to and will be fulfilled by the Lead Contact, Bhagwati P Gupta (guptab@mcmaster.ca).

Materials Availability

All data generated or analyzed in this study are included in this published article and its supplemental information.

Data and Code Availability

The published article includes all data generated or analyzed during this study.

METHODS

All methods can be found in the accompanying Transparent Methods supplemental file.

SUPPLEMENTAL INFORMATION

Supplemental Information can be found online at https://doi.org/10.1016/j.isci.2020.101843.

CellPress OPEN ACCESS

iScience
Article

ACKNOWLEDGMENTS

We thank Hannah Hosein, Sakshi Mehta and Lindyann Lessey for assistance with some of the experiments and Lesley MacNeil for providing feedback on the initial draft. Some of the strains were obtained from CGC, which is funded by the NIH Office of Research Infrastructure Programs (P40OD010440). The tissue-specific promoter plasmids were kindly provided by the Roy lab (McGill). This work was supported by NSERC Discovery grant to BG.

AUTHOR CONTRIBUTIONS

BG and AM designed the study. AM, AR, and WB performed the experiments. BG and AM analyzed the data and wrote the manuscript. All authors reviewed and edited the draft. BG supervised the project.

DECLARATION OF INTERESTS

The authors declare no competing interests.

Received: August 17, 2020
Revised: October 14, 2020
Accepted: November 17, 2020
Published: December 18, 2020

REFERENCES

Apfeld, J., O'Connor, G., McDonagh, T., DiStefano, P.S., and Curtis, R. (2004). The AMP-activated protein kinase AAK-2 links energy levels and insulin-like signals to lifespan in C. elegans. Genes Dev. *18*, 3004–3009.

Arthur, S.T., and Cooley, I.D. (2012). The effect of physiological stimuli on sarcopenia; impact of Notch and Wnt signaling on impaired aged skeletal muscle repair. Int. J. Biol. Sci. *8*, 731–760.

Bansal, A., Kwon, E.S., Conte, D., Jr., Liu, H., Gilchrist, M.J., MacNeil, L.T., and Tissenbaum, H.A. (2014). Transcriptional regulation of Caenorhabditis elegans FOXO/DAF-16 modulates lifespan. Longev Healthspan *3*, 5.

Benedetti, C., Haynes, C.M., Yang, Y., Harding, H.P., and Ron, D. (2006). Ubiquitin-like protein 5 positively regulates chaperone gene expression in the mitochondrial unfolded protein response. Genetics *174*, 229–239.

Brack, A.S., Conboy, M.J., Roy, S., Lee, M., Kuo, C.J., Keller, C., and Rando, T.A. (2007). Increased Wnt signaling during aging alters muscle stem cell fate and increases fibrosis. Science *317*, 807–810.

Burkewitz, K., Zhang, Y., and Mair, W.B. (2014). AMPK at the nexus of energetics and aging. Cell Metab. *20*, 10–25.

Chen, A.T., Guo, C., Itani, O.A., Budaitis, B.G., Williams, T.W., Hopkins, C.E., McEachin, R.C., Pande, M., Grant, A.R., Yoshina, S., et al. (2015). Longevity genes revealed by integrative analysis of isoform-specific daf-16/FoxO mutants of Caenorhabditis elegans. Genetics *201*, 613–629.

Chen, D., Li, P.W., Goldstein, B.A., Cai, W., Thomas, E.L., Chen, F., Hubbard, A.E., Melov, S., and Kapahi, P. (2013). Germline signaling mediates the synergistically prolonged longevity produced by double mutations in daf-2 and rsks-1 in C. elegans. Cell Rep. *5*, 1600–1610.

Chen, J., Ou, Y., Li, Y., Hu, S., Shao, L.W., and Liu, Y. (2017). Metformin extends C. elegans lifespan through lysosomal pathway. Elife *6*, e31268.

Davis, B.O., Jr., Anderson, G.L., and Dusenbery, D.B. (1982). Total luminescence spectroscopy of fluorescence changes during aging in Caenorhabditis elegans. Biochemistry *21*, 4089–4095.

de Lencastre, A., Pincus, Z., Zhou, K., Kato, M., Lee, S.S., and Slack, F.J. (2010). MicroRNAs both promote and antagonize longevity in C. elegans. Curr. Biol. *20*, 2159–2168.

Gouspillou, G., and Hepple, R.T. (2016). Editorial: mitochondria in skeletal muscle health, aging and diseases. Front. Physiol. *7*, 446.

Greer, E.L., Dowlatshahi, D., Banko, M.R., Villen, J., Hoang, K., Blanchard, D., Gygi, S.P., and Brunet, A. (2007a). An AMPK-FOXO pathway mediates longevity induced by a novel method of dietary restriction in C. elegans. Curr. Biol. *17*, 1646–1656.

Greer, E.L., Oskoui, P.R., Banko, M.R., Maniar, J.M., Gygi, M.P., Gygi, S.P., and Brunet, A. (2007b). The energy sensor AMP-activated protein kinase directly regulates the mammalian FOXO3 transcription factor. J. Biol. Chem. *282*, 30107–30119.

Gruber, J., Yee, Z., and Tolwinski, N.S. (2016). Developmental drift and the role of Wnt signaling in aging. Cancers (Basel) *8*, 73.

Hardie, D.G., and Lin, S.C. (2017). AMP-activated protein kinase - not just an energy sensor. F1000Res *6*, 1724.

Hardie, D.G., Ross, F.A., and Hawley, S.A. (2012). AMPK: a nutrient and energy sensor that maintains energy homeostasis. Nat. Rev. Mol. Cell Biol. *13*, 251–262.

Hood, D.A., Memme, J.M., Oliveira, A.N., and Triolo, M. (2019). Maintenance of skeletal muscle mitochondria in health, exercise, and aging. Annu. Rev. Physiol. *81*, 19–41.

Huang, C., Xiong, C., and Kornfeld, K. (2004). Measurements of age-related changes of physiological processes that predict lifespan of Caenorhabditis elegans. Proc. Natl. Acad. Sci. U S A *101*, 8084–8089.

Huraskin, D., Eiber, N., Reichel, M., Zidek, L.M., Kravic, B., Bernkopf, D., von Maltzahn, J., Behrens, J., and Hashemolhosseini, S. (2016). Wnt/beta-catenin signaling via Axin2 is required for myogenesis and, together with YAP/Taz and Tead1, active in IIa/IIx muscle fibers. Development *143*, 3128–3142.

Imanikia, S., Sheng, M., Castro, C., Griffin, J.L., and Taylor, R.C. (2019). XBP-1 remodels lipid metabolism to extend longevity. Cell Rep. *28*, 581–589 e584.

Kenyon, C. (2011). The first long-lived mutants: discovery of the insulin/IGF-1 pathway for ageing. Philos. Trans. R. Soc. Lond. B Biol. Sci. *366*, 9–16.

Kenyon, C., Chang, J., Gensch, E., Rudner, A., and Tabtiang, R. (1993). A C. elegans mutant that lives twice as long as wild type. Nature *366*, 461–464.

Kenyon, C.J. (2010). The genetics of ageing. Nature *464*, 504–512.

Korswagen, H.C., Coudreuse, D.Y., Betist, M.C., van de Water, S., Zivkovic, D., and Clevers, H.C. (2002). The Axin-like protein PRY-1 is a negative regulator of a canonical Wnt pathway in *C. elegans*. Genes Dev. *16*, 1291–1302.

Kwon, E.S., Narasimhan, S.D., Yen, K., and Tissenbaum, H.A. (2010). A new DAF-16 isoform regulates longevity. Nature *466*, 498–502.

Lapierre, L.R., and Hansen, M. (2012). Lessons from C. elegans: signaling pathways for longevity. Trends Endocrinol. Metab. *23*, 637–644.

Lee, H., Cho, J.S., Lambacher, N., Lee, J., Lee, S.J., Lee, T.H., Gartner, A., and Koo, H.S. (2008). The Caenorhabditis elegans AMP-activated protein kinase AAK-2 is phosphorylated by LKB1 and is required for resistance to oxidative stress and for normal motility and foraging behavior. J. Biol. Chem. *283*, 14988–14993.

Lee, S.S., Kennedy, S., Tolonen, A.C., and Ruvkun, G. (2003). DAF-16 target genes that control C. elegans life-span and metabolism. Science *300*, 644–647.

Lezzerini, M., and Budovskaya, Y. (2014). A dual role of the Wnt signaling pathway during aging in Caenorhabditis elegans. Aging Cell *13*, 8–18.

Li, Y.H., and Zhang, G.G. (2016). Towards understanding the lifespan extension by reduced insulin signaling: bioinformatics analysis of DAF-16/FOXO direct targets in Caenorhabditis elegans. Oncotarget *7*, 19185–19192.

Libina, N., Berman, J.R., and Kenyon, C. (2003). Tissue-specific activities of C. elegans DAF-16 in the regulation of lifespan. Cell *115*, 489–502.

Lin, X.X., Sen, I., Janssens, G.E., Zhou, X., Fonslow, B.R., Edgar, D., Stroustrup, N., Swoboda, P., Yates, J.R., 3rd, Ruvkun, G., et al. (2018). DAF-16/FOXO and HLH-30/TFEB function as combinatorial transcription factors to promote stress resistance and longevity. Nat. Commun. *9*, 4400.

Lopez-Otin, C., Blasco, M.A., Partridge, L., Serrano, M., and Kroemer, G. (2013). The hallmarks of aging. Cell *153*, 1194–1217.

Madeo, F., Zimmermann, A., Maiuri, M.C., and Kroemer, G. (2015). Essential role for autophagy in life span extension. J. Clin. Invest. *125*, 85–93.

Mair, W., Morantte, I., Rodrigues, A.P., Manning, G., Montminy, M., Shaw, R.J., and Dillin, A. (2011). Lifespan extension induced by AMPK and calcineurin is mediated by CRTC-1 and CREB. Nature *470*, 404–408.

Mallick, A., and Gupta, B.P. (2020). Vitellogenin-2 acts downstream of PRY-1/Axin to regulate lipids and lifespan in C. elegans. Micropubl Biol. *21*, 2020.

Mallick, A., Ranawade, A., and Gupta, B.P. (2019a). Role of PRY-1/Axin in heterochronic miRNA-mediated seam cell development. BMC Dev. Biol. *19*, 17.

Mallick, A., Taylor, S.K.B., Ranawade, A., and Gupta, B.P. (2019b). Axin family of scaffolding proteins in development: lessons from C. elegans. J. Dev. Biol. *7*, 20.

Marin, T.L., Gongol, B., Zhang, F., Martin, M., Johnson, D.A., Xiao, H., Wang, Y., Subramaniam, S., Chien, S., and Shyy, J.Y. (2017). AMPK promotes mitochondrial biogenesis and function by phosphorylating the epigenetic factors DNMT1, RBBP7, and HAT1. Sci. Signal. *10*, eaaf7478.

Melendez, A., Talloczy, Z., Seaman, M., Eskelinen, E.L., Hall, D.H., and Levine, B. (2003). Autophagy genes are essential for dauer development and life-span extension in C. elegans. Science *301*, 1387–1391.

Mergoud Dit Lamarche, A., Molin, L., Pierson, L., Mariol, M.C., Bessereau, J.L., Gieseler, K., and Solari, F. (2018). UNC-120/SRF independently controls muscle aging and lifespan in Caenorhabditis elegans. Aging Cell *17*, e12713.

Mihaylova, M.M., and Shaw, R.J. (2011). The AMPK signalling pathway coordinates cell growth, autophagy and metabolism. Nat. Cell Biol. *13*, 1016–1023.

Murphy, C.T., McCarroll, S.A., Bargmann, C.I., Fraser, A., Kamath, R.S., Ahringer, J., Li, H., and Kenyon, C. (2003). Genes that act downstream of DAF-16 to influence the lifespan of Caenorhabditis elegans. Nature *424*, 277–283.

Naito, A.T., Shiojima, I., and Komuro, I. (2010). Wnt signaling and aging-related heart disorders. Circ. Res. *107*, 1295–1303.

Narbonne, P., and Roy, R. (2009). Caenorhabditis elegans dauers need LKB1/AMPK to ration lipid reserves and ensure long-term survival. Nature *457*, 210–214.

Ogg, S., Paradis, S., Gottlieb, S., Patterson, G.I., Lee, L., Tissenbaum, H.A., and Ruvkun, G. (1997). The Fork head transcription factor DAF-16 transduces insulin-like metabolic and longevity signals in C. elegans. Nature *389*, 994–999.

Papsdorf, K., and Brunet, A. (2019). Linking lipid metabolism to chromatin regulation in aging. Trends Cell Biol. *29*, 97–116.

Ranawade, A., Mallick, A., and Gupta, B.P. (2018). PRY-1/Axin signaling regulates lipid metabolism in Caenorhabditis elegans. PLoS One *13*, e0206540.

Regmi, S.G., Rolland, S.G., and Conradt, B. (2014). Age-dependent changes in mitochondrial morphology and volume are not predictors of lifespan. Aging (Albany NY) *6*, 118–130.

Ron, D., and Walter, P. (2007). Signal integration in the endoplasmic reticulum unfolded protein response. Nat. Rev. Mol. Cell Biol. *8*, 519–529.

Seetharaman, A., Cumbo, P., Bojanala, N., and Gupta, B.P. (2010). Conserved mechanism of Wnt signaling function in the specification of vulval precursor fates in C. elegans and C. briggsae. Dev. Biol. *346*, 128–139.

Shin, H., Lee, H., Fejes, A.P., Baillie, D.L., Koo, H.S., and Jones, S.J. (2011). Gene expression profiling of oxidative stress response of C. elegans aging defective AMPK mutants using massively parallel transcriptome sequencing. BMC Res. Notes *4*, 34.

Smith, C.M., Hayamizu, T.F., Finger, J.H., Bello, S.M., McCright, I.J., Xu, J., Baldarelli, R.M., Beal, J.S., Campbell, J., Corbani, L.E., et al. (2019). The mouse gene expression database (GXD): 2019 update. Nucleic Acids Res. *47*, D774–D779.

Song, S., Zhang, B., Sun, H., Li, X., Xiang, Y., Liu, Z., Huang, X., and Ding, M. (2010). A Wnt-Frz/Ror-Dsh pathway regulates neurite outgrowth in Caenorhabditis elegans. PLoS Genet. *6*, e1001056.

Stenesen, D., Suh, J.M., Seo, J., Yu, K., Lee, K.S., Kim, J.S., Min, K.J., and Graff, J.M. (2013). Adenosine nucleotide biosynthesis and AMPK regulate adult life span and mediate the longevity benefit of caloric restriction in flies. Cell Metab. *17*, 101–112.

Taylor, R.C., and Dillin, A. (2013). XBP-1 is a cell-nonautonomous regulator of stress resistance and longevity. Cell *153*, 1435–1447.

Tran, H.C., and Van Aken, O. (2020). Mitochondrial unfolded protein-related responses across kingdoms: similar problems, different regulators. Mitochondrion *53*, 166–177.

Twig, G., and Shirihai, O.S. (2011). The interplay between mitochondrial dynamics and mitophagy. Antioxid. Redox Signal. *14*, 1939–1951.

Uhlen, M., Fagerberg, L., Hallstrom, B.M., Lindskog, C., Oksvold, P., Mardinoglu, A., Sivertsson, A., Kampf, C., Sjostedt, E., Asplund, A., et al. (2015). Proteomics. Tissue-based map of the human proteome. Science *347*, 1260419.

Uno, M., and Nishida, E. (2016). Lifespan-regulating genes in C. elegans. NPJ Aging Mech. Dis. *2*, 16010.

Wang, H., Webster, P., Chen, L., and Fisher, A.L. (2019). Cell-autonomous and non-autonomous roles of daf-16 in muscle function and mitochondrial capacity in aging C. elegans. Aging (Albany NY) *11*, 2295–2311.

Weir, H.J., Yao, P., Huynh, F.K., Escoubas, C.C., Goncalves, R.L., Burkewitz, K., Laboy, R., Hirschey, M.D., and Mair, W.B. (2017). Dietary restriction and AMPK increase lifespan via mitochondrial network and peroxisome remodeling. Cell Metab. *26*, 884–896 e885.

Xu, Y., He, Z., Song, M., Zhou, Y., and Shen, Y. (2019). A microRNA switch controls dietary restriction-induced longevity through Wnt signaling. EMBO Rep. *20*, e46888.

Zhang, P., Judy, M., Lee, S.J., and Kenyon, C. (2013a). Direct and indirect gene regulation by a life-extending FOXO protein in C. elegans: roles for GATA factors and lipid gene regulators. Cell Metab. *17*, 85–100.

Zhang, Q., Wu, X., Chen, P., Liu, L., Xin, N., Tian, Y., and Dillin, A. (2018). The mitochondrial unfolded protein response is mediated cell-non-autonomously by retromer-dependent Wnt signaling. Cell *174*, 870–883 e817.

Zhang, Y., Jeffrey, J., Dong, F., Zhang, J., Kao, W.W., Liu, C.Y., and Yuan, Y. (2019). Repressed Wnt signaling accelerates the aging process in mouse eyes. J. Ophthalmol. *2019*, 7604396.

Zhang, Y.L., Guo, H., Zhang, C.S., Lin, S.Y., Yin, Z., Peng, Y., Luo, H., Shi, Y., Lian, G., Zhang, C., et al. (2013b). AMP as a low-energy charge signal autonomously initiates assembly of AXIN-AMPK-LKB1 complex for AMPK activation. Cell Metab. *18*, 546–555.

Zhou, B., Kreuzer, J., Kumsta, C., Wu, L., Kamer, K.J., Cedillo, L., Zhang, Y., Li, S., Kacergis, M.C., Webster, C.M., et al. (2019). Mitochondrial permeability uncouples elevated autophagy and lifespan extension. Cell *177*, 299–314 e216.

iScience, Volume *23*

Supplemental Information

Axin-Mediated Regulation of Lifespan and Muscle Health in *C. elegans* Requires AMPK-FOXO Signaling

Avijit Mallick, Ayush Ranawade, Wouter van den Berg, and Bhagwati P. Gupta

SUPPLEMENTAL INFORMATION

Supplementary Figures

Figure S1: *pry-1* expression in older adults, effect of *pry-1* overexpression on lifespan, and phenotype of *C. briggsae pry-1* mutant, related to Figures 1, and 4.
(A) qPCR analysis showing *pry-1* transcript levels at day-1, 4 and 8 of adulthood. Data represent the means of two replicates and error bars represent the SEM. Significance was calculated using Bio-Rad software (t-test). *$p < 0.05$.
(B) Lifespan phenotype of *hs::pry-1* transgenic animals.
(C) Lifespan phenotype of *Cbr-pry-1(sy5353)* mutant.
(B-C) See Transparent methods and Table S2 for lifespan data and statistical analyses.

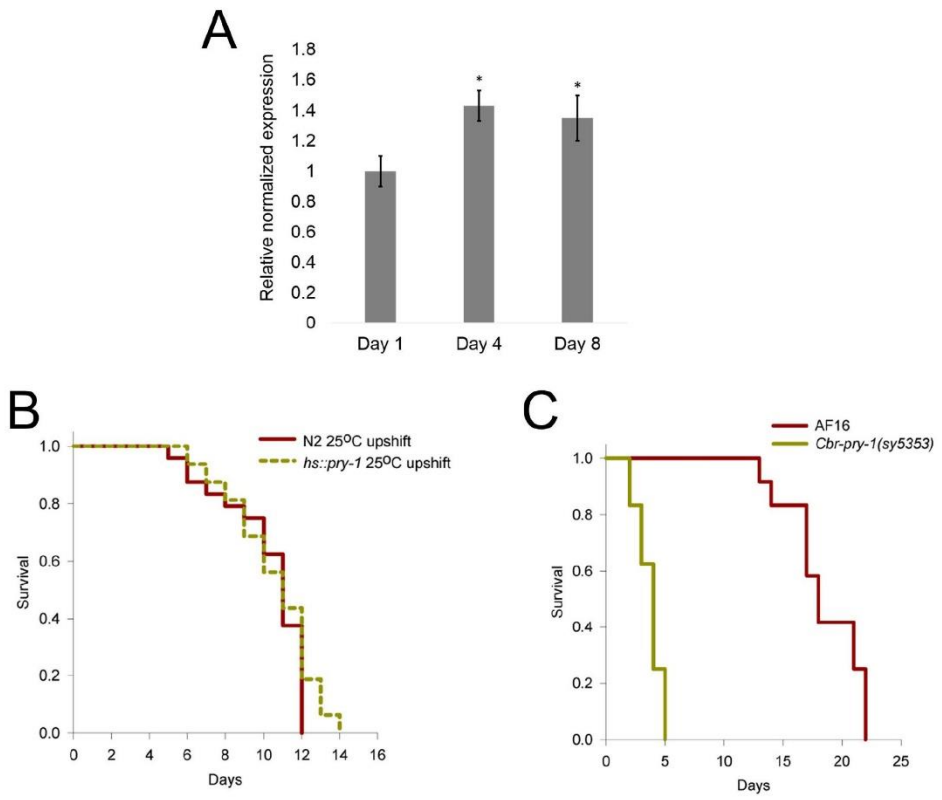

1

Figure S2: Analysis of pharyngeal pumping and body bending in *pry-1(mu38)* animals, related to Figure 2.

(A and B) Pharyngeal pumping and body bending rates in the *pry-1* mutants.

(C and D) Rescue of *pry-1(mu38)* defects by expression of *pry-1* transgene using a *hs::pry-1* construct.

(A-D) Data represent the means of at least two replicates (n ≥ 30 animals) and error bars the standard deviation. Significance was calculated using Student's t-test *$p < 0.05$, **$p < 0.01$.

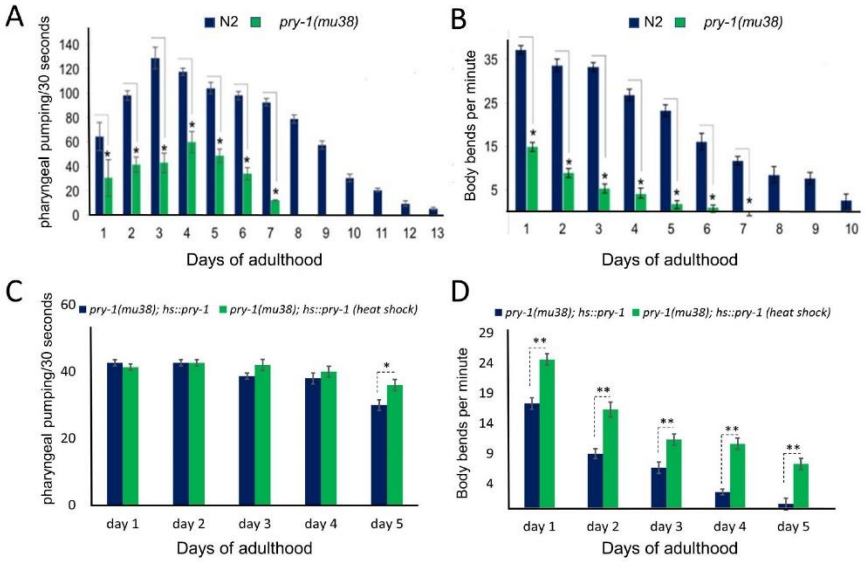

Figure S3: Expression pattern of *pry-1* in *C. elegans*, related to Figure 4.
(A) Expression pattern of *pry-1* in *pry-1p::pry-1::GFP* transgenic animals during larval and adult stages.
(B) Magnified image showing GFP fluorescence in body wall muscles. Nuclei are indicated by arrows.
(C) Arrows point to intestinal nuclei showing GFP fluorescence.

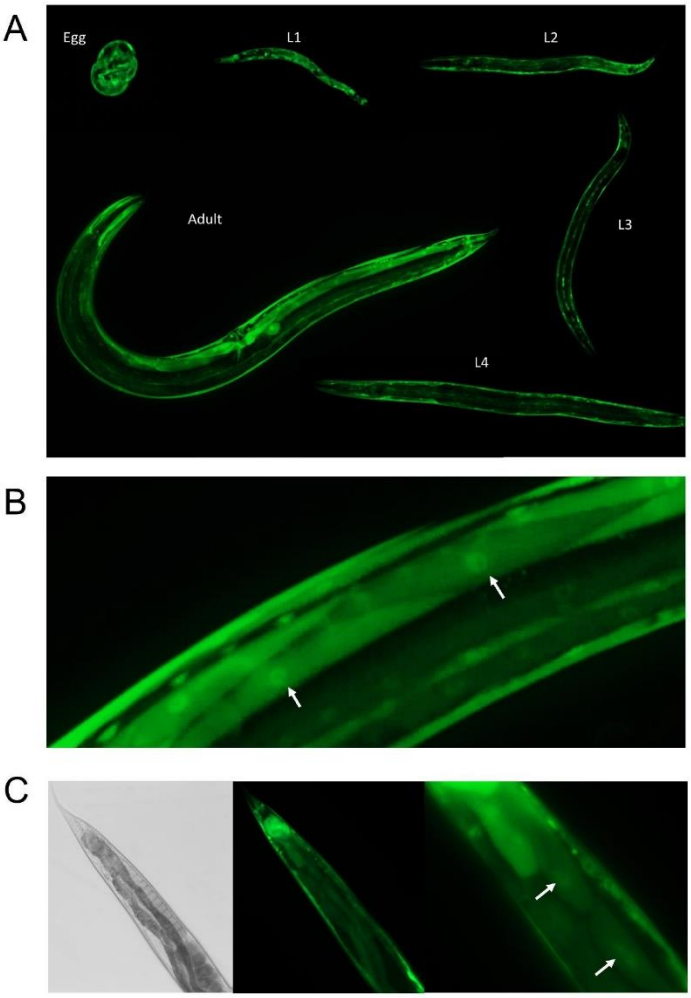

Figure S4: Expression pattern of *pry-1* in *C. briggsae* and the impact of tissue-specific knockdowns of *C. elegans pry-1* on lifespan, related to Figure 4.
(A) Representative images of *C. briggsae pry-1p::GFP* transgenic animals showing GFP fluorescence in muscles of an L4 larva and an adult.
(B) Lifespan phenotype of animals following *pry-1* RNAi knockdown in neurons.
(C) Lifespan phenotype of animals following *pry-1* RNAi knockdown in intestine, hypodermis and germline.
(B-C) See Transparent methods and Table S2 for lifespan data and statistical analyses.

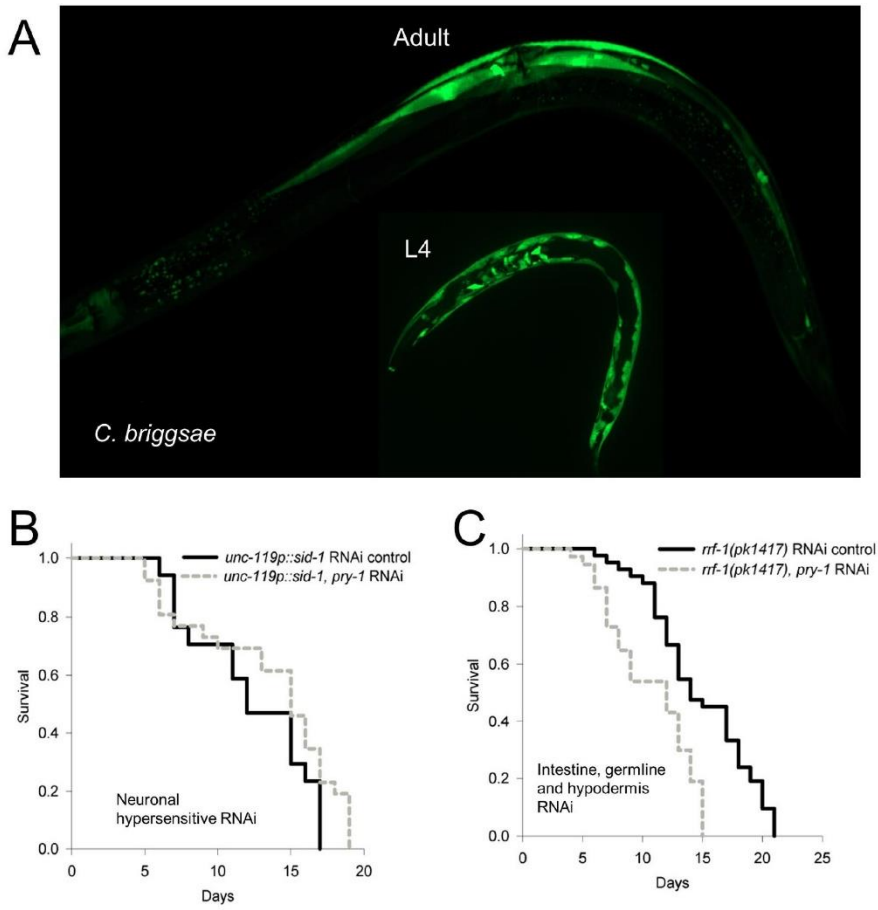

Figure S5: Rescue analysis of *pry-1(mu38)* lifespan defect and the effect of muscle-specific expression of mouse Axin1 in *C. elegans*, related to Figure 5.
(A and B) Lifespan rescue experiments by tissue-specific expression of *pry-1* in hypodermis (A) and muscle.
(C) Lifespan phenotype of animals expressing *mAxin1* in the muscle.
(A-C) See Transparent methods and Table S2 for lifespan data and statistical analyses.
(D and E) Rates of body bending and pharyngeal pumping in *unc-54p::pry-1* animals.
(F) Thrashing rate of *unc-54p::pry-1* between day 8 and 11.
(D-F) Data represent the means of at least two replicates (30 animals each) and error bars the standard deviation. Significance was calculated using Student's t-test $*p < 0.05$, $**p < 0.01$.

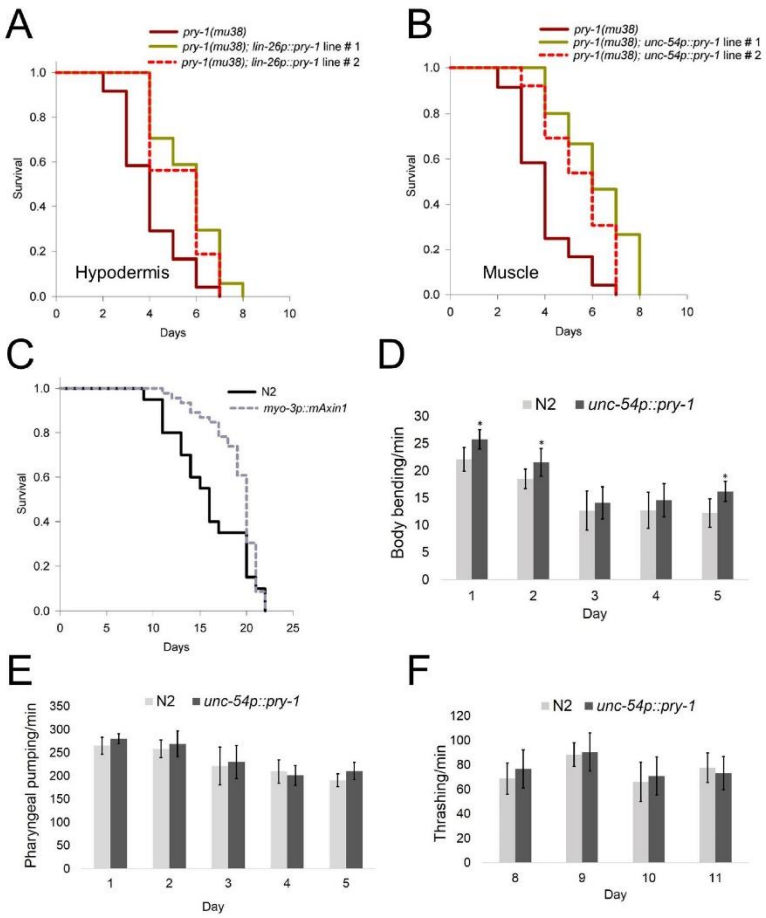

Figure S6: Expression of *daf-16* isoforms, GATA factors *elt-2* and *elt-4*, and *sod-3*. Genetic interactions of *pry-1* with *daf-2* and *daf-16*, related to Figure 6.

(A and B) Transcript levels of *daf-16a, daf-16d/f/h/i/k* and *daf-16* overall in day-1 *pry-1* mutants (A) and *unc-54p::pry-1* animals (B).

(C) Transcript levels of *elt-2* and *elt-4* in day-1 *unc-54p::pry-1* animals.

(A-C) Data represent the means of two replicates and error bars the SEM. Significance was calculated using Bio-Rad software (t-test). $*p < 0.05$, $**p < 0.01$.

(D) Lifespan phenotype of *daf-2* mutants following *pry-1* RNAi.

(E) Lifespan phenotype of *pry-1(mu38); hs::pry-1* animals following *daf-16* RNAi.

(D and E) See Transparent methods and Table S2 for lifespan data and statistical analyses.

(F) *sod-3* transcript analysis in *unc-54p::pry-1* animals. Data represents the mean of two replicates and error bar the SEM. Significance was calculated using Bio-Rad software (t-test). $*p < 0.05$, $**p < 0.01$.

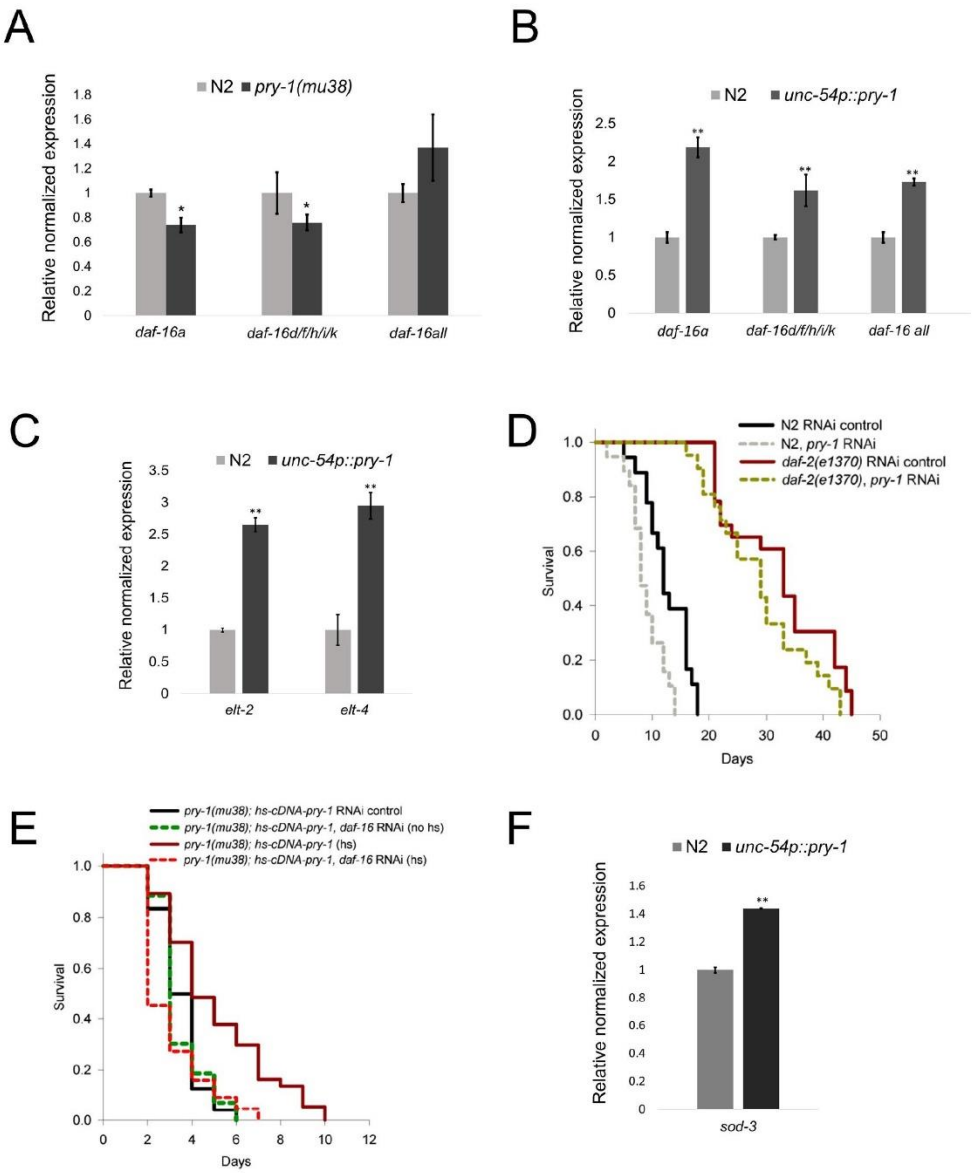
A
N2 pry-1(mu38)
Relative normalized expression
daf-16a
daf-16d/f/h/i/k
daf-16all
B
N2 unc-54p::pry-1
Relative normalized expression
daf-16a
daf-16d/f/h/i/k
daf-16 all
C
N2 unc-54p::pry-1
Relative normalized expression
elt-2
elt-4
D
N2 RNAi control
N2, pry-1 RNAi
daf-2(e1370) RNAi control
daf-2(e1370), pry-1 RNAi
Survival
Days
E
pry-1(mu38); hs-cDNA-pry-1 RNAi control
pry-1(mu38); hs-cDNA-pry-1, daf-16 RNAi (no hs)
pry-1(mu38); hs-cDNA-pry-1 (hs)
pry-1(mu38); hs-cDNA-pry-1, daf-16 RNAi (hs)
Survival
Days
F
N2 unc-54p::pry-1
Relative normalized expression
sod-3

7

Figure S7: Analyses of lipid levels and expression of genes involved in lipid synthesis in *unc-54p::pry-1* animals and genetic interactions of *aak-2* and *par-4* with *pry-1*, related to Figure 7.

(A) Oil red O staining of total lipid droplets in control and *unc-54p::pry-1* day-1 adults. Scale bar is 0.1mm.

(B) Quantification of lipid levels in animals shown in panel A. Data represent the means of at least two replicates ($n \geq 20$ animals each) and error bars the standard deviation. Significance was calculated using Student's t-test, $^{**}p < 0.01$.

(C) qPCR analysis of fatty acid desaturases (*fat-5, fat-6*, and *fat-7*) and SREBP homolog (*sbp-1*) in wild-type (N2) and *unc-54p::pry-1* day-1 adults. Data represent the means of two replicates and error bar the SEM. Significance was calculated using Bio-Rad software (t-test). $^{*}p < 0.05$, $^{**}p < 0.01$.

(D) Representative images of AAK-2::GFP in control and *pry-1(mu38)* animals. Scale bar is 0.2mm. Data represent the means of at least two replicates ($n \geq 20$ animals each) and error bars the standard deviation. Significance was calculated using Student's t-test, $^{**}p < 0.01$.

(E) Representative images of AAK-2::GFP animals. GFP fluorescence is visible in the muscle (arrowhead). Scale bar is 0.1mm.

(F) Dauer survivability phenotype of *pry-1(mu38), pry-1(gk3682),* and *aak-2(ok524)* animals.

(G) Lifespan analysis of *par-4(it57)* animals following control and *pry-1* RNAi knockdowns.

(H) Muscle-specific knockdown of *par-4* in control and *unc-54p::pry-1* animals.

(F-H) See Transparent methods and Table S2 for lifespan data and statistical analyses.

Mallick et al.

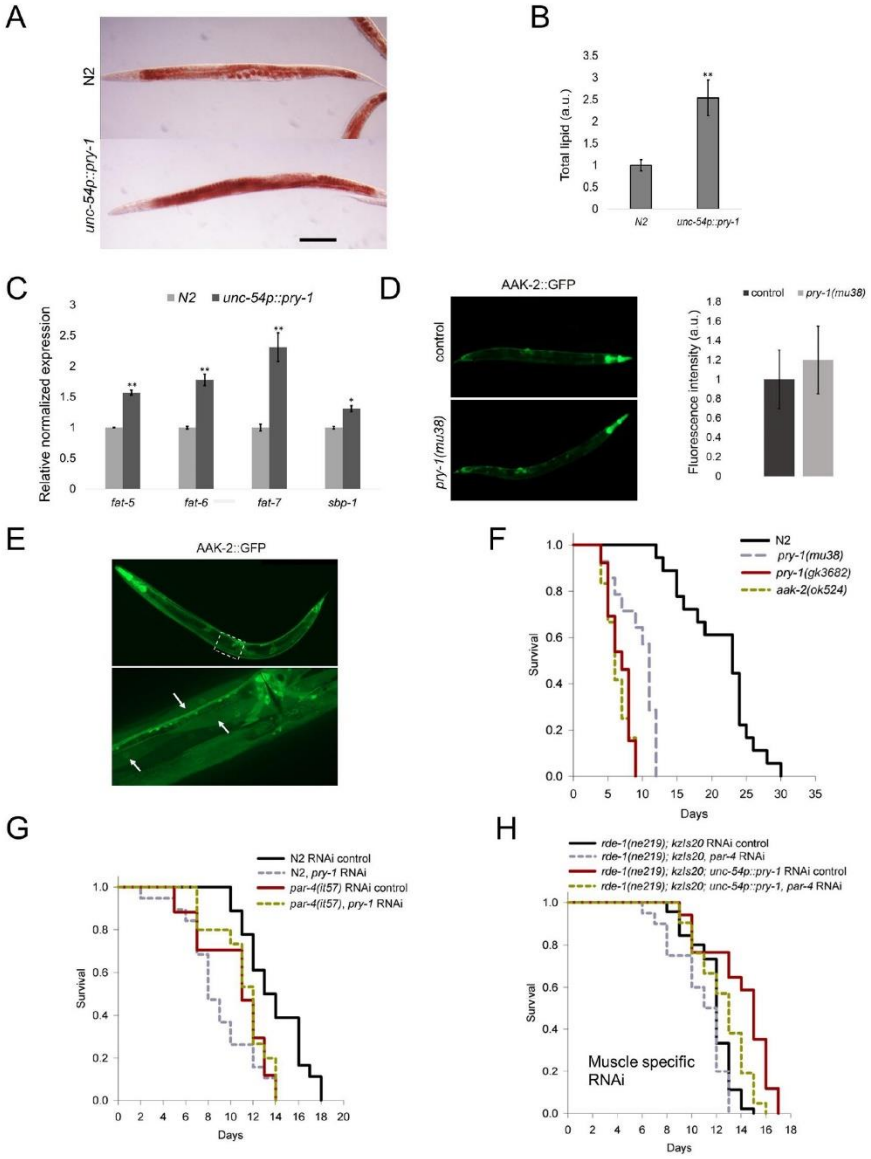

TRANSPARENT METHODS

LEAD CONTACT AND MATERIALS AVAILABILITY

Further information and requests for resources and reagents should be directed to and will be fulfilled by the Lead Contact, Bhagwati Gupta (guptab@mcmaster.ca).

EXPERIMENTAL MODEL AND SUBJECT DETAILS

Worm cultures

C. elegans strains (see Table S8) were maintained on nematode growth medium (NGM) agar-containing plates seeded with OP50 *E. coli* bacteria (Brenner, 1974). Cultures were kept at 20^0C unless otherwise stated.

Strain construction

DY230 strain was created by injecting 100 ng/µl of pGLC37 plasmid into the *pry-1(mu38)* animals. To generate transgenic animals (DY664-668), pGLC153(*unc-54p::pry-1*) or pGLC154(*lin-26p::pry-1*) was injected in N2 animals at 30 ng/µL along with 30 ng/µL of pPD136.64(*myo-3p::YFP*) marker. Two independent lines were established in each case. pGLC153 was also co-injected with 30 ng/µL pPD136.64 in the strains NR350 and VP303 to generate muscle (DY682) and intestine-specific (DY690) RNAi lines. DY679 was generated by injecting 30ng/µL pDC10(*pry-1p::pry-1::GFP*) and co-injection marker 10ng/µL *dat-1p::mCherry* in N2. pDC10 was injected in *C. briggsae* AF16 animals to generate the strain DY160.

METHOD DETAILS

Reagents and resources used in this study are listed in Table S8.

Plasmid construction

pGLC37 was constructed by subcloning full-length *C37A5.9/pry-1* cDNA (1.7kb) downstream of *hsp-16-41* promoter in the vector pPD49.83.

unc-54p::pry-1 plasmid (pGLC153), containing PRY-1 cDNA downstream of muscle-specific promoter *unc-54*, was constructed as follows. Three different fragments, 4.1kbp of *unc-54* promoter, 1.7kbp of *pry-1*-cDNA from pGLC37, and 646bp of *unc-54* 3' UTR from genomic DNA were amplified using primers (Table S8). The purified fragments were cloned into the destination vector using the Multisite Gateway Pro (Thermo Fisher Scientific) protocol.

lin-26p::pry-1 plasmid (pGLC154), containing PRY-1 cDNA downstream of the hypodermis-specific promoter *lin-26*, was constructed as follows. Three different fragments, 4.1kbp of *lin-26*-promoter, 1.7kbp of *pry-1*-cDNA from pGLC37, and 646bp of

unc-54 3' UTR from genomic DNA were amplified using primers (Table S8). The purified fragments were cloned into the destination vector using the Multisite Gateway Pro (Thermofisher) protocol.

pDC10 was kindly provided by Hendrick Korswagen (Korswagen et al., 2002). The plasmid contains a genomic DNA fragment including the complete *C37A5.9/pry-1*-coding sequence and 3.6 kb of upstream sequence inserted in-frame into the *GFP* reporter containing vector pPD95.81.

pry-1 RNAi plasmid (pGLC142) was constructed by inserting a genomic fragment of 2.3kb into the L4440 vector using restriction enzymes *Hind*III and *Xma*I. The fragment was obtained by PCR using the primers GL1343 and GL1344.

RNA extraction and qPCR

Total RNA was extracted from one large plate of worms using the Trizol-based extraction procedure (SIGMA). RNA was DNAse treated according to a protocol (QIAGEN). 1 µg of RNA was used to synthesize cDNA using a SensiFAST cDNA synthesis kit (BIOLINE). SYBR Green (BIORAD) quantitative RT-PCR was performed using the BIORAD CFX-Real Time system and following the BIORAD-CFX Software manual. Data from three biological repeats were analyzed using the comparative 2ΔΔCt method and significance assessed by one-way ANOVA.

RNAi

RNAi-mediated gene silencing was performed using the protocol previously published by our laboratory (Seetharaman et al., 2010). For adult specific RNAi, synchronized worms were cultivated on plates containing OP50 bacteria until the young adult stage and then transferred to RNAi plates. Either L4440 empty vector or GFP RNAi bacteria was used as a control (Kamath et al., 2001). RNAi knockdown of *bar-1* in *pry-1(mu38); hs::pry-1* strain had no effect on the lifespan but did suppress the multivulva phenotype of animals.

RNA-seq data analysis

RNA-seq data for *pry-1(mu38)* animals were published (Ranawade et al., 2018) and deposited in NCBI with accession number GEO GSE94412. GO analysis was carried out with default setting using GoAmigo (http://amigo.geneontology.org). A GO-term containing at least three genes with a *p*-value adjusted for multiple comparisons and < 0.05 (Benjamini-Hochberg method) was counted significant (Carbon et al., 2009). Tissue enrichment analysis was performed using WormBase online TEA tool that employs a tissue ontology (Angeles-Albores et al., 2016).

Lifespan analysis

Lifespan analysis was carried out following an established protocol (Amrit et al., 2014). Each strain was repeated at least twice. A minimum of 50 animals were used per condition, and worms were scored for viability every second day, from day 1 of adulthood (treating the pre-fertile day preceding adulthood as t = 0). *daf-2(e1370)* and *par-4(it57)* animals were grown at 25^0C after reaching adulthood. Young adult worms were transferred to fresh plates every other day and the numbers of dead worms were recorded as events scored. Animals that were lost or burrowed in the medium, exhibiting protruding vulva (intestine protrudes from the vulva), or undergoing bagging (larvae hatching inside the worm body) were censored. SigmaPlot software was used for statistical analysis, and *p* values were calculated using the log-rank (Kaplan-Meier) method.

Dauer longevity assay

Dauers were generated using a starvation protocol. Synchronized gravid adults were plated and allowed to lay eggs for 8 hours following which adults were removed. The plate was then shifted to 27^0C and after 3 days 10 Dauer larvae were randomly picked into a 20 µl drop of double-distilled water suspended under a Petri dish cover. A wet tissue was placed on the bottom of the plate and was sealed with Parafilm. Dauer longevity was monitored daily at 25^oC, and survival was scored as moving response upon exposure to a focused beam of 425-440 nm light as previously described (Narbonne and Roy, 2006). SigmaPlot software was used for statistical analysis, and *p* values were calculated using the log-rank (Kaplan-Meier) method.

Pharyngeal pumping and locomotion

Pharyngeal pumping assay was performed on NGM plates containing a thin bacterial lawn. Worms were bleach synchronized and allowed to grow in the presence of food to late L4 stage. 10 worms were transferred to assay plates, and the number of contractions in the terminal bulb of the pharynx of each animal was counted every 24 hours for 30 sec using a Nikon 80i inverted microscope. Four independent experiments were performed on each day.

The locomotion rate of worms on different days of adulthood was examined using a protocol from the Sternberg lab. Briefly, worms were bleach synchronized and allowed to grow till late L4 stage. Five worms were placed onto separate plates and tested daily for locomotion until death. For testing, a worm was picked onto an NGM plate containing a uniform layer of bacteria and stimulated by contact with the tail. The number of body movements was counted from the trail left on the plate.

Oil Red O staining

Oil Red O (Sigma-Aldrich) staining was performed following the standard protocol (Ranawade et al 2018). Worms were washed with 1x PBS buffer (pH 7.4), and re-

suspended in 60 µl of 1x PBS, 120 µl of 2x MRWB buffer and 60 µl of 4% paraformaldehyde. The worms were then freeze-thawed three times and washed twice with 1x PBS. They were then incubated at room temperature in 60% isopropyl alcohol for 10 minutes for dehydration and stained with freshly prepared Oil Red O solution for at least 48 hours on a shaker. Animals were imaged with a Q-imaging software and Micropublisher 3.3 RTV color camera outfitted with DIC optics on a Nikon 80i microscope. NIH ImageJ software was used to quantify Oil Red O intensities (Soukas et al., 2009). 15 to 30 worms were randomly selected from each category in at least two separate batches.

Fluorescence microscopy

Photomicrographs of GFP-tagged animals were acquired using Axiovision Zeiss microscope (Mallick et al., 2019). Nematodes were mounted on glass slides containing 2% agarose and 0.02M NaN_3 and quickly observed under the microscope (within 10 min.) to minimize stress. The microscopy analysis was independently replicated at least twice.

Western blotting

For native extracts, nematodes were synchronized by bleaching and allowed to grow on OP50 bacteria until day-1 of adulthood. Worms were then washed three times with M9 buffer, pelleted, and mixed with 1mL of native lysis buffer (as described in Gidalevitz et al., 2009). Samples were frozen in -80°C prior to use. Nematodes were thawed on ice and mechanically disrupted using a Precellys (Bertin Instruments) programmed for 8x10s pulses, with 30s between each pulse. Samples were then centrifuged for 5 minutes (13000 g) at 4^0C and supernatant containing total proteins was transferred to fresh tubes.

SDS-PAGE was carried out followed by electrophoretic transfer to nitrocellulose membrane at 100 V for 1 hour at 4°C. Immunoblots were performed according to primary antibody manufacturers' protocols. AAK-2 phosphorylation was probed with rabbit p-AMPKα (T172) antibody (CST). GAPDH was probed as housekeeping gene with 1:1000 mouse GAPDH (Invitrogen). Secondary antibodies, goat-anti-rabbit HRP-linked IgG (CST) and goat-anti-mouse IgG (Invitrogen), were diluted 1:1000 and 1:1500, respectively in 4% milk dissolved in TBST. Signal was detected using Amersham™ ECL™ Western Blotting Detection Reagent (GE Healthcare). The results are representative of two independent experiments.

Quantification and statistical analyses

For lifespan and stress resistance assays, statistics analyses were performed using SigmaPlot software 11. Survival curves were estimated using the Kaplan- Meier test and differences among groups were assessed using the log-rank test. Survival data are expressed relative to the control group. Bio-Rad CFX software was used for qPCR statistical analyses using t-test or one-way ANOVA.

Statistical analyses other than those for muscle mitochondrial morphology were performed using Microsoft Office Excel 365. The mitochondrial data was analyzed using GraphPad prism and p values were calculated using Fisher's exact test. Figure 5 shows values based on normal (tubular) and defective (intermediate and fragmented, combined) mitochondrial phenotypes. Significance was also determined for individual defective categories. The p values are: <0.0001, 0.7583, 0.0429, and 0.048 when comparing tubular with intermediate and <0.0001, 0.5128, 0.0110, and 0.0986 when comparing tubular with fragmented. The genotypes in both cases are: *pry-1(mu38),* whole-animal *pry-1*(RNAi), muscle-specific *pry-1* RNAi, and *unc-54p::pry-1,* respectively. We used the chi square test as well and obtained the following *p* values: <0.0001 for *pry-1(mu38)*, 0.5697 for whole-animal *pry-1*(RNAi), 0.0194 for muscle-specific *pry-1* RNAi, and 0.066 for *unc-54p::pry-1.*

In all cases, differences were considered statistically significant at $p < 0.05$, thereby indicating a probability of error lower than 5%. For hypergeometric probability testing, an online program (http://nemates.org/MA/progs/overlap_stats.html) was used to test statistical significance of the overlap between two gene sets.

Supplemental References

Amrit, F.R.G., Ratnappan, R., Keith, S.A., Ghazi, A., 2014. The *C. elegans* lifespan assay toolkit. Methods 68, 465–475. https://doi.org/10.1016/j.ymeth.2014.04.002

Angeles-Albores, D., Raymond, R.Y., Chan, J., Sternberg, P.W., 2016. Tissue enrichment analysis for *C. elegans* genomics. BMC Bioinformatics 17, 1–10. https://doi.org/10.1186/s12859-016-1229-9

Brenner, S., 1974. The genetics of *Caenorhabditis elegans*. Genetics 77, 71–94. https://doi.org/10.1002/cbic.200300625

Carbon, S., Ireland, A., Mungall, C.J., Shu, S., Marshall, B., Lewis, S., Lomax, J., Mungall, C., Hitz, B., Balakrishnan, R., Dolan, M., Wood, V., Hong, E., Gaudet, P., 2009. AmiGO: Online access to ontology and annotation data. Bioinformatics 25, 288–289. https://doi.org/10.1093/bioinformatics/btn615

Gidalevitz, T., Krupinski, T., Garcia, S., Morimoto, R.I., 2009. Destabilizing protein polymorphisms in the genetic background direct phenotypic expression of mutant SOD1 toxicity. PLoS Genet. 5. https://doi.org/10.1371/journal.pgen.1000399

Kamath, R.S., Martinez-Campos, M., Zipperlen, P., Fraser, A.G., Ahringer, J., 2001. Effectiveness of specific RNA-mediated interference through ingested double-stranded RNA in *Caenorhabditis elegans*. Genome Biol. 2, 1–10. https://doi.org/10.1186/gb-2000-2-1-research0002

Korswagen, H., Coudreuse, D., Betist, M., Water, S., Zivkovic, D., Clevers, H., 2002. The Axin-like protein PRY-1 is a negative regulator of a canonical Wnt pathway in

C. elegans. Genes Dev. 16, 1291–1302.

Mallick, A., Ranawade, A., Gupta, B.P., 2019. Role of PRY-1/Axin in heterochronic miRNA-mediated seam cell development. BMC Dev. Biol. 19, 1–12. https://doi.org/10.1186/s12861-019-0197-5

Narbonne, P., Roy, R., 2006. Inhibition of germline proliferation during *C. elegans* dauer development requires PTEN, LKB1 and AMPK signalling. Development 133, 611–619. https://doi.org/10.1242/dev.02232

Ranawade, A., Mallick, A., Gupta, B.P., 2018. PRY-1/Axin signaling regulates lipid metabolism in *Caenorhabditis elegans*. PLoS One 13, e0206540. https://doi.org/10.1371/journal.pone.0206540

Seetharaman, A., Cumbo, P., Bojanala, N., Gupta, B.P., 2010. Conserved mechanism of Wnt signaling function in the specification of vulval precursor fates in *C. elegans* and *C. briggsae*. Dev. Biol. 346, 128–139. https://doi.org/10.1016/j.ydbio.2010.07.003

Soukas, A.A., Kane, E.A., Carr, C.E., Melo, J.A., Ruvkun, G., 2009. Rictor/TORC2 regulates fat metabolism, feeding, growth, and life span in *Caenorhabditis elegans.* Genes Dev. 496–511. https://doi.org/10.1101/gad.1775409.2004

Chapter 6

Identification and characterization of genes that mediate *pry-1/Axin* function in reproductive structure development, stress responses, and aging

6.1 Preface

This chapter includes the following three articles in its originally published or submitted format: **1)** "Genetic analysis of *Caenorhabditis elegans pry-1/Axin* suppressors identifies genes involved in reproductive structure development, stress responses, and

aging", by Avijit Mallick, Nikita Jhaveri, Jihae Jeon, Yvonne Chang, Krupali Shah, Hannah Hosein and Bhagwati P. Gupta. (G3 Genes|Genomes|Genetics, 15 December 2021; jkab430. DOI: 10.1093/g3journal/jkab430).

2) "Cabin1 domain-containing gene *picd-1* interacts with *pry-1/Axin* to regulate multiple processes in *Caenorhabditis elegans*", by Avijit Mallick, Shane K. B. Taylor, Sakshi Mehta, and Bhagwati P. Gupta. (bioRxiv, 28 September 2021. DOI: 10.1101/2021.09.27.46207, **Submitted in Scientific Reports**).

3) "The FGFR4 homolog KIN-9 regulates lifespan and stress responses in *Caenorhabditis elegans*", by Avijit Mallick, Leo Xu, Sakshi Mehta, Hannah Hossein, and Bhagwati P Gupta (**Submitted in Frontiers in Aging**).

6.2 Mallick *et* al. (2021)- G3 Genes|Genomes|Genetics

In this study, we identified eight genes that function downstream of PRY-1/Axin signalling to regulate developmental and post-developmental processes. Specifically, we focused on a set of differentially expressed genes associated with reproductive structure development in the *pry-1*-mutant transcriptome. Knocking down eight of the genes (*spp-1, clsp-1, ard-1, rpn-7, cpz-1, his-7, cdk-1,* and *rnr-1*) efficiently suppressed the multivulva phenotype of *pry-1* mutants. Our genetic interaction experiments revealed that in addition to their role in vulval development, these genes participate in one or more *pry-1*-mediated biological events. While four of them (*cpz-1, his-7, cdk-1,* and *rnr-1*) function in both stress response and aging, two (*spp-1* and *ard-1*) are specific to stress response. Altogether, these findings demonstrate the important role of *pry-1* suppressors in regulating developmental and post-developmental processes in *C. elegans.*

Contributions: I performed experiments and provided data for Figures 1, 3B, 7, S3, S4A and Table 1. Nikita Jhaveri performed experiments and provided data for Figures 3A, 3C, 4 and Table 2. Jihae Jeon, Yvonne Chang, and Krupali Shah performed experiments and provided data for Figure 2, 5A-H, 6A-B, 6D, S1, S2, S4B and Table 3. Hannah Hossein performed experiments and provided data for Figure 5A-B and 6C. I and Bhagwati Gupta created all the Figures and illustrations. I and Bhagwati Gupta conceived and supervised the project. I, Nikita Jhaveri and Bhagwati Gupta wrote the manuscript. It was finally revised with addressed reviewers concerns by me and Bhagwati Gupta.

OXFORD G3 Genes | Genomes | Genetics

G3, 2022, jkab430
https://doi.org/10.1093/g3journal/jkab430
Advance Access Publication Date: 15 December 2021
Investigation

Genetic analysis of *Caenorhabditis elegans pry-1/Axin* suppressors identifies genes involved in reproductive structure development, stress responses, and aging

Avijit Mallick, Nikita Jhaveri, Jihae Jeon, Yvonne Chang, Krupali Shah, Hannah Hosein, and Bhagwati P. Gupta *

Department of Biology, McMaster University, Hamilton, ON L8S4K1, Canada

*Corresponding author: Email: guptab@mcmaster.ca

Abstract

The Axin family of scaffolding proteins regulates a wide array of developmental and post-developmental processes in eukaryotes. Studies in the nematode *Caenorhabditis elegans* have shown that the Axin homolog PRY-1 plays essential roles in multiple tissues. To understand the genetic network of *pry-1*, we focused on a set of genes that are differentially expressed in the *pry-1*-mutant transcriptome and are linked to reproductive structure development. Knocking down eight of the genes (*spp-1, clsp-1, ard-1, rpn-7, cpz-1, his-7, cdk-1*, and *rnr-1*) via RNA interference efficiently suppressed the multivulva phenotype of *pry-1* mutants. In all cases, the ectopic induction of P3.p vulval precursor cell was also inhibited. The suppressor genes are members of known gene families in eukaryotes and perform essential functions. Our genetic interaction experiments revealed that in addition to their role in vulval development, these genes participate in one or more *pry-1*-mediated biological events. Whereas four of them (*cpz-1, his-7, cdk-1*, and *rnr-1*) function in both stress response and aging, two (*spp-1* and *ard-1*) are specific to stress response. Altogether, these findings demonstrate the important role of *pry-1* suppressors in regulating developmental and post-developmental processes in *C. elegans*. Given that the genes described in this study are conserved, future investigations of their interactions with Axin and their functional specificity promises to uncover the genetic network of Axin in metazoans.

Keywords: *C. elegans*; *pry-1*; Axin; vulva development; stress response; aging; WNT signaling

Introduction

Most genetic research is aimed at linking genes to phenotypes and understanding how changes in gene function affect biological processes. Studies in animal models have demonstrated that genes exert their effects through interactions with other genes that form functional networks. Disruptions of the activity of network components can lead to various defects and in some cases premature death. Therefore, a comprehensive understanding of gene–gene interactions is crucial for the discovery of effective treatments. Our group is currently investigating the genetic network of an Axin family member in the nematode *Caenorhabditis elegans*. Axins are scaffolding proteins that play crucial roles in regulating conserved processes in metazoans; they integrate inputs from multiple interactors to coordinate downstream cellular signaling events. Moreover, Axin mutations have been implicated in multiple abnormalities and diseases (Mallick *et al.* 2019b). Therefore, elucidating the Axin signaling cascade can enhance our understanding of disease progression, and the pathway could be an attractive therapeutic target.

Work from our lab and others have shown that the *C. elegans* Axin homolog PRY-1 is involved in multiple developmental and post-developmental processes, including embryogenesis, neuronal differentiation, vulva formation, seam cell development, lipid metabolism, and lifespan maintenance (Maloof *et al.* 1999; Korswagen *et al.* 2002; Mallick *et al.* 2019b, 2020; Mallick and Gupta 2020). Initial studies on *pry-1* showed that the gene product acts as a negative regulator of canonical WNT signaling (Korswagen *et al.* 2002). PRY-1 forms a destruction complex in the absence of a WNT ligand, leading to inhibition of a WNT effector, the β-catenin homolog BAR-1. Mutations in *pry-1* mimic activated WNT signaling and cause the translocation of BAR-1 to the nucleus, thereby promoting the expression of target genes (Gleason *et al.* 2002). During vulval development, *pry-1* restricts the number of induced vulval precursor cells (VPCs). In a normal worm, three (P5.p, P6.p, and P7.p) of the six Pn.p cells (P3.p through P8.p), termed the VPCs, participate in the formation of the vulva (Sulston and Horvitz 1977; Sternberg 2005). The remaining uninduced VPCs adopt nonvulval fates and fuse with the surrounding hypodermal syncytium (Sternberg and Horvitz 1989). In the absence of *pry-1*, nonvulval cells are inappropriately induced to adopt specific fates, resulting in multiple ectopic ventral protrusions, a phenotype termed multivulva (Muv) (Gleason *et al.* 2002; Seetharaman *et al.* 2010). The mechanism of *pry-1* action during VPC induction and cell fate specification is not well understood.

In addition to its essential function in canonical WNT signaling, *pry-1* participates in the WNT asymmetric pathway to regulate the expression of heterochronic microRNAs and their targets during seam cell development (Mallick *et al.* 2019a). More

Received: October 17, 2021. **Accepted:** November 22, 2021

recently, we discovered additional roles for *pry-1* in the regulation of lipid metabolism, stress response, and aging, and identified its interacting genes in these processes (Mallick *et al.* 2019b, 2020). Whereas these findings demonstrate the essential function of *pry-1* in *C. elegans*, how it controls diverse events and mediates specific cellular interactions remain to be explored. Given that the gene encodes a scaffolding protein, it might recruit many other factors to regulate their activities.

In this study, we set out to investigate the genetic network of *pry-1* by investigating a set of genes that are involved in a wide variety of cellular and molecular processes. The genes are differentially expressed in the *pry-1*-mutant transcriptome and while they are all associated with the GO term "reproductive structure development," many have essential roles in other tissues as well. Our RNAi knockdown experiments revealed that eight of the 26 genes tested (*spp-1*, *clsp-1*, *ard-1*, *rpn-7*, *cpz-1*, *his-7*, *cdk-1*, and *rnr-1*) strongly suppressed the *pry-1* Muv phenotype and ectopic P3.p induction. We examined genetic interactions between the genes and *bar-1* in vulval cells, which revealed that *rpn-7* acts downstream of *pry-1*-*bar-1*-mediated signaling. All of the suppressor genes are conserved in eukaryotes and perform diverse functions such as oxidation-reduction reactions (dehydrogenase family: *ard-1* and reductase family: *rnr-1*), protein degradation (proteasomal complex component: *rpn-7* and peptidase: *cpz-1*), protein phosphorylation (adapter protein: *clsp-1* and kinase: *cdk-1*), transmembrane transportation (channel protein: *spp-1*), and the regulation of gene expression (histone: *his-7*) (Davy *et al.* 2001; Hashmi *et al.* 2004; Boxem 2006; Alper *et al.* 2007; Mori *et al.* 2008; Srinivasan *et al.* 2008; Ossareh-Nazari *et al.* 2016). Four of the genes (*clsp-1*, *his-7*, *cdk-1*, and *rnr-1*) have roles in the cell cycle, DNA damage checkpoint, DNA repair, and DNA replication.

We investigated whether suppressors also participate in other *pry-1*-mediated processes, such as the stress response and lifespan maintenance. Whereas RNAi knockdown of four of the eight genes (*cpz-1*, *his-7*, *cdk-1*, and *rnr-1*) significantly rescued the short lifespan and stress sensitivity of *pry-1* mutants, two of them (*spp-1* and *ard-1*) affected only the stress response but not the lifespan. These results show that *pry-1* utilizes overlapping subsets of genes in distinct processes. Overall, these findings demonstrate that PRY-1 interacts with a diverse set of conserved factors involved in processes such as protein modification, protein homeostasis, DNA replication, DNA repair, gene expression, and the cell cycle to control essential biological events in *C. elegans*.

Materials and methods

Strains

Animals were maintained at 20°C on standard nematode growth media (NGM) plates seeded with OP50 *Escherichia coli* bacterial strains as described by Brenner (1974). Worm strain information can be found in Supplementary Table S1.

RNAi

RNAi mediated gene silencing was performed using a protocol previously published by our laboratory (Ranawade *et al.* 2018). Plates were seeded with *E. coli* HT115 expressing either dsRNA specific to candidate genes or empty vector (L4440). Synchronized gravid adults were bleached, and eggs were plated. Vulva or seam cell phenotypes were analyzed in young adults.

Ahringer RNAi library was the source of bacterial clones (Kamath *et al.* 2003). Initially, GO term searches (in 2017; geneontology.org file "gene_ontology.obo" pulled from the version control on May 3 08:44:20 2017 UTC) had identified 36 upregulated genes associated with reproductive structure development. Of these, 26 clones were present in the RNAi library and tested. The remaining clones were either absent or did not grow. Subsequent GO analysis (performed in 2020) revealed a larger set of upregulated genes (52). Since the work on the initial 26 genes had advanced significantly by this time, additional genes were not tested.

Vulva phenotype and VPC induction analysis

Muv and protruding vulva (Pvl) phenotypes were scored in adults at plate level. Animals with multiple ventral protrusions (pseudovulvae) were termed as Muv and those with a single prominent protrusion as Pvl. VPC induction was determined during the L4 stage under a Nomarski microscope (Seetharaman *et al.* 2010) L4 larvae were mounted on glass slides containing 2% agar pad and the anesthetic sodium azide (1 mM). In a wild-type worm, each of the three VPCs, P5.p, P6.p, and P7.p, are induced to form the vulva (hence the induction score three, one for each precursor). The vulval progeny invaginate and fuse selectively giving rise to a "Christmas tree" appearance during the mid-to-late L4 stage. Animals with more than three induced VPCs (Muv class) show multiple distinct invaginations and are assigned induction scores of greater than three.

Lifespan analysis

All lifespan analysis was done following adult-specific RNAi treatment using a protocol described previously (Mallick *et al.* 2020). Animals were grown on NGM OP50 seeded plates till late L4 stage after which they were transferred to RNAi plates. Plates were then screened daily for dead animals and surviving worms were transferred every other day till the progeny production ceased. Censoring was done for animals that either escaped, burrowed into the medium, showed a bursting of intestine from the vulva or formed a bag of worms (larvae hatches inside the worm and the mother dies). Data from the lifespan experiments are combined and represented by the Kaplan-Meier survival plot coupled with log-rank (Mantel-Cox) test (to get the statistics of average survival time) (Amrit *et al.* 2014).

Stress assay

Oxidative stress experiments were performed by exposing animals to 100 mM paraquat (PQ) for 1 and 2 h using a published protocol (Li *et al.* 2008). Final working concentrations were made in M9 buffer. At least 30 animals were tested for each strain in each replicate. Mean and standard deviation were determined from experiments performed in duplicate. Animals were considered dead if they had no response following a touch using the platinum wire pick and showed no thrashing or swimming movement in M9. Moreover, dead animals usually had an uncurled body posture compared to the normal sinusoidal shape of worms.

Body bending and pharyngeal pumping analysis

Rate of body bending per one min and the rate of pharyngeal pumping per 30 s for adults were analyzed over the period of 4 days (Collins *et al.* 2008). Individual hermaphrodites were analyzed for these phenotypes under the dissecting microscope by placing them on OP50 culture plates. Pharyngeal pumping was assessed by observing the number of pharyngeal contractions for 30 s. For body bending assessment, animals were stimulated by tapping once on the tail of the worm using the platinum wire pick where one body bend corresponded to one complete sinusoidal wave of the worm. Only animals that moved throughout the duration of one min were included in the analysis.

Molecular biology

RNA was extracted from synchronized L3 and day-1 adult animals. Protocols for RNA extraction, cDNA synthesis and qPCR were described earlier (Ranawade *et al.* 2018). Briefly, total RNA was extracted using Trizol (Thermo Fisher, USA), cDNA was synthesized using the SensiFast cDNA synthesis kit (Bioline, USA), and qPCR was done using the SYBR green mix (Bio-Rad, Canada). Primers used for qPCR experiments are listed in Supplementary Table S1.

Nomarski fluorescent microscopy

Animals were anesthetized using 10 mM Sodium Azide and mounted on glass slides with 2% agar pads and covered with glass coverslips. Images were captured using Zeiss Apotome microscope and Zeiss software. Fluorescence of *hsp-4::GFP*, *hsp-60::GFP*, *sod-3::GFP* and *daf-16p::DAF-16::GFP* was examined by analyzing the degree of GFP intensity. Quantification of GFP fluorescence pixel densities was performed with ImageJ™ (https://imagej.nih.gov/ij/).

Statistical analyses

Statistics analyses were performed using Sigma Plot software 11, CFX Maestro 3.1, and Microsoft Office Excel 2016. For lifespan data, survival curves were estimated using the log-rank (Mantel-Cox) test and differences among groups were assessed using the log-rank test. qPCR data were analyzed using Bio-Rad CFX Maestro 3.1 software. For all other assays, data from repeat experiments were pooled and analyzed together and statistical analyses were done using GraphPad Prism 8. *P*-values less than 0.05 were considered statistically significant.

Results

Reproductive structure development genes are misregulated in the *pry-1* mutant

Given that *pry-1* is involved in diverse processes, we aimed to identify its interacting genes that might act in a tissue or process-specific manner. The initial work focused on vulval development, a tissue where *pry-1* plays an essential role but very little is known about the downstream target genes. We used GO enrichment analysis (http://geneontology.org/ and Wormbase release WS258) to filter differentially expressed genes associated with "reproductive structure development" (GO:0048608) in the *pry-1* mutants and identified 149 genes (Supplementary Table S2). Among them, 52 and 97 genes were upregulated and downregulated, respectively, in the *pry-1* mutant transcriptome (Ranawade *et al.* 2018) (Figure 1, A and B, Supplementary Table S2). GO term analysis showed significant enrichment (FDR $p < 0.05$) of processes such as cellular component organization or biogenesis (69), anatomical structure development (61), metabolic process (57), regulation of transcription (27), cell cycle (24), and nervous system development (21) (Supplementary Table S3). When examined for molecular functions, we observed enrichment in categories such as protein binding activity (64), DNA binding activity (27), RNA binding activity (20), hydrolase activity (26), signaling receptor binding activity (8), and protein kinase binding activity (7) (Supplementary Table S3). Many genes were found to be associated with cellular components, including the nucleus (74), protein-containing complexes (65), cytoplasm (52), integral components of the membrane (20), cytoskeleton (17), and nuclear chromosomes (12) (Supplementary Table S3). This suggests that *pry-1* plays an essential role in regulating the expression of diverse sets of genes.

Another type of analysis involved enrichment of tissues and phenotypes linked to misregulated genes (https://wormbase.org/tools/enrichment/tea/tea.cgi, Angeles-Albores *et al.* 2016). The results showed significant enrichment of tissues, such as neurons and P-cell lineages (Supplementary Table S4). The genes were also significantly associated with phenotypes such as Pvl, vulval cell induction increased or decreased, and hermaphrodite reproductive system morphology variants (Supplementary Table S4).

RNAi knockdown of a subset of reproductive structure development genes suppresses the *pry-1* Muv phenotype

We evaluated the role of the upregulated genes in *pry-1*-mediated vulval development. To this end, a subset (26 of 52 genes, 50%) was experimentally tested by RNAi to determine the effect of these genes on the Muv phenotype of *pry-1(mu38)* animals (see *Materials and Methods*, Figure 2). As mentioned previously, adult *pry-1* mutant hermaphrodites exhibit a Muv phenotype owing to the constitutive activation of canonical WNT signaling (Gleason *et al.* 2002). Knockdown of 15 of the genes by RNAi significantly suppressed ectopic pseudovulvae in *pry-1* mutants ($p < 0.05$) (Figure 2). For eight of these, the penetrance of the Muv phenotype was lower than the mean ± 2 standard deviations (95% confidence interval) of control RNAi-treated animals (Figure 2); therefore, we designated them as *pry-1* suppressors.

All eight genes, except one (*spp-1*), have homologs in higher eukaryotes including humans, suggesting their important roles in conserved biological processes. Four of the suppressors encode proteins that possess or regulate enzymatic activities, specifically acting as oxidoreductases (*ard-1* and *rnr-1*), a protease (*cpz-1*), and a regulatory subunit of a proteasome complex (*rpn-7*). Two of the suppressors, *clsp-1* and *cdk-1*, are involved in protein phosphorylation. *cdk-1* is possibly necessary for all cell divisions in *C. elegans* (Boxem 2006). *his-7* is a member of the human H2A family of histones that function in DNA repair and gene expression, and *spp-1* is a homolog of the human gene encoding Saposin-like protein that plays a role in immunity (Table 1).

To investigate the expression of the suppressor genes in the *pry-1(mu38)* strain, we performed qPCR experiments at the L3 stage when VPCs undergo division to produce vulval progeny. Earlier, the transcriptome profiling revealed that all genes were upregulated in the L1 larval stage (Ranawade *et al.* 2018). The pattern was the same in L3 animals, except for *cpz-1*, which was unchanged (Figure 3A). We also carried out qPCR analysis in day-1 adults and found that five of the suppressor genes continued to be expressed at significantly high levels. Of the remaining three, *ard-1* and *rpn-7* were unchanged and *his-7* was downregulated (Figure 3B). Thus, most of the suppressor genes are negatively regulated by *pry-1* in L3 larvae and young adults. The results also suggest that *pry-1* regulates some of the genes in a stage and tissue-specific manner. Thus, it could be that *cpz-1* levels are upregulated in vulval cells but not reflected by whole animal qPCR analysis or that its temporal requirement in vulval cells is different. More work is needed to examine these possibilities. Overall, these results support the key roles of suppressor genes downstream of *pry-1* in vulva formation and their potential involvement in mediating *pry-1* function in adults.

To understand the cellular basis of Muv suppression, the VPC induction pattern was investigated. In control RNAi treatments, *pry-1(mu38)* animals showed an average VPC induction of 3.4 ± 0.6 ($n = 29$), which is higher than the N2 control (Table 2).

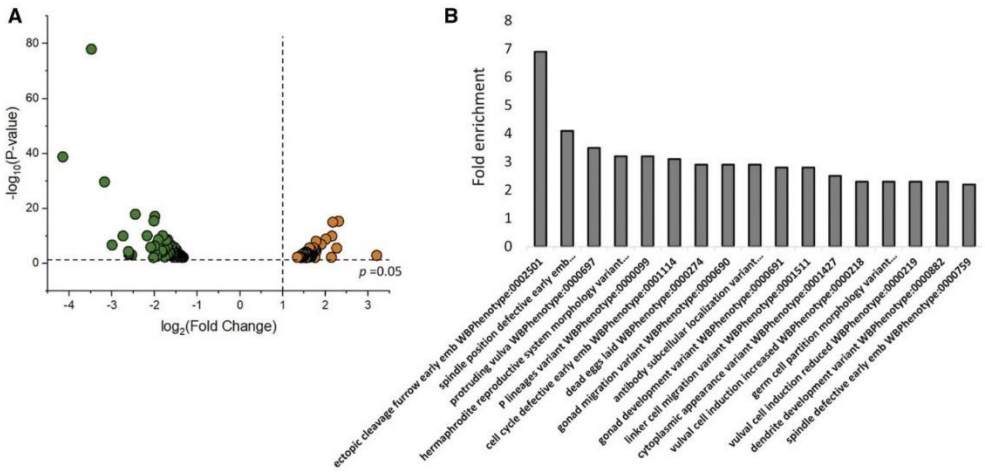

Figure 1 *pry-1* mutant transcriptome is enriched with genes involved in reproductive structure development. (A) Volcano plot showing the 149 differentially expressed genes, with $p < 0.05$, linked to reproductive structure development in *pry-1* mutant animals (Supplementary Table S2). The dotted line on the *x*-axis corresponds to $\log_2$ fold change of 1 and the one on the *y*-axis shows *p*-value of 0.05. Orange and green dots represent significantly upregulated and downregulated genes, respectively. (B) Phenotype-enrichment analysis of genes shown in (A). Not all categories are listed. See Supplementary Table S4 for a complete list.

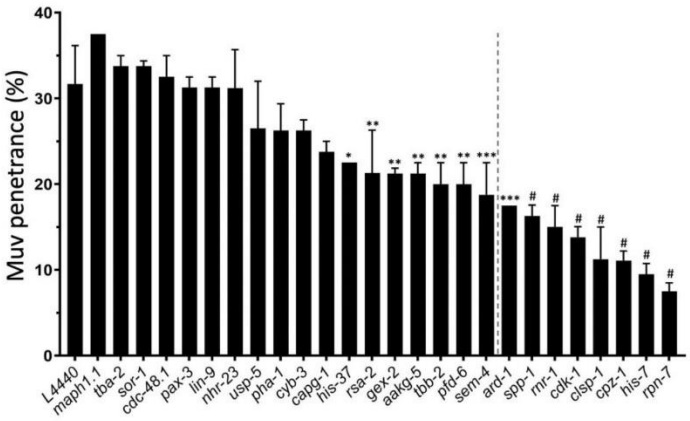

Figure 2 Quantification of the Muv phenotype following RNAi knockdown of 26 upregulated genes in *pry-1(mu38)* animals. Data represent the mean of two replicates ($n > 40$ animals in each replicate) and error bars represent the standard deviation. For eight of the genes, located on the right of the dotted vertical line, Muv penetrance was lower than the mean ± 2x standard deviation of the control (L4440). Statistical analyses were done using one-way ANOVA with Dunnett's *post hoc* test and significant differences are indicated by stars (*): * ($p < 0.05$), ** ($p < 0.01$), *** ($p < 0.001$), # ($p < 0.0001$).

The increase was mainly due to P3.p, and to a lower extent P4.p and P8.p, being ectopically induced. The RNAi knockdown of all eight genes suppressed the P3.p defect in *pry-1* mutant animals (Figure 4C, Table 2) (see *Materials and Methods* for details). For six of the genes (*ard-1, rpn-7, cpz-1, his-7, cdk-1*, and *rnr-1*. *cdk-1* and *rnr-1*) the average VPC induction was also reduced (Figure 4, A and B and Table 2).

We also examined the effects of suppressors on wild-type vulval development. RNAi experiments indicated no significant reduction in VPC induction for any of the genes except *cdk-1* and *rnr-1* (Figure 4, A and D and Table 2). *cdk-1* and *rnr-1* RNAi resulted in 39% and 96.3% reductions in VPC induction, respectively, when compared to that in controls, suggesting that both genes play essential roles in vulva formation. These data, together with expression studies, support our conclusion that all

Table 1 List of the eight suppressor genes, their mammalian homologs, associated GO-biological processes, and function in *C. elegans*

Gene	Mammalian homolog	GO-biological process	Function in *C. elegans*
spp-1	Human SAPLIPs (saposin-like proteins, saposin-B type domain-containing protein)	Pathogenesis; innate immune response; defense response to Gram-negative/positive bacterium; and transmembrane transport	Channel activity
clsp-1	Human CLSPN (claspin)	Mitotic G2 DNA damage checkpoint; activation of protein kinase activity; and mitotic DNA replication checkpoint	Anaphase-promoting complex binding activity; part of the Ataxia telangiectasia and Rad3-related (ATR)/ATL-1 DNA replication checkpoint pathway
ard-1	Human HSD17B10 (hydroxysteroid 17-beta dehydrogenase 10)	Oxidation-reduction process	Dehydrogenase with NADP binding domain
rpn-7	Human PSMD6 (proteasome 26S subunit, non-ATPase 6)	Proteasome-mediated ubiquitin-dependent protein catabolic process	Proteasome 26S complex component; ATP-dependent degradation of ubiquitinated proteins
cpz-1	Human CTSZ (cathepsin Z)	Vulval development; proteolysis; embryo development ending in birth or egg hatching; gonad morphogenesis; ecdysis; collagen and cuticulin-based cuticle	Predicted to have cysteine-type endopeptidase activity
his-7	Human H2AX (histone H2A type 2-B)	DNA repair; chromatin organization; chromatin silencing; and regulation of transcription	Predicted DNA binding activity
cdk-1	Human CDK1 (cyclin-dependent kinase 1)	Cell cycle; cell division; and protein phosphorylation	Serine/threonine kinase activity
rnr-1	Human RRM1 (ribonucleotide reductase catalytic subunit M1)	DNA replication; metabolic process; deoxyribonucleotide biosynthetic process; and oxidation-reduction process	Ribonucleoside-diphosphate reductase activity

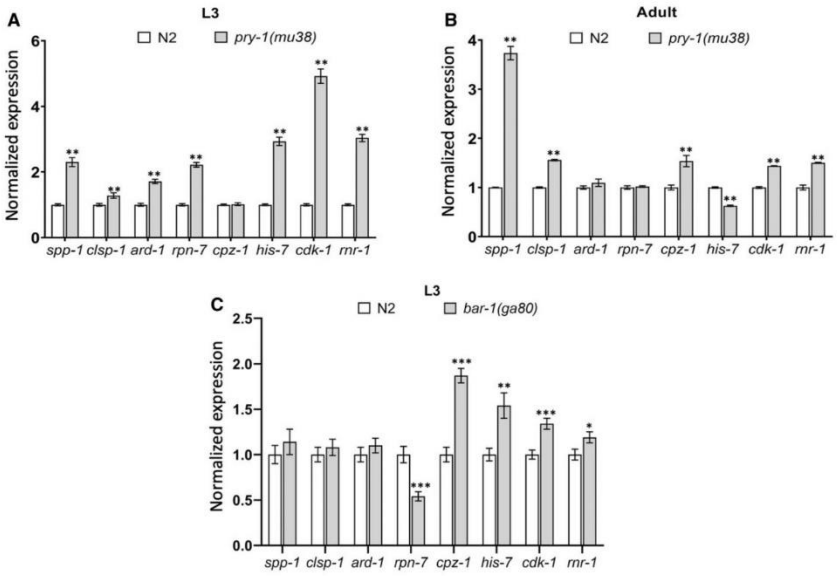

Figure 3 Expression levels of suppressor genes determined by qPCR in *pry-1* and *bar-1* mutants. Normalized expression of suppressor genes in *pry-1(mu38)* L3 larvae and adults (A, B) and *bar-1(ga80)* L3 larvae (C). Each data represents the mean of two replicates and error bars the standard error of means. Significance was calculated using Bio-Rad software (one-way ANOVA) and significant differences are indicated by stars (*): * ($p < 0.05$), ** ($p < 0.01$), *** ($p < 0.001$).

Table 2 Vulval induction analysis in mutants and RNAi-treated animals

Genotype	RNAi target	% Induced VPCs						% Over induced	VPC induction score	*p*-value	N
		P3.p	P4.p	P5.p	P6.p	P7.p	P8.p				
N2	*Control*	0.0	0.0	100.0	100.0	100.0	0.0	NA	3 ± 0	—	40
	ard-1	0.0	0.0	100.0	97.7	100.0	0.0	NA	2.9 ± 0.1	0.360	44
	cdk-1	0.0	0.0	47.5	55.0	77.5	0.0	NA	1.8 ± 0.8	<0.001	40
	clsp-1	0.0	0.0	92.9	97.6	92.9	0.0	NA	2.8 ± 0.6	0.100	42
	cpz-1	0.0	0.0	100.0	100.0	100.0	0.0	NA	3 ± 0	NA	39
	his-7	0.0	0.0	97.2	97.2	97.2	0.0	NA	2.9 ± 0.5	0.314	36
	rnr-1	0.0	0.0	2.8	5.6	2.8	0.0	NA	0.1 ± 0.5	<0.001	36
	rpn-7	0.0	0.0	100.0	100.0	96.7	0.0	NA	2.9 ± 0.1	0.270	30
	spp-1	0.0	0.0	100.0	100.0	100.0	0.0	NA	3 ± 0	NA	43
pry-1(mu38)	*Control*	31.0	3.4	100.0	100.0	100.0	10.3	37.9	3.4 ± 0.6	—	29
	ard-1	0.0	7.9	100.0	97.4	97.4	7.9	15.8	3.1 ± 0.5	0.020	38
	cdk-1	2.5	5	65	32.5	72.5	0	10	1.8 ± 0.9	<0.001	40
	clsp-1	7.0	7.0	95.3	93.0	88.4	16.3	27.9	3.1 ± 0.8	0.068	43
	cpz-1	5.0	5.0	97.5	90.0	75.0	5.0	15.0	2.8 ± 0.9	<0.001	40
	his-7	7.9	0.0	89.5	73.7	84.2	10.5	18.4	2.7 ± 0.9	<0.001	38
	rnr-1	0.0	9.1	54.5	38.6	56.8	9.1	9.1	1.7 ± 1.4	<0.001	44
	rpn-7	2.4	7.1	92.9	85.7	83.3	16.7	23.8	2.9 ± 0.9	0.008	42
	spp-1	0	12.5	100	100	97.5	7.5	15	3.2 ± 0.6	0.096	40
bar-1(ga80)	*Control*	0.0	0.0	78.6	95.2	83.3	0.0	NA	2.5 ± 0.8	—	42
	ard-1	0.0	0.0	59.1	70.5	63.6	0.0	NA	1.9 ± 1.0	0.002	44
	cdk-1	0.0	0.0	40.0	32.5	50.0	0.0	NA	1.2 ± 1.1	<0.001	40
	clsp-1	0.0	0.0	70.5	86.4	75.0	0.0	NA	2.3 ± 0.9	0.181	44
	cpz-1	0.0	0.0	58.3	52.8	63.9	0.0	NA	1.7 ± 1.1	<0.001	36
	his-7	0.0	0.0	66.7	61.1	77.8	0.0	NA	2.0 ± 0.9	0.008	36
	rnr-1	0.0	0.0	0.0	0.0	0.0	0.0	NA	0	<0.001	36
	rpn-7	0.0	0.0	68.4	94.7	91.7	0.0	NA	2.5 ± 0.8	0.690	38
	spp-1	0.0	0.0	51.9	55.6	55.6	0.0	NA	1.6 ± 1.2	<0.001	27

Muv phenotype is indicated by % overinduced. N refers to the total number of animals examined from all batches combined. NA, not applicable.

of the suppressor genes act genetically downstream of *pry-1* to regulate vulval development. In addition, it is possible that *cdk-1* and *rnr-1* act in a pathway parallel to *pry-1*.

Genetic interactions between suppressor genes and *bar-1/β-catenin*

Since PRY-1 is a component of the canonical WNT signaling, we investigated whether any of the suppressor genes function as downstream effectors of the pathway during vulval development. To this end, we used the β-catenin homolog BAR-1, which is negatively regulated by PRY-1 (Eisenmann *et al.* 1998; Gleason *et al.* 2002). Mutations in *bar-1* cause some of the VPCs to remain uninduced. In a *bar-1* null mutant, *bar-1(ga80)*, P3.p and P4.p usually adopt an F (fused) fate. The frequency of the F fate is much lower for the remaining VPCs (12–36% in each case), as they are mostly induced to form the vulva (Eisenmann *et al.* 1998; Eisenmann and Kim 2000). The VPC induction analysis following the RNAi knockdown experiments revealed that for six of the candidate genes—*spp-1*, *ard-1*, *cpz-1*, *his-7*, *cdk-1*, and *rnr-1*—the VPC induction defect of *bar-1(ga80)* was significantly enhanced. *cdk-1* and *rnr-1* RNAi had the most severe effects, and the induction was reduced by 52% and 100%, respectively. In contrast, *clsp-1* and *rpn-7* did not affect VPC induction (Figure 4E and Table 2). We also performed qPCR to examine the levels of suppressor genes in *bar-1(ga80)* animals, which showed that whereas four exhibited increased expression during the L3 stage (*cpz-1*, *his-7*, *cdk-1*, and *rnr-1*), one was reduced (*rnr-7*), and the remaining three were unchanged (*spp-1*, *clsp-1*, and *ard-1*) (Figure 3C). These results, together with interaction experiments involving *pry-1*, are most consistent with the possibility of *rpn-7* acting genetically downstream of the *pry-1-bar-1* pathway to regulate VPC induction. The remaining genes might mediate *pry-1* function in a *bar-1*-independent manner.

Suppressor genes influence *pry-1*-mediated nonvulval processes

PRY-1 plays crucial roles in multiple developmental and post-developmental processes; therefore, we examined the involvement of Muv suppressors in all or subsets of PRY-1 nonvulval functions. The phenotypes examined included an increased seam cell number, molting defect, low brood size, developmental delay, stress sensitivity, increased expression of chaperones (*hsp-4/BiP/GRP78*, *hsp-6/HSP70*, and *hsp-60/HSP60*), and short lifespan (Ranawade *et al.* 2018; Mallick *et al.* 2019a, 2020). The partial or complete loss of function of many of the suppressor genes is known to cause defects similar to that of *pry-1* mutants. These include *ard-1* RNAi leading to sterile progeny and developmental delay (Simmer *et al.* 2003; Sönnichsen *et al.* 2005), *rpn-7* and *cpz-1* RNAi animals showing molting defects (Hashmi *et al.* 2004; Frand *et al.* 2005), *clsp-1* RNAi leading to reduced germ line cell proliferation and increased expression of mitochondrial chaperones (Yoneda *et al.* 2004; Ceron *et al.* 2007), and *his-7* RNAi causing slow growth, larval arrest, and extended dauer survivability of *aak-2* mutants (Lehner *et al.* 2006; Ceron *et al.* 2007; Xie and Roy 2012).

To test whether the suppressor genes participate in *pry-1*-mediated developmental processes outside the vulva system, we first examined the seam cells. During seam cell development, *pry-1* promotes asymmetric cell division, and *pry-1* mutants show increased cell numbers. RNAi of the eight genes did not result in a change in the seam cells in both *pry-1* mutant and wild-type animals (Supplementary Figure S1), suggesting that none of these genes play a role in *pry-1*-mediated signaling in generating seam cells.

Next, we investigated whether suppressor genes interact with *pry-1* to regulate aging. Recent work from our group demonstrated the essential role of *pry-1* in mediating lifespan

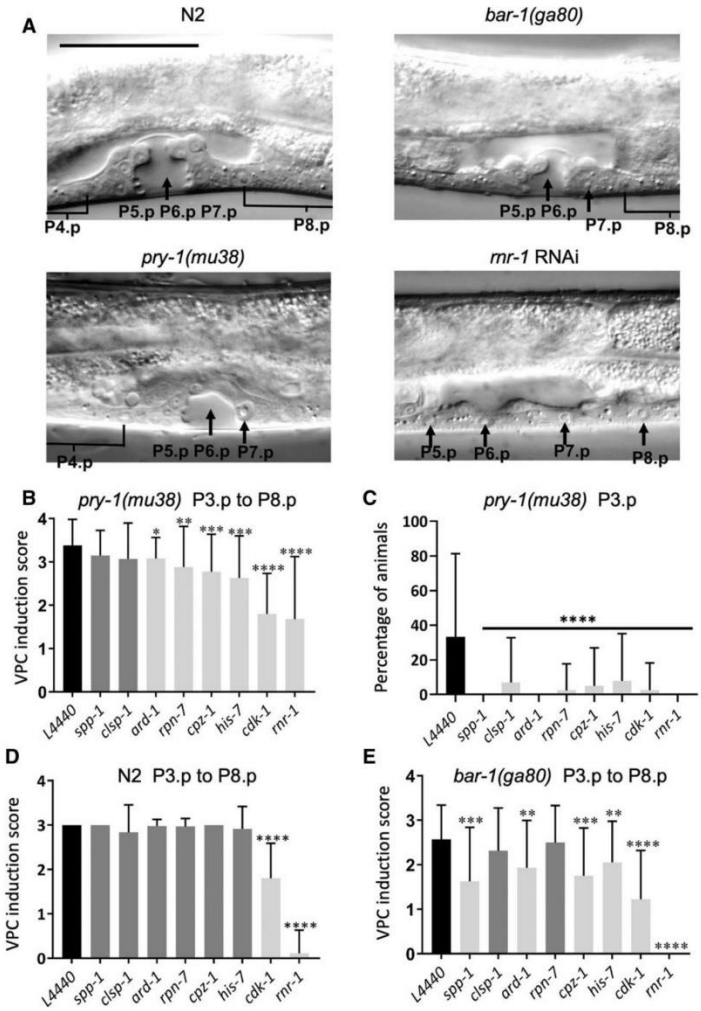

Figure 4 VPC induction analysis following RNAi knockdown of suppressor genes. (A) Representative images of N2, *pry-1(mu38)*, *bar-1(ga80)*, and *rnr-1(RNAi)* animals at the mid-L4 stage. Arrows in N2, *pry-1(mu38)*, and *bar-1(ga80)* animals point to invaginations formed by the progeny of three VPCs (P5.p, P6.p, and P7.p) and to uninduced VPCs in *rnr-1(RNAi)* animal. Not all VPCs and their progeny are shown. Parts of P4.p and P8.p daughter nuclei, where visible, are indicated by half U-shaped lines. Scale bar is 50 μm. (B–E) Panels B, D, and E show average VPC induction (P3.p to P8.p) whereas panel C shows percentage of animals with induced P3.p. Black bars represent control RNAi (L4440), and gray and white represent data that are statistically insignificant and significant, respectively. (B) Knockdown of *ard-1*, *rpn-7*, *cpz-1*, *his-7*, *cdk-1*, and *rnr-1* significantly reduced average VPC induction in *pry-1(mu38)* animals. (C) Same as B, except that the percentage of animals with induced P3.p is plotted. (D) Knockdown of *cdk-1* and *rnr-1* significantly reduced average VPC induction in N2 animals. (E) Knockdown of *spp-1*, *ard-1*, *cpz-1*, *his-7*, *cdk-1*, and *rnr-1* significantly reduced average VPC induction in *bar-1(ga80)* animals. In all cases, data shown in panels B–E represent a cumulative of two replicates ($n > 30$ animals in total for each condition, also see Table 2) and error bars represent the standard deviation. Statistical analyses were done using one-way ANOVA with Dunnett's *post hoc* test and significant differences are indicated by stars (*): * ($p < 0.05$), ** ($p < 0.01$), *** ($p < 0.001$), **** ($p < 0.0001$). Multiple comparison tests were also performed for data in panels B, C, and D using one-way ANOVA for genes that also showed effect in N2 and the results are listed as follows: *cdk-1* RNAi *vs. pry-1(mu38)*; *cdk-1* RNAi ($p > 0.998$), *cdk-1* RNAi *vs. bar-1(ga80)*; *cdk-1* RNAi ($p = 0.061$), *pry-1(mu38)*; *cdk-1* RNAi *vs bar-1(ga80)*; *cdk-1* RNAi ($p = 0.061$), *rnr-1* RNAi *vs pry-1(mu38)*; *rnr-1* RNAi ($p < 0.0001$)****, *rnr-1* RNAi *vs bar-1(ga80)*; *rnr-1* RNAi ($p = 0.999$), *pry-1(mu38)*; *rnr-1* RNAi *vs bar-1(ga80)*; *rnr-1* RNAi ($p < 0.0001$)****.

maintenance in animals (Mallick *et al.* 2020). RNAi of the suppressor genes in *pry-1(mu38)* mutants from the L4 stage revealed that *cpz-1*, *his-7*, *cdk-1*, and *rnr-1* caused a significant extension of the mean lifespan (Figure 5, A–D and Table 3, Supplementary Figure S2). Interestingly, two of these, *cdk-1* and *rnr-1*, also extended the lifespan in wild-type animals, demonstrating their essential function. However, in both cases, increases in the mean lifespan in a *pry-1* mutant background (203% and 170% for *cdk-1* RNAi and

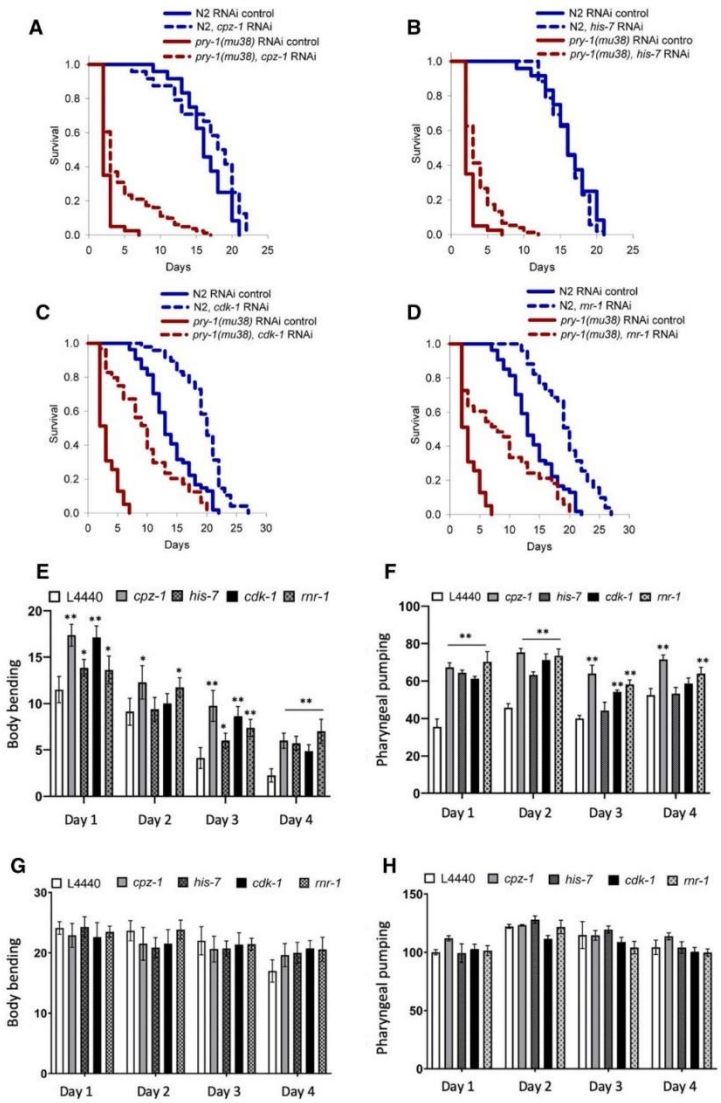

Figure 5 Knockdown of suppressor genes rescue lifespan, body bending and pharyngeal pumping defect of *pry-1* mutants. (A–D) RNAi knockdown of *cpz-1*, *his-7*, *cdk-1*, and *rnr-1* in N2 and *pry-1* mutants (also see Supplementary Figure S2). (A–D) See *Materials and Methods* section and Table 3 for lifespan data and statistical analyses. (E, F) Bar graphs showing the rates of body bending and pharyngeal pumping of *pry-1* mutants over a period of 4 days following RNAi of *cpz-1*, *his-7*, *cdk-1*, *and rnr-1*. (G, H) Bar graphs showing the rates of body bending and pharyngeal pumping of N2 animals. (E–H) Data represent the mean of two replicates (n > 10 animals per replicate) and error bars represent the standard deviation. Statistical analyses for panels E–H were done using one-way ANOVA with Dunnett's *post hoc* test for each day and significant differences are indicated by stars (*): * ($p < 0.05$), ** ($p < 0.01$).

rnr-1 RNAi, respectively) were much higher compared to those observed in wild-type (19.5% and 18.8% for *cdk-1* RNAi and *rnr-1* RNAi, respectively) (Figure 5, C and D; Table 2). The effects of all four genes on body bending and pharyngeal pumping were also examined. We observed that knockdown resulted in significant improvements in both physiological markers of aging in *pry-1* mutants but not in wild-type animals (Figure 5, A–D). Overall, these results allow us to suggest that *cpz-1*, *his-7*, *cdk-1* and *rnr-1* act downstream of *pry-1* in restricting the lifespan of animals.

In addition to its role in aging, *pry-1* is necessary for maintaining the expression of stress response signaling genes (Mallick *et al.* 2020). This led us to examine whether the knockdown of suppressors would decrease the lethality of *pry-1* mutants caused by acute exposure to the nonspecific oxidative stress inducer PQ.

Table 3 Mean, median, and maximum lifespan of N2 and *pry-1(mu38)* animals following control (empty vector L4440) and gene specific RNAi

Genotype	Treatment	Mean lifespan (day)	Median lifespan (day)	Maximum lifespan (day)	N	*p*-value
N2	L4440	16.37 ± 0.64	16	21	51	—
pry-1(mu38)	L4440	3.25 ± 0.26	3	7	79	—
	spp-1 RNAi	2.54 ± 0.19	2	8	80	ns
	clsp-1 RNAi	4.32 ± 0.31	4	9	80	ns
	ard-1 RNAi	3.54 ± 0.45	2	13	79	ns
	rpn-7 RNAi	4.07 ± 0.25	4	10	79	ns
	cpz-1 RNAi	4.67 ± 0.43	3	17	81	<0.001
	his-7 RNAi	4.62 ± 0.26	3	12	75	<0.001
	cdk-1 RNAi	9.86 ± 0.68	10	20	64	<0.001
	rnr-1 RNAi	8.79 ± 1.12	8	20	76	<0.001
N2	*cpz-1* RNAi	16.92 ± 0.97	18	22	45	ns
pry-1(mu38)		4.67 ± 0.43	3	17	81	<0.001
N2	*his-7* RNAi	16.09 ± 0.35	16	21	51	ns
pry-1(mu38)		4.62 ± 0.26	3	12	75	<0.001
N2	*cdk-1* RNAi	19.56 ± 0.54	20	27	48	<0.001
pry-1(mu38)		9.86 ± 0.68	10	20	64	<0.001
N2	*rnr-1* RNAi	19.45 ± 0.60	20	27	51	<0.001
pry-1(mu38)		8.79 ± 1.12	8	20	76	<0.001

In each case, lifespan data are presented as the cumulative of two replicates (see *Materials and Methods* section). N, number of animals examined; ns, not significant.

Except for *clsp-1* and *rpn-7*, RNAi targeting the suppressor genes reduced the stress sensitivity in *pry-1* mutants (Figure 6A). Interestingly, *ard-1* and *cpz-1* RNAi conferred PQ resistance in wild-type animals as well (Supplementary Figure S3), suggesting crucial roles for both of these genes in maintaining PQ sensitivity in animals. These data suggest that *pry-1* inhibits *spp-1*, *his-7*, *cdk-1*, and *rnr-1* to regulate oxidative stress responses in animals. More work is needed to determine whether *ard-1* and *cpz-1* also interact with *pry-1* or act in a parallel pathway.

We investigated whether downregulating the expression of six PQ-responsive genes in *pry-1* mutants could lower cellular stress (Supplementary Figure S4, A and B). This was done using a set of stress response reporters. *pry-1* mutants exhibit increased expression of *hsp-4::GFP* (endoplasmic reticulum unfolded protein response chaperone) and *hsp-60::GFP* (mitochondrial unfolded protein response chaperone) (Supplementary Figure S4B) (Mallick *et al.* 2020). Another stress response reporter that is sensitive to oxidative stress, *sod-3::GFP* (sodium dismutase), was also analyzed. Although *pry-1* mutants do not affect *sod-3::GFP* fluorescence, muscle-specific overexpression of *pry-1* causes an increase in *sod-3* levels (Mallick *et al.* 2020). RNAi targeting all but *spp-1* caused a significant reduction in GFP fluorescence in *hsp-4::GFP* animals (Figure 6B). A similar knockdown in the *sod-3::GFP* strain revealed that the fluorescence was strongly suppressed in the case of *spp-1*, *cpz-1*, *cdk-1*, and *rnr-1* (Figure 6D). There was no significant change in *hsp-60::GFP* expression levels (Figure 6C). Overall, these results show that while there are differences in individual chaperon responses, all six suppressors are involved in *pry-1*-mediated processes and function to maintain the expression of multiple stress-responsive genes.

Discussion

In this study, we analyzed a set of genes that are upregulated in *pry-1* mutants and associated with "reproductive structure development." The genes belong to GO categories that include metabolic processes, transcriptional regulation, and mitotic cell cycle. Among the 26 genes tested, RNAi for eight (*spp-1*, *clsp-1*, *ard-1*, *rpn-7*, *cpz-1*, *his-7*, *cdk-1*, and *rnr-1*) suppressed the Muv phenotype of *pry-1* mutant animals with a threshold of the mean ± 2 standard deviations (95% confidence interval). The ectopic P3.p induction defect was also suppressed in all cases. Further gene expression studies and genetic interactions with a null allele of *bar-1* revealed that whereas all of the suppressors function downstream of *pry-1* to regulate vulva formation, only *rpn-7* is involved in *pry-1-bar-1* signaling. In addition, we found that *cdk-1* and *rnr-1* have essential roles because their downregulation caused defects in VPC induction in wild-type animals.

All eight suppressor genes regulate fundamental cellular processes, such as protein phosphorylation (*cdk-1*) and kinase activation (*clsp-1*), protein breakdown (*rpn-7* and *cpz-1*), DNA replication (*rnr-1*), transcription (*his-7*), mitochondrial oxidation and reduction (*ard-1*), and channel activity (*spp-1*) (Table 1). This is also supported by data showing that *clsp-1*, *his-7*, and *cdk-1* transcripts are enriched in germ line cells (Han *et al.* 2017), and *spp-1*, *ard-1*, *cpz-1*, and *rnr-1* are expressed in the neurons, hypodermis, vulva, gonad, intestine, and muscles (Hashmi *et al.* 2004; Alper *et al.* 2007; Hunt-Newbury *et al.* 2007; Srinivasan *et al.* 2008; Keith *et al.* 2016). Therefore, it is not surprising that perturbations in their function result in multiple phenotypes.

Whereas our work provides the first evidence for the genetic interactions between *pry-1* and these eight genes (see schematic in Figure 7), some of the genes were previously reported to play roles in vulva formation. Specifically, the disruption of *clsp-1* and *ard-1* causes a Pvl phenotype (Simmer *et al.* 2003; Ceron *et al.* 2007). *cpz-1* localizes to the developing vulva, and *cpz-1* RNAi results in defective vulval morphology (Hashmi *et al.* 2004). *cdk-1* regulates *lin-12/Notch* in a cell cycle-dependent manner (Nusser-Stein *et al.* 2012; Weinstein *et al.* 2015). The remaining four genes, *spp-1*, *rpn-7*, *his-7*, and *rnr-1* had no reported function in the vulva system.

In addition to studying vulval development, we investigated the role of the suppressor genes in *pry-1*-mediated post-developmental events. *spp-1*, *rpn-7*, *cdk-1*, and *rnr-1* are known to be involved in aging. Specifically, *rpn-7* and *cdk-1* are both required for *glp-1*-mediated lifespan extension (Ghazi *et al.* 2007; Seidel and Kimble 2015), and *spp-1* and *rpn-7* are required for the longevity of *daf-2* mutants (Murphy *et al.* 2003; Ghazi *et al.* 2007;

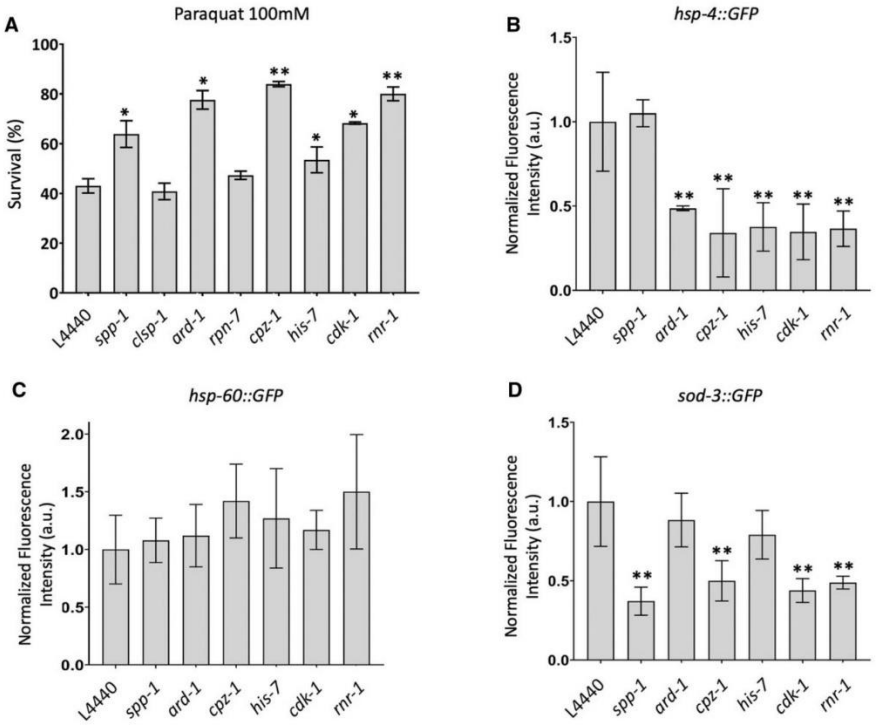

Figure 6 *cpz-1*, *his-7*, *cdk-1*, and *rnr-1* regulate stress sensitivity in *pry-1* mutants. (A) Survivability of *pry-1(mu38)* animals following RNAi knockdown of suppressor genes. The animals were treated with 100 mM PQ solution for 1 h. Data represent mean of two replicates (n > 30 animals). (B) Quantification of fluorescence intensity using *hsp-4::GFP* marker in *pry-1* mutants following RNAi knockdown of *spp-1*, *ard-1*, *cpz-1*, *his-7*, *cdk-1*, and *rnr-1*. (C) Same as (B), except that fluorescence reporter is *hsp-60::GFP* (D) Same as B, except that fluorescence reporter is *sod-3::GFP*. Data represent the mean of two replicates (n > 15 animals per replicate). Error bars represent the standard deviation. Statistical analyses were done using one-way ANOVA with Dunnett's post hoc test for each day and significant differences are indicated by stars (*): * ($p < 0.05$), ** ($p < 0.01$).

Anyanful *et al.* 2009). *rnr-1* is downregulated in long-lived *daf-2* and *eat-2* mutants, consistent with the notion that high levels of *rnr-1* decrease the lifespan (Gao *et al.* 2018). These genes have potential roles in the conserved aging pathway; therefore, we analyzed their requirement in *pry-1* signaling. Our results showed that *cpz-1*, *his-7*, *cdk-1*, and *rnr-1* act downstream of *pry-1* to affect the lifespan of animals. These four genes, along with *spp-1* and *ard-1*, also play roles in *pry-1*-mediated stress response maintenance, as observed in the acute PQ assay and heat shock chaperone analysis. Thus, whereas *pry-1* negatively regulates many genes, it appears to utilize overlapping subsets in different events (Figure 7). We also found that similar to vulval development *cdk-1* and *rnr-1* extend the lifespan of wild-type animals, suggesting their essential roles in multiple tissues. Both genes may also act in a *pry-1*-independent manner. The involvement of *spp-1* and *ard-1* in the stress response but not aging is consistent with the results of other studies describing genes that have unique roles in these two processes (Chen *et al.* 2009; Bennett *et al.* 2014; Richman *et al.* 2018).

Another mechanism by which some of the suppressor genes may mediate *pry-1* signaling is by regulating proteostasis. Whereas the loss of proteostasis contributes to aging and age-associated abnormalities, its enhancement promotes lifespan extension and results in suppression of age-related diseases (Labbadia and Morimoto 2014; Uno and Nishida 2016). Consistent with *pry-1*'s role in proteostasis, we have found that the gene is necessary for the maintenance of stress response. In addition, preliminary work in our lab has revealed that *pry-1* mutants have defects in protein folding and protein degradation.

Our data also suggest that the roles of *spp-1* in *pry-1* and *daf-2* signaling pathways are different, although the extent to which these differences are reflected in its molecular function is unknown. Considering that *spp-1* encodes a channel protein, it is possible that blocking its activity inhibits unwanted signaling in *daf-2* and *pry-1* mutant adults leading to improved responses. However, animals lacking *spp-1* function are expected to be more sensitive to infections as this gene is involved in maintaining the innate immune response (Anyanful *et al.* 2009). Future experiments are needed to make any firm conclusions regarding the mechanism through which *spp-1* functions in the stress response and lifespan maintenance.

In conclusion, this study identified a new set of interactors of *pry-1* in *C. elegans* that are involved in a range of cellular events, such as protein homeostasis, signaling, gene expression, and cell proliferation, by regulating the activities and stability of proteins and changes in DNA, such as replication, the

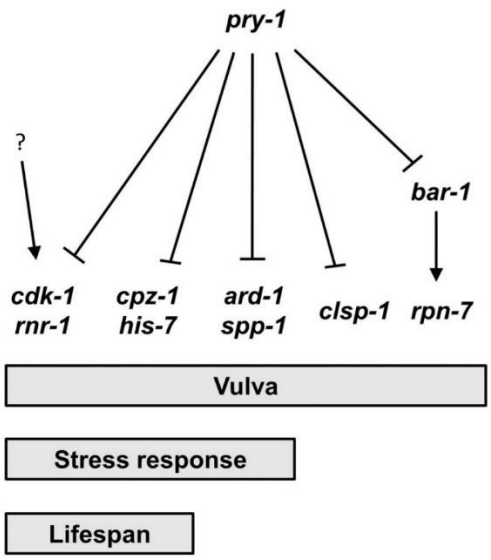

Figure 7 A schematic diagram showing biological processes mediated by *pry*-1 and eight suppressor genes. The genetic relationship is based on the expression and functional data described in this study. While all genes are involved in *pry*-1-mediated vulval development, only six affect stress response and four lifespan. Question mark (?) indicates that *cdk*-1 and *rnr*-1 may also be regulated in a *pry*-1-independent manner.

damage checkpoint, and repair. Some of the suppressors affect multiple *pry*-1-mediated processes, whereas the others appear to have more restricted roles. All of the genes have mammalian homologs or family members, raising the possibility that their interactions with Axin might be conserved. Future studies hold promise to elucidate the mechanism by which these genes mediate tissue-specific functions of Axin in normal and disease conditions.

Data availability

Strains are available upon request. The authors affirm that all data necessary for confirming the conclusions of the article are present within the article, figures, and tables.

Supplementary material is available at G3 online.

Acknowledgments

The authors thank Sakshi Mehta for assistance with certain experiments and Gupta lab members for discussions and suggestions. Some of the strains were obtained from CGC, which is funded by the NIH Office of Research Infrastructure Programs (P40OD010440).

Funding

This work was supported by funds from the Natural Sciences and Engineering Research Council of Canada (NSERC) discovery grant to BPG and NSERC Canada Graduate Doctoral scholarship to AM.

Conflicts of interest

The authors declare that there is no conflict of interest.

Literature cited

Alper S, McBride SJ, Lackford B, Freedman JH, Schwartz DA. 2007. Specificity and complexity of the *Caenorhabditis elegans* innate immune response. Mol Cell Biol. 27:5544–5553.

Amrit FRG, Ratnappan R, Keith SA, Ghazi A. 2014. The *C. elegans* lifespan assay toolkit. Methods. 68:465–475.

Angeles-Albores D, Raymond RY, Chan J, Sternberg PW. 2016. Tissue enrichment analysis for *C. elegans* genomics. BMC Bioinformatics. 17:1–10.

Anyanful A, Easley KA, Benian GM, Kalman D. 2009. Conditioning protects *C. elegans* from lethal effects of enteropathogenic *E. coli* by activating genes that regulate lifespan and innate immunity. Cell Host Microbe. 5:450–462.

Bennett CF, Vander Wende H, Simko M, Klum S, Barfield S, *et al.* 2014. Activation of the mitochondrial unfolded protein response does not predict longevity in *Caenorhabditis elegans*. Nat Commun. 5: 1–10.

Boxem M. 2006. Cyclin-dependent kinases in *C. elegans*. Cell Div. 1: 6–12.

Brenner S. 1974. The genetics of *Caenorhabditis elegans*. Genetics. 77: 71–94.

Ceron J, Rual JF, Chandra A, Dupuy D, Vidal M, *et al.* 2007. Large-scale RNAi screens identify novel genes that interact with the *C. elegans* retinoblastoma pathway as well as splicing-related components with synMuv B activity. BMC Dev Biol. 7:1–16.

Chen D, Thomas EL, Kapahi P. 2009. HIF-1 modulates dietary restriction-mediated lifespan extension via IRE-1 in *Caenorhabditis elegans*. PLoS Genet. 5:e1000486.

Collins JJ, Huang C, Hughes S, Kornfeld K. 2008. The Measurement and Analysis of Age-Related Changes in *Caenorhabditis elegans*. WormBook. doi: 10.1895/wormbook.1.137.1. p. 1–21.

Davy A, Bello P, Thierry-Mieg N, Vaglio P, Hitti J, *et al.* 2001. A protein-protein interaction map of the *Caenorhabditis elegans* 26S proteasome. EMBO Rep. 2:821–828.

Eisenmann DM, Kim SK. 2000. Protruding vulva mutants identify novel loci and WNT signalling factors that function during *Caenorhabditis elegans* vulva development. Genetics. 156: 1097–1116.

Eisenmann DM, Maloof JN, Simske JS, Kenyon C, Kim SK. 1998. The β-catenin homolog BAR-1 and LET-60 Ras coordinately regulate the Hox gene lin-39 during *Caenorhabditis elegans* vulval development. Development. 125:3667–3680.

Frand AR, Russel S, Ruvkun G. 2005. Functional genomic analysis of *C. elegans* molting. PLoS Biol. 3:e312.

Gao AW, Smith RL, van Weeghel M, Kamble R, Janssens GE, *et al.* 2018. Identification of key pathways and metabolic fingerprints of longevity in *C. elegans*. Exp Gerontol. 113:128–140.

Ghazi A, Henis-Korenblit S, Kenyon C. 2007. Regulation of *Caenorhabditis elegans* lifespan by a proteasomal E3 ligase complex. Proc Natl Acad Sci USA. 104:5947–5952.

Gleason JE, Korswagen HC, Eisenmann DM. 2002. Activation of WNT signaling bypasses the requirement for RTK/Ras signaling during *C. elegans* vulval induction. Genes Dev. 16:1281–1290.

Han S, Schroeder EA, Silva-García CG, Hebestreit K, Mair WB, *et al.* 2017. Mono-unsaturated fatty acids link H3K4me3 modifiers to *C. elegans* lifespan. Nature. 544:185–190.

Hashmi S, Zhang J, Oksov Y, Lustigman S. 2004. The *Caenorhabditis elegans* Cathepsin Z-like Cysteine Protease, Ce-CPZ-1, has a

multifunctional role during the worms' development. J Biol Chem. 279:6035–6045.

Hunt-Newbury R, Viveiros R, Johnsen R, Mah A, Anastas D, *et al.* 2007. High-throughput *in* vivo analysis of gene expression in *Caenorhabditis elegans*. PLoS Biol. 5:e237.

Kamath RS, Fraser AG, Dong Y, Poulin G, Durbin R, *et al.* 2003. Systematic functional analysis of the *Caenorhabditis elegans* genome using RNAi. Nature. 421:231–237.

Keith SA, Maddux SK, Zhong Y, Chinchankar MN, Ferguson AA, *et al.* 2016. Graded proteasome dysfunction in *Caenorhabditis elegans* activates an adaptive response involving the conserved SKN-1 and ELT-2 transcription factors and the autophagy-lysosome pathway. PLoS Genet. 12:e1005823.

Korswagen HC, Coudreuse DYM, Betist MC, Van De Water S, Zivkovic D, *et al.* 2002. The Axin-like protein PRY-1 is a negative regulator of a canonical WNT pathway in *C. elegans*. Genes Dev. 16:1291–1302.

Labbadia J, Morimoto RI. 2014. Proteostasis and longevity: when does aging really begin? F1000Prime Rep. 6:7.

Lehner B, Calixto A, Crombie C, Tischler J, Fortunato A, *et al.* 2006. Loss of LIN-35, the *Caenorhabditis elegans* ortholog of the tumor suppressor p105Rb, results in enhanced RNA interference. Genome Biol. 7:R4.

Li J, Ebata A, Dong Y, Rizki G, Iwata T, *et al.* 2008. *Caenorhabditis elegans* HCF-1 functions in longevity maintenance as a DAF-16 regulator. PLoS Biol. 6:e233.

Mallick A, Gupta BP. 2020. Vitellogenin-2 acts downstream of PRY-1/Axin to regulate lipids and lifespan in *C. elegans*. MicroPubl Biol. 1:19–21.

Mallick A, Ranawade A, van den Berg W, Gupta BP. 2020. Axin-mediated regulation of lifespan and muscle health in *C. elegans* requires AMPK-FOXO signaling. iScience. 23:101843.

Mallick A, Ranawade A, Gupta BP. 2019a. Role of PRY-1/Axin in heterochronic miRNA-mediated seam cell development. BMC Dev Biol. 19:1–12.

Mallick A, Taylor SKB, Ranawade A, Gupta BP. 2019b. Axin family of scaffolding proteins in development: lessons from *C. elegans*. J Dev Biol. 7:20–23.

Maloof JN, Whangbo J, Harris JM, Jongeward GD, Kenyon C. 1999. A WNT signaling pathway controls Hox gene expression and neuroblast migration in *C. elegans*. Development. 126:37–49.

Mori C, Takanami T, Higashitani A. 2008. Maintenance of mitochondrial DNA by the *Caenorhabditis elegans* ATR checkpoint protein ATL-1. Genetics. 180:681–686.

Murphy CT, McCarroll SA, Bargmann CI, Fraser A, Kamath RS, *et al.* 2003. Genes that act downstream of DAF-16 to influence *C. elegans* lifespan. Nature. 424:277–283.

Nusser-Stein S, Beyer A, Rimann I, Adamczyk M, Piterman N, *et al.* 2012. Cell-cycle regulation of NOTCH signaling during *C. elegans* vulval development. Mol Syst Biol. 8:1–14.

Ossareh-Nazari B, Katsiarimpa A, Merlet J, Pintard L. 2016. RNAi-Based suppressor screens reveal genetic interactions between the CRL2LRR-1 E3-ligase and the DNA replication machinery in *Caenorhabditis elegans*. G3 (Bethesda). 6:3431–3442.

Ranawade A, Mallick A, Gupta BP. 2018. PRY-1/Axin signaling regulates lipid metabolism in *Caenorhabditis elegans*. PLoS One. 13: e0206540.

Richman C, Rashid S, Prashar S, Mishra R, Selvaganapathy PR, *et al.* 2018. *C. elegans* MANF homolog is necessary for the protection of dopaminergic neurons and ER unfolded protein response. Front Neurosci. 12:544.

Seetharaman A, Cumbo P, Bojanala N, Gupta BP. 2010. Conserved mechanism of WNT signaling function in the specification of vulval precursor fates in *C. elegans* and *C. briggsae*. Dev Biol. 346: 128–139.

Seidel HS, Kimble J. 2015. Cell-cycle quiescence maintains *Caenorhabditis elegans* germline stem cells independent of GLP-1/Notch. eLife. 4:1–28.

Simmer F, Moorman C, Van Der Linden AM, Kuijk E, Van Den Berghe PVE, *et al.* 2003. Genome-wide RNAi of *C. elegans* using the hypersensitive rrf-3 strain reveals novel gene functions. PLoS Biol. 1: e12.

Sönnichsen B, Koski LB, Walsh A, Marschall P, Neumann B, *et al.* 2005. Full-genome RNAi profiling of early embryogenesis in *Caenorhabditis elegans*. Nature. 434:462–469.

Srinivasan S, Sadegh L, Elle IC, Christensen AGL, Faergeman NJ, *et al.* 2008. Serotonin regulates *C. elegans* fat and feeding through independent molecular mechanisms. Cell Metab. 7:533–544.

Sternberg PW. 2005. Vulval Development. WormBook. doi: 10.1895/wormbook.1.6.1. p. 1–28.

Sternberg PW, Horvitz HR. 1989. The combined action of two intercellular signaling pathways specifies three cell fates during vulval induction in *C. elegans*. Cell. 58:679–693.

Sulston JE, Horvitz HR. 1977. Post-embryonic cell lineages of the nematode, *Caenorhabditis elegans*. Dev Biol. 56:110–156.

Uno M, Nishida E. 2016. Lifespan-regulating genes in *Celegans*. NPJ Aging Mech Dis. 2:16010.

Weinstein N, Ortiz-Gutiérrez E, Muñoz S, Rosenblueth DA, Álvarez-Buylla ER, *et al.* 2015. A model of the regulatory network involved in the control of the cell cycle and cell differentiation in the *Caenorhabditis elegans* vulva. BMC Bioinformatics. 16:1–21.

Xie M, Roy R. 2012. Increased levels of hydrogen peroxide induce a HIF-1-dependent modification of lipid metabolism in AMPK compromised *C. elegans* dauer larvae. Cell Metab. 16:322–335.

Yoneda T, Benedetti C, Urano F, Clark SG, Harding HP, *et al.* 2004. Compartment-specific perturbation of protein handling activates genes encoding mitochondrial chaperones. J Cell Sci. 117: 4055–4066.

Communicating editor: M. Zetka

6.2 Mallick *et* al. (2022)- Submitted in Scientific Reports

In this study we characterize a new gene named *picd-1* which is shown to interact with *pry-1* and regulate calcineurin signaling. Such an interaction of this protein in involved in regulating the lifespan and stress response of animals. Our lab and others have established *pry-1*'s essential role in developmental processes that affect the reproductive system, seam cells, and a posterior P lineage cell, P11.p. Additionally, *pry-1* is crucial for lipid metabolism, stress responses, and aging. In this study, we expanded on our previous work on *pry-1* by reporting a novel interacting gene named *picd-1* (***p**ry-1*-**i**nteracting and **C**abin1 **d**omain-containing). PICD-1 protein shares sequence conservation with Cabin1, a component of the HUCA complex. Our findings have revealed that PICD-1 is involved in several *pry-1*-mediated processes, including stress response and lifespan maintenance. *picd-1*'s expression overlapped with that of *pry-1* in multiple tissues throughout the lifespan. Furthermore, PRY-1 and PICD-1 inhibited CREB-regulated transcriptional coactivator homolog CRTC-1, which promotes longevity in a calcineurin-dependent manner. Overall, our study provides the first evidence of a Cabin1 domain-containing protein participating in Axin-mediated signaling.

Contributions: I performed experiments and provided data for Figures 1, 2, 3, 4A, 4C, 5, 6A-C, 7, 8F, 9A-B, 10A, 10C, 10E-G, S1, and S3; Tables 1, 2 and S1; and Videos S1 and S2. Shane Taylor performed experiments and provided data for Figures 8A-C, 9G-H, 10B and 10D. Sakshi Mehta performed experiments and provided data for Figures 4B, 6A-C, 8D-E, 9C-F and S2. I and Bhagwati Gupta created all the Figures and

illustrations. I and Bhagwati Gupta conceived and supervised the project. I, Shane Taylor and Bhagwati Gupta wrote the manuscript.

Cabin1 domain-containing gene *picd-1* interacts with *pry-1/Axin* to regulate multiple processes in *Caenorhabditis elegans*

Avijit Mallick, Shane K. B. Taylor, Sakshi Mehta, and Bhagwati P. Gupta

Department of Biology, McMaster University, 1280 Main Street West, Hamilton ON L8S 4K1, Canada.

Email:
Avijit Mallick mallia1@mcmaster.ca
Shane K. B. Taylor taylos49@mcmaster.ca
Sakshi Mehta mehtas11@mcmaster.ca
Bhagwati P Gupta guptab@mcmaster.ca

Author for correspondence: Bhagwati P Gupta, Telephone: 905-525-9140 x26451

Keywords: *C. elegans, picd-1, pry-1*, Axin, Cabin1, stress response, aging, lifespan, vulva development, gonad, *crtc-1*, calcineurin

ABSTRACT

The Axin family of scaffolding proteins control diverse processes, such as facilitating the interactions between cellular components and providing specificity to signaling pathways. Several proteins that belong to the Axin family have been discovered to date. However, despite its crucial role in metazoans, the mechanism of *pry-1* action is not well understood. The *Caenorhabditis elegans* Axin homolog *pry-1* is a powerful tool for identifying interacting genes and downstream effectors that function in a conserved manner to regulate Axin-mediated signaling. Our lab and others have established *pry-1*'s essential role in developmental processes that affect the reproductive system, seam cells, and a posterior P lineage cell, P11.p. Additionally, *pry-1* is crucial for lipid metabolism, stress responses, and aging. In this study, we expanded on our previous work on *pry-1* by reporting a novel interacting gene named *picd-1* (***p**ry-1*-**i**nteracting and **C**abin1 **d**omain-containing). PICD-1 protein shares sequence conservation with Cabin1, a component of the HUCA complex. Our findings have revealed that PICD-1 is involved in several *pry-1*-mediated processes, including stress response and lifespan maintenance. *picd-1*'s expression overlapped with that of *pry-1* in multiple tissues throughout the lifespan. Furthermore, PRY-1 and PICD-1 inhibited CREB-regulated transcriptional coactivator homolog CRTC-1, which promotes longevity in a calcineurin-dependent manner. Overall, our study provides the first evidence of a Cabin1 domain-containing protein participating in Axin-mediated signaling.

INTRODUCTION

Signaling pathways enable cells to communicate with each other and their environment. Because of their essential role in cells, these pathway components are tightly regulated via interaction with a host of cellular factors. The Axin family is a group of scaffolding proteins that bring together different proteins to facilitate their interactions and regulate their activity [1]. There are two Axin homologs in mammals: Axin1 and Axin2. Axin was initially discovered as a negative regulator of the WNT-mediated signaling cascade. However, subsequent studies revealed a much broader role of these proteins in other pathways, including JNK, AMPK, and TGFβ [1–3]. Axin regulates several processes, including organogenesis, anterior-posterior axis formation, neuronal development, and metabolic homeostasis. Further, loss of Axin function causes lethality, neuroectodermal defects, abnormal body axis patterning, and reduced adipogenesis [1]. However, the mechanism by which

Axin regulates different biological processes and mediates specific interactions is not well understood.

In the nematode *C. elegans*, the Axin homolog PRY-1 controls processes such as embryogenesis, neuronal differentiation, vulval development, P11.p cell fate, and seam cell development [1,4–6]. The WNT-dependent function of PRY-1 in vulval cells involves its interactions with several other proteins to form a destruction complex that results in the phosphorylation and degradation of BAR-1 (β-Catenin) [4]. However, little is known about the factors that interact with PRY-1 in WNT-independent processes. Our lab recently identified differentially expressed mRNA and miRNA genes in *pry-1* mutants, which uncovered novel interacting partners and genetic network of *pry-1* that regulate post-developmental events [5,7]. Specifically, PRY-1 is crucial for lipid metabolism, stress response, and lifespan maintenance, where it interacts with WNT-independent signaling pathway components [7–10]. These include SBP-1/SREBP and vitellogenin involved in fatty acid synthesis and lipid storage, AAK-2/AMPK in the muscle that non-autonomously activates DAF-16/FOXO in the intestine and delays aging [7–9], and the components of the endoplasmic reticulum unfolded protein response (ER-UPR) pathway. Additionally, we identified several other genes regulated by *pry-1* during stress response and lifespan maintenance in animals. These include *cpz-1* (proteolysis), *cdk-1* (cell cycle), *rnr-1* (DNA replication), *his-7* (gene expression), and *ard-1* (mitochondrial oxidation/reduction) [6].

A comprehensive understanding of *pry-1* function would require the identification of its interacting proteins and downstream effectors. We previously performed a transcriptome profiling of *pry-1* that revealed several differentially expressed genes involved in lipid regulation and aging [7]. In this study, we report a novel downstream effector of *pry-1* signaling called *picd-1* that is critical for regulating multiple developmental and post-developmental processes. PICD-1 shares a domain with the mammalian calcineurin-binding protein 1 (Cabin1), a component of the histone H3.3 chaperone complex HUCA[11]. Cabin1 negatively regulates calcineurin signaling, which in turn affects various cellular functions, including stress response and lifespan [12–15]. We show that PICD-1 negatively regulates CREB-regulated transcriptional coactivator (CRTC) homolog, CRTC-1, which promotes longevity mediated by calcineurin signaling [16]. Consistent with the *pry-1*'s role in promoting *picd-1* expression, *pry-1* mutants exhibit nuclear localization of CRTC-1, suggesting

that PICD-1 is involved in PRY-1-mediated CRTC-1 regulation. These results demonstrate the critical role of PICD-1 in *C. elegans* and prompt future studies to investigate the involvement of Cabin1 and calcineurin signaling in Axin-mediated processes in eukaryotes.

RESULTS

picd-1 encodes a Cabin1 domain-containing protein

During a CRISPR-based screening to isolate alleles of *pry-1*, we recovered a secondary mutation (*gk3701*) in *F56E10.1* (WBGene00018975), now named *picd-1* (***p**ry-1* **i**nteracting and **C**abin1 **d**omain-containing, see Methods). The *pry-1(gk3681); picd-1(gk3701)* double mutant exhibited a significant increase in the protruding-vulva (Pvl) phenotype (77%, compared to 66% in *pry-1* mutants alone) and pronounced protrusions that frequently burst in the vulva (**Table 1, Figure 1A and B, Video S1)**. Sequence analysis of *picd-1* identified orthologs in other nematode species (**Figure 1C**), all of which contain a domain similar to the histone transcription regulator 3 (Hir3)/calcineurin-binding protein (Cabin1) family members (IPR033053, https://www.ebi.ac.uk/interpro/) (**Figures 1C and 1D**). The alignments of *picd-1* with human Cabin1 (isoform a) showed 26% (729/2853) identity and 38% (1080/2853) similarity (EMBOSS stretcher pairwise alignment tool; https://www.ebi.ac.uk/Tools/psa/). Human Cabin1 is part of the histone H3.3 chaperone complex HUCA (HIRA/UBN1/Cabin1/ASF1a), involved in nucleosome assembly. Similarly, Gene Ontology (GO) analysis (www.wormbase.org) revealed that *picd-1* is associated with the biological process "DNA replication-independent nucleosome assembly" (GO:0006336) and the cellular component "nucleus" (GO:0005634). Thus, *picd-1* is likely to encode a nuclear protein that functions in chromatin assembly and regulation of gene expression. Furthermore, *in silico* analysis revealed that PICD-1 contains 49 amino acid residues predicted to bind DNA (http://biomine.cs.vcu.edu/servers/DRNApred/#References [17]) (**Table S1**).

picd-1 is expressed in multiple tissues

To gain further insights into the function of *picd-1*, we created transgenic animals carrying the *picd-1::GFP* transcriptional reporter. The analysis of transgenic animals revealed GFP fluorescence during the development of tissues and organs, such as the pharynx, intestine, body

wall muscles, hypodermis (seam cells), gonads, and vulva **(Figure 2)**. This expression pattern resembled that of *pry-1*, which was recently described by our group [8]. As *picd-1::GFP* animals entered adulthood, fluorescence was localized to the intestine and certain head neurons **(Figure 2)**, which persisted throughout the life of the animals (data not shown). A broad range of *picd-1* expression was also supported by previously published RNA-sequencing and microarray studies [18,19]. Overall, our expression analysis suggests that *picd-1* functions in multiple tissues and may play a role in *pry-1*-mediated developmental and post -developmental processes.

Mutations in *picd-1* do not affect vulval induction but cause morphogenetic defects

In addition to using the *gk3701* strain to examine mutant phenotypes, we generated a new allele, *bh40*, which has multiple in-frame stop codons in exon 1 (**see Methods and Figures 3A and 3B**). qPCR analysis showed that *bh40* and *gk3701* greatly reduced *picd-1* transcript levels (**Figure 3C**). Interestingly, while the Pvl phenotype of *pry-1(mu38)* was enhanced by both the alleles (**Figures 1A and B**), neither had an obvious impact on the penetrance of the multivulva (Muv) phenotype in *pry-1(mu38)* animals. In fact, the double mutants showed a slightly less Muv phenotype compared to *pry-1(mu38)* alone (**Table 1, Figure 1B**), which may be due to changes in morphogenetic processes as vulval precursor induction is not affected by any of the *picd-1* mutations (**Figure 3D, Table 1**). Similar phenotypes were observed following *picd-1* RNAi (**Figure S1**). In agreement with this, *picd-1(bh40),* but not *picd-1(gk3701),* exhibited abnormal vulval invagination (**Figure 4A**) and the vulval morphology phenotype of *bh40* was dominant over *pry-1(mu38)***.** Furthermore, adult *picd-1* mutants were Pvl (*gk3701*: 5% and *bh40*: 16.7%) (**Table 1**).

Phenotypic analysis of both *picd-1* mutant strains did not reveal any signs of sickness. Careful examination showed that this gene is involved in the development of the egg-laying system. The *picd-1(bh40)* worms were weakly egg-laying (Egl) (**Figure S2, Video S2**), and their Egl and Pvl phenotypes were enhanced at 25 °C (**Figures 4B and S2**). No Egl phenotype was observed in the *picd-1(gk3701)* strain. Based on the Pvl and Egl penetrance, *bh40* appears to be a stronger loss-of-function allele than *gk3701*.

As the *picd-1::GFP* pattern overlapped with that of *pry-1,* and *picd-1* mutation enhanced the *pry-1* Pvl phenotype, we examined whether *pry-1* affects *picd-1* expression. *picd-1* levels drastically reduced in the *pry-1* mutants (**Figure 4C**), which shows that *picd-1* is required for the development of the reproductive system and is positively regulated by *pry-1*.

***picd-1* mutations worsen the phenotypes of *pry-1* mutants**

Next, we investigated the involvement of *picd-1* in other *pry-1*-mediated developmental and post-developmental processes. *picd-1* mutants grew slowly and took longer to reach adulthood than the wild-type and *pry-1(mu38)* animals (**Figure 5A**). Moreover, the growth defect in the *pry-1; picd-1* double mutant was significantly worse than in the single mutants (**Figure 5A**).

Mutations in *picd-1* enhanced the developmental defects of *pry-1(mu38)* animals, including those involving seam cells and the P lineage cell P11.p. Although 70–80% of *pry-1* mutants showed an extra P12.pa cell in the place of P11.p, the phenotype was fully penetrant in *pry-1(mu38); picd-1(bh40)* double mutant **(Table 1)**. Seam cell defects in *pry-1* mutants are caused by changes in asymmetric cell division at the L2 stage [5,20]. Although RNAi knockdown of *picd-1* did not affect seam cells, it enhanced the phenotype of *pry-1(mu38)* animals (**Figure 5B**). Moreover, both *picd-1* and *pry-1* mutants exhibited defects in alae, which are structures formed by differentiated seam cells (**Figure 5C**) [5]. Hence, these data show that *picd-1* interacts with *pry-1* to affect P11.p and seam cell development.

In addition, we observed several other developmental abnormalities in the *picd-1* mutant animals. The analysis of brood size revealed defects in *picd-1(bh40)* but not in *picd-1(gk3701)* animals (**Figures 6A and 6B**). Although the *bh40* allele did not affect embryonic viability, it drastically reduced the brood count and enhanced the embryonic lethality of *pry-1* mutants ($p < 0.001$) (**Figures 6A–C**). Further analysis revealed that *pry-1(gk3681); picd-1(gk3701)* and *pry-1(mu38)*; *picd-1(bh40)* double mutants had abnormal oocytes and gonads, respectively (**Figures 7A–C**). More specifically, 46 ± 6% (n=45) of *pry-1(mu38)*; *picd-1(bh40)* animals lacked oocytes in the posterior gonad arm (**Figures 7C and 7D**). No such phenotype was observed in either of the single mutants.

***picd-1* mutants are sensitive to stress and exhibit a short lifespan**

We previously reported that *pry-1* plays a role in stress response maintenance [6,8]. The analysis of heat shock chaperones — *hsp-4* (ER-UPR), *hsp-6* (MT-UPR), and *hsp-16.2* (cytosolic heat shock response, HSR) — showed that all three were upregulated in *pry-1* mutant animals (**Figure 8A**). Similar experiments in *picd-1* mutants showed increased expression of *hsp-4, hsp-16.2*, and the oxidative stress response gene *sod-3* (**Figure 8B**). Consistent with these results, both *pry-1* and *picd-1* mutants showed electrotaxis defects (**Figure 8C**), a phenotype observed in animals with abnormalities in the UPR signaling [21].

To further elucidate the stress sensitivity of animals lacking *picd-1* function, we examined the survivability of the animals following chemical treatments. Both *gk3701* and *bh40* alleles were sensitive to paraquat and tunicamycin, although the effect was more pronounced following paraquat exposure **(Figures 8D and 8E)**. Interestingly, *bh40* did not enhance paraquat sensitivity in *pry-1(mu38)* animals (**Figure 8F**), which could be explained by the significantly reduced expression of *picd-1* in *pry-1* mutants. Finally, the responses of *picd-1(bh40)* animals to chemical exposures were more pronounced than *picd-1(gk3701)*.

As increased stress sensitivity can affect the lifespan of an animal, and *pry-1* mutants are short-lived, we analyzed whether *picd-1* plays a role in aging. Neither *picd-1*(gk3701) nor *picd-1*(RNAi) enhanced the lifespan defects of animals lacking *pry-1* function (**Figures 9A and 9B, Table 2**). Considering that *pry-1* mutant animals have a significantly reduced expression of *picd-1* than the wild-type animals, it is conceivable that further reduction in *picd-1* cannot exacerbate the short-lived phenotype. Alternatively, it is plausible that *picd-1* is not involved in lifespan maintenance. To explore this further, we examined the lifespan of *picd-1* mutant and RNAi-treated animals in the absence of other mutations. Both *gk3701* and *bh40* alleles reduced the lifespan of the animals. *picd-1(bh40)* worms had a significantly reduced lifespan at both 20 °C and 25 °C, and *picd-1(gk3701)* exhibited a similar phenotype at 25 °C (**Figures 9B and 9C, Table 2**). These results were also supported by the RNAi experiments. The analysis of age-associated biomarkers revealed a progressive age-associated decline in both body bending and pharyngeal pumping rates (**Figures 9E and 9F**). Overall, the data suggest that while *picd-1* does not enhance the phenotype of *pry-1* mutants, the gene plays an essential role in maintaining the usual lifespan of animals.

We have previously shown that in addition to affecting lifespan, *pry-1* regulates lipid metabolism [7]. This result prompted us to analyze whether *picd-1* affects lipid levels and the expression of genes involved in fatty acid synthesis. The analysis of Δ9 desaturases showed that while *fat-5* and *fat-7* were downregulated, *fat-6* was unaffected (**Figure 9G**). Among the three transcription factors regulating the expression of Δ9 desaturases, *nhr-80* (NHR family) was downregulated, but *sbp-1* (SREBP1 homolog) was upregulated (**Figure 9G**) [22]. We also quantified lipids by Oil Red O staining but saw no change in *picd-1* mutants (**Figure 9H**), possibly due to functional redundancies within the *fat* [23,24] and *nhr* family of genes [22]. Hence, we conclude that *picd-1* is necessary for the expression of a subset of lipid synthesis genes but is not crucial for regulating lipid levels.

Loss of *picd-1* and *pry-1* promotes CRTC-1 nuclear localization

Research has shown that calcineurin (a calcium-activated phosphatase) signaling promotes nuclear localization of CRTC-1, leading to a reduction in the lifespan of *C. elegans* [16]. Given that human Cabin1 negatively regulates calcineurin signaling [12,25], we investigated whether *picd-1* knockdown could affect the subcellular localization of CRTC-1::RFP. The RNAi knockdown of *picd-1* caused nuclear localization of CRTC-1, consistent with the short lifespan of *picd-1* mutants (**Figures 9C, 9D and 10A**). Moreover, CRTC-1 responsive genes, *dod-24* and *asp-12* [26], were upregulated in the *picd-1(bh40)* mutants (**Figure 10B**).

As *pry-1* is necessary for *picd-1* expression, we examined its effect on the CRTC-1::RFP subcellular localization and found that CRTC-1 was nuclear-localized and *dod-24* upregulated in *pry-1* mutants (**Figures 10C and 10D**). To further understand the mechanism of PRY-1-PICD-1-mediated CRTC-1 localization, we examined the involvement of the Wnt canonical pathway component BAR-1/β-catenin. The *bar-1* RNAi did not affect CRTC-1::RFP nuclear localization in *pry-1* mutants **(Figure 10E),** suggesting that PRY-1 may function in a WNT-independent manner to regulate CRTC-1. Next, we examined the involvement of CRTC-1 in PRY-1-mediated lifespan and stress response and found that *crtc-1* RNAi significantly rescued the short lifespan and stress sensitivity defects of *pry-1* mutants (**Figures 10 F–G and Table 2**). Hence, we propose that PRY-1 and PICD-1 inhibit CRTC-1-dependent transcriptional response to delay age-associated processes.

Given that calcineurin and CRTC-1 mediated lifespan regulation involves the *C. elegans* CREB transcription factor homolog 1 (CRH-1), we wanted to know whether PRY-1 and CRH-1 regulate a common set of target genes. Consistent with our hypothesis, we found a significant overlap in differentially expressed genes between *pry-1* and *crh-1* mutant transcriptomes (406 common genes, R.F 2.5, $p < 5.108e\text{-}78$). Furthermore, the number of overlapping sets of genes regulated in an opposite manner between *pry-1* and *crh-1* mutants were also significant (**Figure S3 and Table S2**) and were enriched with GO biological processes such as response to stress (18), metabolic processes (18), and cellular processes (40) (FDR < 0.05). In conclusion, these data demonstrate a novel functional relationship between PRY-1 and CRTC-1 in *C. elegans*.

DISCUSSION

In this study, we identified a new gene, *picd-1*, in *C. elegans* that interacts with *pry-1* and regulates several larval and adult processes. *picd-1* is predicted to encode a nuclear protein containing a conserved Cabin1 domain, which belongs to the HUCA complex in humans [11]. The HUCA complex is implicated in diverse chromatin regulatory events, where it preferentially deposits a histone variant H3.3. This leads to transcriptional activation by nucleosome destabilization or transcriptional repression through heterochromatinization [27]. Cabin1 is expressed in all human tissues and localized to the nucleoplasm and cytoplasm [28,29]. Studies in other systems have also uncovered homologous proteins of Cabin1. For example, the yeast *Saccharomyces cerevisiae* contains Hir1p and Hir2p (both HIRA orthologs) and Hir3, Hpc2, and Asf1p, orthologs of Cabin1, UBN1, and ASF1a, respectively [27].

Our study provides the first genetic evidence of a Cabin1 domain-containing protein regulating biological processes in *C. elegans*. Other complex components in worms include HIRA-1 (HIRA homolog), ASFL-1, and UNC-85 (both ASF1a homologs) [30–32]. However, it remains to be seen if any of these proteins interact with PRY-1. Mutations in *picd-1* led to multiple defects such as Pvl, Egl, small brood size, developmental delay, stress sensitivity, and short lifespan. Interestingly, loss of *picd-1* function enhanced various phenotypes of the *pry-1* mutant, some of which were not seen in the *picd-1* mutant alone. For example, *pry-1; picd-1* double mutant showed a Pvl phenotype and

exhibited P11.p cell fate changes. In addition, *picd-1* RNAi enhanced seam cell defects in the *pry-1* mutants. Interestingly, mutations in *picd-1* did not enhance vulval precursor cell induction or Muv phenotype in *pry-1* mutants. Overall, these results suggest that *picd-1* participates in a subset of *pry-1*-mediated processes.

We also analyzed the role of *picd-1* in other *pry-1*-mediated non-developmental events, such as egg-laying, embryonic survivability, aging, stress response, and lipid metabolism. Loss of *picd-1* function worsened the embryonic lethality of *pry-1* mutants. Moreover, *pry-1; picd-1* double mutant had a very small brood size due to defects in the gonad arms. Similar phenotypes are observed in the mutants of other HIRA complex components. Knockdown of *hira-1* leads to embryonic lethality, *asfl-1* or *unc-85* single mutants have low brood size, and *asfl-1; unc-85* double mutant is sterile [31–33]. Together, these data show that *pry-1* and *picd-1* interact to regulate embryonic viability and fertility in animals. However, it remains to be seen whether PRY-1 and PICD-1 interact with other HIRA complex components to mediate their function.

Furthermore, we found that *picd-1* is required for normal stress response maintenance. *picd-1* mutants showed enhanced sensitivity to paraquat and tunicamycin. The mutant animals also exhibited increased levels of UPR markers. Both *picd-1* and *pry-1* mutants significantly increased *hsp-16.2,* and *hsp-4*, suggesting that these genes function together to regulate ER-UPR and HSR. However, more work is needed to determine whether these two genes uniquely affect MT-UPR and oxidative stress and their biological significance.

Mutants that show sensitivity to stress typically have a short lifespan [34–36]. Similar to *pry-1* mutants, *picd-1(bh40)* animals are short-lived and exhibit defects in age-related physiological markers. This result is consistent with the fact that both genes function together to regulate stress response and aging. However, there are functional differences between the two genes. For example, we found that lipid levels were greatly reduced in *pry-1* but not in *picd-1* mutants. The *nhr-80* and *fat-7* levels were reduced in *picd-1* mutant animals, consistent with the known role of *nhr-80* in regulating *fat-7* expression [24]. However, while *picd-1* is needed for the expression of *fat-5*, *fat-7* and *nhr-80*, a lack of its function does not compromise lipid levels in animals. These results suggest that *picd-1* participates only in a subset of *pry-1*-mediated processes. However, the extent

to which the two genes interact in specific tissues and the precise nature of their interactions is unknown.

A possible mechanism of *picd-1* function in lifespan maintenance may involve calcineurin. AMPK and calcineurin modulation of CRTCs are conserved in mammals and *C. elegans* [16,37–40]. In *C. elegans*, AAK-2 and calcineurin regulate CRTC-1 post-translationally in an opposing manner, where activated AAK-2 causes nuclear exclusion of CRTC-1 and extends lifespan. Such a phenotype was also observed after deactivating calcineurin [16]. Our data showed that loss of *picd-1* function resulted in the nuclear localization of CRTC-1 and activated the CRTC-1 target genes. These findings, together with the fact that mammalian Cabin1 inhibits calcineurin-mediated signaling [12,25,41], suggest that PICD-1 may regulate CRTC-1 via downregulation of calcineurin in *C. elegans*. The loss of *picd-1*/Cabin-1 should lead to increased calcineurin signaling, which may explain the shorter lifespan of *picd-1* mutants.

As *picd-1* is downregulated in *pry-1* mutants, and both genes are needed for the proper subcellular localization of CRTC-1 and its downstream targets, we speculate that PRY-1 and PICD-1 use CRTC-1 to regulate stress response and lifespan of animals. While there is no evidence for the interaction between mammalian Axin and CRTCs, studies have shown that CREB, which associates with CRTCs, is inhibited by Axin-GSK3β signaling [42,43]. Our work provides the first evidence of genetic interactions between *pry-1*, *picd-1*, and *crtc-1* in *C. elegans*, which has uncovered a novel crosstalk between Axin and calcineurin signaling. However, several questions remain unanswered. For instance, the components of *pry-1* signaling affecting CRTC-1 nuclear localization are unknown. In preliminary experiments, *tax-6* RNAi (calcineurin catalytic subunit) did not affect the *pry-1* phenotype (data not shown); however, more experiments are needed to completely ascertain its requirements. Additionally, whether *picd-1* is regulated by *pry-1* in a WNT-dependent manner or it is co-regulated by *pry-1* and *aak-2* [8,10] independently of WNT needs thorough investigation. Moreover, it is unknown whether other HUCA complex components interact with PCID-1 to mediate PRY-1's role during stress response and lifespan, as well as whether PRY-1 and PICD-1 co-regulate a common set of targets during these processes. Further work is needed to investigate these questions and to gain a deeper understanding of the conserved mechanisms involved in Axin-Cabin1 signaling in eukaryotes.

MATERIALS AND METHODS

Worm strains

Cultures were maintained at 20 °C on standard nematode growth media (NGM) plates seeded with OP50 *E. coli* bacteria.

N2 (wild-type)

DY220 *pry-1(mu38)*

VC3710 *pry-1(gk3682)*

VC3709 *pry-1(gk3681); picd-1(gk3701)*

DY725 *pry-1(mu38); picd-1(bh40)*

DY678 *bhEx287[pGLC150(picd-1p::GFP) + myo-3::wCherry]*

DY698 *picd-1(bh40)*

DY694 *picd-1(gk3701)*

RG733 *wIs78[(scm::GFP) + (ajm-1p::GFP)]*

AGD418 *uthIs205[crtc-1p::CRTC-1::RFP::unc-54 3' UTR + rol-6(su1006)]*

DY740 *pry-1(gk3682); uthIs205[crtc-1p::crtc-1::RFP + rol-6(su1006)]*

Mutant allele and transgene generation

The *gk3701* allele of *picd-1* was generated by the CRISPR technique. It carries a 5 bp sequence (GGTGA) mutation in the second exon (flanking 25 nucleotides: GTGAAGAGGATGAGGACAATGGTGA and GGATTCAGAAGAAGAAGATGAAGAA), resulting in multiple premature in-frame stop codons (See primers in **Table S2**).

The other allele *(bh40)* was created using a nested CRISPR technique[44]. We replaced the 84 bp in the first exon with a synthetic sequence containing stop codons in different frames (See primers used in **Table S2**). Both *picd-1* strains were outcrossed twice with the wildtype N2 animals and sequenced to confirm the mutations.

To generate the *picd-1p::GFP* transgenic animals (DY678), pGLC150 was injected in N2 background at 50 ng/µL along with 30 ng/µL of *myo-3::wCherry*. pGLC150 was constructed by

cloning a 3,885 bp PCR-amplified (using the primers GL1372 and GL1373) fragment, spanning the promoter region and a portion of the first exon of the *picd-1* gene, into the vector pPD95.81 using the restriction sites SalI and KpnI.

RNAi

RNAi mediated gene silencing was performed using a protocol previously published by our laboratory[45]. Plates were seeded with *E. coli* HT115 expressing either dsRNA specific to candidate genes or empty vector (L4440). Gravid adult hermaphrodites were treated with a bleach solution, and eggs were plated. Animals were allowed to grow till adulthood and vulva and seam cell phenotypes were examined.

Fluorescent and DIC microscopy

Animals were paralyzed in 10 mM Sodium Azide and mounted on glass slides containing 2% agar pads and covered with glass coverslips. Images were captured using a Zeiss Apotome microscope and Zeiss ZEN software. For acquiring live videos of gonad, animals were suspended in M9 without Sodium Azide. Videos were captured by a high speed camera fitted on a Leica MZ-FLIII fluorescent stereomicroscope[46].

Vulval induction, P11.p, P12.p, body bending, and pharyngeal pumping

Vulval induction and P11.p and P12.p phenotypes were examined in L4 stage animals using a Nomarski microscope. VPCs were considered induced if they gave rise to progeny. Wild-type (N2) animals have three induced VPCs, one each for P5.p, P6.p, and P7.p. Mutants with more than three induced VPCs were termed as 'over-induced'. Muv and Pvl phenotypes were scored in adults.

The P11.p and P12.pa cells are readily distinguished based on their nuclear size and morphology [47–49]. In *pry-1* mutants, two P12.pa-like cells are observed and P11.p is missing.

Body bending per 1 min and pharyngeal pumping per 30 sec were analyzed in young adults over a period of four days [6]. For this, individual hermaphrodites were placed on OP50 plates and examined under a dissecting microscope. Pharyngeal pumping was assessed by observing the number of pharyngeal contractions. For body bending, animals were stimulated by tapping once

on the tail by a platinum wire. Each full sinusoidal motion was counted as one body bend. Only animals that moved actively within 1 min were included in the analysis.

Lifespan analysis

Lifespan experiments of RNAi-treated animals were carried out using a previously described protocol [8]. Synchronized eggs were allowed to grow on NGM OP50 seeded plates till the late L4 larval stage after which they were transferred to RNAi bacteria seeded plates. Cultures were screened daily for dead animals and surviving adults were transferred every other day till the progeny production ceased. Censoring was done for animals that had either escaped, burrowed into the medium, showed a bursting at the vulva, or had progeny hatching inside the uterus [50].

Stress assay

Oxidative and endoplasmic reticulum mediated stress experiments were performed using 100 mM paraquat (Thermo Fisher Scientific, USA) and 25 ng/µL tunicamycin (Sigma-Aldrich, Canada) respectively. Animals were incubated for 1 hr, 2 hr, 3 hr and 4 hr, following a previous published protocol [6]. All the final working concentrations were made in M9. At least 30 animals of each strain were tested in replicates. Means and standard deviations were determined from experiments performed in duplicate. Animals were considered dead if they did not respond to a platinum wire touch and showed no thrashing or swimming movement in M9. Moreover, dead animals usually had an uncurled and straight body shape in comparison to the normal sinusoidal shape of worms.

Oil Red O staining

Neutral lipid staining was done on synchronized day-1 adults using Oil Red O dye (Thermo Fisher Scientific, USA) following a published protocol [9]. Quantifications were performed using ImageJ software as described earlier [51].

Molecular Biology

RNA was extracted from synchronized L3 and day-1 adult animals. Protocols for RNA extraction, cDNA synthesis and qPCR were described earlier [7]. Briefly, total RNA was extracted using Trizol (Thermo Fisher, USA). The RNA was used to prepare cDNA and, subsequently, perform qPCR

using the SensiFast cDNA synthesis kit (Bioline, USA), and SYBR green mix (Bio-Rad, Canada), respectively. Primers are listed in **Table S1**.

Statistical analyses

Statistics analyses were performed using GraphPad prism 9, SigmaPlot software 11, CFX Maestro 3.1 and Microsoft Office Excel 2019. For lifespan data, survival curves were estimated using the Kaplan- Meier test and differences among groups were assessed using the log-rank test. qPCR data was analyzed using Bio-Rad CFX Maestro 3.1 software. For all other assays, data from repeat experiments were pooled and analyzed together, and statistical analyses were done using GraphPad Prism 9. *p* values less than 0.05 were considered statistically significant.

ACKNOWLEDGEMENT

We thank Drs. Andrew Dillin (University of California, Berkeley) and Brent Derry (University of Toronto) for providing the CRTC-1::RFP strain and *crtc-1* RNAi plasmid, respectively. Hannan Minhas assisted with electrotaxis experiments and Wouter van den Berg with the screening of *picd-1* CRISPR allele *bh40*. This work was supported by the NSERC Discovery grant to Bhagwati Gupta and NSERC CGS-D scholarship to Avijit Mallick. Some of the strains were obtained from the *Caenorhabditis* Genetics Center (CGC), which is funded by the NIH Office of Research Infrastructure Programs (P40 OD010440).

AUTHORS CONTRIBUTIONS

AM initially characterized the *picd-1* mutants and generated many reagents for the study. AM, SM and SKBT carried out the experiments. AM, SKBT, and BG analyzed the data. AM wrote the first draft of the manuscript with assistance from SKBT. All authors reviewed the final version. BG supervised the study.

REFERENCES

1. Mallick, A., Taylor, S. K. B., Ranawade, A. & Gupta, B. P. Axin Family of Scaffolding

Proteins in Development: Lessons from C. elegans. *J. Dev. Biol.* **7**, 1–23 (2019).

2. Clevers, H. & Nusse, R. Wnt/β-catenin signaling and disease. *Cell* **149**, 1192–1205 (2012).
3. Luo, W. & Lin, S. C. Axin: A master scaffold for multiple signaling pathways. *NeuroSignals* **13**, 99–113 (2004).
4. Sawa, H. & Korswagen, H. C. Wnt signaling in C. elegans *. *WormBook* 1–30 (2013). doi:10.1895/wormbook.1.
5. Mallick, A., Ranawade, A. & Gupta, B. P. Role of PRY-1/Axin in heterochronic miRNA-mediated seam cell development. *BMC Dev. Biol.* **19**, 1–12 (2019).
6. Mallick, A. *et al.* Genetic analysis of Caenorhabditis elegans pry-1 / Axin suppressors identifies genes involved in reproductive structure development , stress responses , and aging. *G3 Genes, Genomes, Genet.* **jkab430**, (2021).
7. Ranawade, A., Mallick, A. & Gupta, B. P. PRY-1/Axin signaling regulates lipid metabolism in Caenorhabditis elegans. *PLoS One* **13**, e0206540 (2018).
8. Mallick, A., Ranawade, A., van den Berg, W. & Gupta, B. P. Axin-Mediated Regulation of Lifespan and Muscle Health in C. elegans Requires AMPK-FOXO Signaling. *iScience* **23**, 101843 (2020).
9. Mallick, A. & Gupta, B. P. Vitellogenin-2 acts downstream of PRY-1 / Axin to regulate lipids and lifespan in C . elegans. *microPublication Biol.* **1**, 19–21 (2020).
10. Mallick, A. & Gupta, B. P. AXIN-AMPK signaling : Implications for healthy aging [version 1 ; peer review : awaiting peer review]. *F1000Research* **10**, 1–10 (2021).
11. Rai, T. S. *et al.* Human CABIN1 Is a Functional Member of the Human HIRA/UBN1/ASF1a Histone H3.3 Chaperone Complex. *Mol. Cell. Biol.* **31**, 4107–4118 (2011).
12. Sun, L. *et al.* Cabin 1, a negative regulator for calcineurin signaling in T lymphocytes. *Immunity* **8**, 703–711 (1998).
13. Park, Y. J., Yoo, S. A., Kim, M. & Kim, W. U. The Role of Calcium–Calcineurin–NFAT Signaling Pathway in Health and Autoimmune Diseases. *Front. Immunol.* **11**, 1–14 (2020).
14. Park, H. S., Lee, S. C., Cardenas, M. E. & Heitman, J. Calcium-Calmodulin-Calcineurin Signaling: A Globally Conserved Virulence Cascade in Eukaryotic Microbial Pathogens. *Cell Host Microbe* **26**, 453–462 (2019).
15. Bandyopadhyay, J., Lee, J. & Lee, J. Calcineurin, a Calcium/Calmodulin-dependent Protein

Phosphatase, Is Involved in Movement, Fertility, Egg Laying, and Growth in Caenorhabditis elegans. *Mol. Biol. Cell* **13**, 3281–3293 (2002).

16. Mair, W. *et al.* Lifespan extension induced by AMPK and calcineurin is mediated by CRTC-1 and CREB. *Nature* **470**, 404–408 (2011).
17. Yan, J. & Kurgan, L. DRNApred, fast sequence-based method that accurately predicts and discriminates DNA-and RNA-binding residues. *Nucleic Acids Res.* **45**, 1–16 (2017).
18. Grün, D. *et al.* Conservation of mRNA and protein expression during development of C.elegans. *Cell Rep.* **6**, 565–577 (2014).
19. Golden, T. R., Hubbard, A., Dando, C., Herren, M. A. & Melov, S. Age-related behaviors have distinct transcriptional profiles in Caenorhabditis.elegans. *Aging Cell* **7**, 850–865 (2008).
20. Gleason, J. E. & Eisenmann, D. M. Wnt signaling controls the stem cell-like asymmetric division of the epithelial seam cells during C. elegans larval development. *Dev. Biol.* **348**, 58–66 (2010).
21. Taylor, S. K. B. *et al.* C. elegans electrotaxis behavior is modulated by heat shock response and unfolded protein response signaling pathways. *Sci. Rep.* **11**, 1–17 (2021).
22. Watts, J. L. & Ristow, M. Lipid and carbohydrate metabolism in Caenorhabditis elegans. *Genetics* **207**, 413–446 (2017).
23. Brock, T. J., Browse, J. & Watts, J. L. Fatty acid desaturation and the regulation of adiposity in Caenorhabditis elegans. *Genetics* **176**, 865–875 (2007).
24. Brock, T. J., Browse, J. & Watts, J. L. Genetic regulation of unsaturated fatty acid composition in C. elegans. *PLoS Genet.* **2**, 0997–1005 (2006).
25. Lai, M. M., Burnett, P. E., Wolosker, H., Blackshaw, S. & Snyder, S. H. Cain, a novel physiologic protein inhibitor of calcineurin. *J. Biol. Chem.* **273**, 18325–18331 (1998).
26. Burkewitz, K. *et al.* Neuronal CRTC-1 Governs Systemic Mitochondrial Metabolism and Lifespan via a Catecholamine Signal. *Cell* **160**, 842–855 (2015).
27. Szenker, E., Ray-Gallet, D. & Almouzni, G. The double face of the histone variant H3.3. *Cell Res.* **21**, 421–434 (2011).
28. Thul, P. J. *et al.* A subcellular map of the human proteome. *Science (80-.).* **356**, (2017).
29. Uhlén, M. *et al.* Tissue-based map of the human proteome. *Science (80-.).* **347**, (2015).
30. Burkhart, K. B., Sando, S. R., Corrionero, A. & Horvitz, H. R. H3.3 Nucleosome Assembly

Mutants Display a Late-Onset Maternal Effect. *Curr. Biol.* **30**, 2343-2352.e3 (2020).

31. Grigsby, I. F., Rutledge, E. M., Morton, C. A. & Finger, F. P. Functional redundancy of two C. elegans homologs of the histone chaperone Asf1 in germline DNA replication. *Dev. Biol.* **329**, 64–79 (2009).
32. Grigsby, I. F. & Finger, F. P. UNC-85, a C. elegans homolog of the histone chaperone Asf1, functions in post-embryonic neuroblast replication. *Dev. Biol.* **319**, 100–109 (2008).
33. Piano, F. *et al.* Gene Clustering Based on RNAi Phenotypes of Ovary-Enriched Genes in C. elegans. *Curr. Biol.* **12**, 1959–1964 (2002).
34. Morton, E. A. & Lamitina, T. Caenorhabditis elegans HSF-1 is an essential nuclear protein that forms stress granule-like structures following heat shock. *Aging Cell* **12**, 112–120 (2013).
35. Taylor, R. C. & Dillin, A. XXBP-1 Is a cell-nonautonomous regulator of stress resistance and longevity. *Cell* **153**, 1435 (2013).
36. Libina, N., Berman, J. R. & Kenyon, C. Tissue-Specific Activities of C. elegans DAF-16 in the Regulation of Lifespan tissues play an important role in establishing the ani-mal's rate of aging. First, the C. elegans genome con-tains more than 35 insulin-like genes expressed in a. *Cell* **115**, 489–502 (2003).
37. Screaton, R. A. *et al.* The CREB coactivator TORC2 functions as a calcium- and cAMP-sensitive coincidence detector. *Cell* **119**, 61–74 (2004).
38. Koo, S. H. *et al.* The CREB coactivator TORC2 is a key regulator of fasting glucose metabolism. *Nature* **437**, 1109–1114 (2005).
39. Komiya, T. *et al.* Enhanced activity of the CREB co-activator Crtc1 in LKB1 null lung cancer. *Oncogene* **29**, 1672–1680 (2010).
40. Wang, Y., Vera, L., Fischer, W. H. & Montminy, M. The CREB coactivator CRTC2 links hepatic ER stress and fasting gluconeogenesis. *Nature* **460**, 534–537 (2009).
41. Jang, H., Cho, E. J. & Youn, H. D. A new calcineurin inhibition domain in Cabin1. *Biochem. Biophys. Res. Commun.* **359**, 129–135 (2007).
42. Gavagan, M., Fagnan, E., Speltz, E. B. & Zalatan, J. G. The Scaffold Protein Axin Promotes Signaling Specificity within the Wnt Pathway by Suppressing Competing Kinase Reactions. *Cell Syst.* **10**, 515-525.e5 (2020).
43. Fiol, C. J., Wang, A., Roeske, R. W. & Roach, P. J. Ordered multisite protein

phosphorylation. Analysis of glycogen synthase kinase 3 action using model peptide substrates. *J. Biol. Chem.* **265**, 6061–6065 (1990).

44. Vicencio, J., Martínez-Fernández, C., Serrat, X. & Cerón, J. Efficient generation of endogenous fluorescent reporters by nested CRISPR in caenorhabditis elegans. *Genetics* **211**, 1143–1154 (2019).

45. Seetharaman, A., Cumbo, P., Bojanala, N. & Gupta, B. P. Conserved mechanism of Wnt signaling function in the specification of vulval precursor fates in C. elegans and C. briggsae. *Dev. Biol.* **346**, 128–139 (2010).

46. Chalich, Y., Mallick, A., Gupta, B. & Jamal Deen, M. Development of a low-cost, user-customizable, high-speed camera. *PLoS One* **15**, 1–21 (2020).

47. Eisenmann, D. M. & Kim, S. K. Protruding vulva mutants identify novel loci and wnt signalling factors that function during Caenorhabditis elegans vulva development. *Genetics* **156**, 1097–1116 (2000).

48. Walston, T. *et al.* mig-5/Dsh controls cell fate determination and cell migration in C. elegans. *Dev. Biol.* **298**, 485–497 (2006).

49. Jiang, L. I. & Sternberg, P. W. Interactions of EGF, Wnt and HOM-C genes specify the P12 neuroectoblast fate in C. elegans. *Development* **125**, 2337–2347 (1998).

50. Amrit, F. R. G., Ratnappan, R., Keith, S. A. & Ghazi, A. The C. elegans lifespan assay toolkit. *Methods* **68**, 465–475 (2014).

51. Soukas, A. A., Kane, E. A., Carr, C. E., Melo, J. A. & Ruvkun, G. Rictor/TORC2 regulates fat metabolism, feeding, growth, and life span in Caenorhabditis elegans. *Genes Dev.* 496–511 (2009). doi:10.1101/gad.1775409.2004

LIST OF TABLES

Table 1: Analysis of VPC induction, P12.pa cell fate, Pvl, and Muv penetrance in different strains. *Extra P12.pa cell in the place of P11.p.

	VPC induction pattern (% induced)							Over-induced vulva and P12.pa			Pvl and Muv		
Genotype	**P3p**	**P4p**	**P5p**	**P6p**	**P7p**	**P8p**	**N**	**% over-induced**	**% P12pa***	**N**	**% Pvl**	**%Muv**	**N**
N2	0	0	100	100	100	0	20	0	0	20	0	0	20
pry-1(gk3682)	27.3	4.5	100	100	86.4	4.5	22	36.4	72.7	22	65.7	31.3	40
pry-1(mu38)	18.2	0	100	100	81.8	9.1	22	27.2	81.8	22	59.6	34.2	50
picd-1(gk3701)	0	0	100	100	100	0	20	0	0	20	5	0	40
picd-1(bh40)	0	0	100	100	100	0	20	0	0	20	16.7	0	40
pry-1(gk3681); picd-1(gk3701)	21.7	8.7	100	100	87	13	23	39.1	74	23	76.8	22	40
pry-1(mu38); picd-1(bh40)	12.5	12.5	100	100	92	12.5	24	25	100	24	80	20	40

Table 2: Lifespan analysis of animals. Each lifespan assay was carried out in two or more batches (see Methods). N: number of animals examined, ns: not significant.

Genotype	treatment	Mean Lifespan (days)	Median Lifespan (days)	Maximum Lifespan (days)	N	*p* value
N2	-	16.9 ± 0.9	16	23	56	
pry-1(gk3682)	-	3.7 ± 0.1	4	4	45	<0.001
pry-1(gk3681); picd-1(gk3701)	-	3.6 ± 0.1	4	4	50	<0.001
picd-1(gk3701)	-	15.3 ± 0.5	16	21	44	ns
picd-1(bh40)	-	13.7 ± 0.5	14	21	51	<0.001
N2	*empty vector*	16.6 ± 0.9	16	21	75	
	picd-1 RNAi	11.6 ± 0.6	18	22	58	<0.001
	crtc-1 RNAi	20.4 ± 0.9	22	26	63	<0.01
pry-1(mu38)	*empty vector*	3.1 ± 0.3	3	6	79	
	picd-1 RNAi	2.9 ± 0.3	2	6	80	ns
	crtc-1	5.1 ± 0.4	6	8	48	<0.001
pry-1(gk3682)	*empty vector*	4.1 ± 0.3	4	6	52	
	crtc-1 RNAi	7.1 ± 0.7	7	10	64	<0.001
N2	25°C	13.4 ± 0.5	14	20	56	
picd-1(gk3701)	25°C	11.9 ± 0.5	12	16	48	<0.001
picd-1(bh40)	25°C	10.9 ± 0.4	11	17	54	<0.001

LIST OF FIGURES

Figure 1: Phenotype of *picd-1* mutants and sequence similarity of PICD-1 with Cabin1 proteins. (A) Representative images of Pvl phenotype in *pry-1(gk3682)* and *pry-1(gk3681); picd-1(gk3701)* animals. **(B)** *picd-1* mutation enhances Pvl phenotype of *pry-1* mutants. Data represent a cumulative of two replicates (n > 30 animals) and error bars represent the standard deviation. Statistical analyses for panel (**B**) were done using one-way ANOVA with Dunnett's post hoc test and significant differences are indicated by stars (*): ** (p <0.01). **(C)** Sequence comparison of PICD-1 with mammalian Cabin1 and nematode homologs. **(D)** Sequence alignment dendrogram generated by LIRMM (http://www.phylogeny.fr/simple_phylogeny.cgi) using default parameters.

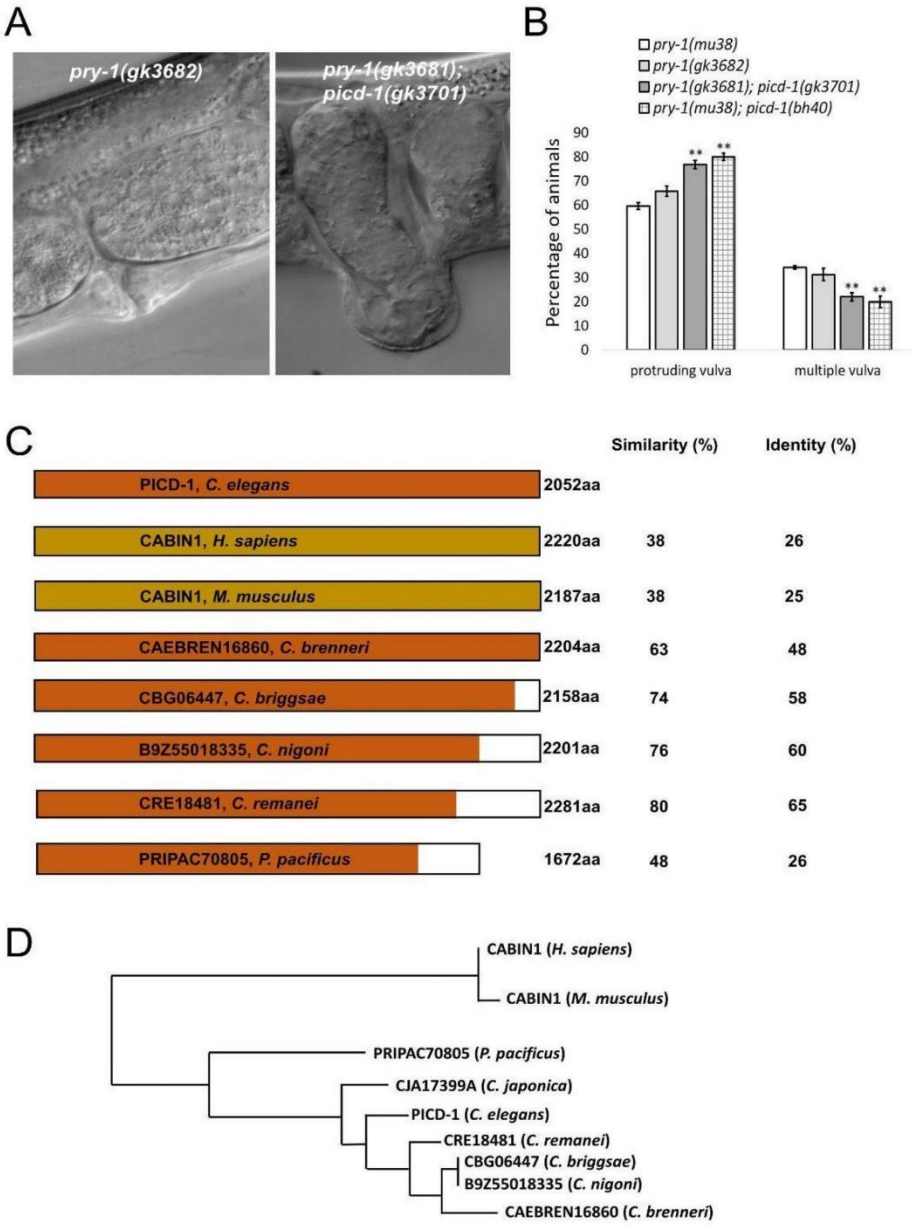
A
pry-1(gk3682)
pry-1(gk3681); picd-1(gk3701)
B
pry-1(mu38)
pry-1(gk3682)
pry-1(gk3681); picd-1(gk3701)
pry-1(mu38); picd-1(bh40)
Percentage of animals
90
80
70
60
50
40
30
20
10
0
**
**
**
**
protruding vulva
multiple vulva
C
Similarity (%)
Identity (%)
PICD-1, C. elegans 2052aa
CABIN1, H. sapiens 2220aa 38 26
CABIN1, M. musculus 2187aa 38 25
CAEBREN16860, C. brenneri 2204aa 63 48
CBG06447, C. briggsae 2158aa 74 58
B9Z55018335, C. nigoni 2201aa 76 60
CRE18481, C. remanei 2281aa 80 65
PRIPAC70805, P. pacificus 1672aa 48 26
D
CABIN1 (H. sapiens)
CABIN1 (M. musculus)
PRIPAC70805 (P. pacificus)
CJA17399A (C. japonica)
PICD-1 (C. elegans)
CRE18481 (C. remanei)
CBG06447 (C. briggsae)
B9Z55018335 (C. nigoni)
CAEBREN16860 (C. brenneri)

22

Figure 2: Expression analysis of *picd-1* in *C. elegans*. Representative images of animals expressing *picd-1::GFP* in larvae and adults. Tissues that show fluorescence include pharynx, gonad, hypodermis, intestine, vulva, body wall muscles and tail. Scale bars representing 100µm and 50µm are shown.

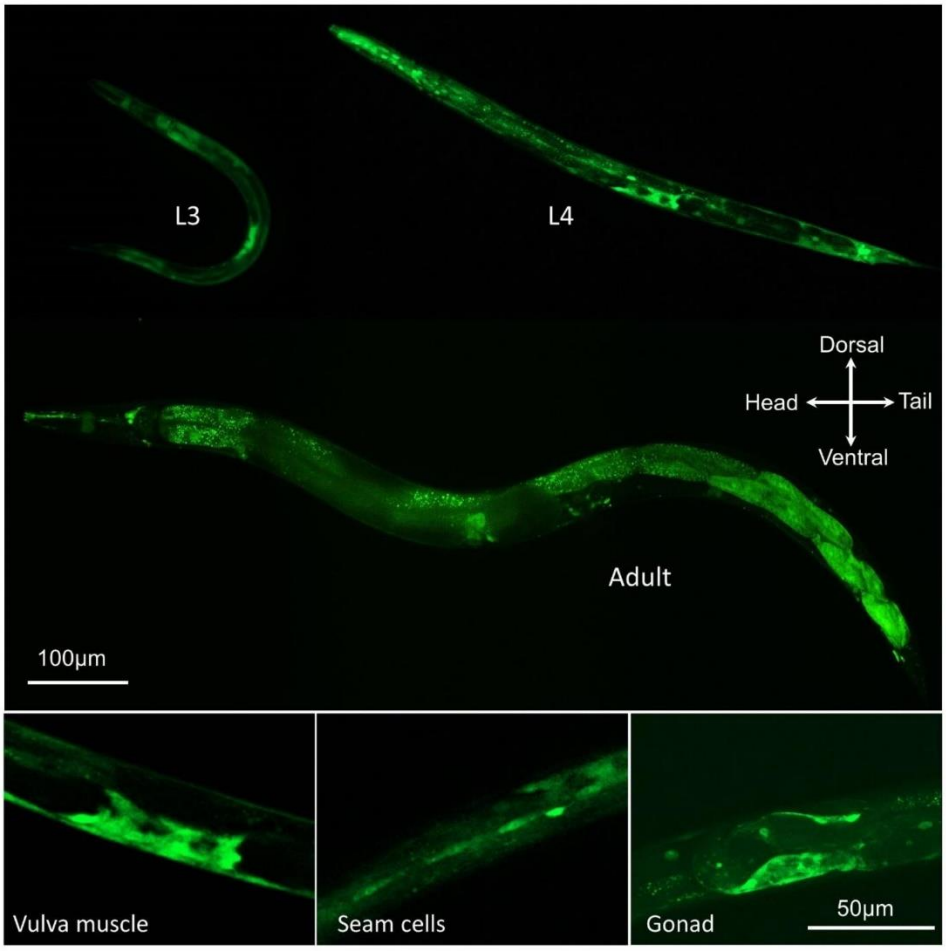

Figure 3: Analysis of *picd-1* alleles and their effect on *pry-1* mutant Pvl phenotype. (A) Schematic diagram of the *picd-1* open reading frame. The approximate locations of *bh40* and *gk3701* mutations have been indicated. **(B)** Sequences for *bh40* and *gk3701* mutations are shown in box. Inserted sequence is shown in italic and stop codons are shown in bold. **(C)** . Expression levels of *picd-1* in *pry-1(gk3682)* and *pry-1(mu38)* mutants at the L1 stage compared to wild-type. Data represent the means of two replicates and error bars represent the standard error of means. *p* values were calculated using Bio-Rad software (one-way ANOVA). **(D)** Bar graph showing VPC induction score in *picd-1* and *pry-1* mutants alone, and *pry-1; picd-1* double mutants compared to N2. Data represent the means of two replicates. The error bars show the standard deviation (n > 15 animals per batch). Statistical analyses were done using one-way ANOVA with Dunnett's post hoc test In panels C and D, significant differences are indicated by stars (*): ** (p <0.01).

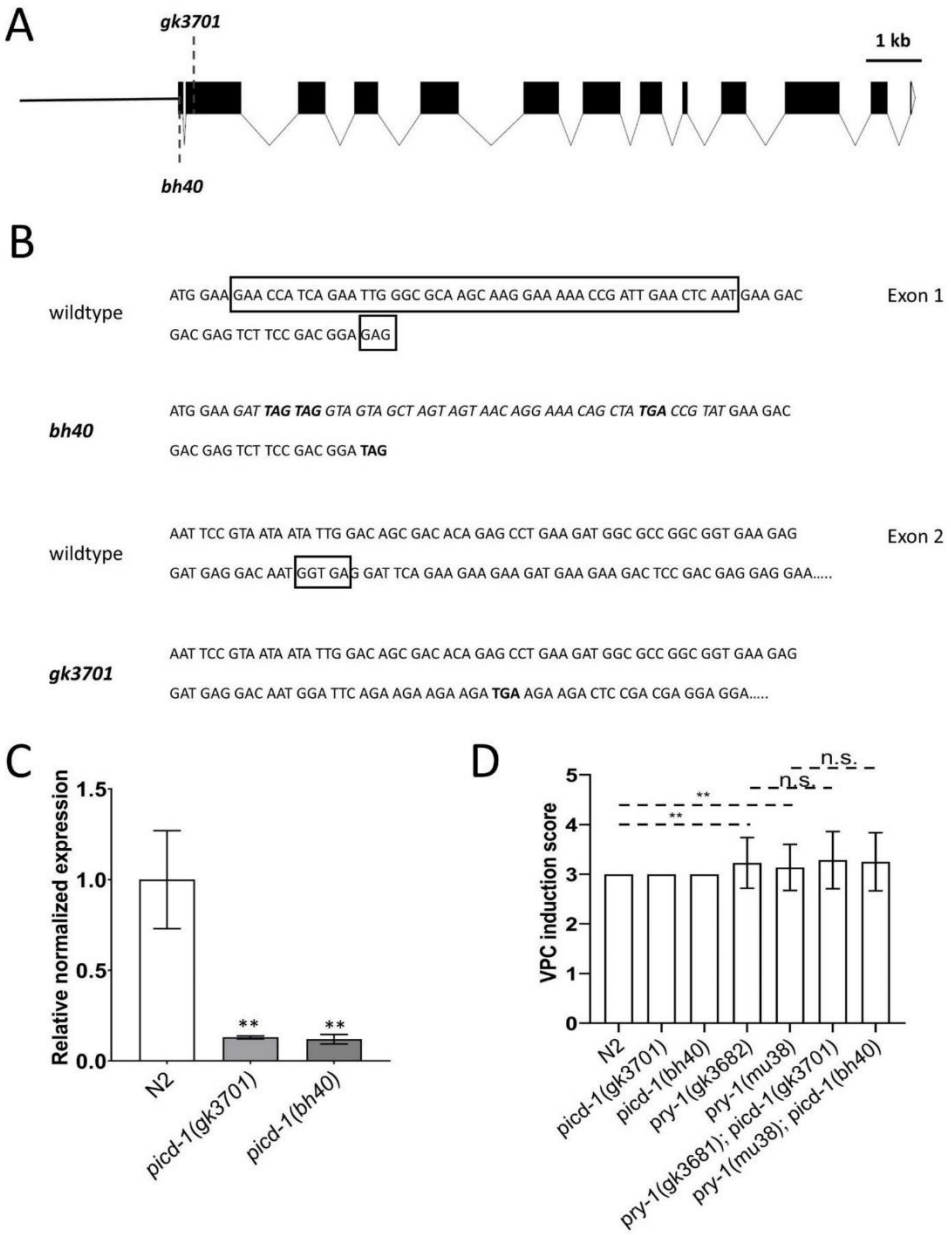
A
gk3701
1 kb
bh40
B
wildtype
ATG GAA GAA CCA TCA GAA TTG GGC GCA AGC AAG GAA AAA CCG ATT GAA CTC AAT GAA GAC
GAC GAG TCT TCC GAC GGA GAG
Exon 1
bh40
ATG GAA GAT TAG TAG GTA GTA GCT AGT AGT AAC AGG AAA CAG CTA TGA CCG TAT GAA GAC
GAC GAG TCT TCC GAC GGA TAG
wildtype
AAT TCC GTA ATA ATA TTG GAC AGC GAC ACA GAG CCT GAA GAT GGC GCC GGC GGT GAA GAG
GAT GAG GAC AAT GGT GAG GAT TCA GAA GAA GAA GAT GAA GAA GAC TCC GAC GAG GAG GAA.....
Exon 2
gk3701
AAT TCC GTA ATA ATA TTG GAC AGC GAC ACA GAG CCT GAA GAT GGC GCC GGC GGT GAA GAG
GAT GAG GAC AAT GGA TTC AGA AGA AGA AGA TGA AGA AGA CTC CGA CGA GGA GGA.....
C
Relative normalized expression
1.5
1.0
0.5
0.0
**
**
N2
picd-1(gk3701)
picd-1(bh40)
D
VPC induction score
5
4
3
2
1
0
**
**
n.s.
n.s.
N2
picd-1(gk3701)
picd-1(bh40)
pry-1(gk3682)
pry-1(mu38)
pry-1(gk3681); picd-1(gk3701)
pry-1(mu38); picd-1(bh40)

619
620

25

Figure 4: *picd-1* regulates vulval morphology. (A) Representative vulval images of wild-type, and *picd-1* and *pry-1* mutants at the mid-L4 stage. Scale bar is 50µm. **(B)** Line graph showing the percentage of *picd-1(bh40)* mutants showing Pvl phenotype at 20C and 25C compared to wild-type controls (Also see Table 1). Data represent a cumulative of two replicates (n > 30 animals) and error bars represent the standard deviation. Statistical analyses were done using one-way ANOVA with Dunnett's post hoc test. **(C)** Expression levels of *picd-1* in *pry-1* mutants. Data represent the means of two replicates and error bars represent the standard error of means. *p* values were calculated using Bio-Rad software (one-way ANOVA). In panels B and C, significant differences are indicated by stars (*): ** (p <0.01).

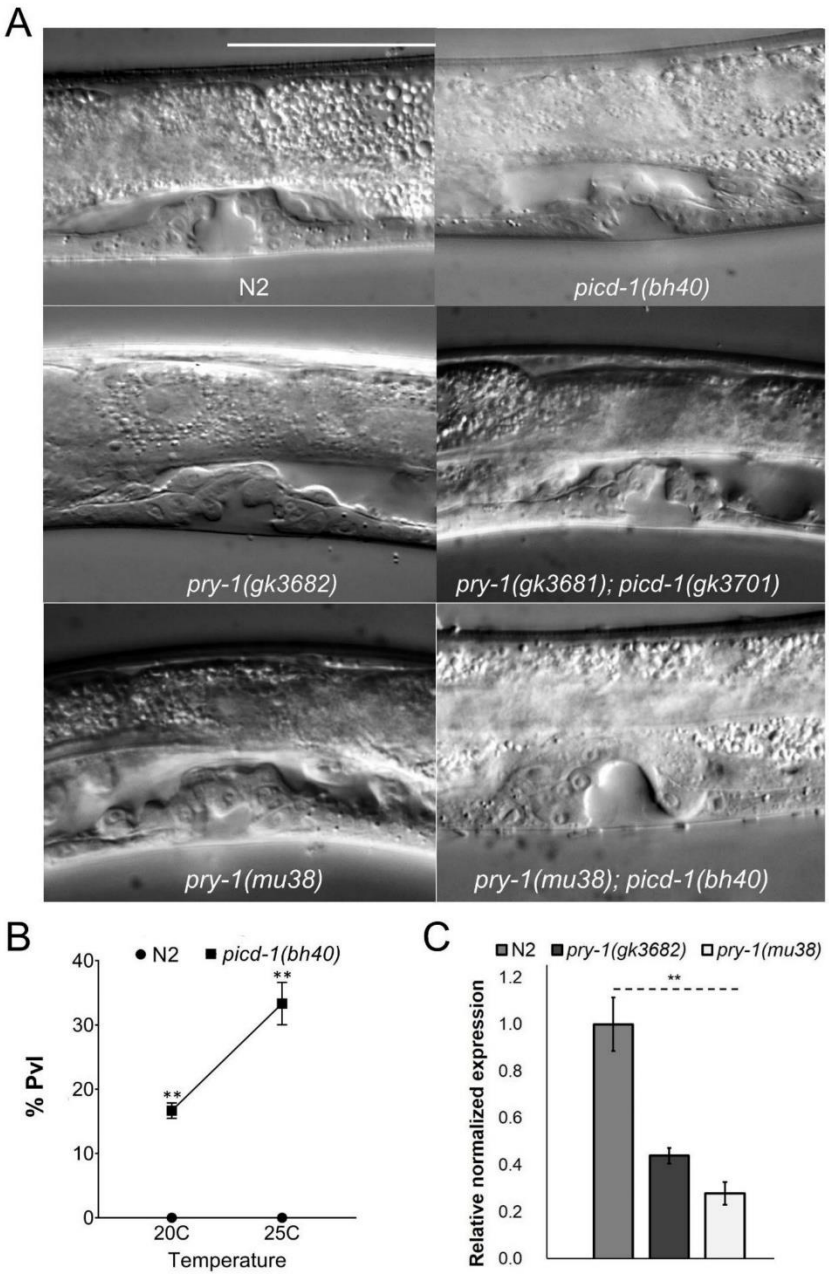
A
N2
picd-1(bh40)
pry-1(gk3682)
pry-1(gk3681); picd-1(gk3701)
pry-1(mu38)
pry-1(mu38); picd-1(bh40)
B
N2
picd-1(bh40)
% Pvl
40
30
20
10
0
**
**
20C
25C
Temperature
C
N2
pry-1(gk3682)
pry-1(mu38)
Relative normalized expression
1.2
1.0
0.8
0.6
0.4
0.2
0.0
**

630
631

Figure 5: *picd-1* regulates developmental timing, seam cell division and alae formation. (A) *picd-1* mutants exacerbate the developmental delay of *pry-1* mutants. The data shows the average time (two replicates, n > 60 animals) taken by *picd-1(bh40), pry-1(mu38)* and *pry-1(mu38); picd-1(bh40)* double mutants to reach adulthood compared to wild-type animals. The error bars represent the standard deviation. **(B)** Bar graph showing the average number of seam cells (two replicates, n > 30 animals) in the wild-type and *pry-1(mu38)* animals following control (L4440) and *picd-1* RNAi. The error bars represent the standard deviation. Statistical analyses were done using one-way ANOVA with Dunnett's post hoc test and significant differences are indicated by stars (*): * (p <0.05). **(C)** Representative images showing alae (white arrowheads) in wild-type N2 and *picd-1(bh40)* animals. Extra alae in the *picd-1* mutant are marked with *. Scale bar is 25µm.

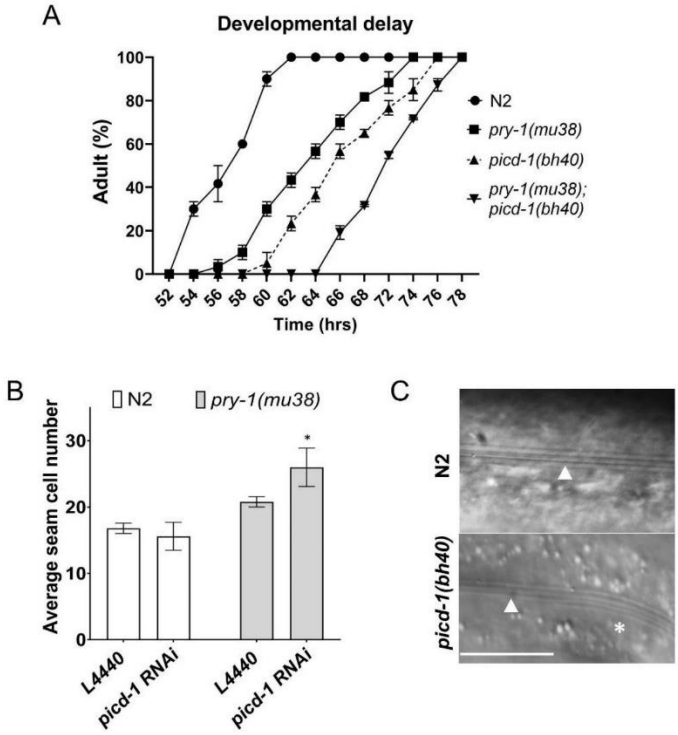

Figure 6: *picd-1* regulates brood size and embryonic viability. Bar graphs showing eggs laid on each day **(A),** totals number of eggs **(B),** and percentage of the hatched eggs. **(C)** by N2 and single and double mutant animals. Data represent a cumulative of two replicates (n > 30 animals) and error bars represent the standard deviation. Statistical analyses were done using one-way ANOVA with Dunnett's post hoc test and significant differences are indicated by stars (*): * (p <0.05), ** (p <0.01), *** (p <0.001).

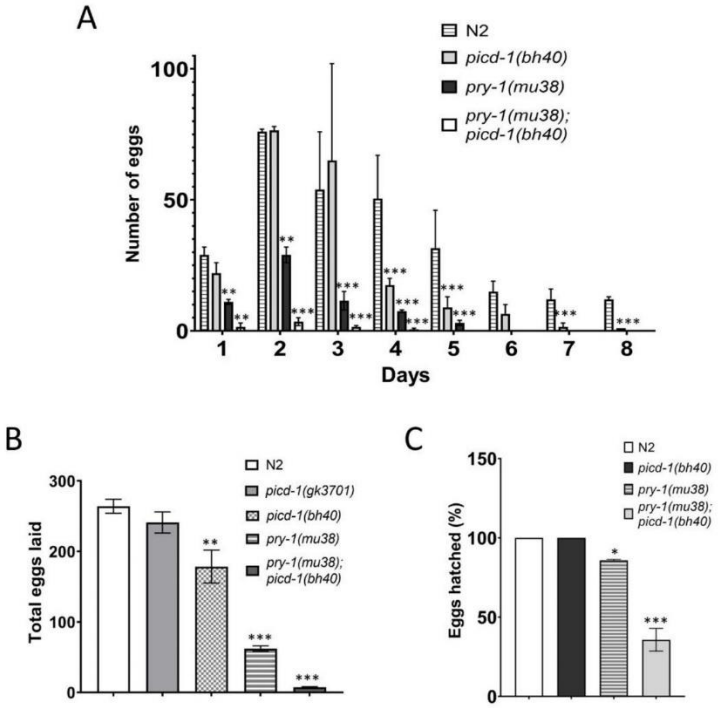

Figure 7: *picd-1* interacts with *pry-1* to regulate oocyte development. (A) *pry-1; picd-1* double mutants show abnormal oocytes and embryos morphology. Scale bar is 25µm. **(B)** Posterior gonad arms of wildtype, *picd-1(bh40), pry-1(mu38)* and *pry-1(mu38); picd-1(bh40)* adults. *pry-1(mu38); picd-1(bh40)* animals have no oocytes in the posterior gonad arm. The spermatheca (Sp), embryos (E), and oocytes (Oo) are marked. Vulva opening is shown (using #) and left to right of figure panels correspond to anterior to posterior direction. Scale bar is 0.1mm.

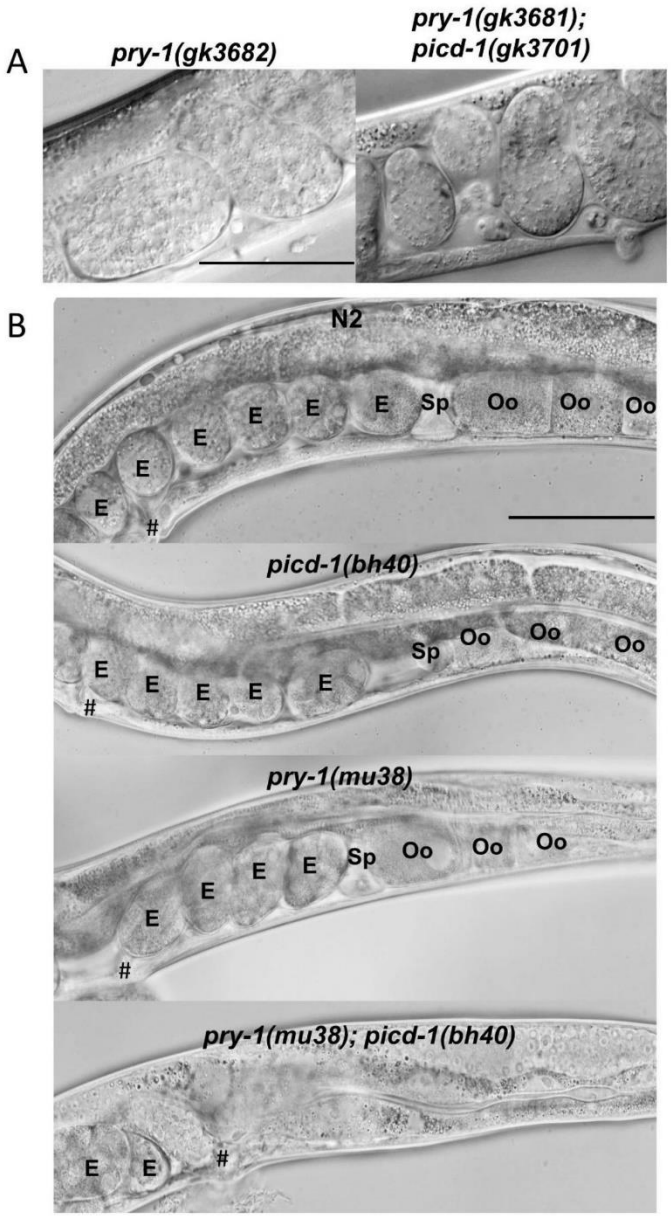
A
pry-1(gk3682)
pry-1(gk3681);
picd-1(gk3701)
B
N2
E
Sp
Oo
#
picd-1(bh40)
pry-1(mu38)
pry-1(mu38); picd-1(bh40)

660
661
662

Figure 8: *picd-1* mutants are stress sensitive. (A-B) Expression levels of *hsp-4, hsp-6, hsp-16.2*, *sod-3* and *hsf-1* in *picd-1(bh40)* and *pry-1(mu38)* young adult animals. Data represent the means of two replicates and error bars represent the standard error of means. *p* values were calculated using Bio-Rad software (one-way ANOVA) and significant differences are indicated by stars (*): ** (p <0.01). **(C)** Box and whisker plots represent normalized electrotaxis speeds of *picd-1(gk3701)*, *picd-1(bh40)*, *pry-1(mu38)* and *pry-1(mu38); picd-1(bh40)* mutants. **(D)** Bar graphs represent percentage survival following 200 mM paraquat exposure for 4 hrs. (**E)** Bar graphs represent percentage survival of animals following 25ng/µl tunicamycin exposure for 4 hrs. **(F)** Bar graphs represent percentage survival of animals following 100 mM paraquat exposure for 2 hr. For panels **C-F**, data are the cumulative of two replicates (n > 30 animals) and error bars represent the standard deviation. Statistical analyses were done using one-way ANOVA with Dunnett's post hoc test and significant differences are indicated by stars (*): * (p <0.05), ** (p <0.01).

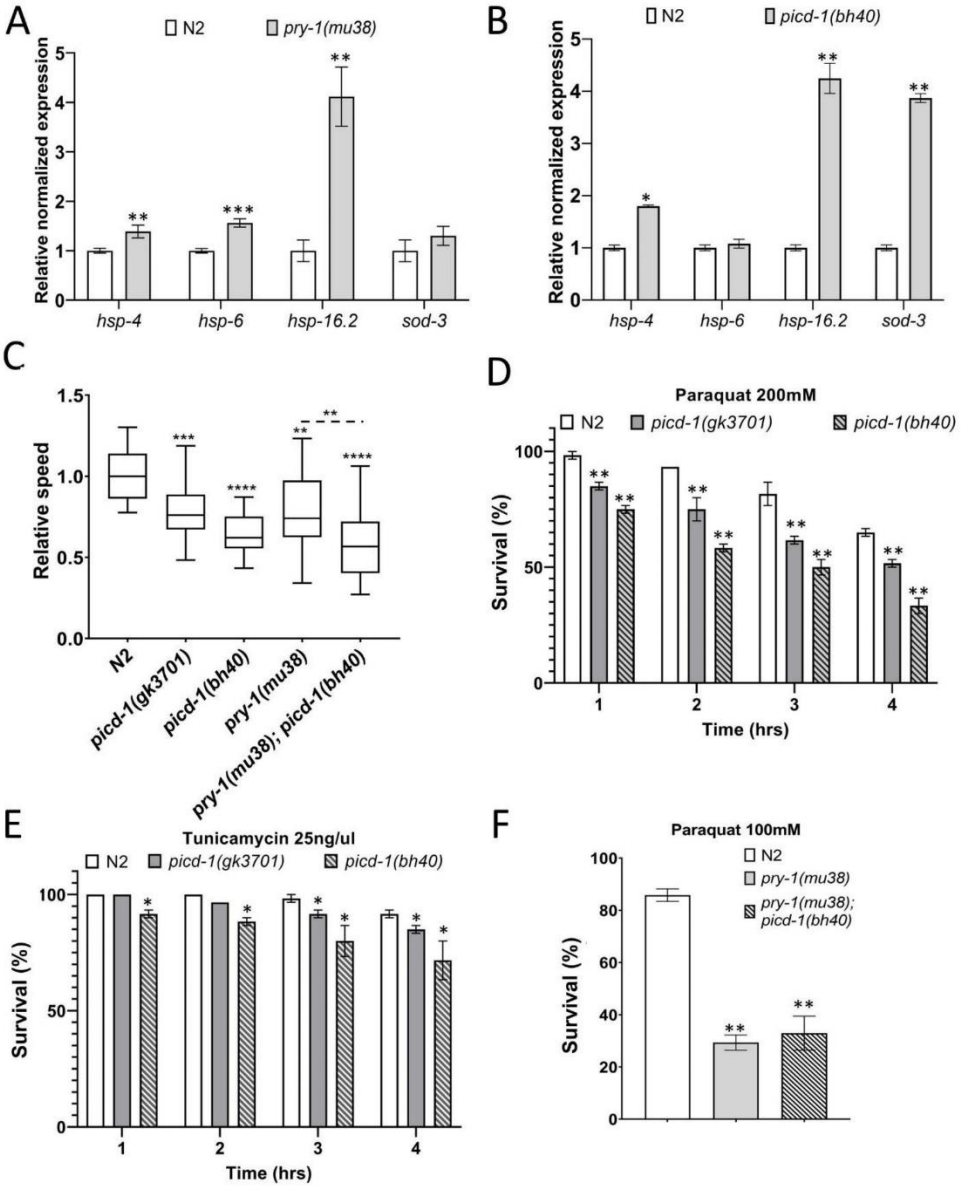

677
678
679

33

Figure 9: *picd-1* mutation reduces lifespan and causes age-associated deterioration. (A) *picd-1* mutation does not affect the lifespan of *pry-1* mutants. **(B)** *picd-1* RNAi reduces the lifespan of control animals but not that of *pry-1* mutants. **(C-D)** Lifespan of *picd-1(gk3701)* and *picd-1(bh40)* mutants at 20 ^{0}C and 25 ^{0}C. See Materials and Methods section and Table 2 for life span data and statistical analyses. **(E-F)** Bar graphs showing the rates of body bending and pharyngeal pumping of *picd-1* mutants compared to wild-type over a period of 5 days. Data represent a cumulative of two replicates (n > 15 animals) and error bars represent the standard deviation. Statistical analyses were done using one-way ANOVA with Dunnett's post hoc test and significant differences are indicated by stars (*): * (p <0.05), ** (p <0.01). **(G)** Expression analysis of *fat-5, fat-6, fat-7, nhr-49*, *nhr-80* and *sbp-1* genes in the *picd-1(bh40)* mutants compared to wild-type. Data represent the means of two replicates and error bars represent the standard error of means. p values were calculated using Bio-Rad software (one-way ANOVA) and significant differences are indicated by stars (*): ** (p <0.01). **(H)** Quantification of total lipid using Oil Red O in the wild-type and *picd-1(bh40)* animals. Data represent a cumulative of two replicates (n > 30 animals) and error bars represent the standard deviation. Statistical analysis was done using one-way ANOVA with Dunnett's post hoc test.

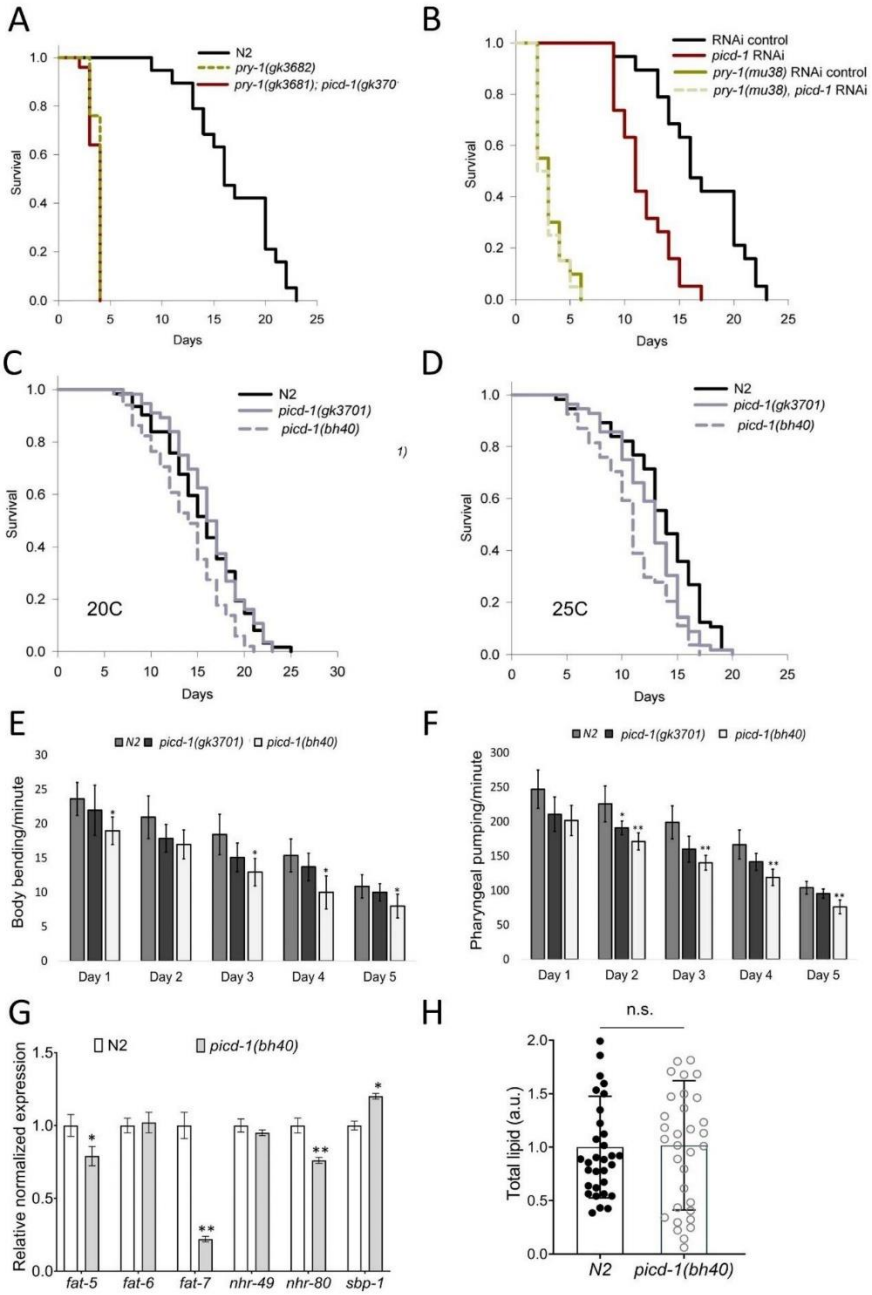
A
N2
pry-1(gk3682)
pry-1(gk3681); picd-1(gk370
Survival
Days
B
RNAi control
picd-1 RNAi
pry-1(mu38) RNAi control
pry-1(mu38), picd-1 RNAi
Survival
Days
C
N2
picd-1(gk3701)
picd-1(bh40)
20C
Survival
Days
D
N2
picd-1(gk3701)
picd-1(bh40)
25C
Survival
Days
E
N2 picd-1(gk3701) picd-1(bh40)
Body bending/minute
Day 1
Day 2
Day 3
Day 4
Day 5
F
N2 picd-1(gk3701) picd-1(bh40)
Pharyngeal pumping/minute
Day 1
Day 2
Day 3
Day 4
Day 5
G
N2
picd-1(bh40)
Relative normalized expression
fat-5
fat-6
fat-7
nhr-49
nhr-80
sbp-1
H
n.s.
Total lipid (a.u.)
N2
picd-1(bh40)

Figure 10: Loss or reduced *picd-1* function promotes CRTC-1 dependent transcriptional response. (A) *picd-1,* but not L4440 control, RNAi causes nuclear accumulation of CRTC-1::RFP fluorescence(). **(B)** qPCR analysis of *dod-24* and *asp-12* in *picd-1(bh40)* animals shows increased expression. **(C, D)** Similar experiments performed in *pry-1* mutants. n > 30 animals were examined for assays in **A** and **C**. For panels **B** and **D**, data represent the means of two replicates and error bars represent the standard error of means. *p* values were calculated using Bio-Rad software (one-way ANOVA) and significant differences are indicated by stars (*): **** (p <0.0001). **(E)** CRTC-1::RFP localization analysis in *pry-1(gk3682)* mutants following L4440 control RNAi and *bar-1* and *crtc-1* RNAi treatments (n > 30 animals). Nuclear fluorescence is absent in the case of *crtc-1* RNAi. **(F)** Lifespan of wild type and *pry-1* mutant animals following L4440 control and *crtc-1* RNAi (also see Table 2). **(G)** Bar graphs represent percentage survival of animals following 100 mM paraquat exposure for 2 hr. Data represent a cumulative of two replicates (n > 30 animals) and error bars represent the standard deviation. Statistical analyses were done using non-parametric *t* test and significant differences are indicated by stars (*): * (p <0.05), ** (p <0.01).

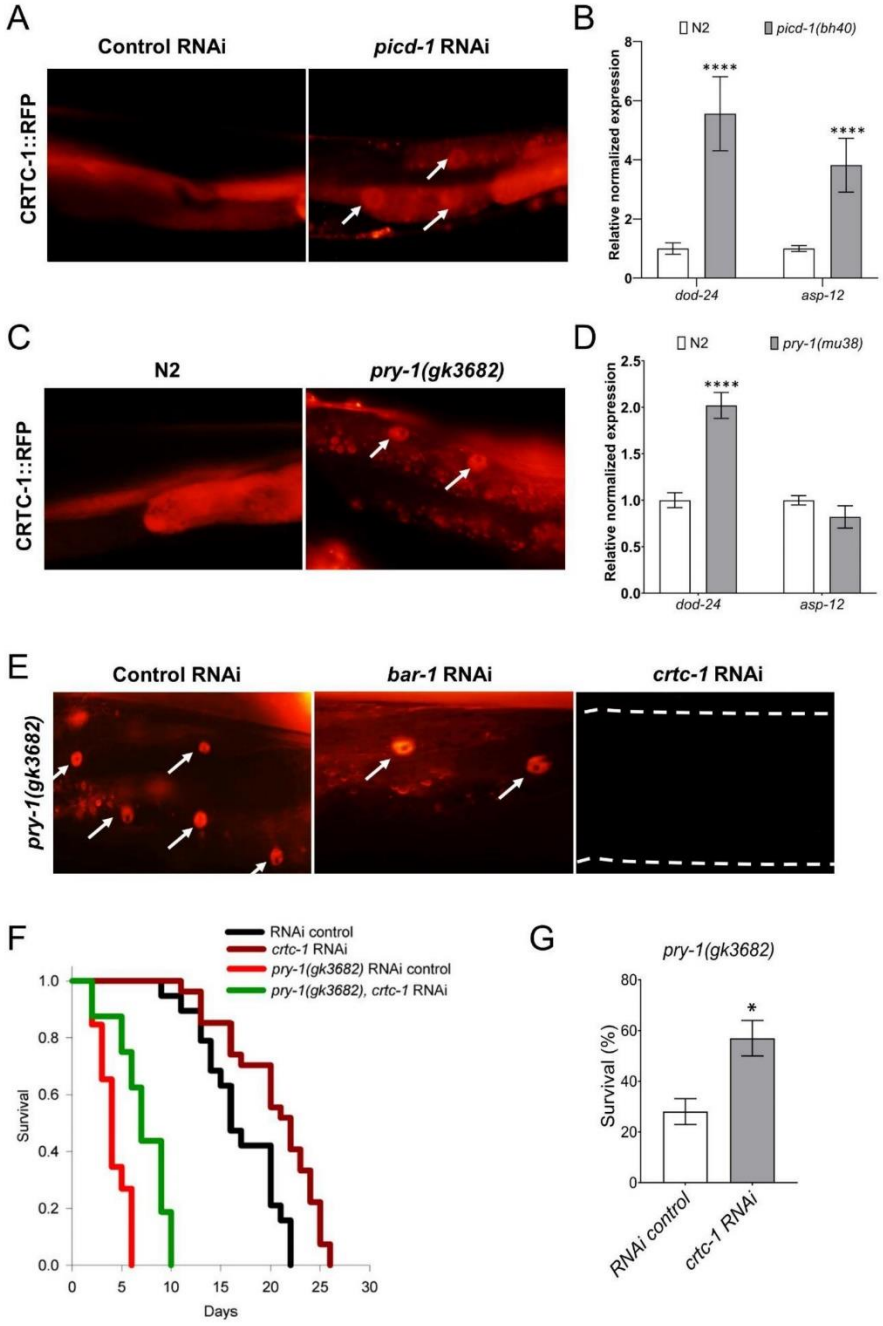
A
Control RNAi
picd-1 RNAi
CRTC-1::RFP
B
N2
picd-1(bh40)
Relative normalized expression
****
****
dod-24
asp-12
C
N2
pry-1(gk3682)
CRTC-1::RFP
D
N2
pry-1(mu38)
Relative normalized expression
****
dod-24
asp-12
E
Control RNAi
bar-1 RNAi
crtc-1 RNAi
pry-1(gk3682)
F
RNAi control
crtc-1 RNAi
pry-1(gk3682) RNAi control
pry-1(gk3682), crtc-1 RNAi
Survival
Days
G
pry-1(gk3682)
Survival (%)
*
RNAi control
crtc-1 RNAi

715

Supplementary material:

Figure S1: *picd-1* RNAi enhances the Pvl phenotype of *pry-1(mu38)* animals. Bar graph showing the percentage of *pry-1* mutants showing Pvl and Muv phenotype following control and *picd-1* RNAi. Data represent a cumulative of two replicates (n > 30 animals) and error bars represent the standard deviation. Statistical analysis was done using one-way ANOVA with Dunnett's post hoc test and significant differences are indicated by stars (*): * (p <0.05), ** (p <0.01).

Figure S2: *picd-1* mutants exhibit Egl phenotype. A graph showing the percentage of control and *picd-1(bh40)* animals with Egl phenotype at 20 ^{0}C and 25 ^{0}C. Data represent a cumulative of two replicates (n > 30 animals) and error bars represent the standard deviation. Statistical analysis was done using one-way ANOVA with Dunnett's post hoc test and significant differences are indicated by stars (*): ** (p <0.01), *** (p <0.001).

Figure S3: Common sets of genes regulated by *pry-1* and *crh-1*. Venn diagrams showing 406 DE genes shared between *pry-1* and *crh-1* mutant transcriptomes as well as overlapping genes with opposite expression trends.

Table S1: List of primers used in the study.

Video S1: Enhanced protruding vulva of *pry-1(mu38); picd-1(bh40)* animal.

Video S2: Egl defect of *picd-1(bh40)* mutants.

Figure S1: *picd-1* RNAi enhances the Pvl phenotype of *pry-1(mu38)* animals.

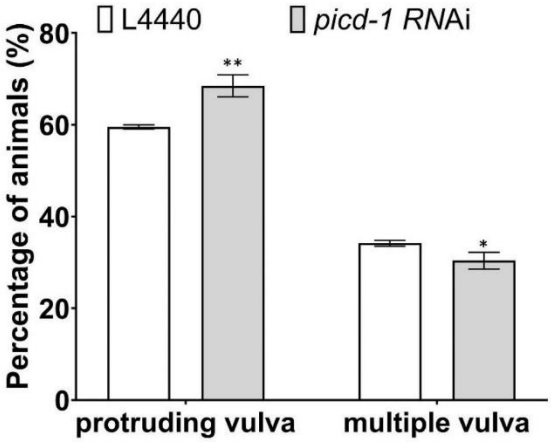

Figure S2: *picd-1* mutants exhibit Egl phenotype.

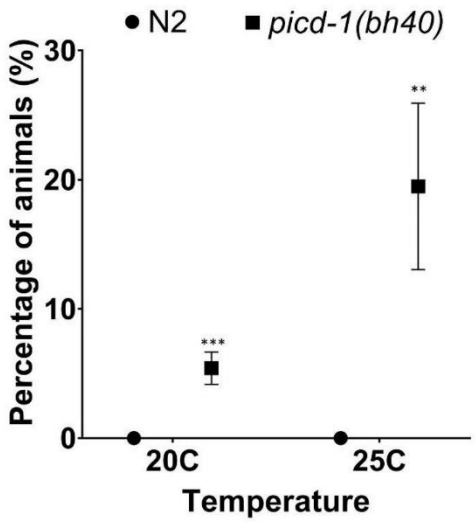

Figure S3: Common sets of genes regulated by *pry-1* and *crh-1*.

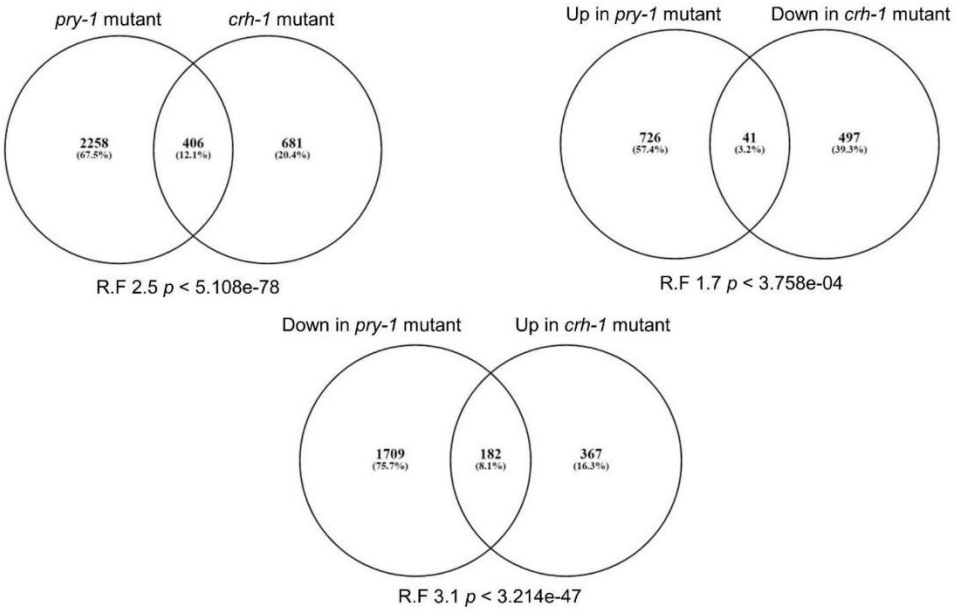

6.3 Mallick *et* al. (2022)- Submitted in Frontiers in Aging

In this study I describe the discovery of a novel FGFR4 homolog KIN-9 in *C. elegans*. Our lab uses the Axin scaffolding protein homolog, PRY-1, in *C. elegans* as a genetic model to investigate the various biological processes that it regulates. We have reported the transcriptomic profiling of *pry-1* mutants where differentially expressed genes are found to be associated with processes like lipid metabolism, stress response, and aging. Subsequently, we have also reported the *pry-1*-miRNA-transcriptome, which revealed six differentially expressed miRNAs. Five of the miRNAs (*lin-4, miR-237, miR-48, miR-84,* and *miR-241*) were upregulated, whereas one miRNA (*miR-246*) was found to be downregulated (Mallick *et al.* 2019a). Though it is evident that PRY-1 regulates both coding and non-coding genes, it remains to be investigated how this master scaffolding protein utilizes miRNAs to regulate the downstream protein-coding genes to modulate a wide range of biological events.

Here we report the role of a miRNA gene, *miR-246,* in *C. elegans* promoting an adaptation against oxidative, endoplasmic, and mitochondrial stress and maintaining normal adult lifespan. Earlier it has been noted that the *miR-246* loss of function leads to slightly reduced lifespan and increased sensitivity to heat stress. Besides, deep sequencing of aged animals revealed that *miR-246* is the highest upregulated miRNA in both wildtype and Insulin/insulin-like growth factor-1 signaling (IIS) receptor homolog *daf-2* mutant as animals got older. Although the underlying mechanism and downstream genes by which *miR-246* elucidate these processes are still unclear. Detailed genetic and gene expression studies in our lab suggest that the *mir-246* loss-induced increased sensitivity to heat, and oxidative stress is mediated by downstream

changes in expression of the target gene *kin-9*. Additionally, *kin-9* knockdown in the *miR-246* mutants rescues the stress sensitivity and short lifespan seen in these animals. Consistently, *kin-9* mutants confer longevity and stress resistivity. Further transcriptional analysis suggests that *kin-9* may be acting downstream of the PRY-1/Axin-POP-1/TCF pathway. Overall, our findings provide new insights into the unique role of the *pry-1* and *miR-246* mediated pathway in stress response.

Contributions: I performed experiments and provided data for Figures 1, 2H-I, 3F-I, 4A-E, S1, S2, S3, S4, S7 and S8; Tables S1, S2 and S3. Leo Xu and Sakshi Mehta performed experiments and provided data for Figure 2A-G. Sakshi Mehta performed experiments and provided data for Figure 3A-D and S6A-B; Table S3. Leo Xu performed experiments and provided data for Figure 4F-H and S9. Hannah Hosein performed experiments and provided data for Figures 3E, S5 and S6C-D; Table S3. I and Bhagwati Gupta created all the Figures and illustrations. I and Bhagwati Gupta conceived and supervised the project. I and Bhagwati Gupta wrote the manuscript.

The FGFR4 homolog KIN-9 regulates lifespan and stress responses in *Caenorhabditis elegans*

Avijit Mallick, Leo Xu+, Sakshi Mehta, Hannah Hossein#, and Bhagwati P Gupta*

Department of Biology, McMaster University, 1280 Main Street West, Hamilton, ON, L8S4K1, Canada

+Current address: Department of Cell and Systems Biology, University of Toronto
#Current address: Department of Biochemistry, McGill University, Montreal, Canada

Email address:
Avijit Mallick mallia1@mcmaster.ca
Leo Xu leor.xu@mail.utoronto.ca
Sakshi Mehta sakshimt@gmail.com
Hannah Hossein hannah.hosein@mail.mcgill.ca
Bhagwati P Gupta guptab@mcmaster.ca

*Author for correspondence: Bhagwati P Gupta

Running title: *kin-9/FGFR4* regulates lifespan and stress response

Keywords: *kin-9*, FGFR4, *pry-1*, *pop-1*, *miR-246*, aging, lifespan, stress response, ER-UPR, WNT signaling, FGF signaling

Brief research report
Frontiers in Aging
4000 words

ABSTRACT

Fibroblast growth factor receptors (FGFRs) are a family of receptor tyrosine kinases that regulate diverse biological processes in eukaryotes. The nematode *C. elegans* is a good system to study the roles of FGFR signaling and their mechanism of regulation. We have identified a new FGFR homolog in *C. elegans*, KIN-9, that has essential functions in aging and stress response maintenance. *kin-9* was discovered as a target of *miR-246*, a microRNA that is positively regulated by the Axin family member *pry-1*. We found that animals lacking *kin-9* function are long-lived and resistant to chemical-induced stress. Furthermore, the endoplasmic reticulum-mediated unfolded protein response (ER-UPR) pathway genes are downregulated, suggesting that *kin-9* is needed to maintain a normal ER-UPR. Among other experiments, we analyzed *kin-9* expression, which revealed its presence in the intestine, a tissue that affects the lifespan of animals. Overall, these findings demonstrate that *kin-9* is regulated by *miR-246* and may function downstream of *pry-1* in *C. elegans*. Our study forms the basis for future investigations to investigate the mechanism of microRNA mediated FGFR signaling in maintaining aging and stress response.

INTRODUCTION

Aging is a gradual deterioration of cellular and tissue function that is regulated by both genetic and environmental factors (Kenyon, 2010; Lapierre and Hansen, 2012; Uno and Nishida, 2016). Genetic factors include components of conserved signaling pathways that are associated with multiple cellular processes. Thus, it is important to identify these factors that facilitate or inhibit this inevitable detrimental process in order to develop effective interventions. We are investigating the function of an Axin scaffolding protein homolog, PRY-1, in regulating stress response and aging in the nematode *C. elegans*. To gain insights into the genetic network of *pry-1,* mRNA and miRNA transcriptome profiling experiments were carried out (Ranawade et al., 2018; Mallick et al., 2019a). These together with biochemical and genetic studies led to the identification of several major factors that interact with PRY-1 including AAK-2/AMPK, DAF-16/FOXO, and CRTC-1/CRTCs (Mallick et al., 2020, 2021b).

The miRNA transcriptome analysis revealed six differentially expressed miRNAs in *pry-1* mutants, five of which (*lin-4, miR-237, miR-48, miR-84,* and *miR-241*) were upregulated, and one (*miR-246*) was downregulated (Mallick et al., 2019a). miRNAs are non-coding RNAs that regulate target gene expression by binding to their conserved 3' untranslated region (UTR), or less common 5' UTR, and coding sequence (Stefani and Slack, 2008; Ambros and Ruvkun, 2018; O'Brien et al., 2018). Studies have shown that miRNAs regulate diverse biological processes (Ambros and Ruvkun, 2018; O'Brien et al., 2018). In this study, we focus on *miR-246* and its target in mediating *pry-1*'s role in aging and stress resistance. The *miR-246* was reported earlier as the highest fold upregulated gene during aging in both wild-type and the long-lived *daf-2* (Insulin/insulin-like

growth factor-1 signaling (IIS) receptor homolog) mutant (De Lencastre et al., 2010; Pincus et al., 2011). However, the mechanism of action of *miR-246* remains unclear.

The data presented in this paper suggest a model where *miR-246* acts downstream of PRY-1 to regulate the expression of a Fibroblast growth factor receptor (FGFR) homolog to promote longevity and stress resistance of animals. Previous studies have reported the regulation of FGF signaling by miRNAs. For example, while *miR-140* regulates *FGF9* during lungs development, *miR-200a*, *miR-20a*, and *miR217* regulate *FGF4, FGF13*, and *FGFR12* respectively during the establishment of neural crest territory (Yin et al., 2015; Copeland and Simoes-Costa, 2020). These findings, together with the essential roles of FGF signaling in development and diseases (DeVore et al., 1995; Ornitz and Itoh, 2015; Xie et al., 2020) underscore the importance of identifying regulatory mechanisms involving miRNA and FGF signaling in metazoans. In this regard, the nematode *C. elegans* serves as an attractive system since it contains conserved microRNA families and FGF signaling that can easily be targeted by forward and reverse genetic approaches. While there are twenty-three FGF family members (FGF1-23) and four fibroblast growth factor receptors (FGFRs) (FGFR1-4) in the mammalian system, *C. elegans* has two known ligands (EGL-17 and LET-756) and a single FGFR (EGL-15) (Borland et al., 2001; Ornitz and Itoh, 2015; Xie et al., 2020). Previously, EGL-17-EGL-15 signaling was shown to be required for sex muscle development (DeVore et al., 1995).

In this study, we report a new FGFR4 family member KIN-9 that is regulated by *miR-246*. KIN-9 has a conserved FGFR receptor tyrosine kinase (RTK) domain and shows a high degree of sequence and structural similarity to mammalian FGFR4s. In agreement with KIN-9 being a FGFR, we found that its overexpression phenotype resembles that of activated FGF signaling in *C. elegans*. The phenotypic analysis revealed that while *kin-9* mutants are long-lived and stress-resistant, *miR-246* mutants show opposite phenotypes. We also found that *kin-9* RNAi fully suppressed the lifespan and stress sensitivity defects of *miR-246* mutants. To further validate the regulatory relationship between *miR-246* and *kin-9*, a chimeric GFP-*kin-9*-3' UTR reporter was utilized, which showed increased fluorescence in *miR-246* mutant animals. These data together with *kin-9* being upregulated in both the *miR-246* and *pry-1* mutants, support our model of *pry-1* positively regulating *miR-246* which in turn inhibits *kin-9* expression.

The analysis of *kin-9::GFP* transgenic animals revealed that the gene is expressed in the pharynx and intestine. The presence in the intestine supports the role of *kin-9* in lifespan maintenance, similar to what has been described for many other long-lived mutants (An and Blackwell, 2003; Libina et al., 2003; Taylor and Dillin, 2013). Since *kin-9* mutants are resistant to stress, we examined the expression of unfolded protein response (UPR) pathway components and chaperons. The results showed that the endoplasmic reticulum (ER) UPR components were downregulated, suggesting that a lower *kin-9* activity is beneficial for protein homeostasis. Overall, the results

described in this study demonstrate that *miR-246* directly regulates the FGFR4 homolog kin-9 to regulate lifespan and stress response in *C. elegans*.

MATERIALS AND METHODS

Strains and worm culture

N2 *C. elegans* wild type
CB3241 *clr-1(e1745)* II
MT15020 *miR-246(n4636) IV*
NH2531 *let-60(ay75)/dpy-20(e1362) IV*
DY662 *kin-9(tm3973) X*
DY691 *unc-119(tm4063) III; bhEx289[pGLC158(kin-9p(4.3kb)::GFP)+unc-119(+)]*
DY692 *unc-119(tm4063) III; bhEx290[pGLC144(kin-9p(2.1kb)::GFP)+unc-119(+)]*
DY676 *bhEx285[pGLC146(hsp-16::kin-9) + pJH1774(myo-3p::wCherry)]*
DY700 *bhEx293[pGLC160(kin-9p(2.1kb)::GFP::kin-9 3'UTR)]*
DY703 *pry-1(mu38) I; bhEx293[pGLC160(kin-9p::GFP::kin-9 3'UTR)]*
DY705 *miR-246(n4636) IV; bhEx293[pGLC160(kin-9p::GFP::kin-9 3'UTR)]*

Plasmid construction and transgenics

Plasmids were constructed as follows. To design pGLC144, a 2,182 bp PCR-amplified (using the primers GL1350 and GL1352) fragment, spanning the promoter region and a portion of the first exon of *kin-9b.1* and *kin-9c.1*, was subcloned into the vector pPD95.81, using SphI and SalI. For pGLC158, we cloned a 4,378 bp PCR-amplified (using the primers GL1431 and GL1432) fragment, spanning the promoter region and a portion of the first exon of the *kin-9a.1* gene, into the vector pPD95.81, using the restriction sites SalI and KpnI. The pGLC160 was derived from pGLC144. This was done by replacing the unc-54 3' UTR in pGLC144 with the *kin-9* 3' UTR using the restriction sites SpeI and EcoRI. The 554 bp of *kin-9* fragment was obtained by PCR (using the primers GL1497 and GL1498). For pGLC146, we cloned a 4,715 bp PCR-amplified (using the primers GL1353 and GL1354) fragment, spanning the full-length coding sequence of the *kin-9* gene, into the vector pPD49.83, using the restriction sites KpnI and SacI.

To generate the DY691 and DY692 transgenic lines, *unc-119(tm4063)* mutants were injected with pGLC158 and pGLC144 plasmids (50 ng/µL) respectively, along with the rescue plasmid unc-119(+) (40 ng/µL). DY700 strain was generated by injecting 50 ng/µL of the pGLC160 plasmid in the N2 background. DY676 strain was generated by injecting 20 ng/µL of the pGLC146 plasmid with 30 ng/µL of the coinjection marker pJH1774 (*myo-3::wCherry*) in the N2 background.

RNAi

RNAi-mediated gene silencing was performed using a protocol previously published by our laboratory (Mallick et al., 2021a). Plates were seeded with Escherichia coli HT115 expressing either dsRNA specific to candidate genes or empty vector (L4440). Synchronized gravid adults were bleached, and eggs were plated. After becoming young adults, animals were analyzed for stress sensitivity and lifespan (Mallick et al., 2021a).

Fluorescent microscopy

Animals were paralyzed in 10mM Sodium Azide and mounted on glass slides with 2% agar pads and covered with glass coverslips for immediate image acquisition using Zeiss Apotome microscope and software.

Body bending and pharyngeal pumping

The rate of body bending per 1 min and the rate of pharyngeal pumping per 30 sec for adults were analyzed over the period of 4 days6. Hermaphrodites were analyzed for these phenotypes under the dissecting microscope in isolation on OP50 plates. Pharyngeal pumping was assessed by observing the number of pharyngeal contractions for 30 sec. For body bending assessment, animals were stimulated by tapping once on the tail of the worm using the platinum wire pick where one body bend corresponded to one complete sinusoidal wave of the worm. Only animals that moved throughout the duration of 1 min were included in the analysis.

Lifespan analysis

Lifespan experiments were done following adult-specific RNAi treatment using a previously described protocol (Mallick et al., 2020). Animals were grown on NGM OP50 seeded plates till the late L4 stage after which they were transferred to RNAi plates. For lifespan analysis at different temperatures, animals were grown till the late L4 stage at 20C following which they were shifted to either 15C or 25C. Plates were then screened daily for dead animals and surviving worms were transferred every other day till the progeny production ceased. Censoring was done for animals that either escaped, burrowed into the medium, showed a bursting of intestine from the vulva, or underwent bagging of worms (larvae hatch inside the worm and the mother dies).

Stress assay

Oxidative (paraquat) and endoplasmic reticulum mediated stress (tunicamycin) stress experiments were performed using 100mM paraquat (PQ) (Thermo Fisher Scientific, USA) and 25ng/µL tunicamycin (Sigma-Aldrich, Canada) respectively. Animals were incubated, for 2hr or over a period of 6hr, following the previously published protocol. All the final working concentrations were made in M9 instead of water. At least 50 animals were tested for each strain in each replicate. Heat stress experiments were performed by incubating the NGM plate containing at least 50 adult animals at 35C for either 2hr or over a period of 12hr. Mean and standard deviation was determined from experiments performed in duplicate. Animals were considered dead if they had no response

following a touch using the platinum wire pick and showed no thrashing or swimming movement in M9. Moreover, dead animals usually had an uncurled and straight body shape in comparison to the normal sinusoidal shape of worms.

Oil Red O staining

Neutral lipid staining was done on synchronized day-1 adult animals using Oil Red O dye (Thermo Fisher Scientific, USA) following the previously published protocol. Quantification was then done using ImageJ software as described previously.

Molecular Biology

RNA was extracted from synchronized L3 and day-1 adult animals. Protocols for RNA extraction, cDNA synthesis, and qPCR were described earlier. Briefly, total RNA was extracted using Trizol (Thermo Fisher, USA), cDNA was synthesized using the SensiFast cDNA synthesis kit (Bioline, USA), and qPCR was done using the SYBR green mix (Bio-Rad, Canada). Primers used for qPCR experiments are listed in **Supplementary Table 1**.

Statistical analyses

Statistics analyses were performed using GraphPad prism 9, SigmaPlot software 11, CFX Maestro 3.1, and Microsoft Office Excel 2019. For lifespan data, survival curves were estimated using the Kaplan- Meier test, and differences among groups were assessed using the log-rank test. qPCR data were analyzed using Bio-Rad CFX Maestro 3.1 software. For all other assays, data from repeat experiments were pooled and analyzed together and statistical analyses were done using GraphPad Prism 9. p values less than 0.05 were considered statistically significant.

RESULTS

kin-9 expression is regulated by *miR-246* and its 3' UTR contains miRNA consensus binding sites

We previously reported that PRY-1 regulates the expression of a set of miRNAs involved in heterochronic development that included *lin-4* and *let-7* family members (Mallick et al., 2019a). Another miRNA that was discovered as part of the study is *miR-246*, which is known to affect aging and stress response maintenance (De Lencastre et al., 2010). We found that *miR-246* did not affect the heterochronic phenotype of *pry-1*. Furthermore, its expression was downregulated in *pry-1(mu38)* larvae and adults (Mallick et al., 2019a).

In this study, we focus on *miR-246* and its downstream target that may modulate these biological processes. A better understanding of the biological role of miRNAs requires the identification of their direct targets. In general, miRNAs negatively regulate their target gene activity, meaning that a phenotypic consequence caused by a miRNA deletion is mediated by increasing the activity of

its target(s). We, therefore, hypothesized that *miR-246* loss-induced short lifespan and enhanced stress sensitivity would be suppressed by depletion of its target gene activity. Computational algorithms, such as TargetScan (Jan et al., 2011), PicTar (Lall et al., 2006), PITA (Kertesz et al., 2007) and STarMirDB (Rennie et al., 2016) which predict miRNA targets based on 3' UTR seed matches, were used to generate a list of *miR-246* target candidates (**Supplementary Figure 1; Supplementary Table 2**).

We tested three top listed targets: *cah-4*, *kin-9* and *pbs-5* for transcript levels in a deletion mutant of *miR-246* that deletes the entire transcript and 5' upstream sequence (*n4636:* 518bp length) (Miska et al., 2007) (**Figures 1A, B**). Based on the mechanism of miRNA function, the transcript level of a target gene is supposed to be higher than normal in the miRNA mutant background. Our results revealed that *kin-9* expression was significantly upregulated compared to control whereas no change was observed in the level of *cah-4* and *pbs-5* (**Figure 1B; Supplementary Figure 2**).

Sequence analysis revealed that KIN-9 is a homolog of the fibroblast growth factor receptor-4 (FGFR4) (http://www.wormbase.org). The receptor tyrosine kinase (RTK) domain in KIN-9 is roughly 53% similar to the mouse and human FGFR4 proteins (**Figures 1C, D**). Outside of this domain, no significant sequence similarity with FGFR4 could be detected (**Figure 1C**). We also used the secondary structure prediction tool Jpred4 (http://www.compbio.dundee.ac.uk/jpred/) (Drozdetskiy et al., 2015), which confirmed the KIN-9 homology to human FGFR4 (PDB ID: 6jpj, 6jpe, 5jkg, 4uxq, 4qrc and 4qqt). Finally, to determine whether the KIN-9 RTK domain possesses conserved tyrosine kinase phosphorylation sites present in FGFR, the online program Group-based prediction system (GPS 5) was utilized (http://gps.biocuckoo.cn/online.php) (Xue et al., 2011). The analysis revealed six such sites that, together with the secondary structure prediction, establish KIN-9 as a bona fide FGFR family member in *C. elegans* (**Supplementary Figure 3**). It is worth mentioning that a previously characterized FGFR in *C. elegans*, EGL-15, shares 50% sequence similarity with KIN-9 in the RTK domain (**Figure 1E; Supplementary Figure 4**) (Schutzman et al., 2001). The KIN-9 orthologs are also found in other nematode species (http://www.wormbase.org) (**Figures 1F**).

The *kin-9* gene is predicted to produce three isoforms of varied size (478 aa, 585aa, and 615aa), all of which have the conserved RTK domain. The longest isoforms (b and c) also possess the N-terminus signal sequence and a transmembrane alpha-helix domain (**Figures 1G, H**).

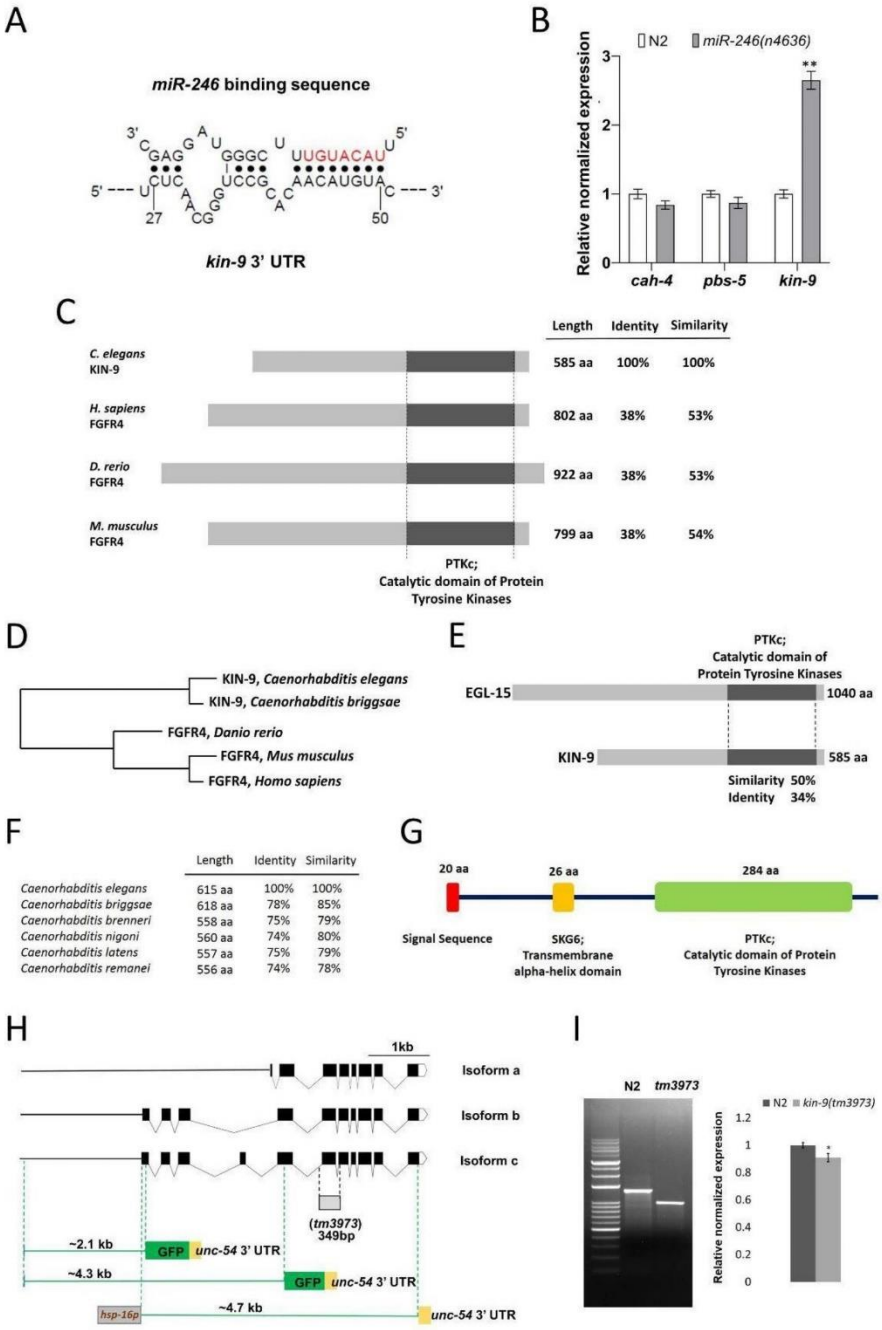
A
miR-246 binding sequence
UUGUACAU
kin-9 3' UTR
B
N2
miR-246(n4636)
Relative normalized expression
cah-4
pbs-5
kin-9
C
Length Identity Similarity
C. elegans KIN-9 585 aa 100% 100%
H. sapiens FGFR4 802 aa 38% 53%
D. rerio FGFR4 922 aa 38% 53%
M. musculus FGFR4 799 aa 38% 54%
PTKc; Catalytic domain of Protein Tyrosine Kinases
D
KIN-9, Caenorhabditis elegans
KIN-9, Caenorhabditis briggsae
FGFR4, Danio rerio
FGFR4, Mus musculus
FGFR4, Homo sapiens
E
PTKc; Catalytic domain of Protein Tyrosine Kinases
EGL-15 1040 aa
KIN-9 585 aa
Similarity 50%
Identity 34%
F
Length Identity Similarity
Caenorhabditis elegans 615 aa 100% 100%
Caenorhabditis briggsae 618 aa 78% 85%
Caenorhabditis brenneri 558 aa 75% 79%
Caenorhabditis nigoni 560 aa 74% 80%
Caenorhabditis latens 557 aa 75% 79%
Caenorhabditis remanei 556 aa 74% 78%
G
20 aa
26 aa
284 aa
Signal Sequence
SKG6; Transmembrane alpha-helix domain
PTKc; Catalytic domain of Protein Tyrosine Kinases
H
1kb
Isoform a
Isoform b
Isoform c
(tm3973) 349bp
~2.1 kb
GFP unc-54 3' UTR
~4.3 kb
GFP unc-54 3' UTR
hsp-16p
~4.7 kb
unc-54 3' UTR
I
N2 tm3973
N2 kin-9(tm3973)
Relative normalized expression

266

8

Figure 1: *miR-246* mutants show overexpression of *kin-9*. (A) The predicted binding site of *miR-246* at the 3' UTR of *kin-9* mRNA. **(B)** Expression analysis of three candidate genes cah-4, pbs-5 and *kin-9* in the *miR-246* mutants. **(C)** Schematic representation of KIN-9 and FGFR4 proteins from Caenorhabditis elegans, Homo sapiens, Danio rerio, and Mus musculus with percent identity and similarity indicated relative to *C. elegans* KIN-9. Conserved domains are aligned and are depicted with sizes, all presented to scale. **(D)** Phylogenetic tree of proteins shown in panel **(C)**. **(E)** Schematic representation of Caenorhabditis elegans KIN-9 and EGL-15 proteins with percent identity and similarity indicated. **(F)** Similarities and identities between the KIN-9 proteins in the Caenorhabditis genus. **(G)** Protein domains and structure of KIN-9 protein. **(H)** Schematic dendrograms showing all the isoforms and tm3973 deletion allele of *kin-9* with exons (black solid boxes), introns (bent lines) and upstream sequences (solid straight line). Regions used for creating transcriptional reporters and heat shock promoter-driven *kin-9* overexpression are also shown. **(I)** PCR and qPCR analyses of the tm3973 allele. Gel image showing the shorter fragment of *kin-9* transcript and bar graph showing *kin-9* mRNA levels in the tm3973 mutants. **(B and I)** Each data represents the mean of two replicates and error bars the standard error of means. Significance was calculated using Bio-Rad software (one-way ANOVA) and significant differences are indicated by stars (*): * ($p < 0.05$), ** ($p < 0.01$).

***kin-9* mutants are stress resistant and long-lived whereas *hs::kin-9* animals are stress sensitive and die prematurely**

A deletion mutant of *kin-9*, *tm3973*, was obtained from the National BioResource Project and confirmed by sequencing (https://shigen.nig.ac.jp/c.elegans). The allele carries a 349 bp long deletion (flanking 25 nucleotides: TTTTGGAGTGCAACTAGTGGTCAAC and TCGCCTACCATCCTCATCTTGTGTC) which removes a portion of the RTK domain and leads to a premature stop codon resulting in truncated proteins for the three isoforms (167 aa, 271 aa and 304 aa) (**Figure 1H**). Interestingly, cDNA analysis revealed the presence of a truncated mRNA transcript in *kin-9(tm3973)* worms indicating that readthrough transcription occurs despite the presence of 17 inframe nonsense mutations. Analysis of the cDNA band intensity and qPCR analysis of *kin-9* transcript revealed a slight difference between the control and the mutant animal (**Figure 1I**). While it is unclear whether *tm3973* allows translation to occur, any products arising from this allele would be expected to be non-functional.

The *kin-9(tm3973)* animals exhibit no obvious morphological defects but appear to have a slight growth delay, lay significantly fewer eggs, and L1 larvae show resistance to starvation (**Figures 2A-D**). Since brood size and L1 survival may be affected by lipid levels (Watts and Ristow, 2017; Ranawade et al., 2018), we carried out Oil Red O staining but found no change in neutral lipid levels (**Figure 2C**). The *tm3973* animals also show increased resistance to paraquat and tunicamycin but are sensitive to heat stress (**Figures 2E-G**). These data suggest that *kin-9* plays an important role in stress response maintenance. Further support to this conclusion also comes

from the expression analysis of ER-UPR pathway components. We found that *kin-9* mutants affect the ER-UPR pathway, as judged by reduced expression of the pathway components *ire-1, pek-1, xbp-1* and the chaperone *hsp-4* (**Figures 2H, I**). Consistent with these results, mutants exhibit electrotaxis defects associated with chronic stress (**Figure 2J**) (Taylor et al., 2021). No change in mitochondrial UPR components was detected in the absence of *kin-9* function (**Figures 2H, I**).

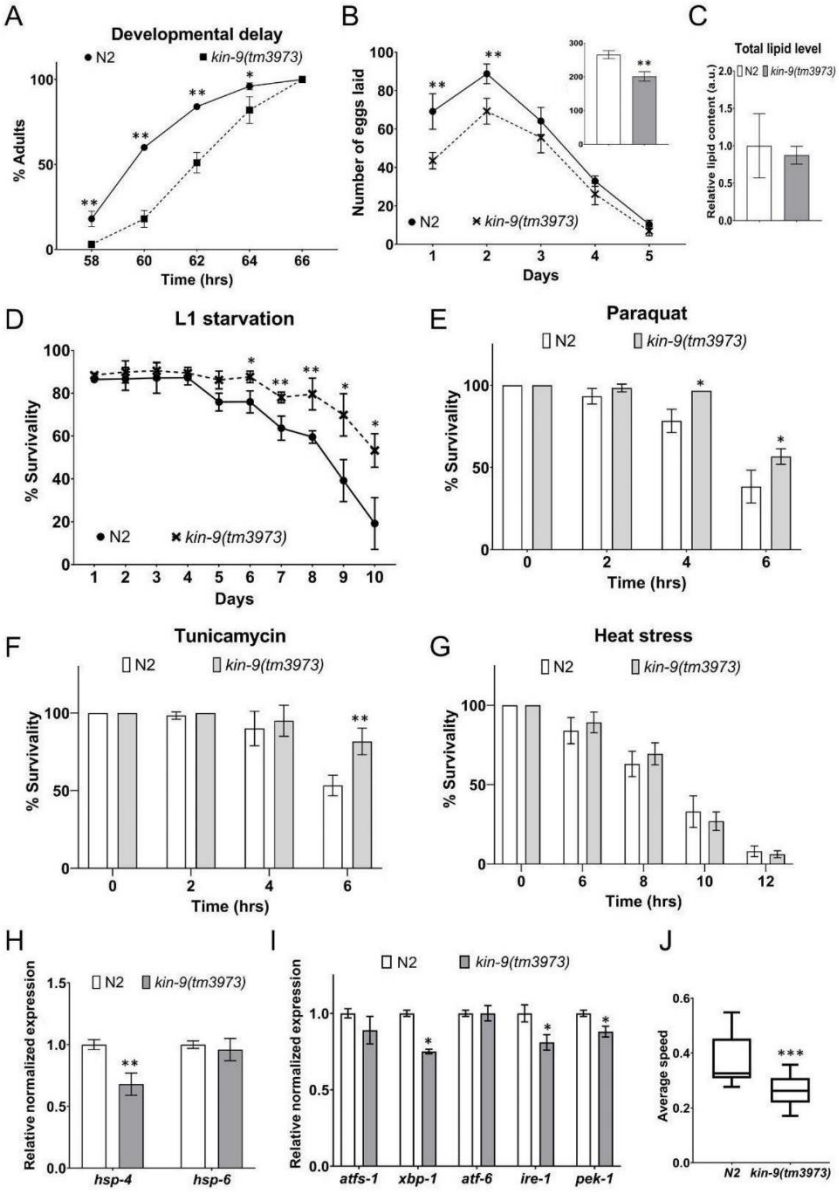

Figure 2: *kin-9* mutants exhibit resistance to heat and chemical-induced stress. (B) Line graph showing the number of eggs laid by *kin-9* mutants compared to N2. Smaller bar graph showing the total number of eggs laid (N2- clear bar; *kin-9(tm3973)* grey bar). **(C)** Quantification of neutral lipids using Oil Red O staining. **(D)** Survival graph of *kin-9(tm3973)* L1 worms upon starvation

compared to N2. **(E-F)** Bar graph showing the survivability of *kin-9* mutants compared to N2 following paraquat (200mM) and tunicamycin (25ng/uL) over a period of six hours. **(G)** Survivability of *kin-9* mutants compared to N2 at 35°C over a period of 12 hours. **(H-I)** qPCR analysis of *hsp-4, hsp-6, atfs-1, xbp-1, atf-6, ire-1,* and *pek-1* in *kin-9(tm3973)* adults compared to N2. Data in **(H-I)** represent the mean of two replicates and error bars the standard error of means. Significance was calculated using Bio-Rad software (one-way ANOVA) and significant differences are indicated by stars (*): * ($p < 0.05$), ** ($p < 0.01$). **(J)** Electrotaxis analysis of day-1 *kin-9(tm3973)* adults. **(A-G and I)** Data represent the mean of two replicates (n > 40 animals in each replicate) and error bars represent the standard deviation. Statistical analyses were done using multiple unpaired t-tests and significant differences are indicated by stars (*): * ($p < 0.05$), ** ($p < 0.01$), *** ($p < 0.001$).

Since *miR-246* mutants are short-lived (De Lencastre et al., 2010), we examined the lifespan phenotype of animals lacking *kin-9* function. Consistent with *kin-9* being a downstream target, mutant animals show an extension in lifespan (**Figures 3A; Supplementary Table 3**). Similar lifespan changes were observed in RNAi-treated animals (**Figure 3B; Supplementary Table 3**). The mutants exhibit slightly increased body bending rates but no change in pharyngeal pumping (**Figures 3C, D**).

If the absence of *kin-9* results in lifespan extension, then increased levels of the gene should give rise to an opposite phenotype. To test this possibility, *hsp::kin-9* transgenic lines were generated to overexpress *kin-9* by subjecting animals to heat treatments (See Methods). A high level of *kin-9* expression in these animals was confirmed using qPCR (**Supplementary Figure 5**). Consistent with a longer lifespan of *kin-9* mutants, transgenic animals overexpressing *kin-9* were small, short-lived, and showed slower pharyngeal pumping and body bending (**Figures 3F, G; Supplementary Figure 6, 7**). The aging phenotype was similar at other growth temperatures (15C and 25C, **Supplementary Figure 6; Supplementary Table 3)**. Moreover, *hsp::kin-9* animals exhibited increased stress sensitivity to both paraquat and tunicamycin (**Figures 3H, I**). Altogether, these data demonstrate an important role of *kin-9* in regulating the normal lifespan and stress responses of animals.

Interestingly, we observed that the *hsp::kin-9* animals were unusually transparent when grown at 25C (**Supplementary Figure 7**), an appearance that resembled 'clear (clr)' phenotype reported earlier in *C. elegans* that have activated FGF signaling (**Supplementary Figure 7**) (Borland et al., 2001). Clr phenotype is characterized by the accumulation of clear fluid within the pseudocoelomic cavity. Thus, animals appear to have a floating intestine with fluid-filled body cavities as well as being short, immobile, and sterile (Borland et al., 2001; Schutzman et al., 2001). Such a phenotype is also seen in other FGF pathway component mutants (Schutzman et al., 2001).

However, whether such an attribute in *hsp::kin-9* animals is caused by changes in FGF pathway components is currently unknown.

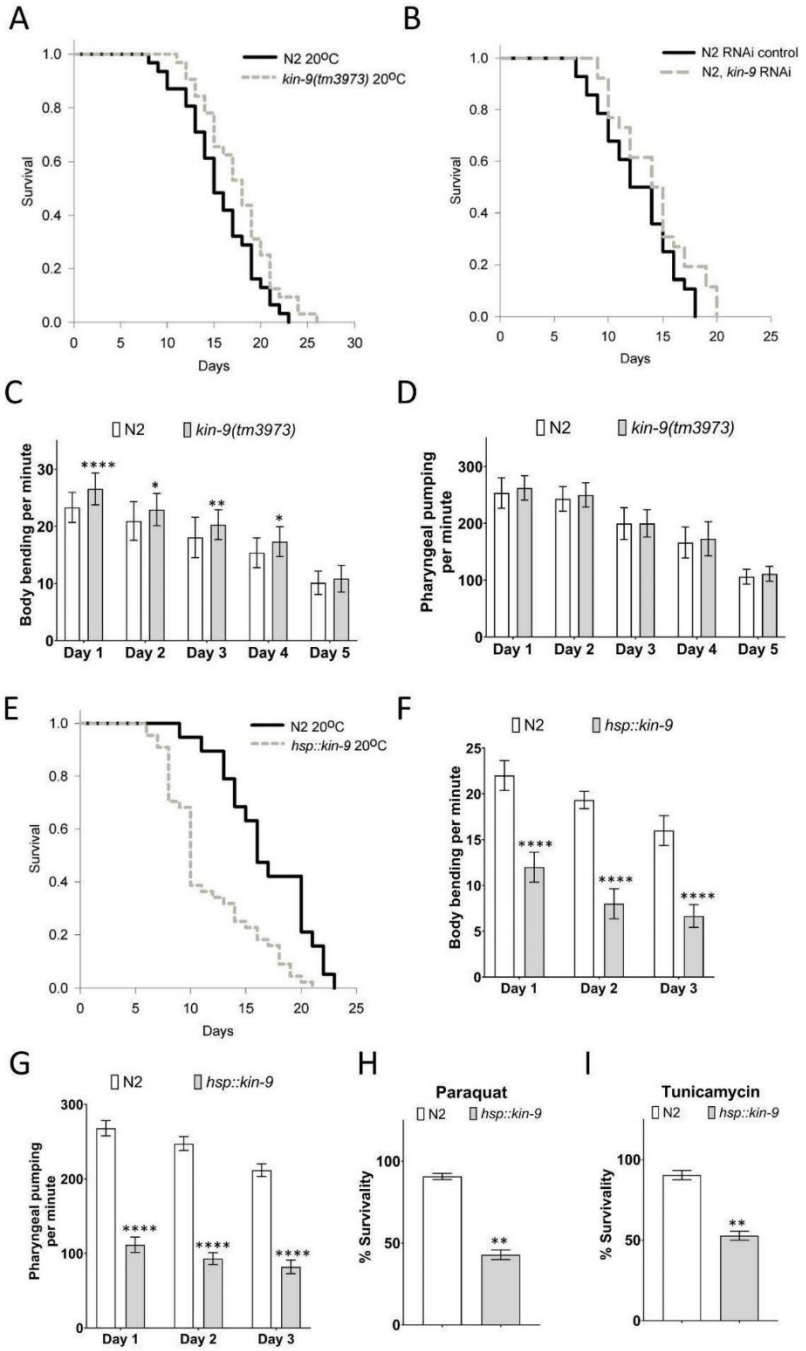
A
N2 20ºC
kin-9(tm3973) 20ºC
Survival
Days
B
N2 RNAi control
N2, kin-9 RNAi
Survival
Days
C
N2
kin-9(tm3973)
Body bending per minute
Day 1
Day 2
Day 3
Day 4
Day 5
D
N2
kin-9(tm3973)
Pharyngeal pumping per minute
Day 1
Day 2
Day 3
Day 4
Day 5
E
N2 20ºC
hsp::kin-9 20ºC
Survival
Days
F
N2
hsp::kin-9
Body bending per minute
Day 1
Day 2
Day 3
G
N2
hsp::kin-9
Pharyngeal pumping per minute
Day 1
Day 2
Day 3
H
Paraquat
N2
hsp::kin-9
% Survivality
I
Tunicamycin
N2
hsp::kin-9
% Survivality

361

14

Figure 3: Loss of *kin-9* function causes a reduced lifespan. (A) Lifespan graphs of *kin-9(tm3973)* mutants compared to N2 **(B)** Lifespan analysis of animals following control and *kin-9* RNAi knockdown during adulthood. **(C-D)** Bar graphs showing the rate of body bending and pharyngeal pumping in *kin-9* mutants compared to N2 over a period of five days. **(E)** Lifespan graphs of *hsp::kin-9* animals compared to N2. **(A-B, E)** See the Methods section and **Supplementary Table 3** for statistics performed. **(F-G)** Bar graph showing the survivability of *hsp::kin-9* adults compared to N2 following paraquat (200mM) and tunicamycin (25ng/uL) exposure for 2hrs. **(C-D, F-I)** Data represent the mean of two replicates (n > 10/day animals in each replicate for **C-D** and **F-G**; n> 50 animals in each replicate for **H-I**) and error bars represent the standard deviation. Statistical analyses were done using multiple unpaired t-tests with Welch correction and significant differences are indicated by stars (*): ** ($p < 0.01$), *** ($p < 0.001$).

***kin-9* is expressed in the pharynx, intestine, and tail region**

Given the *kin-9's* essential role in *C. elegans*, we wanted to identify cells and tissues where the gene is expressed. To this end, transgenic strains carrying *kin-9::GFP* reporters were generated. Two different constructs were utilized (see Methods), the longest of which (4.3 kb) contains a part of an exon that is common to all isoforms whereas the shorter one (2.1 kb) is specific to isoforms b and c (**Figure 1H**). GFP fluorescence analysis of transgenic lines showed expression throughout the lifespan, which agrees well with the previously published transcriptomic data (Grun et al 2014, Golden et al 2008). We found that *kin-9p(2.1kb)::GFP* adults have GFP fluorescence in the pharynx, intestine, and certain cells located in the tail (**Figure 4A**). While the *kin-9p(4.3kb)::GFP* animals exhibit a similar pattern, interestingly no fluorescence was observed in the posterior region (**Supplementary Figure 8**). It may be that the longer fragment has certain inhibitory sequences that contribute to expression differences. More experiments involving dissection of regulatory sequences are needed to investigate this possibility. The intestinal expression of *kin-9* and its persistence during adulthood aligns with many other genes with known roles in lifespan extension and stress response maintenance (An and Blackwell, 2003; Libina et al., 2003; Taylor and Dillin, 2013). The specific role of *kin-9* in the pharynx remains to be determined.

***kin-9* 3'UTR is targeted by *miR-246* and *kin-9* RNAi rescues *miR-246(n4636)* defects**

Since miRNAs function mainly through binding to the 3' UTR of target genes (Ambros and Ruvkun, 2018; O'Brien et al., 2018), we decided to examine whether *miR-246* affects transcriptional regulation of *kin-9*. To this end, transgenic lines were generated containing a chimera of GFP and *kin-9* 3' UTR under the control of the *kin-9* promoter (*kin-9p(2.1kb)::GFP::kin-9UTR*) (See methods; **Figure 4B**). As expected, the GFP fluorescence showed a roughly four-fold increase when the construct was introduced in *miR-246(n4636)* animals (**Figure 4C**). Since *miR-246* is positively regulated by *pry-1* (Mallick et al., 2019a), we also examined *kin-9p(2.1kb)::GFP::kin-9UTR* fluorescence in *pry-1* mutants and found a similar upregulation (**Figure 4C**). Consistent with this, the qPCR analysis revealed that *kin-9* transcript

levels were high in animals lacking *pry-1* function (**Figure 4D**). Altogether, these data show that *pry-1* and *miR-246* negatively regulate *kin-9* expression.

As the *kin-9* expression is upregulated in *miR-246* mutants and that *miR-246* directly regulates *kin-9* transcript levels, it led us to test whether *miR-246(n4636)* phenotypes can be rescued by reducing *kin-9* function. The lifespan and stress sensitivity defects of *miR-246* mutants were indeed fully rescued upon *kin-9* RNAi (**Figures 4E-H; Supplementary Figure 9, Supplementary Table 3**). Together with transcript analysis and data in previous sections, the results demonstrate that *kin-9* is involved in lifespan regulation and acts downstream of *miR-246*. Interestingly, no phenotypic rescue was observed by knocking down *kin-9* in *pry-1* mutant animals (**Supplementary Table 3)**, which suggests that *kin-9* is not the sole effector of *pry-1* function in aging-related processes. The findings are consistent with *pry-1* interacting with multiple pathway components to regulate aging and stress response in *C. elegans*.

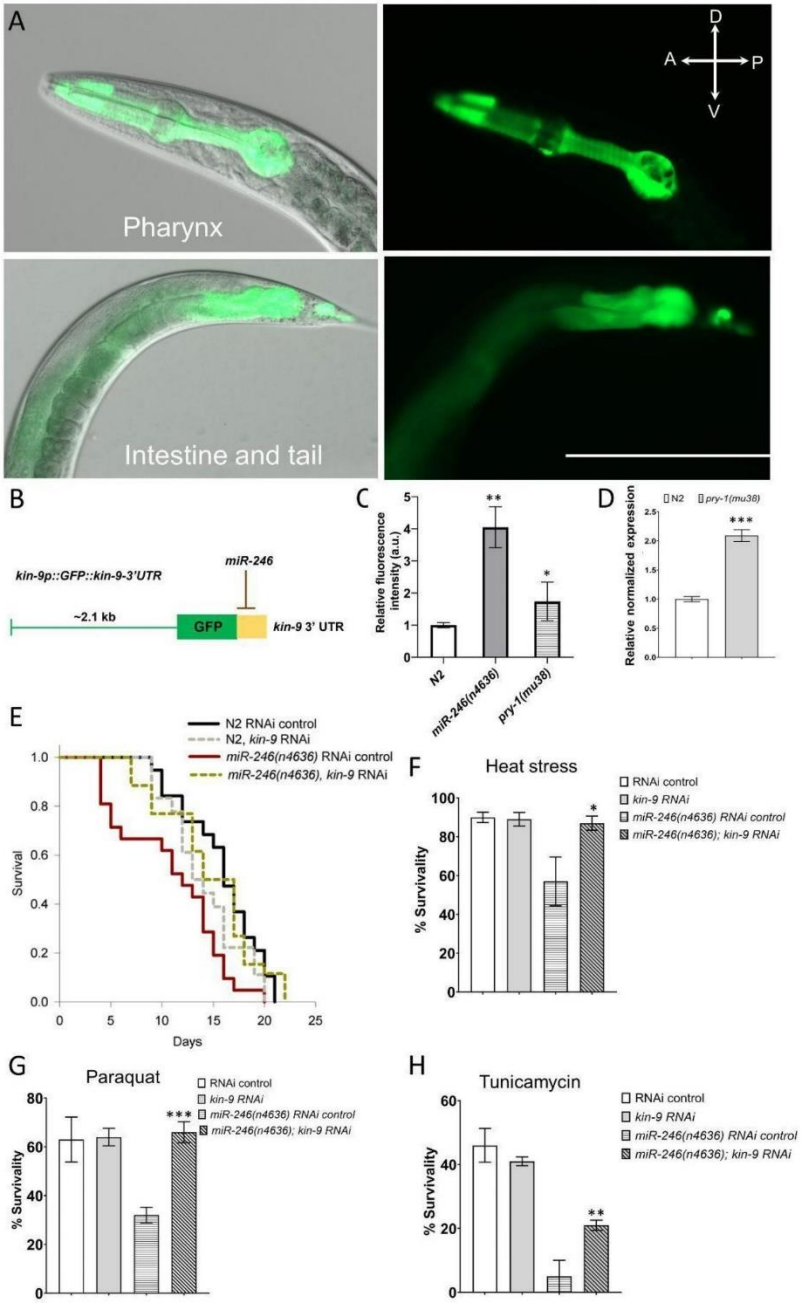
A
Pharynx
D
A
P
V
Intestine and tail
B
kin-9p::GFP::kin-9-3'UTR
miR-246
~2.1 kb
GFP
kin-9 3' UTR
C
Relative fluorescence intensity (a.u.)
N2
miR-246(n4636)
pry-1(mu38)
D
N2
pry-1(mu38)
Relative normalized expression
E
N2 RNAi control
N2, kin-9 RNAi
miR-246(n4636) RNAi control
miR-246(n4636), kin-9 RNAi
Survival
Days
F
Heat stress
RNAi control
kin-9 RNAi
miR-246(n4636) RNAi control
miR-246(n4636); kin-9 RNAi
% Survivality
G
Paraquat
RNAi control
kin-9 RNAi
miR-246(n4636) RNAi control
miR-246(n4636); kin-9 RNAi
% Survivality
H
Tunicamycin
RNAi control
kin-9 RNAi
miR-246(n4636) RNAi control
miR-246(n4636); kin-9 RNAi
% Survivality

Figure 4: Lowering *kin-9* activity suppresses *miR-246* mutant defects. (A) *kin-9p(2.1kb)::GFP* analysis shows expression in the pharynx, intestine, and tail neurons. **(B)** Schematic diagram of a *kin-9p::GFP::kin-9 3' UTR* construct showing potential *miR-246* binding at the 3' UTR of the kin-9 mRNA transcript. **(C)** Bar graph showing the GFP analysis using the array *kin-9p::GFP::kin-9 3' UTR* in *miR-246*(n4636) and *pry-1(mu38)* adults compared to control. Data represent the mean of two replicates (n > 25 animals in each replicate) and error bars represent the standard deviation. Statistical analyses were done using one-way ANOVA with Dunnett's post hoc test and significant differences are indicated by stars (*): * ($p < 0.05$), ** ($p < 0.01$). **(D)** qCPR analysis of *kin-9* gene in the *pry-1(mu38)* adults compared to control. Data represent the mean of two replicates and error bars the standard error of means. Significance was calculated using Bio-Rad software (one-way ANOVA) and significant differences are indicated by stars (*): *** ($p < 0.001$). **(E)** Lifespan analysis of N2 and *miR-246(n4636)* animals following control and *kin-9* RNAi knockdown. See the Methods section and **Supplementary Table 3** for statistics performed. **(F-H)** Bar graphs showing survivability of N2 and *miR-246(n4636)* animals following control and *kin-9* RNAi when exposed to heat stress (35C), paraquat (200mM for 2 hours) and tunicamycin (25ng/uL for 2 hours). Data represent the mean of two replicates (n > 50 animals in each replicate) and error bars represent the standard deviation. Statistical analyses were done using one-way ANOVA with Dunnett's post hoc test and significant differences are indicated by stars (*): * ($p < 0.05$), ** ($p < 0.01$).

DISCUSSION

We have identified *kin-9* as a new target of the microRNA *miR-246* and demonstrated its essential function in regulating stress responses and lifespan in *C. elegans*. The sequence analysis of KIN-9 protein has revealed that it is a member of the FGFR family, specifically FGFR4. Further support to KIN-9 being a *C. elegans* FGFR comes from our data showing that overexpression of *kin-9* causes a Clr phenotype which is associated with activated FGF signaling (Borland et al., 2001; Schutzman et al., 2001).

Our work has revealed that *kin-9* is a direct target of the microRNA *miR-246*. The *miR-246* was identified earlier in a transcriptomic study in our lab that is positively regulated by *pry-1* (Mallick et al., 2019a). Given that *miR-246* is necessary for lifespan maintenance (De Lencastre et al., 2010), we were interested in identifying its targets to further understand the downstream components of the *pry-1-miR-246* genetic network. While the silico analysis revealed three genes with consensus *miR-246* binding sites in their 3' UTR, *kin-9* was the only one with increased expression in the *miR-246* mutant background. Consistent with *kin-9* being a bona fide target of *miR-246*, a GFP transgene containing *kin-9* 3' UTR responded to the *miR-246* activity, i.e., in the absence of *miR-246*, GFP fluorescence was significantly upregulated.

The analysis of *kin-9* mutants has revealed that the gene is necessary for regulating the stress response and aging. While animals lacking *kin-9* function showed resistance to stress treatments, reduced expression of heat shock chaperon and ER-UPR genes, and a longer lifespan, the transgenic lines overexpressing *kin-9* showed opposite phenotypes. Consistent with these roles, *kin-9* is expressed in the intestine, a tissue known to be the primary player involved in nutrient uptake and metabolic activities (Libina et al., 2003; Rera et al., 2013). Studies on aging have shown that the intestine communicates with other parts of the body such as neurons and muscles and leads to activation of downstream effectors. The IIS transcription factor DAF-16 that functions mainly in the neurons and intestine, affects muscle health and mitochondrial mass suggesting cross-talks between these tissues (Libina et al., 2003; Uno and Nishida, 2016; Wang et al., 2019; Mallick et al., 2020; Gupta, 2022). Thus, it is conceivable that *kin-9* regulates the stress responses and lifespan by maintaining a healthy gut which in turn signals other tissues to promote their health.

The work described here suggests that FGFR signaling in *C. elegans* is regulated by a microRNA. Our data support a model where *pry-1* promotes *miR-246* expression which in turn inhibits *kin-9*. However, the precise mechanism of this genetic relationship remains to be investigated. While our data showed that *kin-9* expression is inhibited by *pry-1*, its knock down was unable to suppress the *pry-1* phenotype, suggesting that *kin-9* alone is not sufficient to modulate *pry-1* signaling. Additionally, it is unknown whether *kin-9* may be regulated by *pry-1* in a WNT-dependent manner. Previous studies on *pry-1*/Axin have revealed its genetic network that includes multiple signaling components (Mallick et al., 2019b). For example, PRY-1 interacts with AAK-2/AMPK in the muscle in a cell nonautonomous manner to regulate DAF-16 in the intestine to promote the lifespan and muscle health of animals (Mallick et al., 2020). PRY-1 also regulates CABIN1 domain-containing protein PICD-1 to affect calcineurin signaling and CRTC-1 dependent transcription (Mallick et al., 2021b). More recently, we have identified several genes (cpz-1/CTSZ, cdk-1/CDK1, rnr-1/RRM1, his-7/H2AX, and ard-1/HSD17B10) that function downstream of PRY-1 to regulate the lifespan and stress response of animals (Mallick et al., 2021a). Taken together these findings demonstrate that *pry-1* is a master regulator of aging-related processes and functions by coordinating activities of diverse genes and pathways.

KIN-9 is the first FGFR family member in *C. elegans* that plays essential roles in aging and stress response maintenance. Earlier, it was found that the homologs of transmembrane protein Klotho (KLO-1 and KLO-2) require EGL-15-EGL-17 to promote similar processes (Château et al., 2010). Studies in higher eukaryotes have also shown that Klotho promotes lifespan and functions as a co-receptor of FGFRs (Kuro-o et al., 1999; Ornitz and Itoh, 2015). Consistent with the interaction between Klotho and FGFRs, there is some evidence that mammalian FGFs affect aging related changes. For example, the age-associated impairment of human mesenchyme-derived progenitor cells can be reversed by FGF2 treatment (Hurley et al., 2016). Additionally, the activated FGF2 pathway causes an increased fat accumulation in aged human skeletal muscles (Mathes et al., 2021).

The genetic analysis of *kin-9* as a target of *miR-246* and its potential role in the *pry-1* network provides opportunities to investigate the underlying mechanism and its conservation. Whether *kin-9* utilizes known downstream components of the FGF signaling remains to be determined. In this regard, it is interesting to note that *kin-9* RNAi was found to delay the development of *let-60* mutant animals (Byrne et al., 2007). The identification of *kin-9* pathway components and their interactions with *pry-1* hold significant promise to advance our understanding of Axin function in stress maintenance and aging.

ACKNOWLEDGEMENTS

This work was supported by the NSERC Discovery grant to Bhagwati Gupta and NSERC CGS-D scholarship to Avijit Mallick. Some of the strains were obtained from the *Caenorhabditis* Genetics Center (CGC), which is funded by the NIH Office of Research Infrastructure Programs (P40 OD010440).

REFERENCES

Ambros, V., and Ruvkun, G. (2018). Recent molecular genetic explorations of caenorhabditis elegans microRNAs. *Genetics* 209, 651–673. doi:10.1534/genetics.118.300291.

An, J. H., and Blackwell, T. K. (2003). SKN-1 links C. elegans mesendodermal specification to a conserved oxidative stress response. *Genes Dev.* 17, 1882–1893. doi:10.1101/gad.1107803.

Borland, C. Z., Schutzman, J. L., and Stern, M. J. (2001). Fibroblast growth factor signaling in Caenorhabditis elegans. *BioEssays* 23, 1120–1130. doi:10.1002/bies.10007.

Byrne, A. B., Weirauch, M. T., Wong, V., Koeva, M., Dixon, S. J., Stuart, J. M., et al. (2007). A global analysis of genetic interactions in Caenorhabditis elegans. *J. Biol.* 6. doi:10.1186/jbiol58.

Château, M. T., Araiz, C., Descamps, S., and Galas, S. (2010). Klotho interferes with a novel FGF-signalling pathway and insulin/Igf-like signalling to improve longevity and stress resistance in Caenorhabditis elegans. *Aging (Albany. NY).* 2, 567–581. doi:10.18632/aging.100195.

Copeland, J., and Simoes-Costa, M. (2020). Post-transcriptional tuning of FGF signaling mediates neural crest induction. *Proc. Natl. Acad. Sci. U. S. A.* 117, 33305–33316. doi:10.1073/PNAS.2009997117.

De Lencastre, A., Pincus, Z., Zhou, K., Kato, M., Lee, S. S., and Slack, F. J. (2010). MicroRNAs both promote and antagonize longevity in C. elegans. *Curr. Biol.* 20, 2159–2168. doi:10.1016/j.cub.2010.11.015.

DeVore, D. L., Horvitz, H. R., and J.Stern, M. (1995). An FGF receptor signaling pathway is required for the normal cell migrations of the sex myoblasts in C. elegans hermaphrodites. *Cell* 83, 611–620. doi:10.1016/0092-8674(95)90101-9.

Drozdetskiy, A., Cole, C., Procter, J., and Barton, G. J. (2015). JPred4: A protein secondary

structure prediction server. *Nucleic Acids Res.* 43, W389–W394. doi:10.1093/nar/gkv332.
Gupta, B. P. (2022). AXIN-AMPK signaling : Implications for healthy aging [version 1 ; peer review : 2 approved with reservations] Avijit Mallick. 1–13.
Hurley, M. M., Gronowicz, G., Zhu, L., Kuhn, L. T., Rodner, C., and Xiao, L. (2016). Age-Related Changes in FGF-2, Fibroblast Growth Factor Receptors and β-Catenin Expression in Human Mesenchyme-Derived Progenitor Cells. *J. Cell. Biochem.* 117, 721–729. doi:10.1002/jcb.25357.
Jan, C. H., Friedman, R. C., Ruby, J. G., and Bartel, D. P. (2011). Formation, regulation and evolution of Caenorhabditis elegans 3'UTRs. *Nature* 469, 97–103. doi:10.1038/nature09616.
Kenyon, C. J. (2010). The genetics of ageing. *Nature* 464, 504–512. doi:10.1038/nature08980.
Kertesz, M., Iovino, N., Unnerstall, U., Gaul, U., and Segal, E. (2007). The role of site accessibility in microRNA target recognition. *Nat. Genet.* 39, 1278–1284. doi:10.1038/ng2135.
Kuro-o, M., Matsumura, Y., Arawa, H., Kawaguchi, H., Suga, T., Utsugi, T., et al. (1999). Mutation of the mouse klotho gene leads to a syndrome resembling ageing. *Chemtracts* 12, 703–707.
Lall, S., Grün, D., Krek, A., Chen, K., Wang, Y. L., Dewey, C. N., et al. (2006). A genome-wide map of conserved MicroRNA targets in C. elegans. *Curr. Biol.* 16, 460–471. doi:10.1016/j.cub.2006.01.050.
Lapierre, L. R., and Hansen, M. (2012). Lessons from C. elegans: Signaling pathways for longevity. *Trends Endocrinol. Metab.* 23, 637–644. doi:10.1016/j.tem.2012.07.007.
Libina, N., Berman, J. R., and Kenyon, C. (2003). Tissue-Specific Activities of C. elegans DAF-16 in the Regulation of Lifespan tissues play an important role in establishing the ani-mal's rate of aging. First, the C. elegans genome con-tains more than 35 insulin-like genes expressed in a. *Cell* 115, 489–502. Available at: www.cell.com/cgi/content/full/115/4/489/DC1.
Mallick, A., Jhaveri, N., Jeon, J., Chang, Y., Shah, K., and Hosein, H. (2021a). Genetic analysis of Caenorhabditis elegans pry-1 / Axin suppressors identifies genes involved in reproductive structure development , stress responses , and aging. *G3 Genes, Genomes, Genet.* jkab430. doi:10.1093/g3journal/jkab430.
Mallick, A., Ranawade, A., and Gupta, B. P. (2019a). Role of PRY-1/Axin in heterochronic miRNA-mediated seam cell development. *BMC Dev. Biol.* 19, 1–12. doi:10.1186/s12861-019-0197-5.
Mallick, A., Ranawade, A., van den Berg, W., and Gupta, B. P. (2020). Axin-Mediated Regulation of Lifespan and Muscle Health in C. elegans Requires AMPK-FOXO Signaling. *iScience* 23, 101843. doi:10.1016/j.isci.2020.101843.
Mallick, A., Taylor, S. K. B., Mehta, S., and Gupta, B. P. (2021b). picd-1, a gene that encodes CABIN1 domain-containing protein, interacts with pry-1/Axin to regulate multiple processes in Caenorhabditis elegans. *bioRxiv*, 1–37. doi:10.1101/2021.09.27.462077.
Mallick, A., Taylor, S. K. B., Ranawade, A., and Gupta, B. P. (2019b). Axin Family of Scaffolding Proteins in Development: Lessons from C. elegans. *J. Dev. Biol.* 7, 1–23. doi:10.3390/jdb7040020.
Mathes, S., Fahrner, A., Ghoshdastider, U., Rüdiger, H. A., Leunig, M., Wolfrum, C., et al. (2021). FGF-2–dependent signaling activated in aged human skeletal muscle promotes intramuscular adipogenesis. *Proc. Natl. Acad. Sci. U. S. A.* 118, 1–12.

doi:10.1073/pnas.2021013118.
Miska, E. A., Alvarez-Saavedra, E., Abbott, A. L., Lau, N. C., Hellman, A. B., McGonagle, S. M., et al. (2007). Most Caenorhabditis elegans microRNAs are individually not essential for development or viability. *PLoS Genet.* 3, 2395–2403. doi:10.1371/journal.pgen.0030215.
O'Brien, J., Hayder, H., Zayed, Y., and Peng, C. (2018). Overview of microRNA biogenesis, mechanisms of actions, and circulation. *Front. Endocrinol. (Lausanne).* 9, 1–12. doi:10.3389/fendo.2018.00402.
Ornitz, D. M., and Itoh, N. (2015). The fibroblast growth factor signaling pathway. *Wiley Interdiscip. Rev. Dev. Biol.* 4, 215–266. doi:10.1002/wdev.176.
Pincus, Z., Smith-Vikos, T., and Slack, F. J. (2011). MicroRNA predictors of longevity in caenorhabditis elegans. *PLoS Genet.* 7. doi:10.1371/journal.pgen.1002306.
Ranawade, A., Mallick, A., and Gupta, B. P. (2018). PRY-1/Axin signaling regulates lipid metabolism in Caenorhabditis elegans. *PLoS One* 13, e0206540. doi:10.1371/journal.pone.0206540.
Rennie, W., Kanoria, S., Liu, C., Mallick, B., Long, D., Wolenc, A., et al. (2016). STarMirDB: A database of microRNA binding sites. *RNA Biol.* 13, 554–560. doi:10.1080/15476286.2016.1182279.
Rera, M., Azizi, M. J., and Walker, D. W. (2013). Organ-specific mediation of lifespan extension: More than a gut feeling? *Ageing Res. Rev.* 12, 436–444. doi:10.1016/j.arr.2012.05.003.
Schutzman, J. L., Borland, C. Z., Newman, J. C., Robinson, M. K., Kokel, M., and Stern, M. J. (2001). The Caenorhabditis elegans EGL-15 Signaling Pathway Implicates a DOS-Like Multisubstrate Adaptor Protein in Fibroblast Growth Factor Signal Transduction . *Mol. Cell. Biol.* 21, 8104–8116. doi:10.1128/mcb.21.23.8104-8116.2001.
Stefani, G., and Slack, F. J. (2008). Small non-coding RNAs in animal development. *Nat. Rev. Mol. Cell Biol.* 9, 219–230. doi:10.1038/nrm2347.
Taylor, R. C., and Dillin, A. (2013). XBP-1 Is a cell-nonautonomous regulator of stress resistance and longevity. *Cell* 153, 1435. doi:10.1016/j.cell.2013.05.042.
Taylor, S. K. B., Minhas, M. H., Tong, J., Selvaganapathy, P. R., Mishra, R. K., and Gupta, B. P. (2021). C. elegans electrotaxis behavior is modulated by heat shock response and unfolded protein response signaling pathways. *Sci. Rep.* 11, 1–17. doi:10.1038/s41598-021-82466-z.
Uno, M., and Nishida, E. (2016). Lifespan-regulating genes in c. Elegans. *npj Aging Mech. Dis.* 2. doi:10.1038/npjamd.2016.10.
Wang, H., Webster, P., Chen, L., and Fisher, A. L. (2019). Cell-autonomous and non-autonomous roles of daf-16 in muscle function and mitochondrial capacity in aging C. elegans. *Aging (Albany. NY).* 11, 2295–2311. doi:10.18632/aging.101914.
Watts, J. L., and Ristow, M. (2017). Lipid and carbohydrate metabolism in Caenorhabditis elegans. *Genetics* 207, 413–446. doi:10.1534/genetics.117.300106.
Xie, Y., Su, N., Yang, J., Tan, Q., Huang, S., Jin, M., et al. (2020). FGF/FGFR signaling in health and disease. *Signal Transduct. Target. Ther.* 5. doi:10.1038/s41392-020-00222-7.
Xue, Y., Liu, Z., Cao, J., Ma, Q., Gao, X., Wang, Q., et al. (2011). GPS 2.1: Enhanced prediction of kinase-specific phosphorylation sites with an algorithm of motif length selection. *Protein Eng. Des. Sel.* 24, 255–260. doi:10.1093/protein/gzq094.
Yin, Y., Castro, A. M., Hoekstra, M., Yan, T. J., Kanakamedala, A. C., Dehner, L. P., et al. (2015). Fibroblast Growth Factor 9 Regulation by MicroRNAs Controls Lung Development and Links DICER1 Loss to the Pathogenesis of Pleuropulmonary Blastoma. *PLoS Genet.*

11, 1–22. doi:10.1371/journal.pgen.1005242.

SUPPLEMENTAL MATERIALS

Supplementary Table 1: List of primers used in the study.
Supplementary Table 2: List of *miR-246* target genes.
Supplementary Table 3: Table with the mean, median, and maximum lifespan of animals.

Supplementary Figure 1: *miR-246* has a conserved binding site at the 3' UTR region of the kin-9 transcript. The conserved *miR-246* binding region (7mer-m8) is shown in red. This prediction is generated with the TargetScanWorm software and default parameters (http://www.targetscan.org/worm_52/).

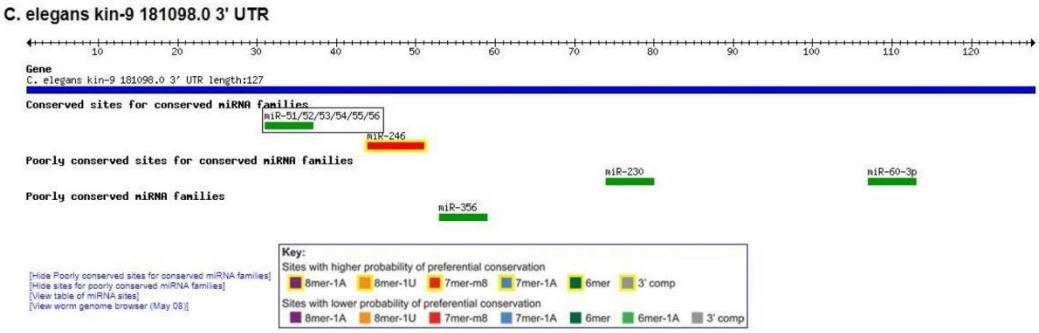

Supplementary Figure 2: qCPR analysis of *kin-9c* isoform and *kin-9* isoforms (a, b and c) together show significant upregulation in the *miR-246* mutants. Data represent the mean of two replicates and error bars the standard error of means. Significance was calculated using Bio-Rad software (one-way ANOVA) and significant differences are indicated by stars (*): * ($p < 0.05$), ** ($p < 0.01$).

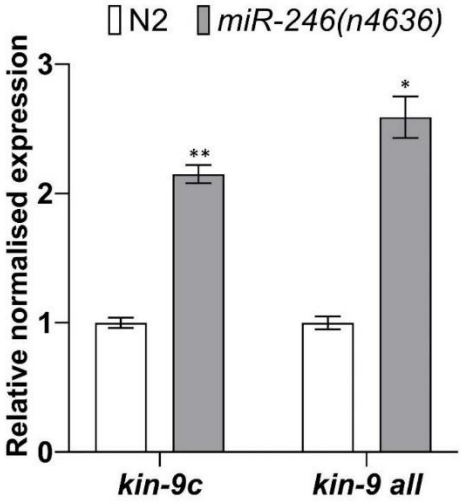

Supplementary Figure 3: Analysis showing the conserved Tyrosine kinase phosphorylation sites of FGFR family in the 284aa (273-557aa) region of the kinase domain of KIN-9 using the Group-based Prediction System (GPS 5) (http://gps.biocuckoo.cn/online.php) (Yu Xue et al 2011). Tyrosine kinase domain on the KIN-9 protein is predicted using the NCBI protein blast function.

```
    QIHPGQRTQLLRDCPVAVKMLPSFADDAARSDFMQEINFMKSLAYHPHLV   #     50
    SMLGFVADRKSPYLLVEFCEHGDLLHMIRNRRQEIINGPTENPDGLKIKD   #    100
    LLMFSWQISNGLEYLNNIGCIHRDIAARNVLVDSANTCKIGDFGLCRLTD   #    150
    SLLYTARGGRLPLKWMAPESLATYEYSYKSDVWSYGVLLWELFSLGEVPY   #    200
    GEVQTTELLQTHRSGKRLLKPEWCPEEIYDVMRLCWQELPDDRPAFQQTC   #    250
    AVLAQMLENATENYGYLIPKHFNNQTRDPSEQCDNV                 #    300
%1  ..................................................   #     50
%1  ............Y.....................................   #    100
%1  .............Y....................................   #    150
%1  ............................Y......................Y   #    200
%1  ............................Y.....................   #    250
%1  ................Y...................
```

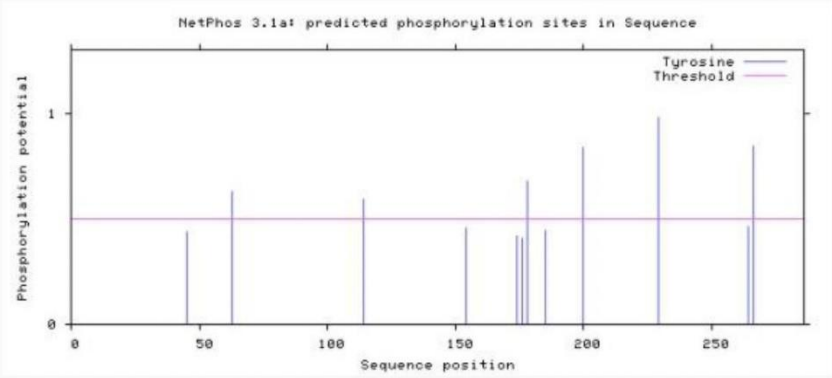

Supplementary Figure 4: Protein blast of KIN-9 with EGL-15 shows sequence conservation in the region of the tyrosine kinase domain. Sequence comparison showing similarities (denoted by +) and identities between the sequences of the kinase domain of EGL-15 (613-937aa) and KIN-9 (244-561aa).

```
613  KRMNSENTVLSEYEVDSDPVWEVERSKLSLVHM--LGEGAFGEVWKATYK-ETENNEI--  667
     K++N   T L          W ++R+ L + +   LG GAF  V+K     E   ++I
244  KKVNDYETQLDSPAYSIHDPWLLDRNNLEINYSKKLGSGAFCNVFKGKINGEAPVSQIHP  303

668  ----------AVAVKKLKMSAHEKELIDLVSEMETFKVIGEHENVLRLIGCCTGAGPLYV  717
                VAVK L   A +    D + E+   K +  H +++ ++G        Y+
304  GQRTQLLRDCPVAVKMLPSFADDAARSDFMQEINFMKSLAYHPHLVSMLGFVADRKSPYL  363

718  VVELCKHGNLRDFLRAHRPKEEKAKKSSQELTDYLEPRKASDKDDIELIPNLTQRHLVQF  777
     +VE C+HG+L   +R  R          QE+ +   P +  D         L  + L+ F
364  LVEFCEHGDLLHMIRNRR----------QEIIN--GPTENPD--------GLKIKDLLMF  403

778  AWQVAQGMNFLASKKIIHRDLAARNVLVGDGHVLKISDFGLSRDVHCNDYYRKRGNGRLP  837
     +WQ++ G+ +L +   IHRD+AARNVLV   +  KI DFGL R +  +  Y  RG GRLP
404  SWQISNGLEYLNNIGCIHRDIAARNVLVDSANTCKIGDFGLCR-LTDSLLYTARG-GRLP  461

838  IKWMALEALDSNVYTVESDVWSYGVLLWEIMTLGGTPYPTIAMPELYANLKEGYRMEPPH  897
     +KWMA E+L +  Y+ +SDVWSYGVLLWE+ +LG  PY  +   EL    + G R+  P
462  LKWMAPESLATYEYSYKSDVWSYGVLLWELFSLGEVPYGEVQTTELLQTHRSGKRLLKPE  521

898  LCPQEVYHLMCSCWREKLEERPSFKTIVDYLDWMLTMTNE  937
      CP+E+Y +M  CW+E  ++RP+F+     L  ML    E
522  WCPEEIYDVMRLCWQELPDDRPAFQQTCAVLAQMLENATE  561
```

Supplementary Figure 5: qPCR analysis of *kin-9* in the *hsp::kin-9* adult animals. Data represent the mean of two replicates and error bars the standard error of means. Significance was calculated using Bio-Rad software (one-way ANOVA) and significant differences are indicated by stars (*): ** (p <0.01).

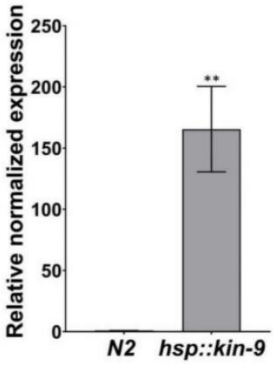

Supplementary Figure 6: Graphs showing the lifespan of *kin-9(tm3973)* and *hsp::kin-9* animals at different temperatures. See the Methods section and **Supplementary Table 3** for statistics performed.

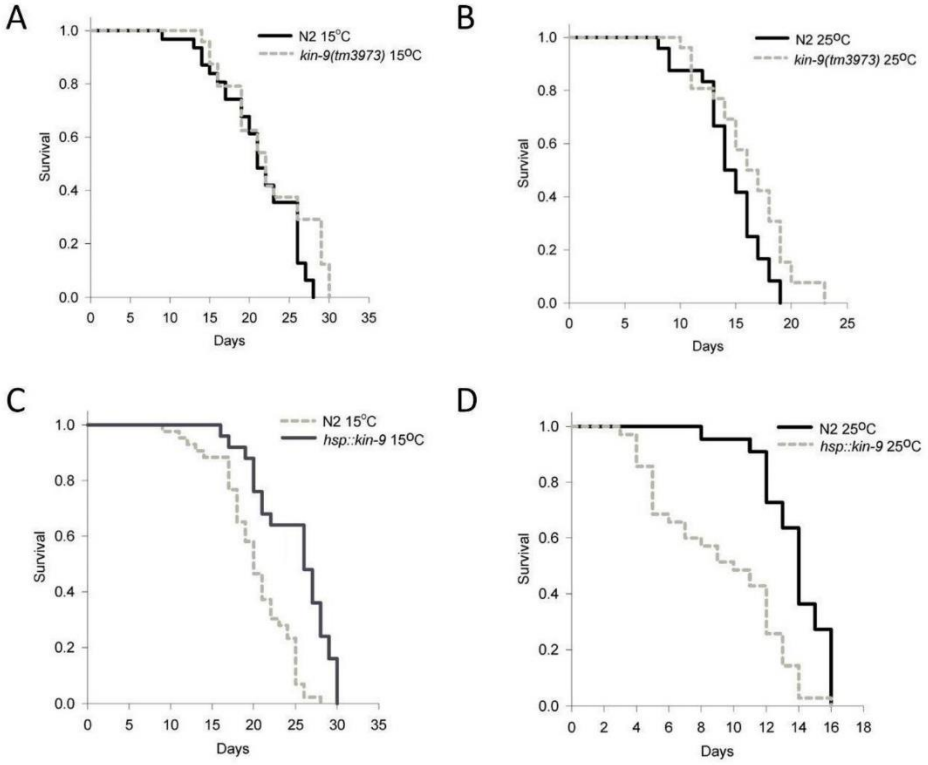

Supplementary Figure 7: Representative images of FGF pathway component mutants compared to wild-type animals. Similar to *clr-1* loss of function and *let-60* gain of function mutants, animals with *kin-9* overexpression show clear phenotype.

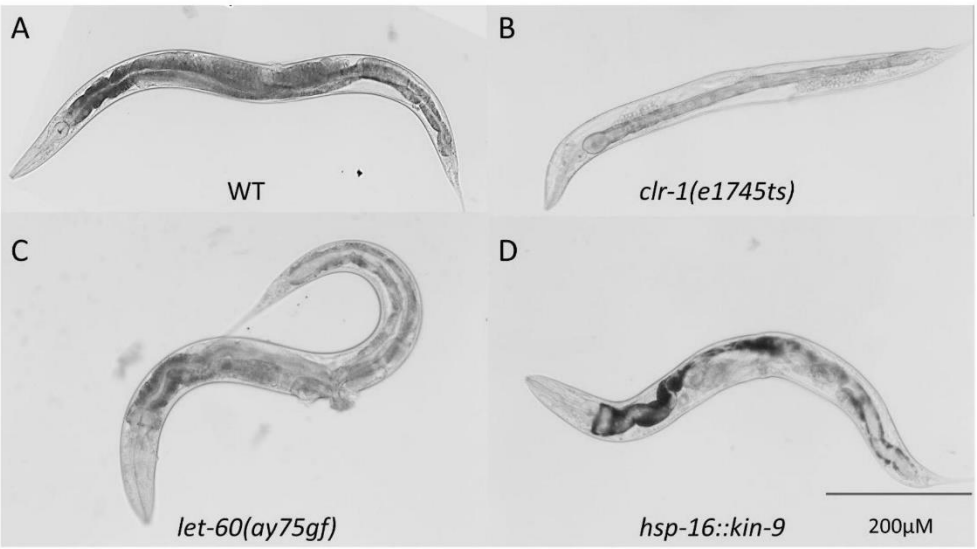

Supplementary Figure 8: Expression of *kin-9p(4.3kb)::GFP* animals.

30

Supplementary Figure 9: Expression analysis of *kin-9* in the N2 and *miR-246(n4636)* animals following control and *kin-9* RNAi knockdown. Data represent the mean of two replicates and error bars the standard error of means. Significance was calculated using Bio-Rad software (one-way ANOVA) and significant differences are indicated by stars (*): ** (p <0.01), *** (p < 0.001).

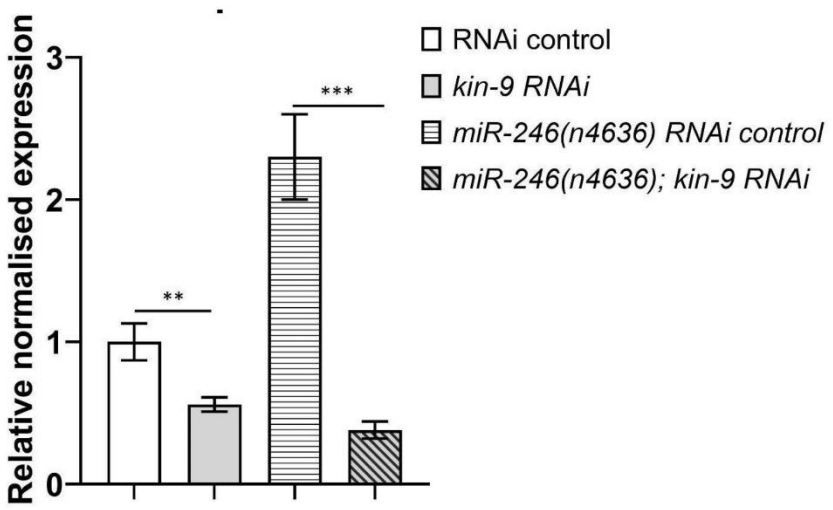

Chapter 7

Conclusion and future directions

7.1 Key findings of the thesis

I have described the findings of my thesis in **Chapters 3-6**. The research objective of my Ph.D. work focused on understanding the role of Axin in *C. elegans*. During my tenure, my work not only focused on the developmental events regulated by PRY-1 for which WNT signaling is very well known but also explored mechanisms of PRY-1 function that are WNT independent and regulate post-developmental processes in animals. As such, I have briefly summarised the findings on the role of PRY-1/Axin in the following sections.

7.1.1 PRY-1 regulates seam cell development and miRNA expression

In this chapter, we have shown that PRY-1/Axin functions in the asymmetric pathway to regulate WRM-1 and SYS-1 localization which in turn affects POP-1 localization in the nucleus of seam cells. Loss of *pry-1* function causes an increase in seam cell number and upregulates expression of heterochronic miRNAs: *lin-4, miR-237, miR-241, miR-48*, and *miR-84*. Interestingly, one other miRNA (*miR-246*) is also found to be misregulated and is not involved in the heterochronic pathway. Rather *miR-246* has known roles in aging and stress response. Such a phenotype and miRNA regulation by PRY-1 appears to be conserved in the closely related species *C. briggsae* too.

7.1.2 PRY-1 regulates lipid metabolism

In this chapter, we have reported the role of PRY-1/Axin in regulating lipid synthesis. To start with we carried out the mRNA transcriptomics analysis in the *pry-1* mutants which revealed differentially expressed genes associated with lipid synthesis, transportation, and breakdown. Subsequent genetic, molecular and mass spectrometry analyses demonstrated the function of PRY-1 in regulating the expression of fatty acid desaturases, and yolk lipoproteins (vitellogenin). Specifically, PRY-1 utilizes the SREBP transcription factor homolog SBP-1 to regulate fatty acid synthesis genes and BAR-1/β-catenin to regulate vitellogenins (*vit-1* to *vit-6*).

7.1.3 PRY-1 regulates aging and muscle health

In this chapter, we have discovered a novel aging pathway that regulates longevity and muscle health in aging animals. While PRY-1's role in developmental events is well

documented, we show for the first time its function in post-developmental processes. First, we explored the tissue-specific role of PRY-1 and found that PRY-1 plays a conserved role in the muscle of animals where it is necessary for both muscle development and maintenance. Moreover, PRY-1 forms a complex with AAK-2, the catalytic subunit homolog of AMPK, to cell non autonomously activate DAF-16/FOXO in the intestine. This signaling is not only required for the normal lifespan but also to maintain the lipid levels of animals. We have also shown that the PRY-1/Axin function is necessary to activate (phosphorylate) the energy sensor AMPK and all the benefits contributed by AMPK signaling are abolished in the absence of PRY-1 function.

7.1.4 Downstream effectors of PRY-1 signaling

The final chapter describes genes that function downstream of PRY-1 to regulate vulva development, stress response, and aging. Firstly, I have identified eight suppressors of *pry-1* mutants' phenotypes with known functions in gene expression, proteostasis, and oxidation-reduction process. Interestingly, all the eight *pry-1* suppressors (*spp-1, clsp-1, ard-1, rpn-7, cpz-1, his-7, cdk-1,* and *rnr*-1) identified contain mammalian homologs. Whereas four of them (*cpz-1, his-7, cdk-1,* and *rnr-1*) function in both stress response and aging, two (*spp-1* and *ard-1*) are specific to the stress response. Secondly, I have identified the CABIN1 homolog PICD-1 in *C. elegans*, which enhances the *pry-1* mutant phenotype. Here, I show that *pry-1* and *picd-1* negatively regulates calcineurin signaling thus promoting the nuclear function of the CRTC-1/CRTCs transcription factor. This mode of regulation regulates the normal lifespan and stress response of animals. Finally, *pry-1* has also been shown to affect FGF signaling via a microRNA,

miR-246, that negatively regulates the expression of the newly discovered *FGFR4* homolog *kin-9*. Such a regulatory network is necessary for delaying aging and conferring stress resistance of animals. Altogether, these findings demonstrate the important role of *pry-1* interacting genes in regulating developmental and post-developmental processes in *C. elegans.*

7.2 Future directions

My work has contributed to a growing body of study demonstrating the essential role of the Axin homolog PRY-1 in *C. elegans* during developmental and post-developmental periods in animals. More specifically, a comprehensive genetic and molecular analysis of this gene has been carried out that uncovered multiple genetic pathways that interact with PRY-1. As a scaffolding protein, PRY-1 recruits many different factors and affects diverse signaling pathways and downstream effectors. For example, *pry-1* functions cell non-autonomously in the muscles to activate AAK-2/AMPK and DAF-16/FOXO in the intestine to regulate the lifespan of animals utilizes the CABIN1 domain-containing protein PICD-1 to negatively regulate calcineurin signaling and promotes a microRNA, *miR-246*, expression to inhibit the KIN-9/FGFR signaling.

While it is evident that PRY-1 is an important genetic factor that forms a nexus between independent pathways, it remains to be investigated how many of these interactions are specific to any tissue or cell types and processes. All these findings reported in the

previous chapters opened up new possibilities and will serve as the foundation for understanding regulatory mechanisms mediating core cellular processes in the eukaryotes.

My work has informed that the role of PRY-1 could be studied at three different levels: **1)** Tissue/cellular level (**Section 7.2.1**), **2)** Broader biological processes (**Section 7.2.2**), and **3)** Molecular interactions or signaling pathways (**Section 7.2.3** and see **Figure 7.1**). At the tissue or cell level, we can investigate which tissues or organelles require PRY-1 function to mediate these different biological processes that include aging, stress response, metabolism, and immunity. Moreover, it is not fully understood what type of post-translational modifications of PRY-1 influence the sub-cellular localization of this protein.

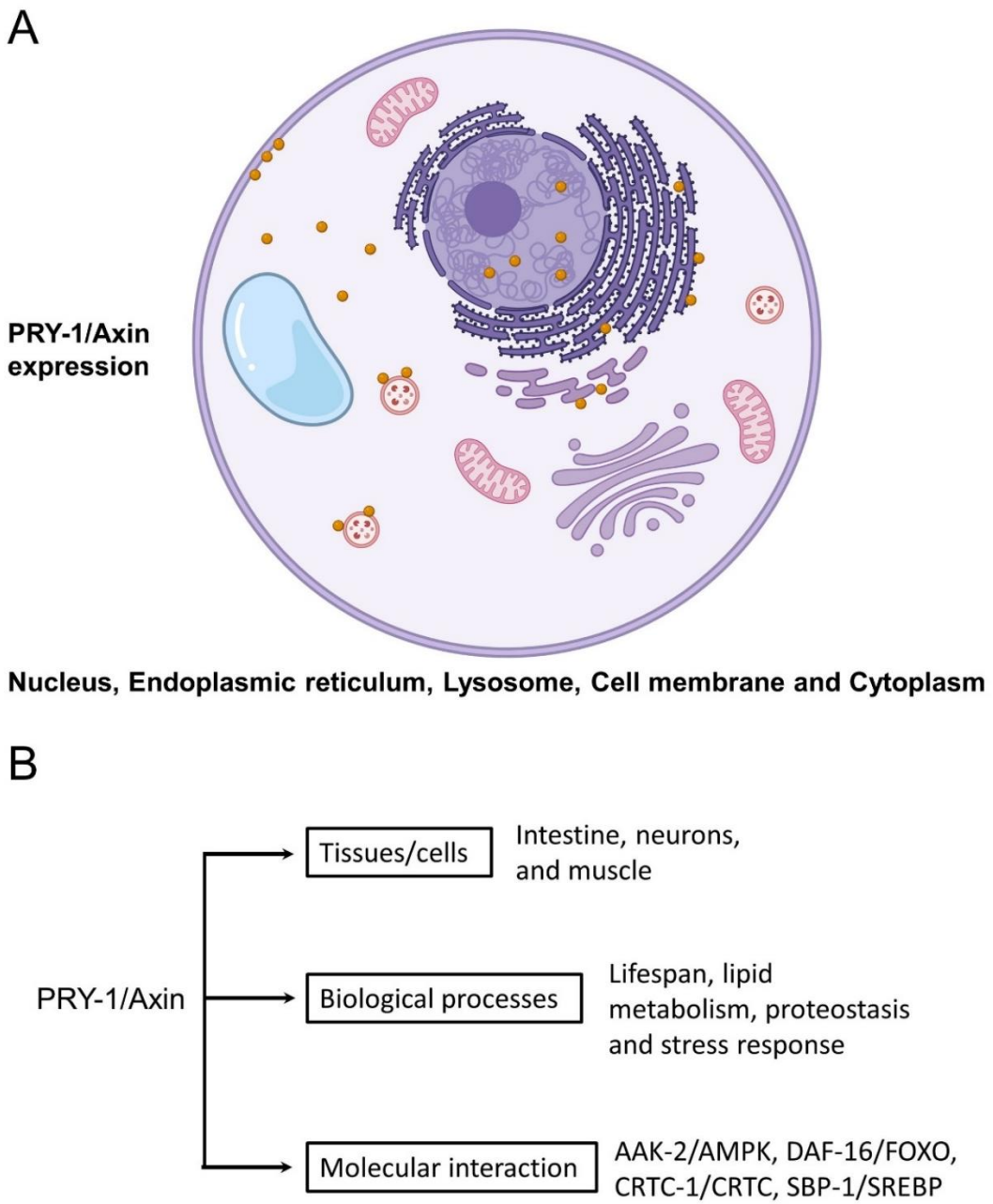

Figure 7.1: Localization and function of PRY-1/Axin in different tissues and cell types. (A) Schematic diagram of a cell showing the known subcellular localization of PRY-1/Axin (Orange colored ball; Prepared using Biorender.com). **(B)** PRY-1 function

can be investigated at various levels (Cellular, biological processes, and molecular interactors).

7.2.1 Tissue and cell-specific function

My work has shown that PRY-1 is expressed in the nucleus, cytoplasm, and endoplasmic reticulum of cells. Moreover, loss of *pry-1* function affects mitochondria health and morphology. However, it is unclear what role PRY-1 plays in these subcellular locations. Thus, future investigations should shed light on this area which will uncover the role and interacting partners of PRY-1 in these organelles. I have described a few possible investigations on this line which are listed in the next sections.

Does PRY-1 affect lysosomal function?

As mentioned previously, mammalian Axin forms a complex with AMPK in the lysosomal membrane upon glucose starvation. Such an organelle-specific complex formation has been reported in *C. elegans* using the Axin homolog AXL-1. But it remains to be seen whether the other major Axin homolog PRY-1 is also present in this lysosomal complex. Support towards such as possibility comes from my recent data showing the requirement of PRY-1 function for metformin and glucose-deprived induced benefits.

Understanding the role of PRY-1 in the endoplasmic reticulum

Recently my high-resolution confocal imaging using the PRY-1::GFP animals revealed that PRY-1 is expressed in the endoplasmic reticulum. Given that the endoplasmic reticulum (ER) is the site for protein synthesis, folding, trafficking, and certain lipid and

cholesterol synthesis, it is expected that *pry-1* mutants may show defects in these macromolecule metabolisms. Consistently, *pry-1* mutants show a reduction in the lipid content and fatty acid synthesis and increased aggregation of unfolded toxic protein. Additionally, these mutants are also very sensitive to environmental stresses that aggravate protein misfolding and aggregation. As such, *pry-1* mutants affect all the UPR^{ER} pathways that are devoted to solving or reverting defective protein folding.

Thus, together with the experiments proposed in the previous section, it is important to uncover how PRY-1 affects protein translation and folding in the ER. To address this objective, I am proposing two sets of experiments**: 1)** Analyse the vesicle formation and trafficking from the ER and **2)** whether protein secretion is normal from the cells with PRY-1/Axin function.

How is PRY-1 involved in maintaining mitochondrial health?

We have demonstrated for the first time the role of *pry-1* in maintaining mitochondrial morphology where *pry-1* is necessary to delay mitochondrial fragmentation (**Chapter 5**). While it is evident that PRY-1 promotes mitochondrial fusion, the actual mechanism or function of PRY-1 in this process is unclear. Interestingly, my recent work at the Dillin lab revealed that PRY-1 is expressed in the endoplasmic reticulum but not mitochondria of muscles which suggests that the gene may not be affecting the mitochondrion directly but rather via the endoplasmic reticulum. This is in agreement with the role of protein (nuclear-encoded and ER translated) trafficking affecting mitochondrial biogenesis (Higuchi-Sanabria *et al.* 2018; Anderson and Haynes 2020).

Thus, it will be of great interest to investigate the role of PRY-1 in affecting mitochondrial protein trafficking and finally its biogenesis.

What factors affect PRY-1 nuclear localization?

While most of the research has focused on the role of Axin in the cytoplasm, it is mostly unknown what it does in the nucleus (**Figure 7.1**). My recent expression analysis mentioned above also confirmed the localization of PRY-1 in the nucleus of muscle and intestinal cells and the presence of a large set of differentially expressed genes in the *pry-1* mutants linked to gene expression regulation suggest that the important role of this protein in the nucleus. Supporting this hypothesis, research in the mammalian system has shown that Axin is regulated (both in the nucleus and cytoplasm) by a cell cycle gene cyclin-dependent kinase 5 (*Cdk5*) during axon formation in the neuronal cells (Fang *et al.* 2011). The same group has subsequently shown that the interaction of Axin with GSK-3β in the cytoplasm is critical for intermediate progenitor (IP) amplification whereas that with β-catenin in the nucleus promotes neuronal differentiation (Fang *et al.* 2013). However, it is unclear what dictates the change in the subcellular localization of Axin which can be investigated in the future.

7.2.2 Regulation of biological processes

In this section, I outline the proposed future objectives that can be pursued to understand the role of this master scaffolding protein PRY-1 in important cellular processes such as lipid metabolism, proteostasis, and immune response to pathogenic attack.

PRY-1 and lipid metabolism

PRY-1 is necessary for fatty acid synthesis and preliminary data demonstrate that it may utilize SREBP homolog SBP-1 to transcribe the fatty acid desaturases. Interestingly, lowering vitellogenins could also rescue the lipid defect of *pry-1* mutants. However, there is no evidence of the role of *vits* in fatty acid synthesis but lipid transportation. Thus, it is unclear how *vit* RNAi is sufficient to rescue the lipid levels in these mutants. Moreover, as mammalian AMPK inhibits fatty acid synthesis by phosphorylating SREBP, leading to a reduction in lipid synthesis, it is unclear whether Axin is involved in this process.

PRY-1 and proteostasis

All the above-mentioned chapters suggest that PRY-1 plays an important role in maintaining the UPR pathways. Together with the data that *pry-1* is expressed in the endoplasmic reticulum and affects mitochondrial health, allows me to propose that the protein also regulates protein quantity, quality, and localization in animals. To better understand these processes and to analyze whether this hypothesis is true, proteomics analysis in the *pry-1* mutants and *pry-1* overexpression lines will be immensely helpful. This study will allow us to explore the relationship between PRY-1 and proteostasis.

PRY-1 and immunity

Our *pry-1* miRNA transcriptomic analysis revealed differentially expressed miRNAs (*miR-48/84/241*) involved in innate immunity (Ren and Ambros 2015). Thus it is plausible that *pry-1* may regulate immunity in *C. elegans*. Moreover, *pry-1* affects mitochondrial health, $UPR^{mt,}$ and UPR^{ER}. Because UPR-regulated innate immunity provides resistance to infection (Pellegrino *et al.* 2014; Gallotta *et al.* 2020), this will

be of great interest to investigate the possible roles of PRY-1 in these processes leading to enhanced immune response.

7.2.3 Identification of genes and signaling pathways that mediate the *pry-1* function

In this section, I have outlined the unanswered questions regarding the major signalings (described in **Chapter 6**) discovered to interact with PRY-1 that should be pursued in the future. These are the Axin-AMPK signaling, Calcineurin signaling, miRNA-FGFR pathway, and WNT signaling.

Axin-AMPK signaling

We and others have shown that Axin-AMPK signaling is essential for maintaining muscle health, muscle metabolism, aging, and metformin-induced benefits. While a lot has been done in the last 5 years or so to identify the downstream targets of this pathway, a little has been explored to understand the mechanistic differences between inducers of canonical AMPK and Axin-AMPK pathway. Moreover, it is unclear whether the Axin-AMPK pathway is present in all the tissue types, or it is tissue-specific. Thus, I have listed some of the unresolved questions below.

While it has been shown that the Axin homologs in both *C. elegans* (PRY-1 and AXL-1) and mammalian systems (Axin1 and Axin2) can activate AMPK (Zhang *et al.* 2013; Chen *et al.* 2017; Zong *et al.* 2019; Mallick *et al.* 2020), the redundancies between the homologs and their tissue-specific interactions with AMPK are unknown. Moreover,

the differences in lifespan and lipid metabolism phenotypes between the two Axin mutants in *C. elegans* raise the question of functional equivalency with regards to AMPK activation in physiological conditions. Future research along these directions promises to refine our understanding of Axin-AMPK signaling and its conservation in eukaryotes.

An important aspect of modulating a signaling cascade is to properly understand its limiting factors. The following four research directions are expected to contribute to the molecular mechanism of the pathway. Firstly, it is unclear if there is a conformational change in AMPK following Axin binding similar to that reported for the AMP-dependent mechanism. Secondly, whether post-translational modifications of Axin influence its role in activating AMPK. Thirdly, identification of a specific region of the multidomain Axin protein required for AMPK interaction may unravel competitors that may modulate Axin-AMPK signaling. And, finally, the discovery of factors influencing subcellular localization of both Axin and AMPK and, in turn, affecting their interactions.

Other modes of regulation of Axin-AMPK signaling may involve pathways that affect Axin expression. Axin is well characterized for its role as the negative regulator of the WNT signaling and Axin is a target of the pathway (Jho *et al.* 2002; Ranawade *et al.* 2018). Consistent with this, PRY-1/Axin is required for MOM-2/WNT mediated lifespan regulation (Mallick *et al.* 2020) and MOM-2 is expressed in the body wall muscles of *C. elegans*. It remains to be explored whether Axin function in muscles is regulated in a WNT-dependent manner in eukaryotes. Please see the published article

at the end of this chapter for an in-depth discussion on Axin-AMPK signaling **(Section 7.3**; **Mallick and Gupta, 2021).**

Calcineurin signaling

Among the identified downstream effectors of PRY-1 signaling is the CRTC homolog, CRTC-1, which promotes longevity mediated by calcineurin signaling (**Chapter 6**). I have shown that PRY-1 utilizes the CABIN1 domain-containing protein PICD-1 to negatively regulate CRTC-1 mediated transcription. Notably, PRY-1 interacting protein AAK-2 has also been shown to inhibit CRTC-1 function. Thus it is unknown whether PRY-1 interacts with AAK-2 in this pathway. Moreover, it remains to be investigated whether the other components (HIRA-1, ASFL-1, and UNC-85) of the histone H3.3 chaperone complex HUCA, which CABIN1 is part of, are also involved in this regulation.

***miR-246-FGFR* pathway**

While I have shown that *pry-1* mediated regulation of *kin-9/FGFR* utilizes *miR-246*, it is still unclear whether this affects the canonical FGF signaling. Future experiments should investigate this relationship in detail using both genetic and molecular means. Specifically, FGF pathway components should be knocked down in the *miR-246* and *pry-1* mutants to check whether this is sufficient to suppress the mutant phenotypes. Moreover, it will be also interesting to see whether such inhibition by *miR-246* is tissue-specific or not.

Signaling mediated by WNT and non-WNT pathway components

The work described in **chapter 5** demonstrates the role of PRY-1/Axin in muscle maintenance and development. However, the findings suggest that PRY-1 does possess an opposite role in aging when it comes to its functions in other tissues. While PRY-1 role in the muscle appears to be WNT independent, it is likely involved in other WNT-dependent tissue-specific regulation of aging such as in the neurons. Such a hypothesis is also supportive of the fact that different WNT ligand mutants have opposite aging phenotypes. Thus, it will be interesting to investigate in the future whether EGL-20/WNT mediated neuronal cell non-autonomous signaling requires PRY-1. Moreover, with the fact that PRY-1 is expressed in multiple tissues and WNT mediated *pry-1* transcription is most active in the intestine, it will be important to analyze PRY-1 role on lifespan in the absence of WNT canonical signaling or BAR-1/β-catenin function. These analyses will allow us to know whether there is any beneficial role of PRY-1 (WNT independent) in these tissues (neurons and intestine) that have active canonical WNT signaling.

Downstream effectors

Recently, I integrated the muscle-specific and endogenous promoter-driven transgenic overexpression lines of PRY-1 in the Dillin lab at UC Berkeley. Now these homogenous muscle-specific and native promoter-driven PRY-1 overexpressed animals can be used to do whole animal transcriptomic and metabolomic analyses. These will lead to the identifications of genes that are differentially expressed and metabolites that are affected when this signaling cascade is ‘ON’ only in the muscle compared to the whole body. Subsequently, these data can be further utilized to narrow down markers that can

predict muscle health and lifespan of animals. Such a proposed investigation will be very powerful for future Axin research as this will be done for the first time in any animal model. In summary, the results obtained from these experiments will not only allow us to dissect targets of muscle-mediated PRY-1 signaling but also identify targets that are either WNT-specific or independent.

7.3 Mallick and Gupta (2021)- F1000Reseach

7.3.1 Preface

This section of Chapter 7 includes the following review article in its originally published format: "AXIN-AMPK signaling: Implications for healthy aging", by Avijit Mallick and Bhagwati P. Gupta. (F1000Research 8 Dec 2021; 10:1259. DOI: 10.12688/f1000research.74220.1). This is an open-access article distributed under the terms of the Creative Commons Attribution Unported License, which permits unrestricted use, distribution, and reproduction in any medium, provided the original work is properly cited.

Contributions: I and Bhagwati Gupta contributed to gathering information from various articles and wrote the initial draft. I made all the Figures. I and Bhagwati Gupta edited and finalised the manuscript.

F1000Research F1000Research 2021, 10:1259 Last updated: 18 JAN 2022

Check for updates

OPINION ARTICLE

AXIN-AMPK signaling: Implications for healthy aging [version 1; peer review: 1 approved, 2 approved with reservations]

Avijit Mallick, Bhagwati P. Gupta

Department of Biology, McMaster University, Hamilton, Ontario, L8S4K1, Canada

v1 **First published:** 08 Dec 2021, **10**:1259
https://doi.org/10.12688/f1000research.74220.1
Latest published: 08 Dec 2021, **10**:1259
https://doi.org/10.12688/f1000research.74220.1

Abstract

The energy sensor AMP kinase (AMPK) and the master scaffolding protein, AXIN, are two major regulators of biological processes in metazoans. AXIN-dependent regulation of AMPK activation plays a crucial role in maintaining metabolic homeostasis during glucose-deprived and energy-stressed conditions. The two proteins are also required for muscle function. While studies have refined our knowledge of various cellular events that promote the formation of AXIN-AMPK complexes and the involvement of effector proteins, more work is needed to understand precisely how the pathway is regulated in response to various forms of stress. In this review, we discuss recent data on AXIN and AMPK interaction and its role in physiological changes leading to improved muscle health and an extension of lifespan. We argue that AXIN-AMPK signaling plays an essential role in maintaining muscle function and manipulating the pathway in a tissue-specific manner could delay muscle aging. Therefore, research on understanding the factors that regulate AXIN-AMPK signaling holds the potential for developing novel therapeutics to slow down or revert the age-associated decline in muscle function, thereby extending the healthspan of animals.

Keywords

Axin, AMPK, muscle, aging, C. elegans, LKB1, AAK-2, PRY-1

Open Peer Review

Reviewer Status ? ? ✓

	Invited Reviewers		
	1	**2**	**3**
version 1 08 Dec 2021	? report	? report	✓ report

1. **Jonathan S. Oakhill**, University of Melbourne, Melbourne, Australia
2. **Anindya Ghosh Roy**, Nationa Brain Research Centre, Gurgaon, India
3. **Stefan Taubert**, University of British Columbia, Vancouver, Canada

Any reports and responses or comments on the article can be found at the end of the article.

Corresponding author: Bhagwati P. Gupta (guptab@mcmaster.ca)

Author roles: Mallick A: Conceptualization, Data Curation, Formal Analysis, Validation, Writing – Original Draft Preparation, Writing – Review & Editing; **Gupta BP**: Conceptualization, Funding Acquisition, Project Administration, Resources, Supervision, Writing – Original Draft Preparation, Writing – Review & Editing

Competing interests: No competing interests were disclosed.

Grant information: This work was supported by Natural Sciences and Engineering Research Council (NSERC) Discovery grant to BPG and NSERC CGS-D graduate scholarship to AM.
The funders had no role in study design, data collection and analysis, decision to publish, or preparation of the manuscript.

How to cite this article: Mallick A and Gupta BP. **AXIN-AMPK signaling: Implications for healthy aging [version 1; peer review: awaiting peer review]** F1000Research 2021, **10**:1259 https://doi.org/10.12688/f1000research.74220.1

First published: 08 Dec 2021, **10**:1259 https://doi.org/10.12688/f1000research.74220.1

F1000Research 2021, 10:1259 Last updated: 08 DEC 2021

Introduction

With aging, there is a decline in skeletal muscle mass and function. Aging muscle undergoes a shift in the balance between myogenic potential and fibrogenic activity that leads to reduced capacity of the muscle to repair and regenerate.[1] Studies have shown that age-associated decline in muscle function is multifactorial and affected by genetic and environmental factors. While many genes have been identified that contribute to muscle development and function, their mechanisms of action are not well understood.

This review discusses a novel signaling network involving AXIN and AMP-activated protein kinase (AMPK) in maintaining muscle health that offers a new perspective on promoting healthy aging. Both these proteins are conserved in metazoans. AXIN is an established scaffolding protein that acts to integrate inputs from multiple signaling molecules, leading to the regulation of downstream effectors.[2] AMPK plays a crucial role in sensing intracellular energy levels and keeping a balance between cellular metabolism and growth.[3]

AXIN-AMPK signaling

Recent findings from our lab and other published studies involving AXIN and its interacting partner AMPK provide a potential clue into the mechanism of muscle health maintenance. Work in the nematode *C. elegans* has revealed that the AXIN family member PRY-1 is necessary for animals' normal motility and health, and its activated form promotes longevity by maintaining muscle mitochondrial homeostasis.[4] A similar function was previously ascribed to the AMPK catalytic subunit homolog AAK-2.[5,6] The genetic and biochemical experiments revealed that PRY-1 and AAK-2 work together, likely through protein-protein interaction, and PRY-1 is required for AAK-2-mediated beneficial effect on muscle health and lifespan (Figure 1). The interaction between PRY-1 and AAK-2 is not a unique phenomenon, as other AXIN family members also interact with AMPK in different biological contexts. For example, another *C. elegans* AXIN homolog AXL-1 forms a complex with AAK-2 following metformin treatment. Here, AXL-1 is necessary for metformin-mediated lysosomal localization and activation of AAK-2 in a VHA-3-LMTR-3-PAR-4 (v-ATPase-Ragulator-LKB1) complex dependent manner[7] (Figure 2).

The Axin-containing complexes are also reported in mammalian systems. Following metformin treatment and glucose deprivation,[8–10] the AXIN-based lysosomal pathway, consisting of v-ATPase-Ragulator complex (v-ATPase-Ragulator-AXIN/LKB1-AMPK), promotes AMPK phosphorylation by LKB1, leading to AMPK activation. In a separate study

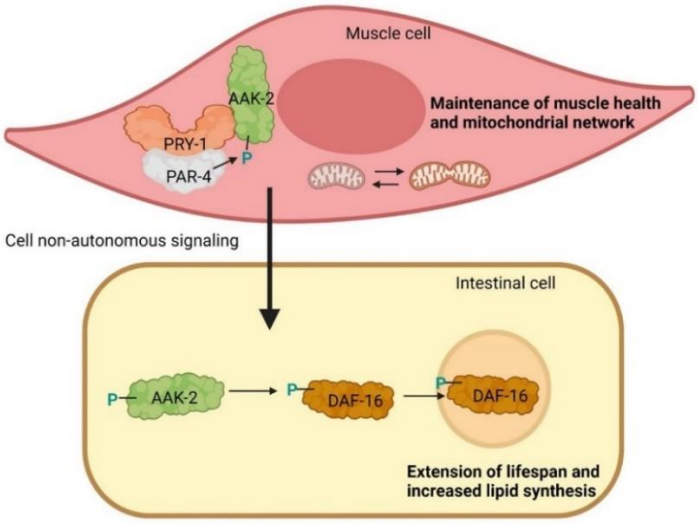

Figure 1. PRY-1/AXIN function in the muscle is necessary to maintain muscle health, mitochondrial biogenesis and longevity. Genetic and biochemical studies have shown that PRY-1/AXIN interacts with PAR-4/LKB1 and AAK-2/AMPK in muscles to promote AAK-2/AMPK phosphorylation. AAK-2 in turn activates DAF-16/FOXO cell non-autonomously in the intestine and promotes DAF-16/FOXO nuclear localization. Green colored P indicates activating phosphorylation.

F1000Research 2021, 10:1259 Last updated: 08 DEC 2021

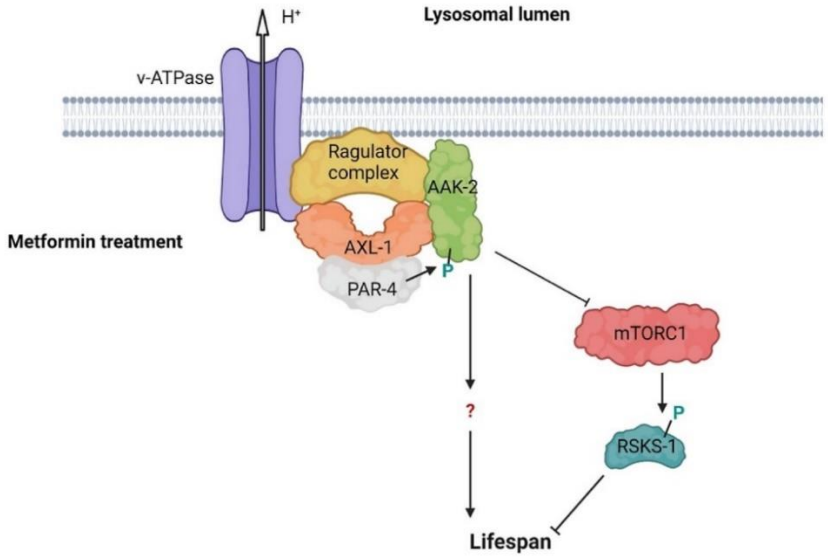

Figure 2. AXL-1/AXIN is required for metformin-mediated AAK-2/AMPK phosphorylation and longer lifespan in *C. elegans*. Metformin treatment induces formation of AXL-1/AXIN-based lysosomal VHA-3-LMTR-3-AXL-1/PAR-4-AAK-2 (v-ATPase-Ragulator-AXIN/LKB1-AMPK) complex that is required for AAK-2/AMPK activation. The effect of metformin is partially attained via inhibition of mTORC1, but other targets of the pathway remain unknown. Green colored P shows activating phosphorylation.

involving myotubes and mice gastrocnemius muscle tissue, exercise stimulated both AMPK and Rac1 while increasing the cellular levels of AXIN1. Accordingly, reducing the AXIN1 function blocked GTP loading of Rac1, AMPK activation, and glucose uptake in the exercising muscles.[11] Additionally, it was shown that muscle-specific knockout (KO) of the AXIN1-binding Ragulator subunit LAMTOR1 completely abolished treadmill exercise-stimulated AMPK activation in gastrocnemius muscle.[10] Together, these data demonstrate the crucial role of AXIN tethering in activating AMPK, which promotes muscle metabolism and benefits linked to exercise.

Investigations of cellular mechanisms underlying AXIN and AMPK interaction have revealed a regulatory relationship that depends on AMP levels[12] (Figure 3). While low glucose triggered AMP-dependent activation of AMPK through the AXIN-based lysosomal pathway, a modest increase in AMP resulted in AXIN-dependent activation of both lysosomal and cytosolic AMPK. Finally, extreme nutrient starvation or high AMP concentrations caused phosphorylation of AMPK independently of AXIN function.[12]

Intriguingly, it was shown recently that skeletal muscle-specific AXIN1 knockout (AXIN1 imKO) mice are phenotypically normal and exhibited no impairment of AMPK regulation or glucose uptake.[13] Such a phenotype may be explained by redundancies between AXIN1 and its homolog AXIN2. Both proteins are expressed in skeletal muscles, and AXIN2 can functionally replace AXIN1 in regulating AMPK.[12,14] Moreover, AXIN2, a negative regulator of WNT signaling, appears to be essential for myogenesis, as increased WNT signaling in aged skeletal muscle promoted fibrogenesis, thereby accelerating aging.[15–17]

Consistent with the role of AXIN in AMPK activation and myogenesis, AMPK is shown to be crucial for regulating skeletal muscle development, growth, and degradation.[18] In skeletal muscle, AMPK signaling has been linked to both acute and chronic exercise adaptations, in addition to a broad range of skeletal muscle disease states and ageing.[19,20] Together these data support the growing evidence that both AXIN and AMPK and their signaling cascade are crucial to maintaining healthy muscles and slowing organismal deterioration with aging.

F1000Research 2021, 10:1259 Last updated: 08 DEC 2021

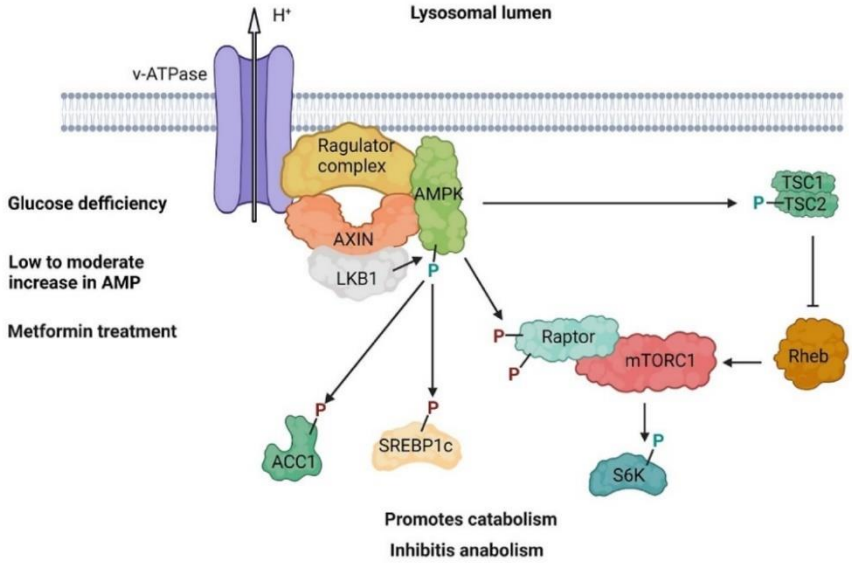

Figure 3. AXIN forms a lysosomal complex, v-ATPase-Ragulator-AXIN/LKB1-AMPK, that is crucial for AMPK activation and the maintenance of energy homeostasis during stress-inducing conditions. The complex is formed following glucose deprivation, low to moderate increases in AMP levels, and metformin treatment. Once activated, AXIN-AMPK signaling promotes catabolism and inhibits anabolism by phosphorylating downstream targets that include ACC1, SREBP1c, Raptor and TSC2. Green and purple colored P indicate activating and inhibitory phosphorylation, respectively.

Downstream effectors of AXIN-AMPK signaling

Studies in mammalian models revealed that both metformin and glucose deprivation inhibit the mechanistic target of rapamycin complex 1 (mTORC1) activity, a master regulator of anabolic pathways.[8,10] Both these treatments cause the mTORC1 components, RAPTOR and mTOR, to dissociate from the v-ATPase-Ragulator and facilitate the formation of the v-ATPase-Ragulator-AXIN/LKB1-AMPK complex. Similarly, research in *C. elegans* has demonstrated that the VHA-3-LMTR-3-AXL-1/PAR-4-AAK-2 complex negatively regulates phosphorylation of the mTORC1 target S6 kinase B1 (S6K) homolog RSKS-1.[7] As the beneficial effects of AXIN-AMPK signaling in the *C. elegans* study were not directly attributed to mTORC1 inhibition, the authors suggested that the signaling cascade may utilize additional factors[7] (Figure 2).

The downstream effectors of AXIN-AMPK have been reported in several other studies. Specifically, in a low glucose condition, the pathway phosphorylates proteins such as acetyl-CoA carboxylase (ACC1) and endoplasmic reticulum-localized sterol regulatory element-binding protein-1c (SREBP1c), thereby inhibiting fatty acid synthesis[12] (Figure 3). Interestingly, in *C. elegans*, PRY-1 promotes transcription of SREBP1 homolog SBP-1 to regulate fatty acid synthesis[4,21]; however, the precise mechanism of this regulatory relationship is unknown. Another effector of PRY-1 appears to be the CREB-regulated transcriptional coactivator (CRTC) homolog.[22] CRTC-1 is known to function downstream of AAK-2 and affects calcineurin-mediated lifespan and stress regulation in *C. elegans*.[23,24] While AMPK and calcineurin signaling in mammalian systems regulate CRTCs in an antagonistic manner, the involvement of Axin in this regulatory network remains to be determined.[25–28]

Given that AMPK regulates many targets, it is expected that a subset may be co-regulated by AXIN. We recently reported that both *pry-1* and *aak-2* mutant transcriptomes significantly overlap with mutually up and downregulated genes. These common differentially expressed genes are associated with muscle structure development, muscle contraction, aging, and lipid metabolism. Moreover, we found that PRY-1-AAK-2 signaling functions in muscles leading to activation of AAK-2 in a cell-non-autonomous manner and phosphorylation and translocation of the FOXO transcription factor homolog DAF-16 into the intestinal cell nuclei[4] (Figure 1). These results are supported by previous studies showing that activated

DAF-16 is indispensable for muscle mitochondria homeostasis and lifespan extension. It is worth mentioning that FOXO3 is also phosphorylated by AMPK in the mammalian system; however, the involvement of AXIN in this process and the function of activated FOXO3 are unknown.[29]

Unlike *C. elegans*, little is known about the role of AXIN and AMPK in regulating muscle health in another leading invertebrate model, namely the fruit fly *D. melanogaster*. Overexpression of *D-axin* in wing disc-associated myoblasts in larvae causes partial to complete loss of indirect flight muscles.[30] However, the precise role of *D-axin* and the involvement of AMPK and TORC1 in adult muscles is unknown. In terms of other processes, it has been reported that a hypomorphic allele of *D-axin* alters the expression of metabolic genes and is hypersensitive to metabolic stress induced by fasting. Such a phenotype depends on TORC1 activity and involves increased ROS production.[31]

Gaps in our knowledge

While much has been learned about Axin, AMPK, and their interactions, there are gaps in our understanding of the mechanisms regulating the complex formation, downstream effectors, and their role in maintaining muscle health. Some of the relevant questions are discussed below.

Is AXIN expression beneficial for muscle health?

The existing data supports that AXIN function in the muscle is beneficial. AXIN2 is required for myogenesis and linked to muscle aging, whereas AXIN1 mediated signaling is necessary for glucose uptake in the exercising muscles.[11,15,17] Both AXIN1 and AXIN2 are expressed in the skeletal muscle. Research in *C. elegans* hints that muscle-specific overexpression of *pry-1* promotes mitochondrial network, muscle development, and muscle physiology.[4] Whether such a role of Axin is conserved in higher eukaryotes is unknown.

Are AXIN1 and AXIN2 redundant in activating AMPK?

While AXIN1 and AXIN2 possess similar domains, they show differences in their regulation and expression pattern (subcellular localization and cell type-specific expression).[14,32] Additionally, AXIN2 is required for muscle development. Interestingly, exercise-induced glucose uptake requires AXIN1 in skeletal muscles. While it remains to be seen whether AXIN2 plays a redundant role in this process and regulates AMPK, Li *et al.*[13] reported no change in AMPK activation following AXIN1 imKO in the skeletal muscle. Furthermore, Zong *et al.*[12] showed that AXIN2 could substitute AXIN1 in forming a complex between LKB1 and AMPK.

In *C. elegans*, PRY-1 and AXL-1 possess the characteristic domains for the AXIN family of proteins[5] and negatively regulate WNT signaling.[33,34] It has been shown that AXL-1 functions redundantly with PRY-1 to regulate the WNT effector protein BAR-1/β-catenin during the formation of the vulva and migration of Q neuroblast. However, both AXINs are functionally not equivalent and play roles independently to control specific processes. For example, PRY-1 is necessary for lipid metabolism, healthspan, lifespan, and seam cell development, whereas AXL-1 regulates excretory cell development.[4,21,33–36] Recent experiments from our lab also highlight functional differences between the two Axin proteins. While PRY-1 and AXL-1 are necessary for metformin-induced lifespan extension,[7] only PRY-1 is required for glucose deprivation mediated longevity in *C. elegans* (Mallick *et al.*, unpublished). These same treatments, i.e., metformin and glucose deprivation, are known to extend the lifespan in an AAK-2-dependent manner.[37,38] Overall, these studies demonstrate that AXIN homologs in every system have shared as well as unique functions. However, whether these proteins can redundantly activate AMPK remains to be investigated.

What factors limit AXIN-AMPK signaling?

Recent reports demonstrate that the lysosomal AXIN-AMPK signaling can be activated by glucose deprivation independently of AMP/ATP ratios. However, the medium-to-high elevation of AMP extends the activation of both cytosolic and lysosomal AMPK, which is also dependent on AXIN1.[12] By contrast, very high AMP levels phosphorylate AMPK in a manner that does not involve AXIN1 and probably occurs via a conformational change in AMPK. Whether AXIN-dependent activation of AMPK also requires a similar change in AMPK conformation is unclear. Furthermore, it is unknown how glucose levels facilitate the complex formation and differential activation of AMPK by LKB1.

Several other factors may also limit AXIN and AMPK mediated signaling. One of these is post-translational modification. AXIN activity is known to be regulated by phosphorylation.[2,39,40] Another could be subcellular localization. While the AXIN-AMPK complex is localized to lysosomes and cytoplasm, the changes in their activities in response to external stimuli are poorly understood.[10,12] Both factors are broadly expressed and in overlapping domains; however, whether their interactions are global or restricted to specific tissues remains to be determined. In this regard, it is worth mentioning that AMPK functions cell non-autonomously in *C. elegans*,[24] and we have reported that the protein is needed in both muscles and intestine to mediate beneficial effects of constitutive expression of AXIN in muscles.[4]

What are the effectors of AXIN-AMPK signaling?

Given that AMPK is involved in many different processes and regulates many downstream targets, one might expect that AXIN-AMPK interaction co-regulates a subset of the targets. In support of this, a recent paper suggests that AXIN-AMPK signaling phosphorylates targets that are different from ATP/AMP-dependent AMPK signaling.[12] As mentioned above, our analysis of *C. elegans pry-1* and *aak-2* transcriptomes has revealed many overlapping genes that are differentially expressed. However, more work is needed to identify and validate common targets of AXIN-AMPK signaling that are involved in maintaining muscle health in different systems. Identification of such target genes could lead to a better understanding of molecular mechanisms underlying the signaling network and the development of diagnostic markers and therapeutic interventions to promote muscle health.

New research directions

We envisage several exciting research avenues involving AXIN-AMPK signaling. While substantial knowledge has been gained in terms of processes that each one participates in and mechanisms underlying their function, little is known how the interactions between the two proteins are regulated, leading to changes in the expression of target genes that carry out various roles. Below are some of the potential research directions to address the questions in the previous section.

While it has been shown that the AXIN homologs in both *C. elegans* (PRY-1 and AXL-1) and mammalian systems (AXIN1 and AXIN2) can activate AMPK,[4,7,9,12] the redundancies between the homologs and their tissue-specific interactions with AMPK are unknown. Moreover, the differences in lifespan and lipid metabolism phenotypes between the two AXIN mutants in *C. elegans* raise the question of functional equivalency regarding AMPK activation in physiological conditions. Future research along these lines should refine our understanding of AXIN-AMPK signaling and its conservation in eukaryotes.

Depending on the context, signaling pathways may utilize different mechanisms to regulate their responses. In this regard, research in the following areas should improve our understanding of the regulatory mechanism of AXIN-AMPK signaling. First, whether a conformational change in AMPK following AXIN binding occurs similar to the AMP-dependent mechanism. Second, the role of post-translational modification of AXIN in activating AMPK. Third, identifying a specific region of the multidomain AXIN protein required for AMPK interaction that, in turn, may uncover potential competitors to modulate the signaling. And, finally, the discovery of factors affecting subcellular localizations of both AXIN and AMPK and, in turn, their interactions.

Other modes of regulation of AXIN-AMPK signaling may include spatial and temporal changes in AXIN expression. AXIN is not only a negative regulator but also a downstream target of the WNT signaling.[21,41] Consistent with this, PRY-1/AXIN is required for MOM-2/WNT mediated lifespan regulation,[4] and MOM-2 is expressed in the body wall muscles of *C. elegans*. It remains to be explored whether AXIN function in muscles is regulated in a WNT-dependent manner in eukaryotes.

Research from our group has shown that overexpression of PRY-1/AXIN in *C. elegans* extends the lifespan and improves muscle health in older adults. Whether forced expression of mammalian AXIN in muscles may also promote the healthspan of animals by activating AXIN-AMPK signaling requires investigation. In line with this, expression analysis of AXIN1 and AXIN2 in old adults and patients with a muscle disease should prove valuable.

As mentioned above, AXIN and AMPK are crucial for muscle development and physiology. Furthermore, exercise promotes the activation of AMPK in an AXIN-dependent manner. Given that exercise promotes muscle health and delays aging,[42–44] it is conceivable that AXIN and AMPK are involved in this process. More work is needed to understand the role of AXIN-AMPK signaling in exercise-mediated benefits.

Conclusion

AXIN family of scaffolding proteins control a wide array of cellular processes by recruiting multiple factors and forming protein complexes. One of the interactors of AXIN is the well-known energy sensor AMPK. AMPK functions as a nexus between energy conservation and aging, and perturbations of its function lead to various age-related pathologies. AXIN-AMPK signaling promotes muscle health and delays age-associated deterioration. Future studies on the pathway, its interacting proteins, and tissue-specific effectors hold promise to uncover key candidates that may be targeted in the future to delay age-associated muscle degeneration and improve muscle health during aging.

Data availability

No data are associated with this article.

Acknowledgements

Authors thank Gupta lab members for discussions on the topic and feedback on the manuscript. Figures were created using BioRender.

References

1. Wang Y, Wehling-Henricks M, Samengo G, *et al.*: **Increases of M2a macrophages and fibrosis in aging muscle are influenced by bone marrow aging and negatively regulated by muscle-derived nitric oxide.** *Aging Cell.* 2015; **14**(4): 678–688.
PubMed Abstract | Publisher Full Text | Free Full Text
2. Mallick A, Taylor SKB, Ranawade A, *et al.*: **Axin Family of Scaffolding Proteins in Development: Lessons from C. elegans.** *J. Dev. Biol.* 2019; **7**(4): 1–23.
3. Hardie DG, Ross FA, Hawley SA: **AMPK: A nutrient and energy sensor that maintains energy homeostasis.** *Nat. Rev. Mol. Cell Biol.* 2012; **13**(4): 251–262.
PubMed Abstract | Publisher Full Text | Free Full Text
4. Mallick A, Ranawade A, van den Berg W, *et al.*: **Axin-Mediated Regulation of Lifespan and Muscle Health in C. elegans Requires AMPK-FOXO Signaling.** *iScience.* 2020; **23**(12): 101843.
PubMed Abstract | Publisher Full Text | Free Full Text
5. Lee H, Jeong SC, Lambacher N, *et al.*: **The Caenorhabditis elegans AMP-activated protein kinase AAK-2 is phosphorylated by LKB1 and is required for resistance to oxidative stress and for normal motility and foraging behavior.** *J. Biol. Chem.* 2008; **283**(22): 14988–14993.
PubMed Abstract | Publisher Full Text | Free Full Text
6. Weir HJ, Yao P, Huynh FK, *et al.*: **Dietary Restriction and AMPK Increase Lifespan via Mitochondrial Network and Peroxisome Remodeling.** *Cell Metab.* 2017; **26**(6): 884–896.e5.
PubMed Abstract | Publisher Full Text | Free Full Text
7. Chen J, Ou Y, Li Y, *et al.*: **Metformin extends C. Elegans lifespan through lysosomal pathway.** *elife.* 2017; **6**: 1–17.
Publisher Full Text
8. Zhang CS, Li M, Ma T, *et al.*: **Metformin Activates AMPK through the Lysosomal Pathway.** *Cell Metab.* 2016; **24**(4): 521–522.
PubMed Abstract | Publisher Full Text
9. Zhang YL, Guo H, Zhang CS, *et al.*: **AMP as a low-energy charge signal autonomously initiates assembly of axin-ampk-lkb1 complex for AMPK activation.** *Cell Metab.* 2013; **18**(4): 546–555.
PubMed Abstract | Publisher Full Text
10. Zhang CS, Jiang B, Li M, *et al.*: **The lysosomal v-ATPase-ragulator complex is a common activator for AMPK and mTORC1, acting as a switch between catabolism and anabolism.** *Cell Metab.* 2014; **20**(3): 526–540.
PubMed Abstract | Publisher Full Text
11. Yue Y, Zhang C, Zhang X, *et al.*: **An AMPK/Axin1-Rac1 signaling pathway mediates contraction-regulated glucose uptake in skeletal muscle cells.** *Am. J. Physiol. Endocrinol. Metab.* 2020; **318**(3): E330–E342.
PubMed Abstract | Publisher Full Text
12. Zong Y, Zhang CS, Li M, *et al.*: **Hierarchical activation of compartmentalized pools of AMPK depends on severity of nutrient or energy stress.** *Cell Res.* 2019; **29**(6): 460–473.
PubMed Abstract | Publisher Full Text | Free Full Text
13. Li J, Knudsen JR, Henriquez-Olguin C, *et al.*: **AXIN1 knockout does not alter AMPK/mTORC1 regulation and glucose metabolism in mouse skeletal muscle.** *J. Physiol.* 2021; **599**(12): 3081–3100.
PubMed Abstract | Publisher Full Text
14. Uhlén M, Fagerberg L, Hallström BM, *et al.*: **Tissue-based map of the human proteome.** *Science (80-).* 2015; **347**(6220).
PubMed Abstract | Publisher Full Text
15. Huraskin D, Eiber N, Reichel M, *et al.*: **Wnt/β-catenin signaling via Axin2 is required for myogenesis and, together with YAP/Taz and tead1, active in IIa/IIx muscle fibers.** *Dev.* 2016; **143**(17): 3128–3142.
PubMed Abstract | Publisher Full Text
16. Arthur ST, Cooley ID: **The effect of physiological stimuli on sarcopenia; Impact of Notch and Wnt signaling on impaired aged skeletal muscle repair.** *Int. J. Biol. Sci.* 2012; **8**(5): 731–760.
PubMed Abstract | Publisher Full Text | Free Full Text
17. Brack AS, Conboy MJ, Roy S, *et al.*: **Increased Wnt signaling during aging alters muscle stem cell fate and increases fibrosis.** *Science (80-).* 2007; **317**(5839): 807–810.
PubMed Abstract | Publisher Full Text
18. Thomson DM: **The role of AMPK in the regulation of skeletal muscle size, hypertrophy, and regeneration.** *Int. J. Mol. Sci.* 2018; **19**(10).
PubMed Abstract | Publisher Full Text | Free Full Text
19. Jensen TE, Wojtaszewski JFP, Richter EA: **AMP-activated protein kinase in contraction regulation of skeletal muscle metabolism: Necessary and/or sufficient?.** *Acta Physiol.* 2009; **196**(1): 155–174.
PubMed Abstract | Publisher Full Text
20. Kjøbsted R, Hingst JR, Fentz J, *et al.*: **AMPK in skeletal muscle function and metabolism.** *FASEB J.* 2018; **32**(4): 1741–1777.
PubMed Abstract | Publisher Full Text | Free Full Text
21. Ranawade A, Mallick A, Gupta BP: **PRY-1/Axin signaling regulates lipid metabolism in Caenorhabditis elegans.** *PLoS One.* 2018; **13**(11): e0206540.
PubMed Abstract | Publisher Full Text | Free Full Text
22. Mallick A, Taylor SKB, Mehta S, *et al.*: **picd-1, a gene that encodes CABIN1 domain-containing protein, interacts with pry-1/Axin to regulate multiple processes in Caenorhabditis elegans.** *bioRxiv.* 2021; 1–37.
23. Mair W, Morantte I, Rodrigues APC, *et al.*: **Lifespan extension induced by AMPK and calcineurin is mediated by CRTC-1 and CREB.** *Nature.* 2011; **470**(7334): 404–408.
PubMed Abstract | Publisher Full Text | Free Full Text
24. Burkewitz K, Morantte I, Weir HJM, *et al.*: **Neuronal CRTC-1 Governs Systemic Mitochondrial Metabolism and Lifespan via a Catecholamine Signal.** *Cell.* 2015; **160**(5): 842–855.
PubMed Abstract | Publisher Full Text | Free Full Text
25. Screaton RA, Conkright MD, Katoh Y, *et al.*: **The CREB coactivator TORC2 functions as a calcium- and cAMP-sensitive coincidence detector.** *Cell.* 2004; **119**(1): 61–74.
PubMed Abstract | Publisher Full Text
26. Koo SH, Flechner L, Qi L, *et al.*: **The CREB coactivator TORC2 is a key regulator of fasting glucose metabolism.** *Nature.* 2005; **437**(7062): 1109–1114.
PubMed Abstract | Publisher Full Text
27. Komiya T, Coxon A, Park Y, *et al.*: **Enhanced activity of the CREB co-activator Crtc1 in LKB1 null lung cancer.** *Oncogene.* 2010; **29**(11): 1672–1680.
PubMed Abstract | Publisher Full Text | Free Full Text
28. Wang Y, Vera L, Fischer WH, *et al.*: **The CREB coactivator CRTC2 links hepatic ER stress and fasting gluconeogenesis.** *Nature.* 2009; **460**(7254): 534–537.
PubMed Abstract | Publisher Full Text | Free Full Text
29. Greer EL, Oskoui PR, Banko MR, *et al.*: **The energy sensor AMP-activated protein kinase directly regulates the mammalian FOXO3 transcription factor.** *J. Biol. Chem.* 2007; **282**(41): 30107–30119.
Publisher Full Text
30. Benchabane H, Xin N, Tian A, *et al.*: **Jerky/Earthbound facilitates cell-specific Wnt/Wingless signalling by modulating β-catenin-TCF activity.** *EMBO J.* 2011; **30**(8): 1444–1458.
PubMed Abstract | Publisher Full Text | Free Full Text
31. Zhang T, Liao Y, Hsu FN, *et al.*: **Hyperactivated Wnt Signaling Induces Synthetic Lethal Interaction with Rb Inactivation by Elevating TORC1 Activities.** *PLoS Genet.* 2014; **10**(5): e1004357.
PubMed Abstract | Publisher Full Text | Free Full Text
32. Thul PJ, Akesson L, Wiking M, *et al.*: **A subcellular map of the human proteome.** *Science (80-).* 2017; **356**(6340).
PubMed Abstract | Publisher Full Text
33. Oosterveen T, Coudreuse DYM, Yang PT, *et al.*: **Two functionally distinct Axin-like proteins regulate canonical Wnt signaling in C. elegans.** *Dev. Biol.* 2007; **308**(2): 438–448.
PubMed Abstract | Publisher Full Text
34. Korswagen HC, DYM C, Betist MC, *et al.*: **The Axin-like protein PRY-1 is a negative regulator of a canonical Wnt pathway in C. elegans.**

Genes Dev. 2002; **16**(10): 1291–1302.
PubMed Abstract | Publisher Full Text | Free Full Text

35. Mallick A, Ranawade A, Gupta BP: **Role of PRY-1/Axin in heterochronic miRNA-mediated seam cell development.** *BMC Dev. Biol.* 2019; **19**(1): 1–12.

36. Mallick A, Gupta BP: **Vitellogenin-2 acts downstream of PRY-1/Axin to regulate lipids and lifespan in C. elegans.** *microPublication Biol.* 2020; **1**: 19–21.

37. Onken B, Driscoll M: **Metformin induces a dietary restriction-like state and the oxidative stress response to extend C. elegans healthspan via AMPK, LKB1, and SKN-1.** *PLoS One.* 2010; **5**(1): e8758.
PubMed Abstract | Publisher Full Text | Free Full Text

38. Schulz TJ, Zarse K, Voigt A, *et al.*: **Glucose Restriction Extends Caenorhabditis elegans Life Span by Inducing Mitochondrial Respiration and Increasing Oxidative Stress.** *Cell Metab.* 2007; **6**(4): 280–293.
PubMed Abstract | Publisher Full Text

39. Tacchelly-Benites O, Wang Z, Yang E, *et al.*: **Axin phosphorylation in both Wnt-off and Wnt-on states requires the tumor suppressor APC.** *PLoS Genet.* 2018; **14**(2): 1–24.
Publisher Full Text

40. Wang Z, Tacchelly-Benites O, Yang E, *et al.*: **Dual Roles for Membrane Association of Drosophila Axin in Wnt Signaling.** *PLoS Genet.* 2016; **12**(12): 1–26.
Publisher Full Text

41. Jho E, Zhang T, Domon C, *et al.*: **Wnt/β-Catenin/Tcf Signaling Induces the Transcription of Axin2, a Negative Regulator of the Signaling Pathway.** *Mol. Cell. Biol.* 2002; **22**(4): 1172–1183.
PubMed Abstract | Publisher Full Text | Free Full Text

42. Hartman JH, Smith LL, Gordon KL, *et al.*: **Swimming Exercise and Transient Food Deprivation in Caenorhabditis elegans Promote Mitochondrial Maintenance and Protect Against Chemical-Induced Mitotoxicity.** *Sci. Rep.* 2018; **8**(1): 1–16.

43. Laranjeiro R, Harinath G, Burke D, *et al.*: **Single swim sessions in C. elegans induce key features of mammalian exercise.** *BMC Biol.* 2017; **15**(1): 1–17.
Publisher Full Text

44. Laranjeiro R, Harinath G, Hewitt JE, *et al.*: **Swim exercise in Caenorhabditis elegans extends neuromuscular and gut healthspan, enhances learning ability, and protects against neurodegeneration.** *Proc. Natl. Acad. Sci. U. S. A.* 2019; **116**(47): 23829–23839.
PubMed Abstract | Publisher Full Text | Free Full Text

Appendix A

PRY-1 is autoregulated via canonical WNT signaling

A.1 Preface

In this chapter, I report the autoregulation of PRY-1 that is dependent on the canonical WNT signaling. Overall, we show a unique feature of the *pry-1* transcriptional response which is dependent on the WNT canonical components *bar-1/β-catenin* and *pop-1/TCF*. Such feedback is also known for one of the Axin homologs, Axin2 in mammals. Additionally, we also discovered a new transcription factor BLMP-1, which is the *C. elegans* homolog of the human BLIMP1, that also regulates *pry-1* expression in a dose dependent manner. Some of the data reported here is contributed by Jessica Knox and Hannah Hosein from the lab.

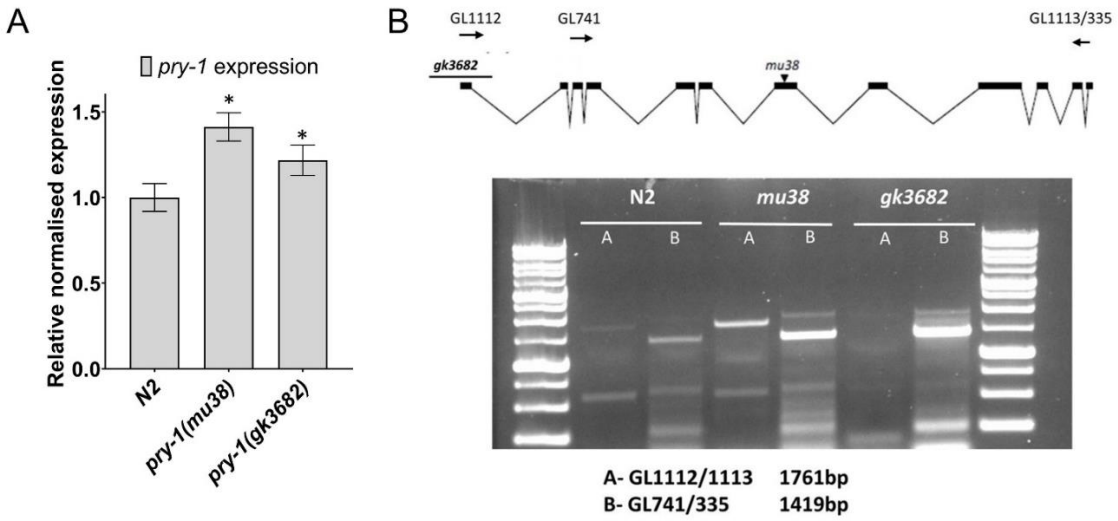

Figure A.1: *pry-1* mutants exhibit increased *pry-1* transcript levels. (A) Expression analysis of *pry-1* in the two *pry-1* mutant background. Data represents the mean of two replicates and error bars the standard error of mean. Significance was calculated using Bio-Rad software (one-way ANOVA) and significant differences are indicated by stars (*): ** (p <0.01). **(B)** PCR confirmation of transcripts for *pry-1(mu38)* and *pry-1(gk3682)* mutants. Only *pry-1(mu38)* makes the full length transcript but not *pry-1(gk3682)*. PCR validates qPCR data from panel **(A)**.

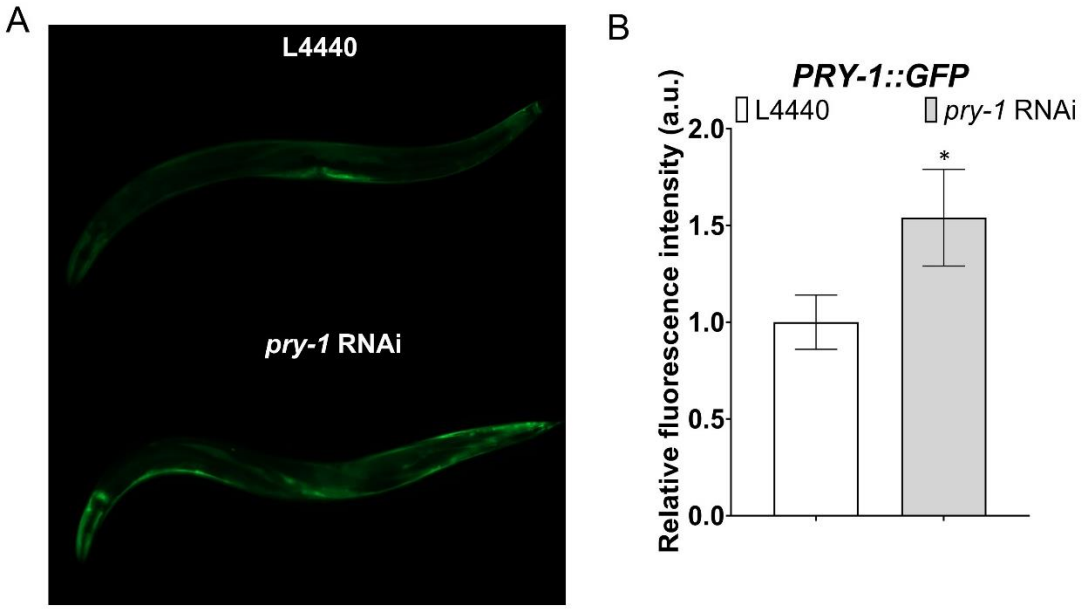

Figure A.2: *pry-1* autoregulation following *pry-1* RNAi reflects in the protein levels too. (A) Representative images of *pry-1p::PRY-1::GFP* animals following control (L4440) and pry-1 RNAi knockdown. **(B)** Bar graph represents the quantification of GFP intensity in PRY-1::GFP animals from panel **(A).** In all cases data represent a cumulative of two replicates (n > 30 animals in total for each condition) and error bars represent the standard deviation. Statistical analyses were done using one-way ANOVA

with Dunnett's post hoc test and significant differences are indicated by stars (*): * (p <0.05). This experiment was conducted by Hannah Hosein.

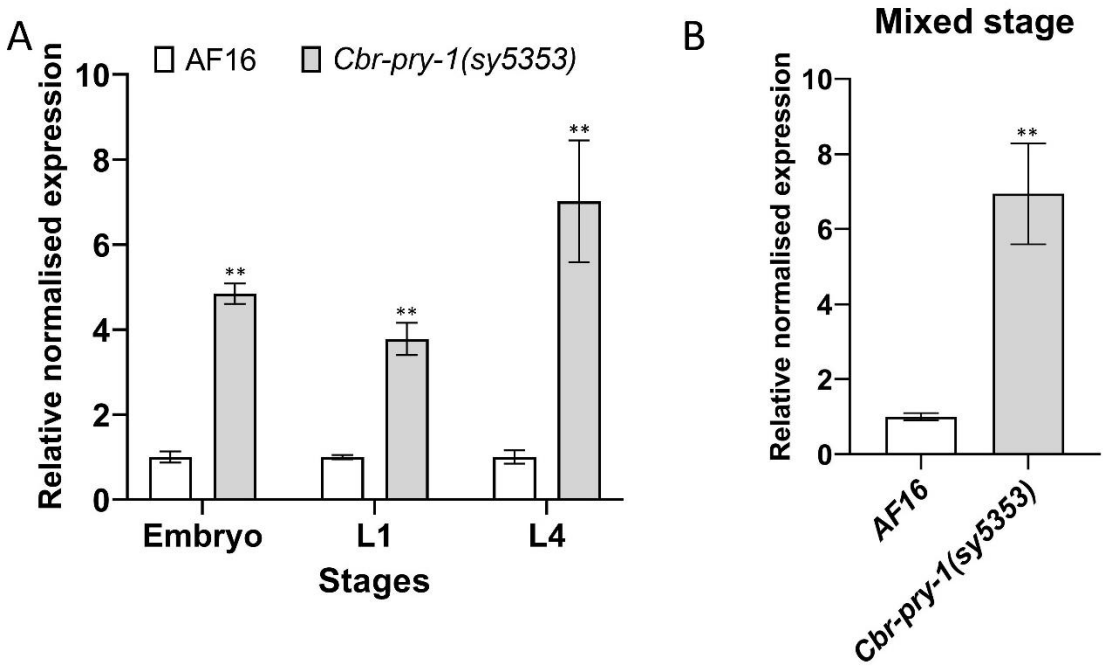

Figure A.3: *pry-1* autoregulation is also conserved in *C. briggsae*. (A) qPCR analysis of *Cbr-pry-1* expression in the *Cbr-pry-1(sy5353)* mutants at embryo, L1 and L4 stages. **(B)** qPCR analysis of *Cbr-pry-1* expression in the *Cbr-pry-1(sy5353)* mutants at the mixed stage compared to AF16 animals. Data represents the mean of two replicates and error bars the standard error of mean. Significance was calculated using Bio-Rad software (one-way ANOVA) and significant differences are indicated by stars (*): ** (p <0.01). This experiment has been carried by Jessica Knox.

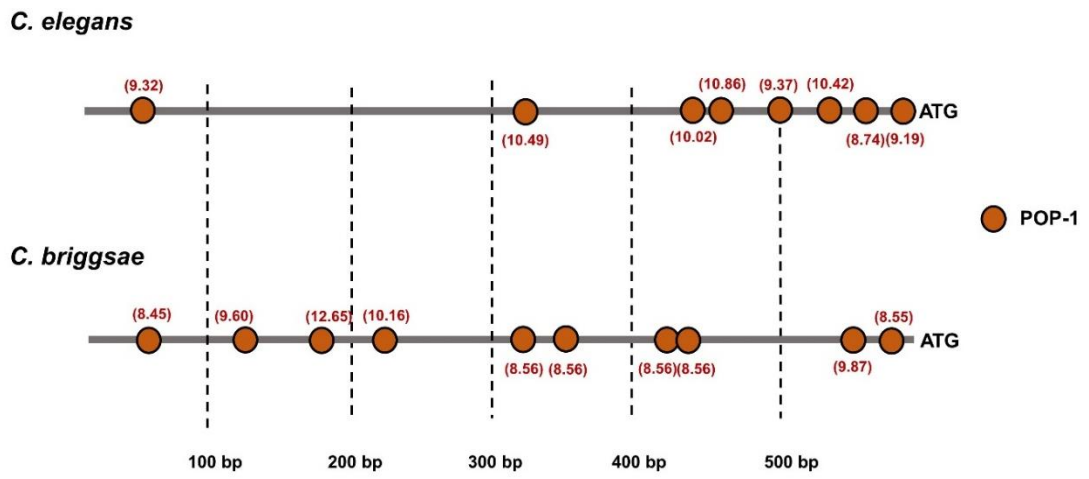

Figure A.4: Multiple conserved POP-1 binding sites in the *pry-1* promoter region. Schematic diagram of the POP-1 binding sites at the 5' upstream sequence of the *pry-1* promoter sequence in both *C. elegans* and *C. briggsae*. This data has been plotted using the CISBP platform (http://cisbp.ccbr.utoronto.ca/). For scores noted at the bottom, binding is at the reverse strand.

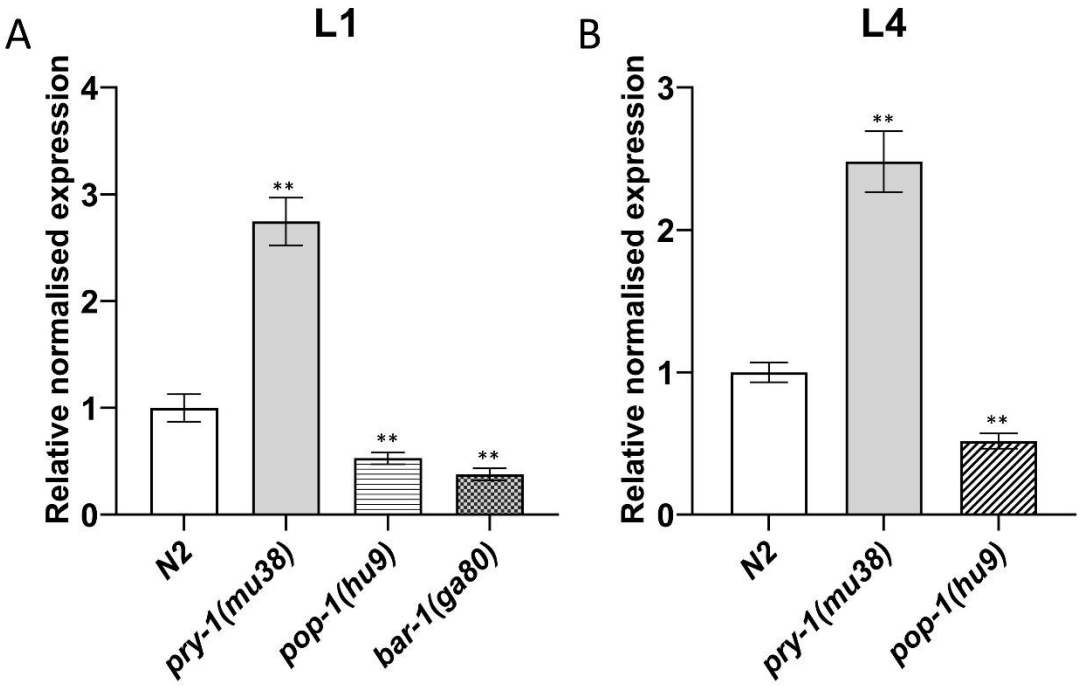

Figure A.5: *bar-1* and *pop-1* are needed for *pry-1* expression. **(A)** qPCR analysis of *pry-1* expression in the *pry-1*, *pop-1* and *bar-1* mutants compared to control at the L1 stage. **(B)** qPCR analysis of *pry-1* expression in the *pry-1* and *pop-1* mutants compared to control at the L4 stage. Data represents the mean of two replicates and error bars the standard error of mean. Significance was calculated using Bio-Rad software (one-way ANOVA) and significant differences are indicated by stars (*): ** (p <0.01). This experiment has been carried by Jessica Knox.

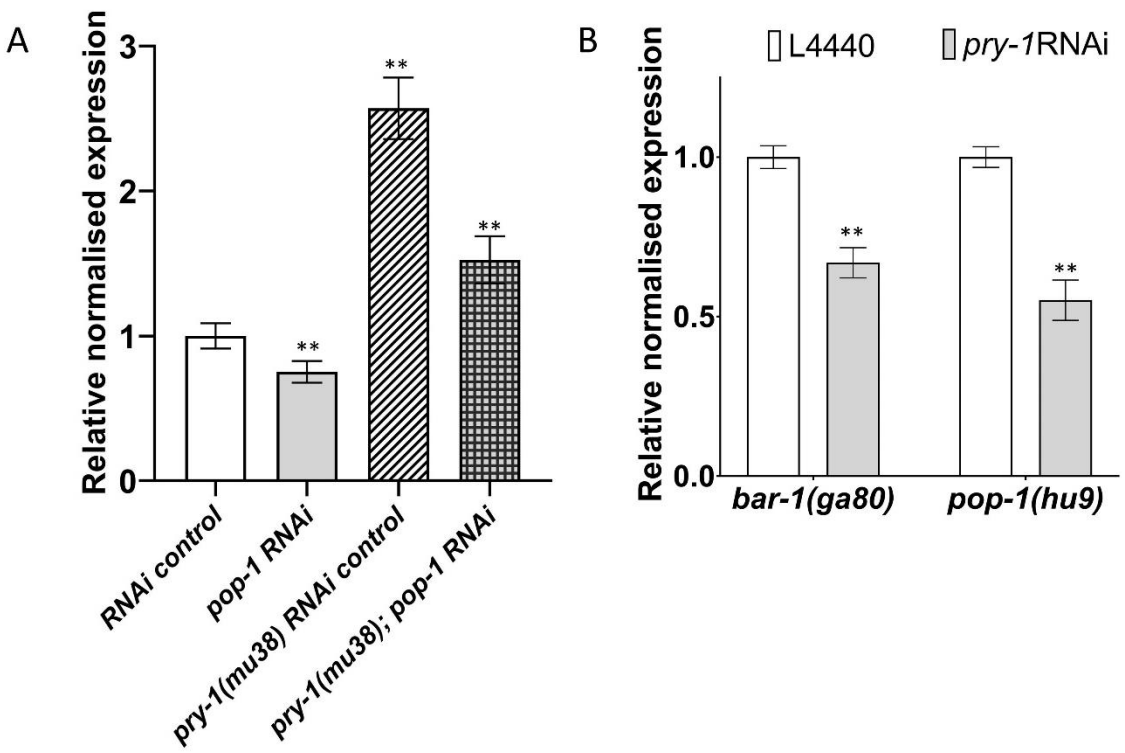

Figure A.6: *pry-1* autoregulation is dependent on BAR-1-POP-1 function. (A) qPCR analysis of *pry-1* expression in the *pry-1* mutants following control (L4440) and *pop-1* RNAi compared to wild type animals. **(B)** qPCR analysis of *pry-1* expression in the *bar-1* and *pop-1* mutants following control (L4440) and *pry-1* RNAi. Data represents the mean of two replicates and error bars the standard error of mean. Significance was calculated using Bio-Rad software (one-way ANOVA) and significant differences are indicated by stars (*): ** (p <0.01).

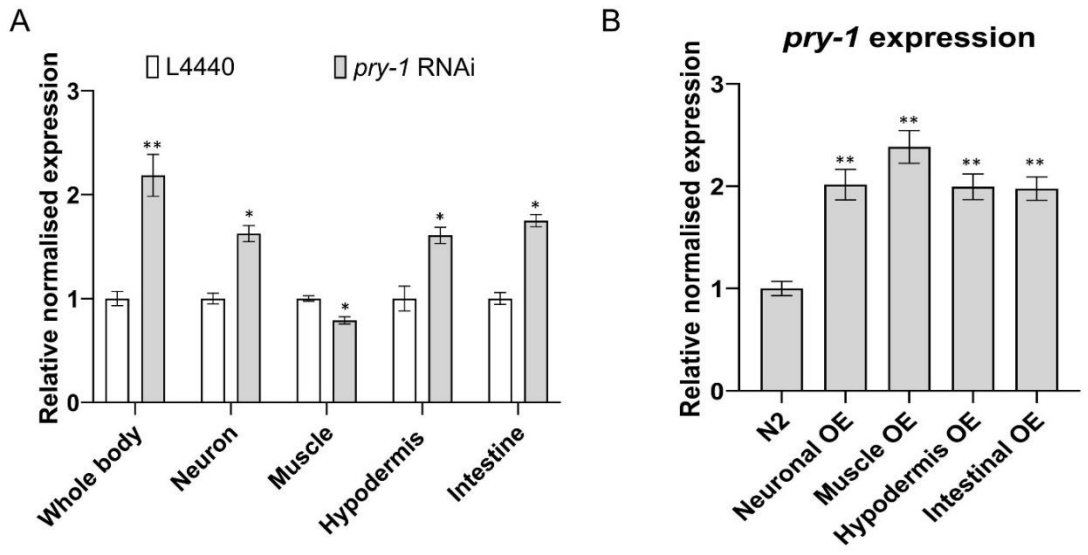

Figure A.7: Muscle tissue appears to have reduced *pry-1* autoregulation. (A) qPCR analysis of *pry-1* expression in the tissue-specific RNAi sensitive strains following control (L4440) and *pry-1* RNAi. **(B)** qPCR analysis of *pry-1* expression in the tissue-specific *pry-1* overexpression strains compared to wild type animals. Data represents the mean of two replicates and error bars the standard error of mean. Significance was calculated using Bio-Rad software (one-way ANOVA) and significant differences are indicated by stars (*): * (p <0.05), ** (p <0.01).

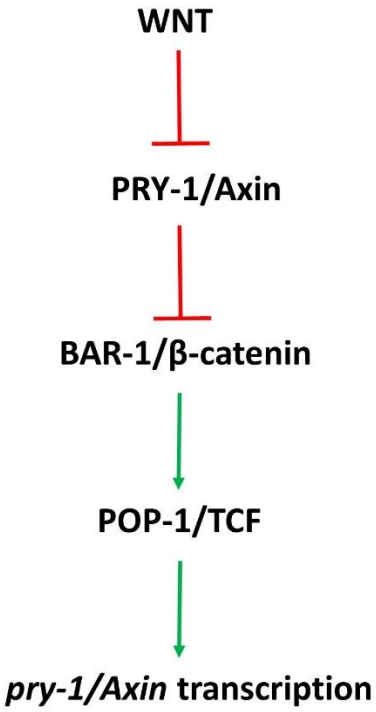

Figure A.8: Proposed model of *pry-1* negative feedback loop. This model proposes that pry-1 expression is partly dependent on the (WNT signaling) BAR-1-POP-1 mediated transcriptional activation. But it is highly plausible that *pry-1* expression requires other transcription factors that are independent of WNT signaling.

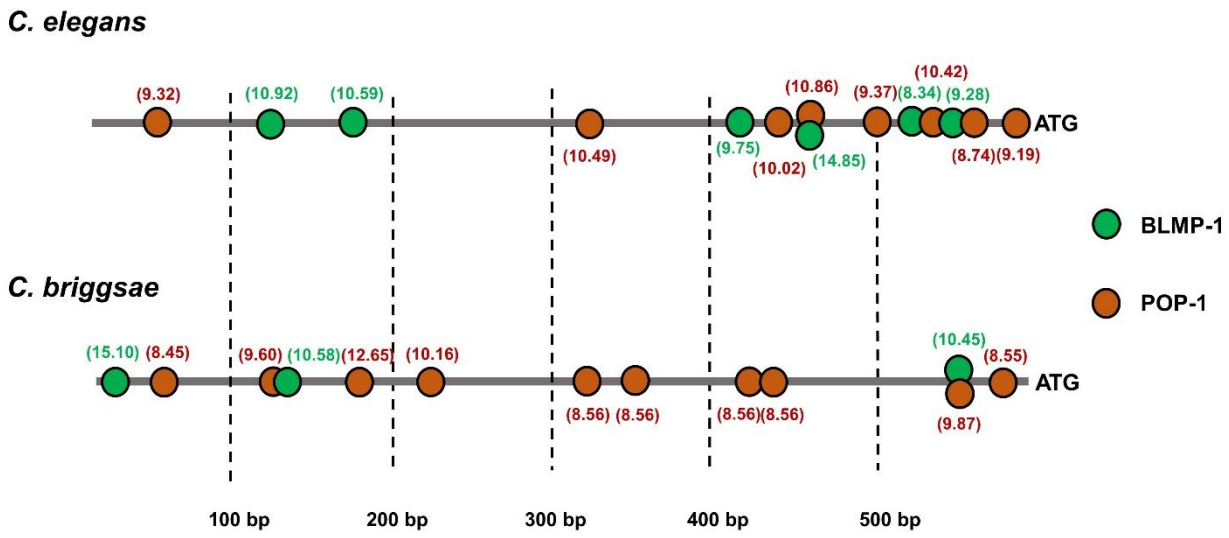

Figure A.9: Multiple conserved POP-1 and BLMP-1 binding sites in the *pry-1* promoter region. Schematic diagram of the POP-1 and BLMP-1 binding sites at the 5' upstream sequence of the *pry-1* promoter sequence in both *C. elegans* and *C. briggsae*. This data has been plotted using the CISBP platform (http://cisbp.ccbr.utoronto.ca/). For scores noted at the bottom, binding is at the reverse strand.

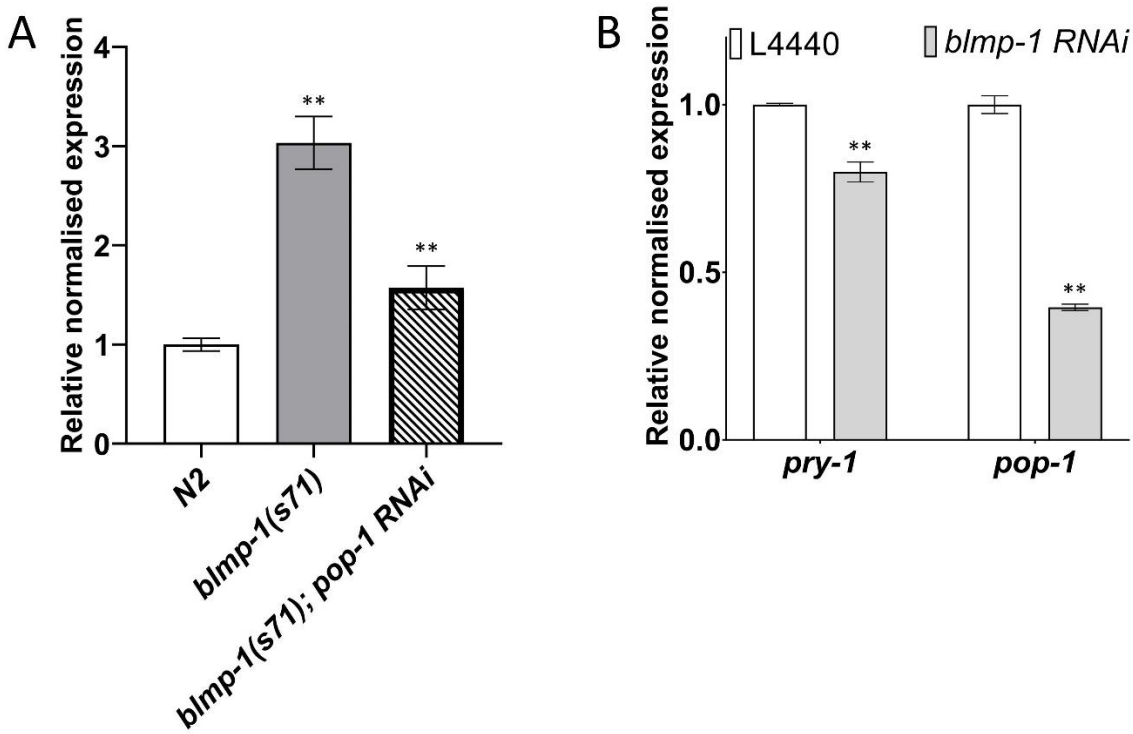

Figure A.10: BLMP-1 regulates *pry-1* expression in a dose dependent manner. (A) qPCR analysis of *pry-1* expression in the *blmp-1* mutant following control (L4440) and *pop-1* RNAi compared to wild type animals. **(B)** qPCR analysis of *pry-1* and *pop-1* expression following control (L4440) and *blmp-1* RNAi. Data represents the mean of two replicates and error bars the standard error of mean. Significance was calculated using Bio-Rad software (one-way ANOVA) and significant differences are indicated by stars (*): ** (p <0.01).

Appendix B

Characterising a receptor tyrosine kinase *F09A5.2* in *C. elegans*

B.1 Preface

In this chapter, I characterise another receptor tyrosine kinase receptor F09A5.2 which has high similarity with the KIN-9/FGFR4 protein described in Appendix B. *F09A5.2* is predicted to be a receptor tyrosine kinase and is expressed in multiple tissues. Specifically, it is expressed in the head and tail neurons, body wall muscles and intestine. We have acquired two deletion alleles of this gene, *tm7493* and *ok1900*. While *tm7493* is 93bp deletion that does not change the frame and is supposed to produce a protein of 834aa, *ok1900* allele is a larger deletion of 1135bp that is expected to translate a truncated protein of 243aa only. Consistent with this, *F09A5.2(tm7493)* mutants show

no significant change in lifespan compared to control animals. But the other mutant, *F09A5.2(ok1900)* is found to be long lived. It will be interesting to characterise these mutants in detail which will allow us to understand the function of this genes in *C. elegans*. Moreover, it is also possible that while the *tm7493* allele show no obvious lifespan defect, it may possess other phenotypes.

B.2 F09A5.2 is more similar to KIN-9 than EGL-15

While analyzing the homologs of *kin-9* in *C. elegans*, we found *egl-15/FGFR* as expected. Interestingly, our analysis revealed another tyrosine kinase receptor *F09A5.2* which has higher similarity and identity with *kin-9* compared to *egl-15* (Figure C.1). This finding is also supported by a previously published article by Popovici et al (1999) where they report a phylogenetic tree based on the alignment of the tyrosine kinase domain of RTKs with four RTKs (*F09A5.2*, *F09G2.1*, *F08F1.1* (*kin-9*), and *C24G6.2*) grouped together (bootstrap value of >900). *kin-9 egl-15* and *F09A5.2* are all located on chromosome X. Moreover, *F09A5.2* was also found to be differentially expressed in the *pry-1* mutants transcriptome data. Given such similarity and potential downstream target candidate of *pry-1* signaling, we went on to characterize the role and expression of *F09A5.2* in *C. elegans*.

A

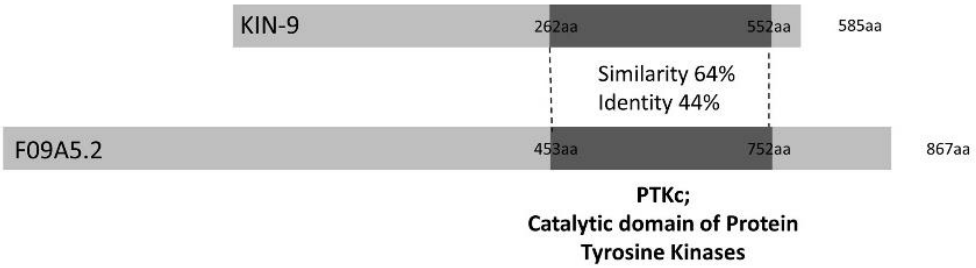

B

Score	Expect	Method	Identities	Positives	Gaps
290 bits(741)	1e-87	Compositional matrix adjust.	137/314(44%)	203/314(64%)	9/314(2%)

```
Query  262  DPWLLDRNNLEINYSKKLGSGAFCNVFKGKINGEAPVSQIHPGQRTQLLRD----CPVAV  317
            D W +D  NL +     LG+GAF NV+KG + G+ P+  ++      +  +       A+
Sbjct  453  DIWEIDTKNLLVQEDHLLGNGAFANVYKGIVKGKIPLLVVNNSLNMTVESENNGHYEAAI  512

Query  318  KMLPSFADDAARSDFMQEINFMKSLAYHPHLVSMLGFVADRKSPYLLVEFCEHGDLLHMI  377
            K LP+ AD+    DF  EI+FMK L +HPH++SMLG V++   P ++VE+C  GDLL  +
Sbjct  513  KKLPAHADEQNHLDFFHEIDFMKRLGHHPHVISMLGCVSNPYEPLIVVEYCARGDLLKFL  572

Query  378  RNRRQEII-----NGPTENPDGLKIKDLLMFSWQISNGLEYLNNIGCIHRDIAARNVLVD  432
            R  +  ++     + P E    L+IKDL+  +WQ+++G+ YL +   IHRD+AARN+L+
Sbjct  573  RRHKDYVLMNKTDDCPIEADMCLRIKDLVSIAWQVADGMSYLASKNFIHRDLAARNILLT  632

Query  433  SANTCKIGDFGLCRLTDSLLYTARGGRLPLKWMAPESLATYEYSYKSDVWSYGVLLWELF  492
             + T K+ DFGLCR  DS LYTA+GGRLP+KWM+ E+L  YE+S K+DVWS+GVLL+E+F
Sbjct  633  KSLTAKVSDFGLCRYMDSALYTAKGGRLPIKWMSVEALKLYEFSTKTDVWSFGVLLFEIF  692

Query  493  SLGEVPYGEVQTTELLQTHRSGKRLLKPEWCPEEIYDVMRLCWQELPDDRPAFQQTCAVL  552
            S+G+VPY  +Q  ++L+   +G RL +P  CP EI+++M+ CW E P+DRP F +    +
Sbjct  693  SMGDVPYPTIQQVDMLEHLLAGGRLSQPLKCPNEIFNIMQKCWAEKPEDRPEFNEMRGEI  752

Query  553  AQMLENATENYGYL  566
              ML    E+YGYL
Sbjct  753  TVMLNLDDESYGYL  766
```

Figure B.1: F09A5.2 another tyrosine kinase receptor is closely related to KIN-9. (A) Both these proteins have homology in the tyrosine kinase domain with a similarity of 64% and an identity of 44%. This is also supported by a previously published article by Popovici et al (1999). (**B)** Showing the amino acid residues that are similar and identical between the proteins in the tyrosine kinase domain.

B.3 *F09A5.2* is expressed in multiple tissues throughout lifespan

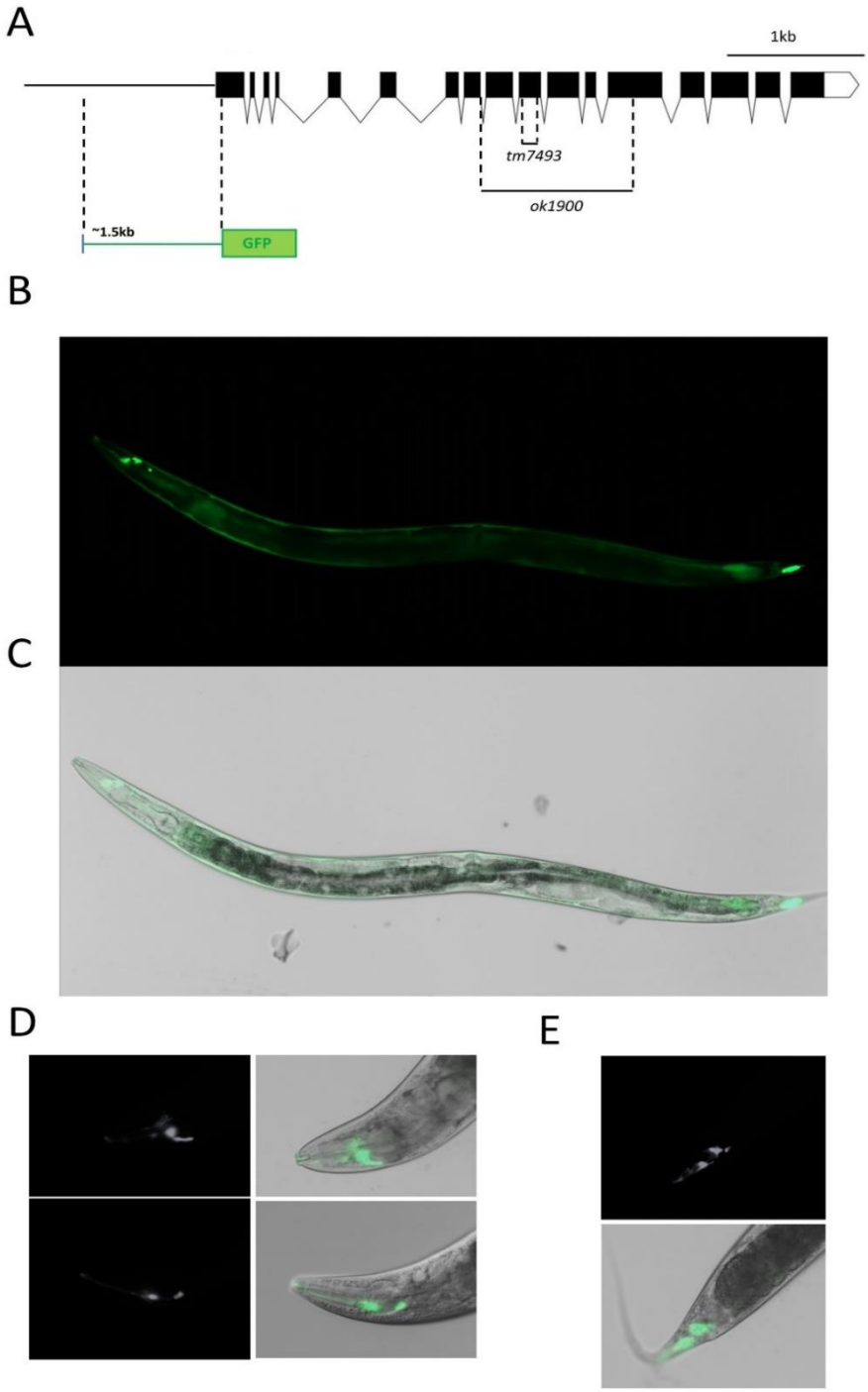

Figure B.2: Expression analysis of the tyrosine kinase receptor *F09A5.2* in *C. elegans*. (A) Panel showing the region used to make the transcriptional reporter and the regions deleted in the mutant alleles. **(B-C)** Animals showing expression of GFP driven by the *F09A5.2* promoter. GFP is seen in the head and tail neurons, body wall muscles, and posterior intestine. **(D-E)** 63X images of fluorescence seen in the head and tail neurons.

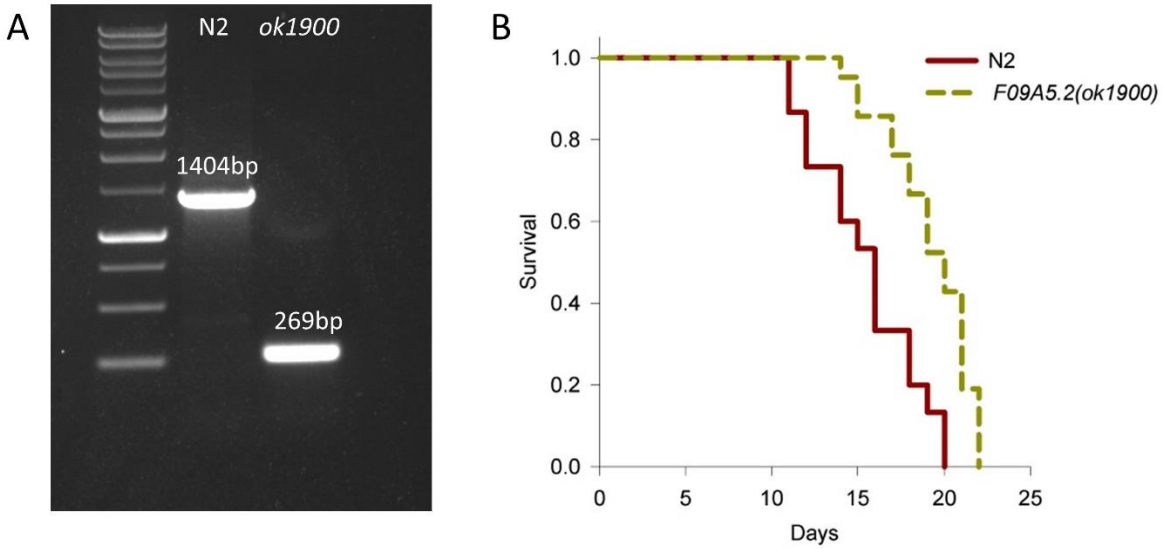

Figure B.3: *F09A5.2* mutants have a 1135bp deletion and exhibit a longer lifespan compared to control animals. (A) Gel image of PCR confirmation for the deletion in *F09A5.2(ok1900)* mutants. **(B)** *F09A5.2(ok1900)* animals have a mean lifespan of 19.23 ± 0.54 days compared to 15.47 ± 0.80 days for control.

Bibliography

Anderson, N. S., and C. M. Haynes, 2020 Folding the Mitochondrial UPR into the Integrated Stress Response. Trends Cell Biol. 30: 428–439.

Arnold, H. K., X. Zhang, C. J. Daniel, D. Tibbitts, J. Escamilla-Powers *et al.*, 2009 The Axin1 scaffold protein promotes formation of a degradation complex for c-Myc. EMBO J. 28: 500–512.

Brack, A. S., M. J. Conboy, S. Roy, M. Lee, C. J. Kuo *et al.*, 2007 Increased Wnt signaling during aging alters muscle stem cell fate and increases fibrosis. Science (80-.). 317: 807–810.

Brenner, S., 1974 THE GENETICS OF CAENORHABDZTZS ELEGANS. Genetics 77: 71–94.

Chen, J., Y. Ou, Y. Li, S. Hu, L. W. Shao *et al.*, 2017 Metformin extends C. Elegans lifespan through lysosomal pathway. Elife 6: 1–17.

Clevers, H., 2006 Wnt/β-Catenin Signaling in Development and Disease. Cell 127: 469–480.

Clevers, H., and R. Nusse, 2012 Wnt/β-catenin signaling and disease. Cell 149: 1192–1205.

Costa, R., R. Peruzzo, M. Bachmann, G. D. Montà, M. Vicario *et al.*, 2019 Impaired Mitochondrial ATP Production Downregulates Wnt Signaling via ER Stress Induction. Cell Rep. 28: 1949-1960.e6.

DeCarolis, N. A., K. A. Wharton, and A. J. Eisch, 2008 Which way does the Wnt blow? Exploring the duality of canonical Wnt signaling on cellular aging. BioEssays 30: 102–106.

Essers, M. A. G., L. M. M. De Vries-Smits, N. Barker, P. E. Polderman, B. M. T. Burgering *et al.*, 2005 Functional interaction between β-catenin and FOXO in oxidative stress signaling. Science (80-.). 308: 1181–1184.

Fang, W. Q., W. W. Chen, A. K. Y. Fu, and N. Y. Ip, 2013 Axin directs the amplification and differentiation of intermediate progenitors in the developing cerebral cortex. Neuron 79: 665–679.

Fang, W. Q., J. P. K. Ip, R. Li, Y. P. Ng, S. C. Lin *et al.*, 2011 Cdk5-mediated phosphorylation of Axin directs axon formation during cerebral cortex development. J. Neurosci. 31: 13613–13624.

Folke, J., B. Pakkenberg, and T. Brudek, 2019 Impaired Wnt Signaling in the Prefrontal Cortex of Alzheimer's Disease. Mol. Neurobiol. 56: 873–891.

Gallotta, I., A. Sandhu, M. Peters, M. Haslbeck, R. Jung *et al.*, 2020 Extracellular proteostasis prevents aggregation during pathogenic attack. Nature 584: 410–414.

Hansen, M., T. Flatt, and H. Aguilaniu, 2013 Reproduction, fat metabolism, and life span: What is the connection? Cell Metab. 17: 10–19.

Hart, M. J., R. De Los Santos, I. N. Albert, B. Rubinfeld, and P. Polakis, 1998 Downregulation of β-catenin by human Axin and its association with the APC tumor suppressor, β-catenin and GSK3β. Curr. Biol. 8: 573–581.

Higuchi-Sanabria, R., P. A. Frankino, J. W. Paul, S. U. Tronnes, and A. Dillin, 2018 A Futile Battle? Protein Quality Control and the Stress of Aging. Dev. Cell 44: 139–163.

Jho, E., T. Zhang, C. Domon, C.-K. Joo, J.-N. Freund *et al.*, 2002 Wnt/β-Catenin/Tcf Signaling Induces the Transcription of Axin2, a Negative Regulator of the Signaling Pathway. Mol. Cell. Biol. 22: 1172–1183.

Kenyon, C. J., 2010 The genetics of ageing. Nature 464: 504–512.

Komiya, Y., and R. Habas, 2008 Wnt signal transduction pathways. Organogenesis 4: 68–75.

Lai, C. H., C. Y. Chou, L. Y. Ch'ang, C. S. Liu, and W. C. Lin, 2000 Identification of novel human genes evolutionarily conserved in Caenorhabditis elegans by comparative proteomics. Genome Res. 10: 703–713.

Lapierre, L. R., and M. Hansen, 2012 Lessons from C. elegans: Signaling pathways for longevity. Trends Endocrinol. Metab. 23: 637–644.

Lezzerini, M., and Y. Budovskaya, 2014 A dual role of the Wnt signaling pathway during aging in Caenorhabditis elegans. Aging Cell 13: 8–18.

Liu, H., M. M. Fergusson, R. M. Castilho, J. Liu, L. Cao *et al.*, 2007 Augmented Wnt signaling in a mammalian model of accelerated aging. Science (80-.). 317: 803–806.

Liu, C. C., C. W. Tsai, F. Deak, J. Rogers, M. Penuliar *et al.*, 2014 Deficiency in LRP6-Mediated Wnt Signaling Contributes to Synaptic Abnormalities and Amyloid Pathology in Alzheimer's Disease. Neuron 84: 63–77.

Logan, C. Y., and R. Nusse, 2004 The Wnt signaling pathway in development and disease. Annu. Rev. Cell Dev. Biol. 20: 781–810.

Mallick, A., A. Ranawade, W. van den Berg, and B. P. Gupta, 2020 Axin-Mediated Regulation of Lifespan and Muscle Health in C. elegans Requires AMPK-FOXO Signaling. iScience 23: 101843.

Mallick, A., A. Ranawade, and B. P. Gupta, 2019a Role of PRY-1/Axin in heterochronic miRNA-mediated seam cell development. BMC Dev. Biol. 19: 1–12.

Mallick, A., S. K. B. Taylor, A. Ranawade, and B. P. Gupta, 2019b Axin Family of Scaffolding Proteins in Development: Lessons from C. elegans. J. Dev. Biol. 7: 1–23.

Marchand, A., F. Atassi, A. Gaaya, P. Leprince, C. Le Feuvre *et al.*, 2011 The

Wnt/beta-catenin pathway is activated during advanced arterial aging in humans. Aging Cell 10: 220–232.

Marzo, A., S. Galli, D. Lopes, F. McLeod, M. Podpolny *et al.*, 2016 Reversal of Synapse Degeneration by Restoring Wnt Signaling in the Adult Hippocampus. Curr. Biol. 26: 2551–2561.

McLeod, F., A. Bossio, A. Marzo, L. Ciani, S. Sibilla *et al.*, 2018 Wnt Signaling Mediates LTP-Dependent Spine Plasticity and AMPAR Localization through Frizzled-7 Receptors. Cell Rep. 23: 1060–1071.

Mello, C. C., J. M. Kramer, D. Stinchcomb, and V. Ambros, 1991 Efficient gene transfer in C.elegans: Extrachromosomal maintenance and integration of transforming sequences. EMBO J. 10: 3959–3970.

Miller, W. L., and H. S. Bose, 2011 Early steps in steroidogenesis: Intracellular cholesterol trafficking. J. Lipid Res. 52: 2111–2135.

Nijholt, D. A. T., A. Nölle, E. S. van Haastert, H. Edelijn, R. F. Toonen *et al.*, 2013 Unfolded protein response activates glycogen synthase kinase-3 via selective lysosomal degradation. Neurobiol. Aging 34: 1759–1771.

Nusse, R., and H. Clevers, 2017 Wnt/β-Catenin Signaling, Disease, and Emerging Therapeutic Modalities. Cell 169: 985–999.

Pakos-Zebrucka, K., I. Koryga, K. Mnich, M. Ljujic, A. Samali *et al.*, 2016 The integrated stress response. EMBO Rep. 17: 1374–1395.

Palomer, E., J. Buechler, and P. C. Salinas, 2019 Wnt signaling deregulation in the aging and Alzheimer's brain. Front. Cell. Neurosci. 13: 1–8.

Papsdorf, K., and A. Brunet, 2019 Linking Lipid Metabolism to Chromatin Regulation in Aging. Trends Cell Biol. 29: 97–116.

Pellegrino, M. W., A. M. Nargund, N. V. Kirienko, R. Gillis, C. J. Fiorese *et al.*, 2014 Mitochondrial UPR-regulated innate immunity provides resistance to pathogen infection. Nature 516: 414–417.

Purro, S. A., E. M. Dickins, and P. C. Salinas, 2012 The secreted Wnt antagonist dickkopf-1 is required for amyloid β-mediated synaptic loss. J. Neurosci. 32: 3492–3498.

Ranawade, A., A. Mallick, and B. P. Gupta, 2018 PRY-1/Axin signaling regulates lipid metabolism in Caenorhabditis elegans. PLoS One 13: e0206540.

Ren, Z., and V. R. Ambros, 2015 Caenorhabditis elegans microRNAs of the let-7 family act in innate immune response circuits and confer robust developmental timing against pathogen stress. Proc. Natl. Acad. Sci. U. S. A. 112: E2366–E2375.

Taylor, R. C., and C. Hetz, 2020 Mastering organismal aging through the endoplasmic reticulum proteostasis network. Aging Cell 19: 1–12.

Uno, M., and E. Nishida, 2016 Lifespan-regulating genes in c. Elegans. npj Aging

Mech. Dis. 2:.

Watts, J. L., and M. Ristow, 2017 Lipid and carbohydrate metabolism in Caenorhabditis elegans. Genetics 207: 413–446.

Xu, Y., Z. He, M. Song, Y. Zhou, and Y. Shen, 2019 A micro RNA switch controls dietary restriction-induced longevity through Wnt signaling . EMBO Rep. 20: 1–14.

Yue, Y., C. Zhang, X. Zhang, S. Zhang, Q. Liu *et al.*, 2020 An AMPK/Axin1-Rac1 signaling pathway mediates contraction-regulated glucose uptake in skeletal muscle cells. Am. J. Physiol. - Endocrinol. Metab. 318: E330–E342.

Zhang, Y. L., H. Guo, C. S. Zhang, S. Y. Lin, Z. Yin *et al.*, 2013 AMP as a low-energy charge signal autonomously initiates assembly of axin-ampk-lkb1 complex for AMPK activation. Cell Metab. 18: 546–555.

Zhang, C. S., B. Jiang, M. Li, M. Zhu, Y. Peng *et al.*, 2014a The lysosomal v-ATPase-ragulator complex is a common activator for AMPK and mTORC1, acting as a switch between catabolism and anabolism. Cell Metab. 20: 526–540.

Zhang, C. S., M. Li, T. Ma, Y. Zong, J. Cui *et al.*, 2016 Metformin Activates AMPK through the Lysosomal Pathway. Cell Metab. 24: 521–522.

Zhang, T., Y. Liao, F. N. Hsu, R. Zhang, J. S. Searle *et al.*, 2014b Hyperactivated Wnt Signaling Induces Synthetic Lethal Interaction with Rb Inactivation by Elevating TORC1 Activities. PLoS Genet. 10:.

Zhang, Q., Z. Wang, W. Zhang, Q. Wen, X. Li *et al.*, 2021 The memory of neuronal mitochondrial stress is inherited transgenerationally via elevated mitochondrial DNA levels. Nat. Cell Biol. 23: 870–880.

Zhang, Q., X. Wu, P. Chen, L. Liu, N. Xin *et al.*, 2018 The Mitochondrial Unfolded Protein Response Is Mediated Cell-Non-autonomously by Retromer-Dependent Wnt Signaling. Cell 174: 870-883.e17.

Zhou, J. yi, D. gui Huang, M. Zhu, C. qi Gao, H. chao Yan *et al.*, 2020 Wnt/β-catenin-mediated heat exposure inhibits intestinal epithelial cell proliferation and stem cell expansion through endoplasmic reticulum stress. J. Cell. Physiol. 235: 5613–5627.

Zong, Y., C. S. Zhang, M. Li, W. Wang, Z. Wang *et al.*, 2019 Hierarchical activation of compartmentalized pools of AMPK depends on severity of nutrient or energy stress. Cell Res. 29: 460–473.